NASA CONTRACTOR REPORT

NASA CR-1916

DESIGN AND EVALUATION OF ACTIVE COOLING SYSTEMS FOR MACH 6 CRUISE VEHICLE WINGS

by W. A. McConarty and F. M. Anthony

Prepared by
BELL AEROSPACE COMPANY
Buffalo, N.Y.
for Langley Research Center

NATIONAL AERONAUTICS AND SPACE ADMINISTRATION • WASHINGTON, D. C. • DECEMBER 1971

1. Report No.	2. Government Accession No.	3. Recipient's Catalog No.
NASA CR-1916		

4. Title and Subtitle	5. Report Date
Design and Evaluation of Active Cooling Systems for Mach 6 Cruise Vehicle Wings	December 1971
	6. Performing Organization Code

7. Author(s)	8. Performing Organization Report No.
W. A. McConarty and F. M. Anthony	7305-901001
	10. Work Unit No. 760-75-01-02
9. Performing Organization Name and Address	11. Contract or Grant No.
Bell Aerospace Company Post Office Box One Buffalo, New York	NAS1-7468
	13. Type of Report and Period Covered
12. Sponsoring Agency Name and Address	Contractor Report
National Aeronautics and Space Administration Washington, D.C. 20546	14. Sponsoring Agency Code

15. Supplementary Notes

16. Abstract

Active cooling systems, which included transpiration, film, and convective cooling concepts, are examined. Coolants included hydrogen, helium, air, and water. Heat shields, radiation barriers, and thermal insulation are considered to reduce heat flow to the cooling systems. Wing sweep angles are varied from 0° to 75° and wing leading edge radii of 0.05 inch and 2.0 inches are examined. Structural temperatures are varied to allow comparison of aluminum alloy, titanium alloy, and superalloy structural materials. Cooled wing concepts are compared among themselves, and with the uncooled concept on the basis of structural weight, cooling system weight, and coolant weight.

1. Hypersonic Aircraft
2. Airfoils - Cooling
3. Heat Transfer
4. Cooling Systems

17. Key Words (Suggested by Author(s))	18. Distribution Statement
Equilibrium temperatures Hypersonic heat loads Hypersonic transport	Unclassified-Unlimited

19. Security Classif. (of this report)	20. Security Classif. (of this page)	21. No. of Pages	22. Price*
Unclassified	Unclassified	271	$3.00

*For sale by the National Technical Information Service, Springfield, Virginia 22151

FOREWORD

This is one of three final reports on a program to design and evaluate active cooling systems for a Mach 6 cruise vehicle. The work has been accomplished by the Bell Aerospace Company under contract NAS1-7468 with the National Aeronautics and Space Administration, Langley Research Center, Hampton, Virginia. F. M. Anthony was program manager, and the principal investigator during the course of the contract was either W. H. McConarty or R. G. Helenbrook. Other personnel contributing to this program were W. N. Meholick (structural design and analysis), M. S. Janis (heat transfer analyses), D. L. Gillis (technical analyses), J. Witmer, H. Yee, J. Witsil, and P. Mitchell. D. E. Fetterman and P. L. Lawing were the NASA contract monitors. Final reports have been prepared for each of three parts.

Part I - Design and Evaluation of Active Cooling Systems for Mach 6 Cruise Vehicle Wings.

Part II - Evaluation of Active Cooling Systems for a Mach 6 Hypersonic Transport Airframe.

Part III - Design of a Convective Cooling System for a Mach 6 Hypersonic Transport Airframe.

Results of Part I are presented in this report.

CONTENTS

	Page
SUMMARY	1
INTRODUCTION	2
SYMBOLS	3
BASELINE DATA	6
HEAT TRANSFER AND AERODYNAMIC DATA	13
IDENTIFICATION OF COOLING SYSTEMS	29
RADIATION AUGMENTED ACTIVE COOLING	55
TRANSPIRATION COOLING SYSTEM SELECTION STUDIES	73
CONVECTIVE AND SPRAY COOLING SYSTEM SELECTION STUDIES	116
STRUCTURAL STUDIES	159
COOLING SYSTEM REFINEMENTS	199
SUMMARY OF ACTIVE COOLING SYSTEMS	212
CONCLUSIONS AND RECOMMENDATIONS	224
SYMBOLS (APPENDICES)	230
APPENDIX A - Geometrical Considerations	233
APPENDIX B - Determination of Local Flow Fields	240
APPENDIX C - Aerodynamic Heating	243
APPENDIX D - Transpiration Cooling	259
APPENDIX E - Aerodynamic Structural Loads	261
REFERENCES	263

DESIGN AND EVALUATION OF ACTIVE COOLING SYSTEMS FOR MACH 6 CRUISE VEHICLE WINGS

by W. A. McConarty and F. M. Anthony
Bell Aerospace Company

SUMMARY

An analytical study was made of active cooling systems for wings of a Mach 6 cruise aircraft. Transportation, film, spray, and convective cooling concepts were examined. Coolants included hydrogen, helium, air, and water. Wing structural temperatures were varied to allow comparison of aluminum alloy, titanium alloy, and superalloy construction materials. Heat shields, radiation barriers, and thermal insulation were considered to reduce heat flow to cooled structures. Wing leading edge radii of 0.05 inch and 2.0 inches were examined and the wing leading edge sweep angle was varied from 0° to 75°. The cooled wing concepts were compared among themselves and with the uncooled concept on the basis of structural weight, cooling system weight, and coolant weight.

The results of this study indicate that indirect convective cooling concepts and transpiration cooling concepts are attractive for cooling the wing structure of hypersonic aircraft, and that the weights of wings cooled by any of several techniques are equal to or less than the weight of an uncooled wing.

SECTION 1

INTRODUCTION

In the development of advanced flight systems such as hypersonic cruise vehicles the establishment of a firm technological base is essential before a major aircraft program is undertaken. To establish this firm technological base a quantitative definition of the design interactions of major systems is necessary. The objective of the work reported herein was to realistically define, evaluate and compare actively cooled concepts for hypersonic cruise vehicles and to identify the technological problems requiring further investigation.

The severe environmental conditions induced by hypersonic cruise flight within the atmosphere make a detailed evaluation of the complex interplay of aerodynamic, thermal and structural design variables imperative in order to achieve an optimum airframe design. Available structural materials are severely taxed by long service life requirements. Ablatives can reduce demands on structural materials, but refurbishment is costly and time consuming. It is appropriate, therefore, to investigate the ability of active cooling concepts to mitigate the adverse effects of hypersonic flight on the vehicle airframe.

The wing of a typical hypersonic cruise vehicle was chosen for study because the design of this component is strongly influenced by aerodynamic, thermal and structural interactions. A variety of cooling system concepts and coolants were investigated so that the influence of active cooling on the overall vehicle configuration and performance could be meaningfully defined and compared with alternate approaches. Studies undertaken also included wing geometry variations. Active cooling system concepts studied included transpiration systems, film cooling systems, and convective cooling systems. Possibilities of hybrid systems of the above were also investigated. A radiation cooled configuration was included for reference. Analysis methods are given in the Appendix.

SYMBOLS

A_{Ref}	area of underwing
b	wing span dimension
Bu	mass transfer driving function
C	wing chord dimension
C_D	drag coefficient
C_F	skin friction coefficient
C_L	lift coefficient
C_p	specific heat
D	diameter of hemicylindrical nose
dA	nodal surface area
F	equation of arbitrary surface
$\overline{F_c C_F}$	postulated function defined by Spalding
F_R	postulated function defined by Spalding
H	enthalpy
h	heat transfer coefficient
K	thermal conductivity
L	unit vector parallel to leading edge
M	Mach number
N	normal vector to surface
Nu	Nusselt number
P	pressure
P_R	Prandtl number
q	heat flux
R	gas constant
R_E	Reynolds number
R_N	radius of hemicylindrical leading edge
$\frac{S}{R_N}$	normalized distance perpendicular to leading edge
T	temperature

SYMBOLS (CONT)

T	tangent vector
t	wing thickness
V	velocity
w	mass flow rate
$\frac{X}{R_N}$	normalized distance from leading edge in streamwise direction

GREEK

α	direction cosine with respect to X axis
α_θ	time varying body angle of attack
β	direction cosine with respect to Y axis
β	velocity gradient at stagnation line
β_i	deflected stream angle
δ	direction cosine with respect to Z axis
δ	angular location of stagnation line
δ	boundary layer displacement thickness
δ_i	compliment of flow deflection angle
Λ	sweep angle
μ	viscosity
ρ	density
ϕ	wedge angle

SUBSCRIPTS

AU	aft upper surface
QW	adiabatic wall conditions
B	blast pressure component
e	effective angle
FU	forward upper surface
H	hemicylindrical surface
i	element number
L	vector normal to leading edge

N	normal to surface
SN	surface normal
u	unit vector
V	vector tangent to velocity vector
VL	velocity vector normal to leading edge
w	wall conditions
δ	local free stream conditions
0	stagnation conditions
1	conditions upstream of shock
2	conditions downstream of shock
02	conditions on surface at stagnation line
∞	free stream conditions

SECTION 2

BASELINE DATA

The baseline configuration used for this study was developed in Reference 1. Figure 1 shows this baseline delta wing vehicle configuration defining fuel tank locations, location of passenger and cargo compartments and location of primary control surfaces. Figure 2 presents a typical mission profile for such a vehicle cruising at Mach 6 and at an altitude slightly above 100,000 feet.

Before wing geometry variations were chosen a baseline wing configuration was established as shown in Figure 3. Wing geometrical variations were made by holding the wing area (6954 ft^2) and the wing span (114 ft) constant while varying sweep angle (0° through 65°) and leading edge radius (0.05 in. to 2.0 in.). The wing sweep variations shown in Figures 4 through 7 are for sweep angles of 0°, 30°, 45° and 65°. A 75° sweep angle case was also included as a special case and is shown in Figure 8. For a 75° sweep angle it was not possible to keep a 114 ft span, a 6954 ft^2 area and a trailing edge perpendicular to the body centerline. Therefore, the span was reduced sufficiently to hold the other variables constant.

The variation in vehicle weight and fuel flow is shown in figure 9. The vehicle takeoff weight is approximately 520,000 pounds, and the landing weight is 335,000 pounds. During the constant Mach number climb to cruise altitude (M = 6), the vehicle angle of attack is 8.31°. During cruise at maximum lift to drag ratio, however, the angle of attack is 5.14°. Because a detailed heating analysis for this aircraft throughout its mission profile was not available, the design point for this study was chosen to be Mach 6, at an altitude of 100,000 feet, and angle of attack of 8.31°. Since the wing is offset from the fuselage reference axis by 2°, the design wing angle of attack is 10.31°. The hydrogen fuel flow at this condition is 147,000 lb/hr.

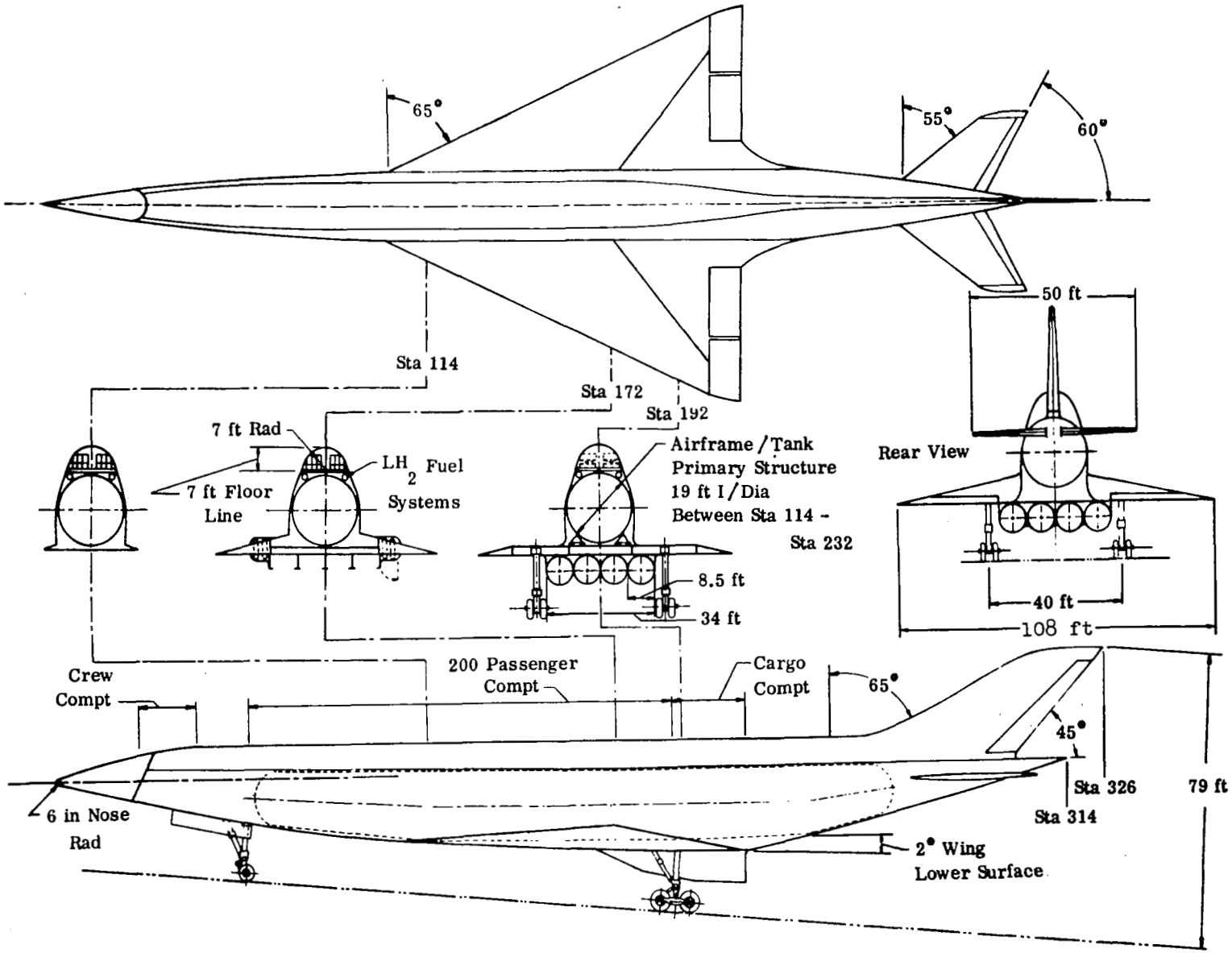

Figure 1. Delta Wing Configuration (from Reference 1).

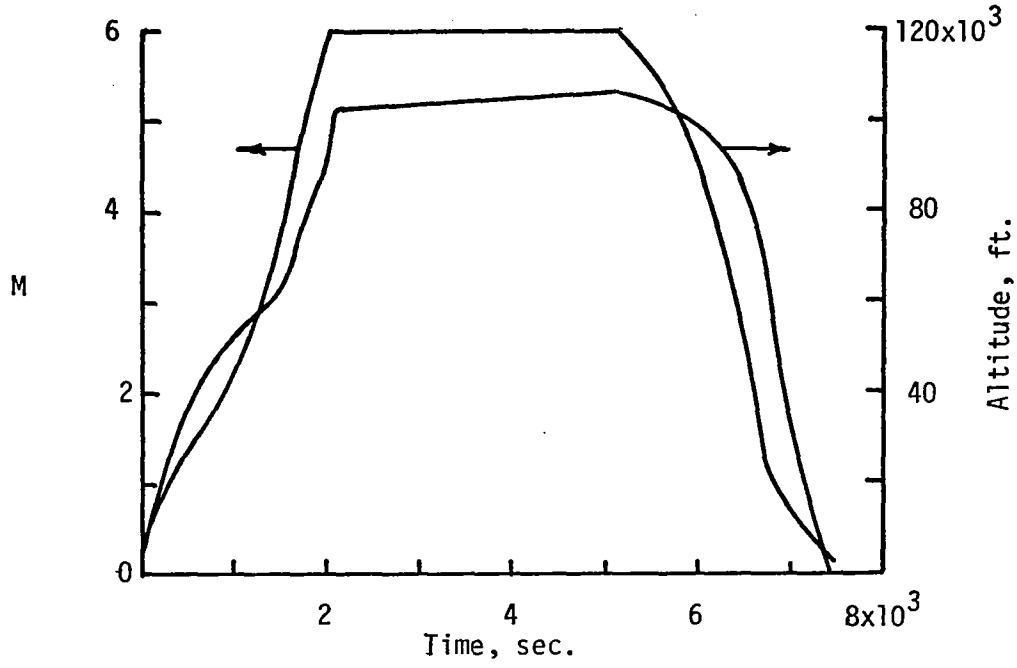

Figure 2.- MISSION PROFILE.

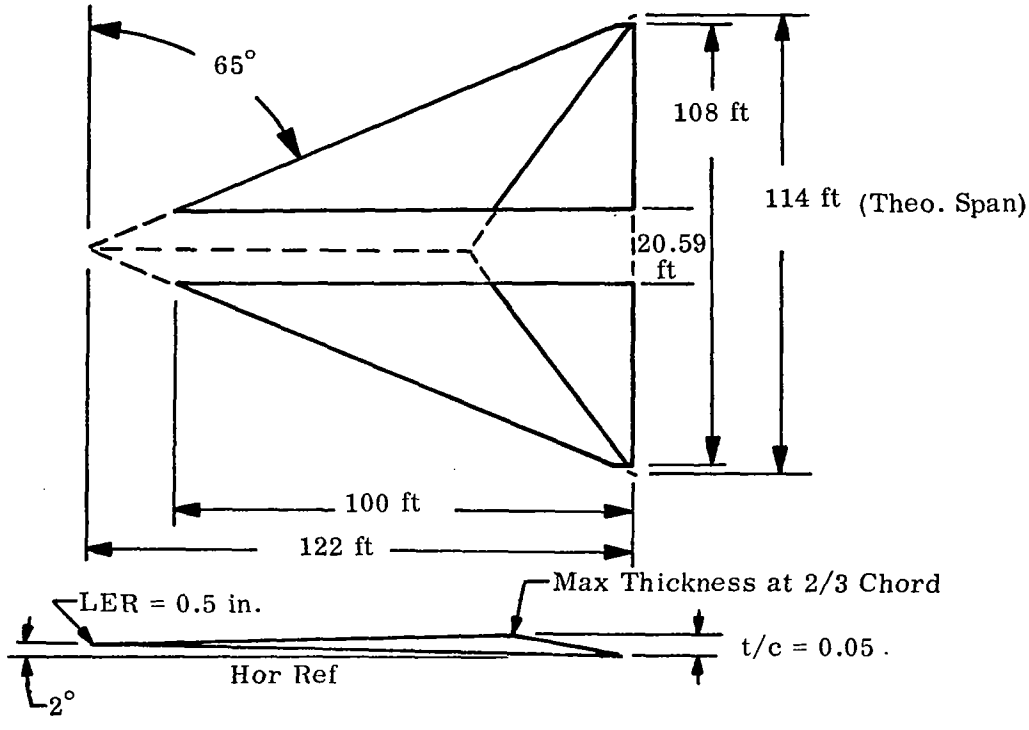

Figure 3. Baseline Wing

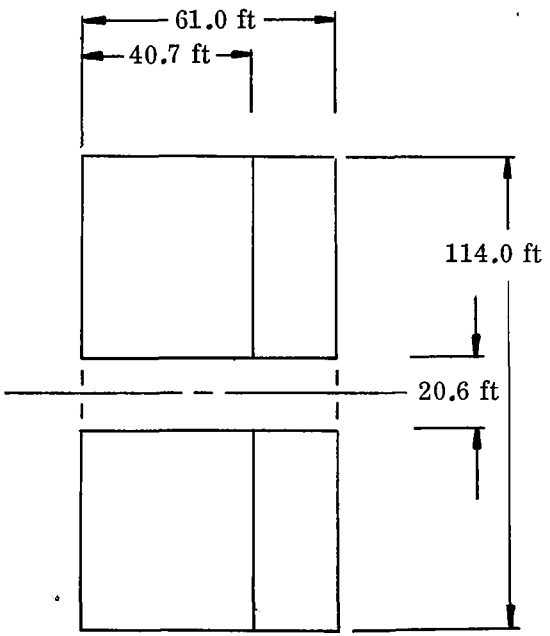

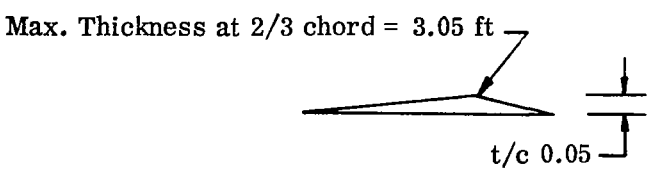

Figure 4. 0° Sweep Wing Configuration

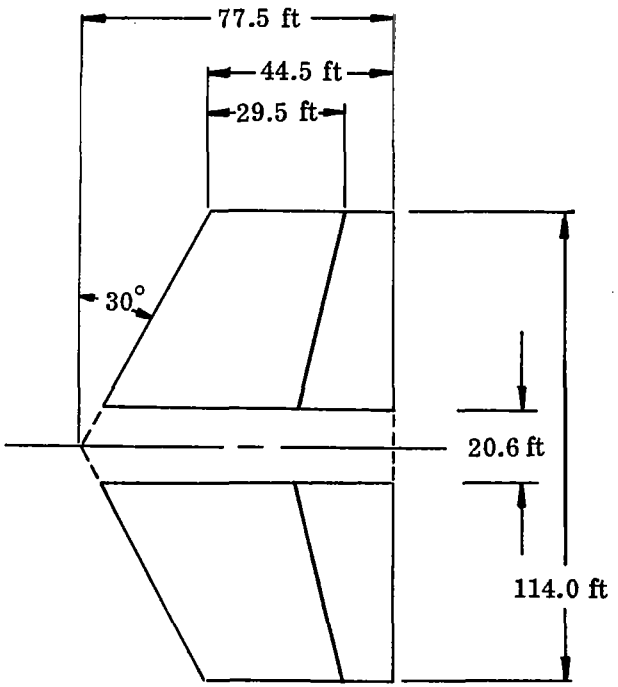

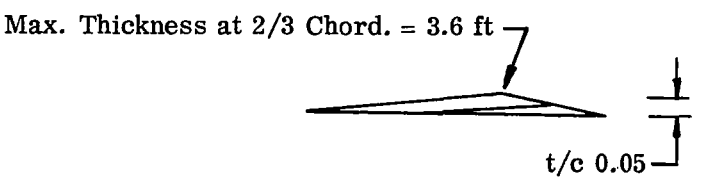

Figure 5. 30° Sweep Wing Configuration

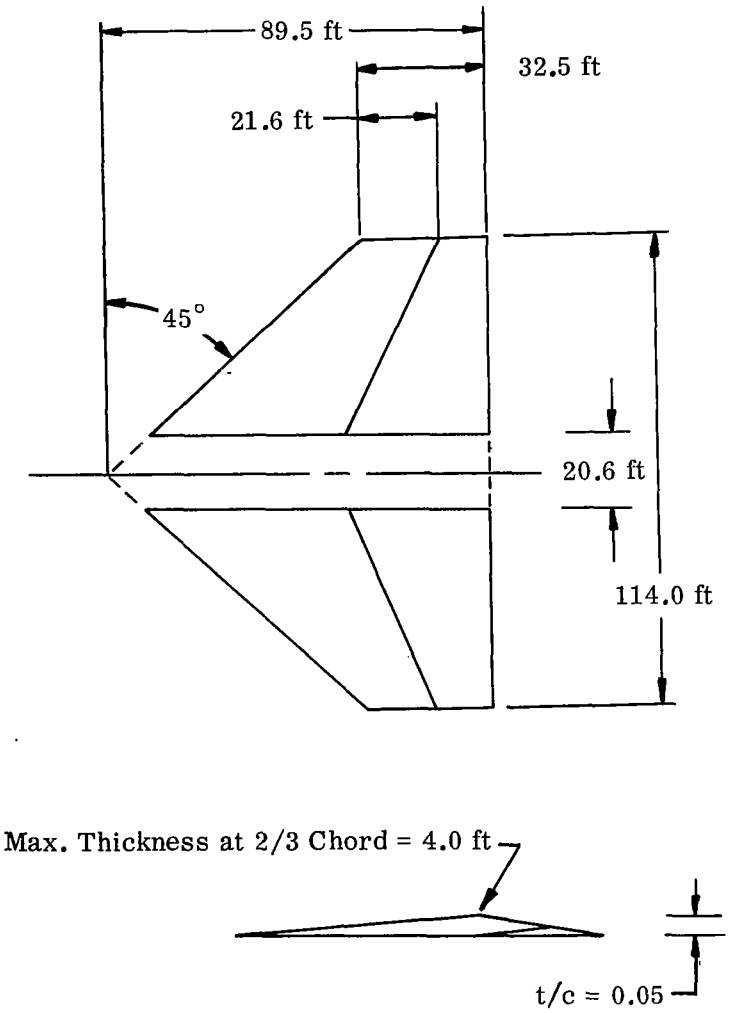

Figure 6. 45° Sweep Wing Configuration

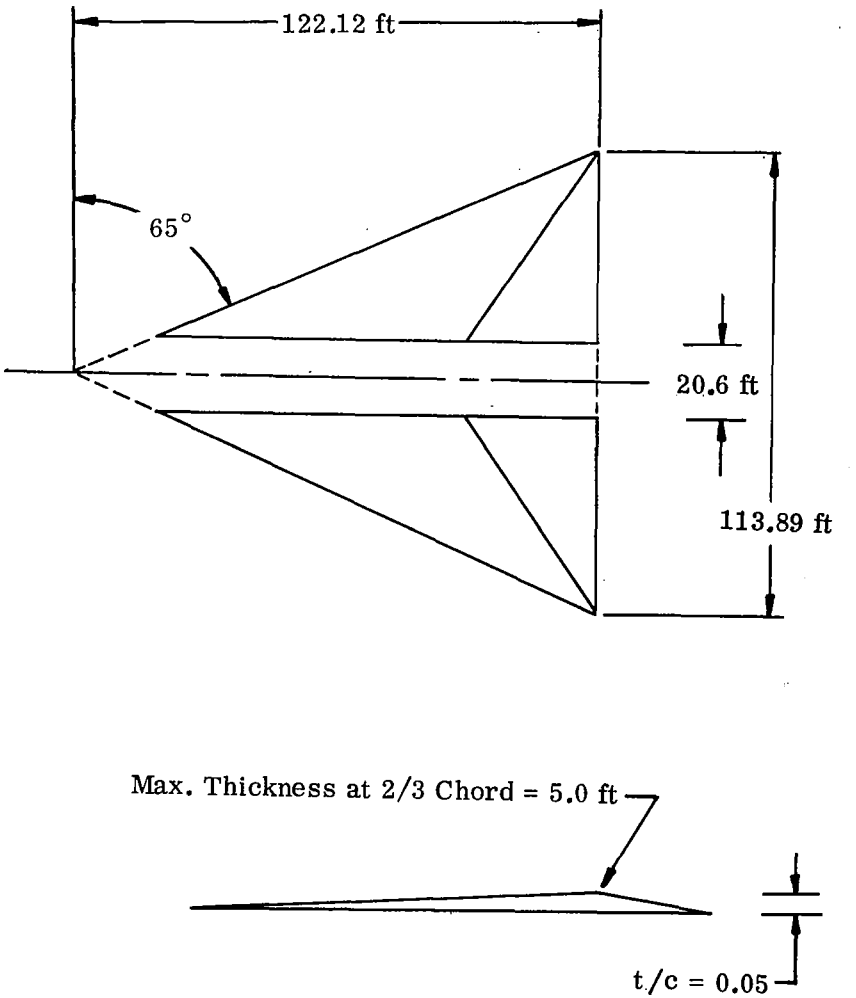

Figure 7. 65° Sweep Wing Configuration

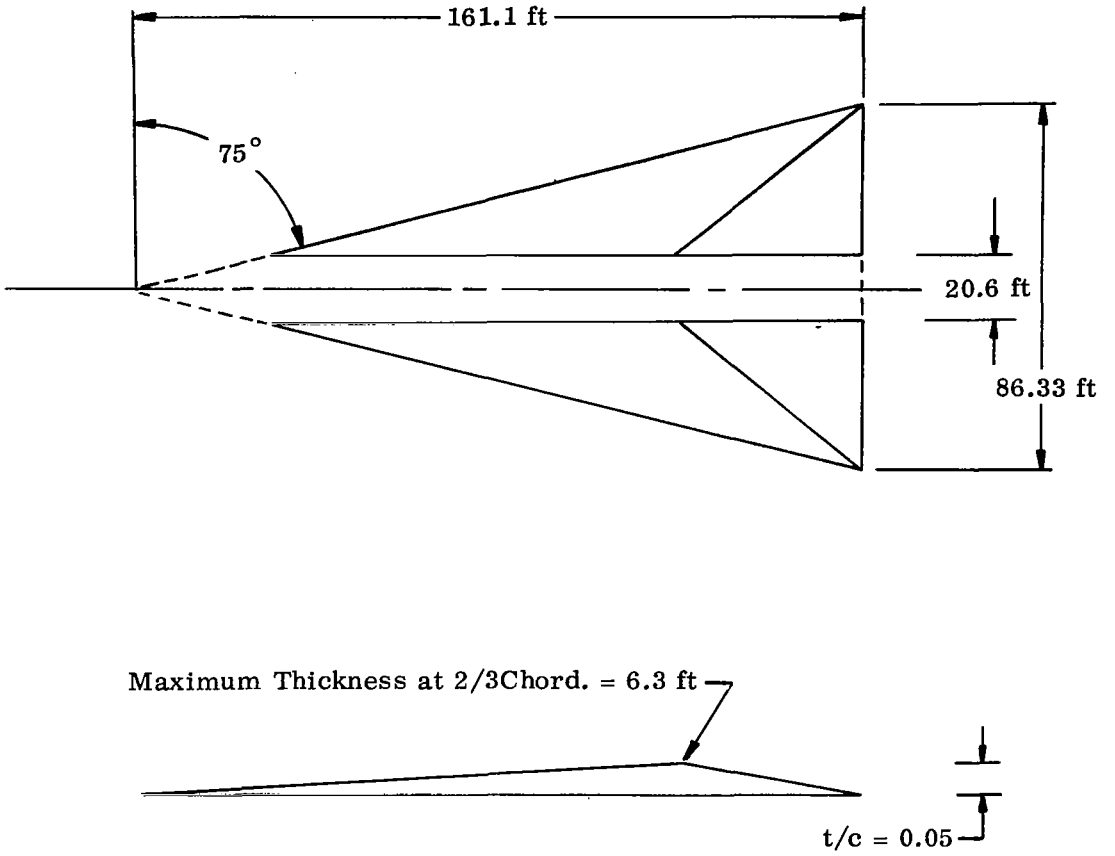

Figure 8. 75° Sweep Wing Configuration

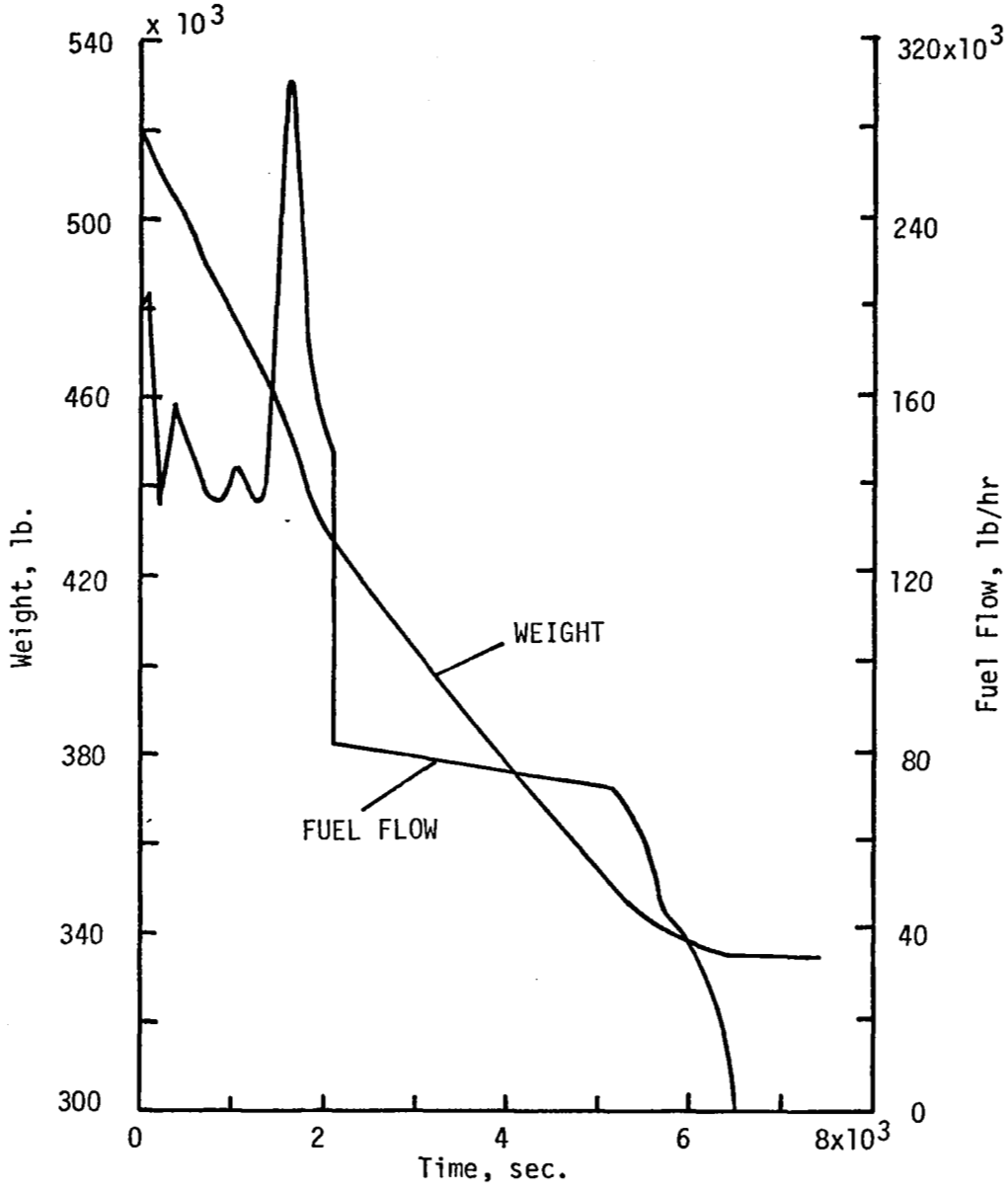

Figure 9. WEIGHT AND FUEL FLOW VARIATION FOR BASELINE VEHICLE.

SECTION 3

HEAT TRANSFER AND AERODYNAMIC DATA

In this section the aerodynamic heat transfer data necessary for active cooling system studies is presented and discussed. Pressure distributions, radiation equilibrium wall temperatures and lift and drag coefficients are also included. This data is presented as a function of leading edge sweep angle for two values of leading edge radius. All data presented in this section is for a dry wing surface.

A. EQUIVALENT STEADY-STATE TIME

For preliminary comparisons of actively cooled systems transient analyses are relatively expensive with respect to computational time, and were shown to be unnecessary in Reference 2. This reference defined a technique for calculating an equivalent steady-state time which yields system weight predictions about 10% higher than those based upon detailed transient analyses. The "equivalent steady-state time" technique was successfully applied to the comparative study of fluid cooled cabin wall concepts for hypersonic cruise vehicles in Reference 3. Therefore, the same technique was employed for this study. The representative mission profile and the related heating ratios and temperatures which were used herein to determine an equivalent time are shown in figures 10 and 11.

Equivalent times were determined in the following manner. For an insulated surface the shape of the heat input curve for the surface closely follows the radiation equilibrium surface temperature curve. Thus, if the surface is insulated an equivalent time for application of the steady-state heat flux is found by dividing the area under the radiation equilibrium surface temperature curve by the steady-state radiation equilibrium surface temperature. Using Figure 11, this equivalent time is 1.4 hours. For an uninsulated surface the shape of the heat input curve for the surface closely follows the cold wall heat flux curve (hT_R curve). Thus, if the surface is not insulated an equivalent time for application of the steady-state heat flux is found by dividing the area under the cold wall heat flux curve by some value of cold wall heating rate. Looking at Figure 11, it is seen that the cold wall heating rate has no steady-state value. The value of cold wall heat flux selected must roughly correspond to the point at which steady-state aerodynamic data is to be generated. For this study a point at Mach 6 and 100,000 ft was selected from Figure 2 for steady-state computations. The value of cold wall heating flux corresponding to this point is approximately 15,000 Btu/ft^2-hr. Using this value for cold wall heat flux the steady-state equivalent time is 1.5 hours. For design purposes in this program a value of 1.5 hours is used for the Mach 6 vehicle.

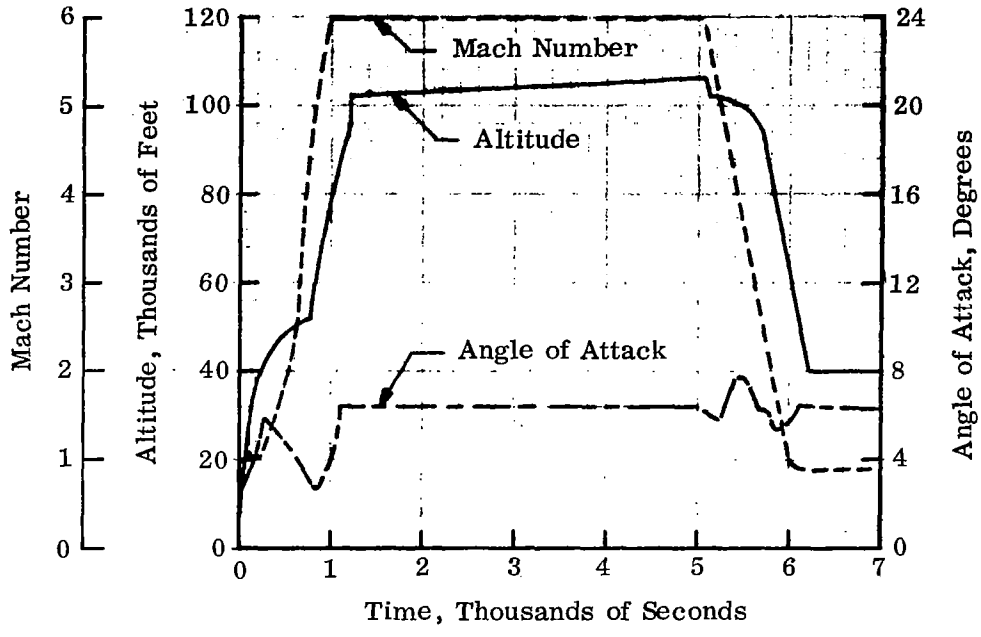

Figure 10. Mission Profile for Equivalent Time Calculation, Mach 6 Cruise Vehicle

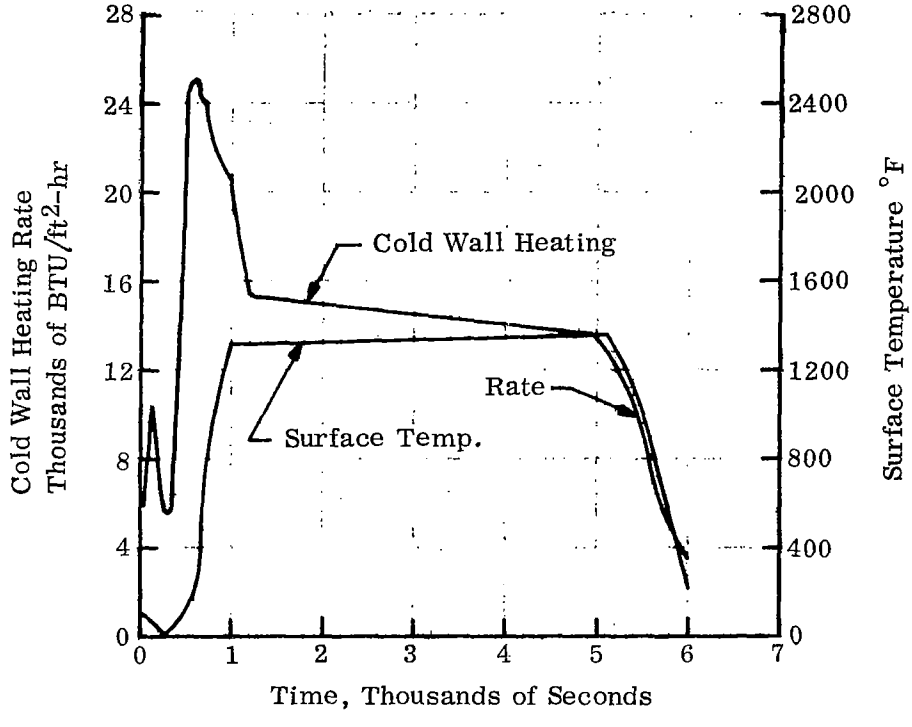

Figure 11. Transient Heat Transfer Data, Mach 6 Cruise Vehicle, Calculated for a 5° Cone 10 ft. Aft of the Nose on the Lower Surface

If any other hot surface on the vehicle is chosen and transient calculations performed to yield data as shown in Figure 11 and new equivalent times are found they will not be far from the above 1.5 hours. Prior studies have found that a cooling system designed using a properly determined equivalent steady-state time will perform very satisfactorily under transient conditions.

B. HEAT TRANSFER COEFFICIENTS

Heat transfer data was generated using a two-dimensional flow assumption neglecting all body and tip effects. With these assumptions lines of constant temperature, heat transfer coefficient and pressure are parallel to the leading edge (excluding the rear wedge). Thus heat transfer data was generated along lines perpendicular to the leading edge.

For the wing configurations chosen the bottom surface of the wing is a compression region with pressures about four times greater than free stream pressures. Depending upon sweep angle and leading edge diameter, flow conditions on the lower surface range from laminar flow at the leading edge with transition to turbulent flow aft of the leading edge, to turbulent flow from the leading edge rearward. The top surface of the wing is in an expansion region and pressures are near or below free stream pressure except near the leading edge. Flow conditions on the top surface range from laminar flow at the leading edge with a transition to turbulent flow aft of the leading edge, to turbulent flow from the leading edge rearward. Behind the maximum thickness line the flow is so greatly expanded that there is no significant heating. The methods used for calculations in the flow regimes mentioned are described in detail in the Appendix and summarized below.

Laminar leading edge heat transfer data was generated using a modified form of the stagnation point heat transfer coefficient correlation by Reshotko and Cohen, Reference 4, which accounts for leading edge diameter. This correlation was corrected for effective sweep angle using methods discussed in Reference 5. The method of Lees, Reference 6, was used to obtain laminar flow distribution aft of the stagnation point on the hemicylindrical leading edge.

Bushnell, Reference 7, has shown that the presence of a forebody has a destabilizing effect on the leading edge flow causing an early onset of transition to turbulent flow. A curve fit to experimental data was used to predict transition to turbulent flow on the swept leading edge. Turbulent leading edge heat transfer data was generated using the method of Beckwith and Gallagher, Reference 8. Aft of the hemicylinder shoulder, heat transfer data was generated using a method outlined by Bertram and Neal, Reference 9, employing the Von Karman form of the Reynolds analogy in conjunction with the Spalding and Chi skin friction function, Reference 10.

Laminar flow flat plate data was generated by methods discussed in Reference 5. A modified form of the Spalding and Chi relation as proposed by Neal and Bertram, Reference 9, was chosen from turbulent flow flat plate analyses.

The onset of transition from laminar to turbulent flow was computed on the basis of the streamwise Reynolds number by conservatively assuming that as soon as the streamwise Reynolds number exceeds a critical Reynolds number turbulent flow commences. Thus, a step change in the heat transfer coefficient variation results rather than the

continuous variation which actually exists. The critical Reynolds number for 0° sweep was assumed to be 500,000. The value of the critical Reynolds number is corrected for a premature onset of turbulence due to a swept leading edge. The above criteria are described in detail in the Appendix.

Heat transfer coefficient data presented in this report is referenced to the radiation equilibrium wall temperatures which result from an adiabatic wall assumption. Studies were conducted to determine the effect of wall temperature deviations from the adiabatic case and resulted in the conclusion that wall temperature effects could be neglected for the present study. This decision is substantiated in the Appendix.

Figures 12 through 17 present typical heat transfer results for the range of variables of interest. Since active cooling systems must be designed to accommodate the maximum heat load on the vehicle, steady-state heat transfer data was generated for the maximum heating conditions. The choice of this combination of parameters was made using data from Reference 1. All heat transfer data presented in this section is for a Mach 6 wing at 100,000 feet with an angle of attack of 10.31°.

Figures 12 and 13 show heat transfer coefficient variations for the minimum (0.05 in.) and maximum (2.0 in.) radii studied. Before discussing the data in these figures the coordinate system should be explained. The zero h line represents the wing surface and values of increasing h are plotted perpendicular to this surface on a uniform grid. The true distance along the surface (zero h line) is found by multiplying the value of n by the conversion factor given (0.00873 or 0.34907). For example, for n = 9 (at the hemicylinder shoulder) the distance to the shoulder is 0.07857 inch for R = 0.05 inch and 3.1416 inch for R = 2.0 inch.

For the 0.05 inch leading edge radius, laminar flow exists on the leading edge hemicylinder for all sweep angles studied (0° to 75°). Although only 0° and 65° sweep values are shown in Figure 12, values of h for other sweep angles are readily approximated by assuming a cosine variation of h with sweep angle. The 2.0 inch leading edge radius encounters both laminar and turbulent flow in the sweep angle range studied. At 0° sweep the heat transfer coefficient is about 48.0 Btu/hr-ft^2-°F at the stagnation point ($n \simeq -1.0$) and the leading edge is in a laminar flow regime. As sweep angle increases, a transition to turbulent flow occurs between 30° and 45° sweep. At 45° sweep, for a 2.0 inch radius, the flow is turbulent and heat transfer coefficients exceed those for the laminar flow 0° sweep case. For sweep angles beyond 45° the leading edge is in a turbulent flow regime for R = 2.0 inches.

Figures 14 through 17 present heat transfer coefficient data for the flat surfaces. Semi-logarithmic graph paper was used to magnify the area near the leading edge. Figures 14 and 15 are for the top surface while Figures 16 and 17 are for the bottom surface. It should be noted that h is near or below 2.0 Btu/hr-ft^2-°F for the majority of the top surface and near or below 10.0 Btu/hr-ft^2-°F for the majority of the bottom surface. For the top surface, 0.05 inch leading edge radius case, the flow for all sweep angles is laminar in the vicintiy of the leading edge with a transition to turbulent flow occurring between 10.0 and 100.0 inches aft of the leading edge. The discontinuities shown on both curves in Figure 14 indicate the onset of transition. In Figure 15 the effect of the

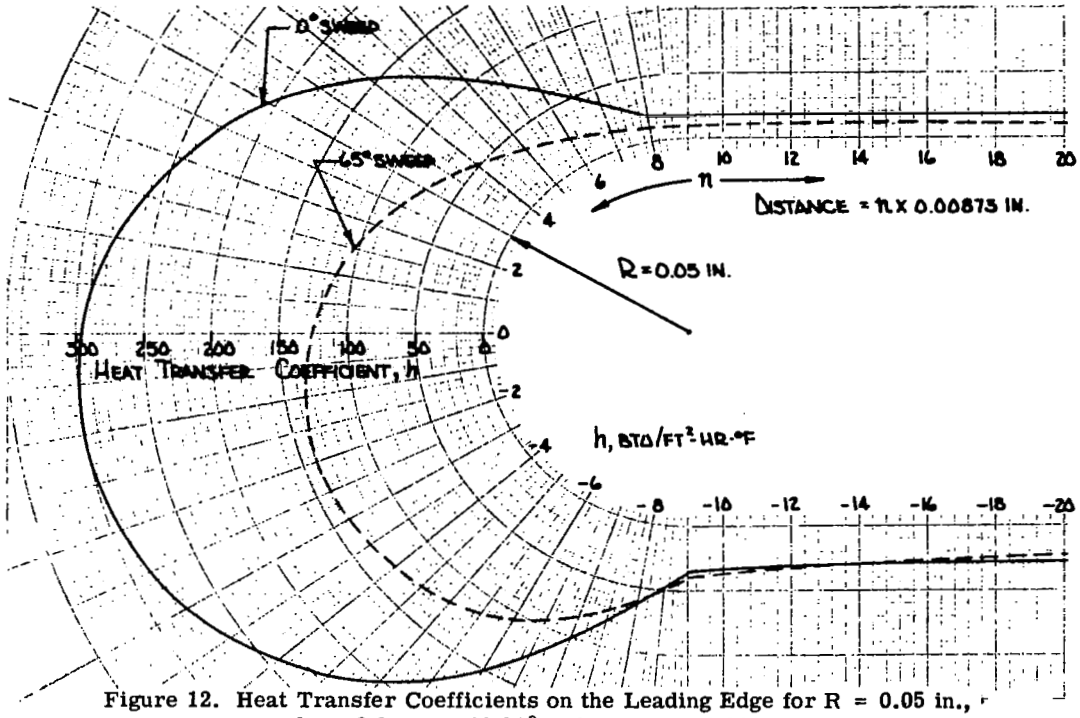

Figure 12. Heat Transfer Coefficients on the Leading Edge for R = 0.05 in., M = 6.0, α = 10.31°, Altitude = 100,000 ft

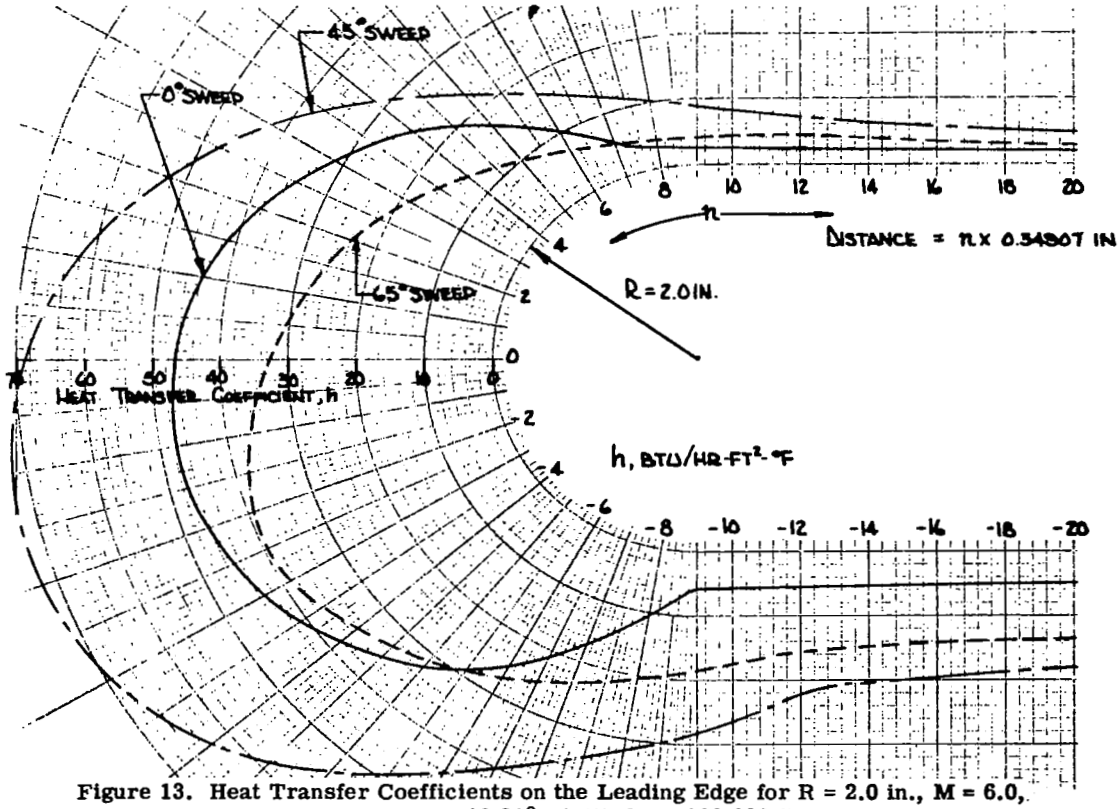

Figure 13. Heat Transfer Coefficients on the Leading Edge for R = 2.0 in., M = 6.0, α = 10.31°, Altitude = 100,000 ft

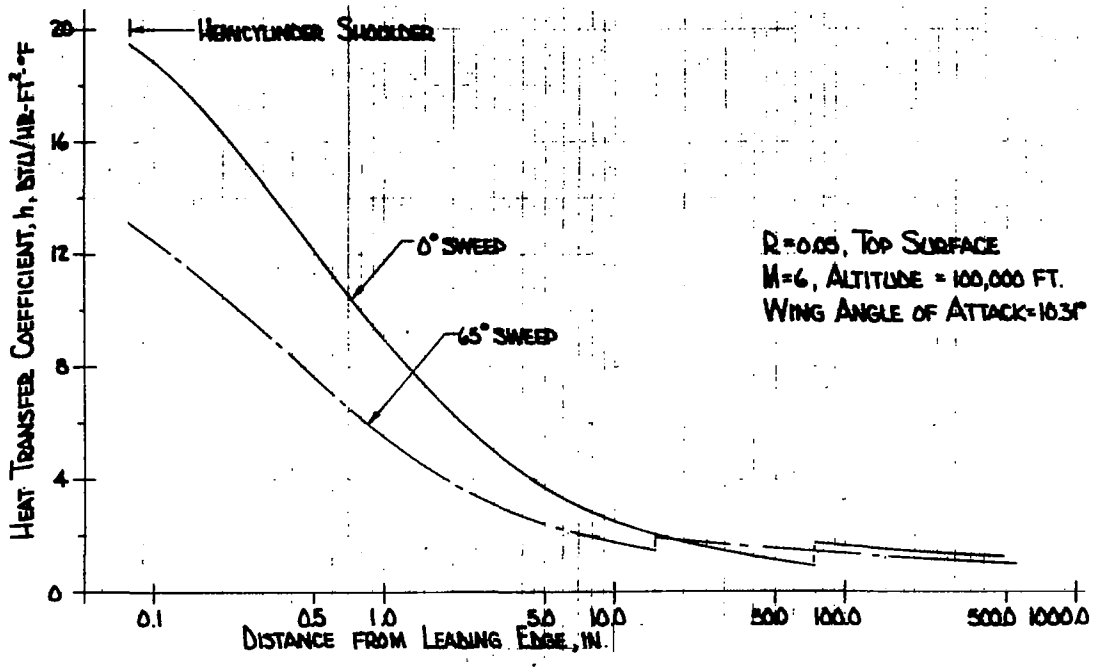

Figure 14. Heat Transfer Coefficients on the Top Surface for a 0.05 in. Leading Edge Radius, M = 6.0, α = 10.31°, Altitude = 100,000 ft

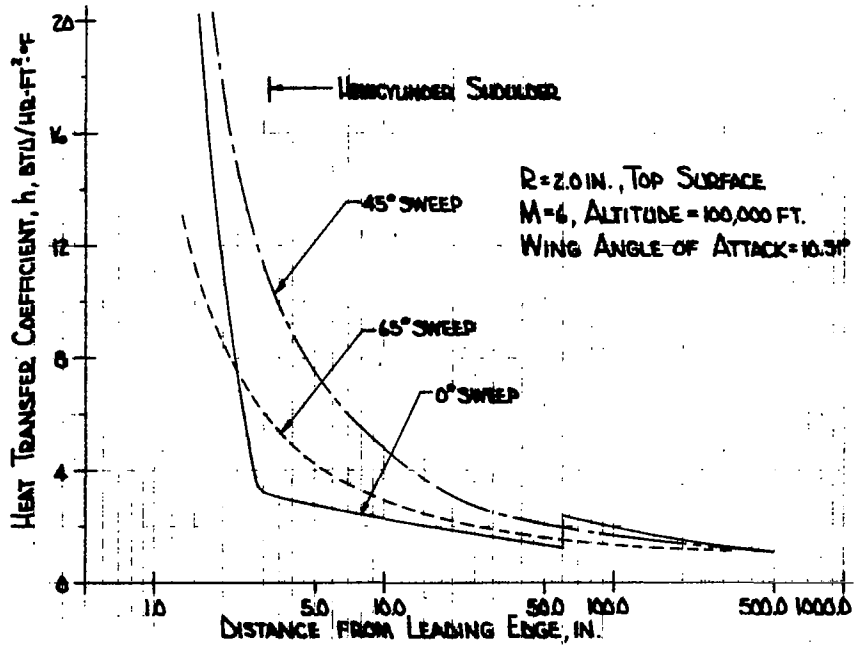

Figure 15. Heat Transfer Coefficients on the Top Surface for a 2.0 in. Leading Edge Radius, M = 6.0, α = 10.31°, Altitude = 100,000 ft

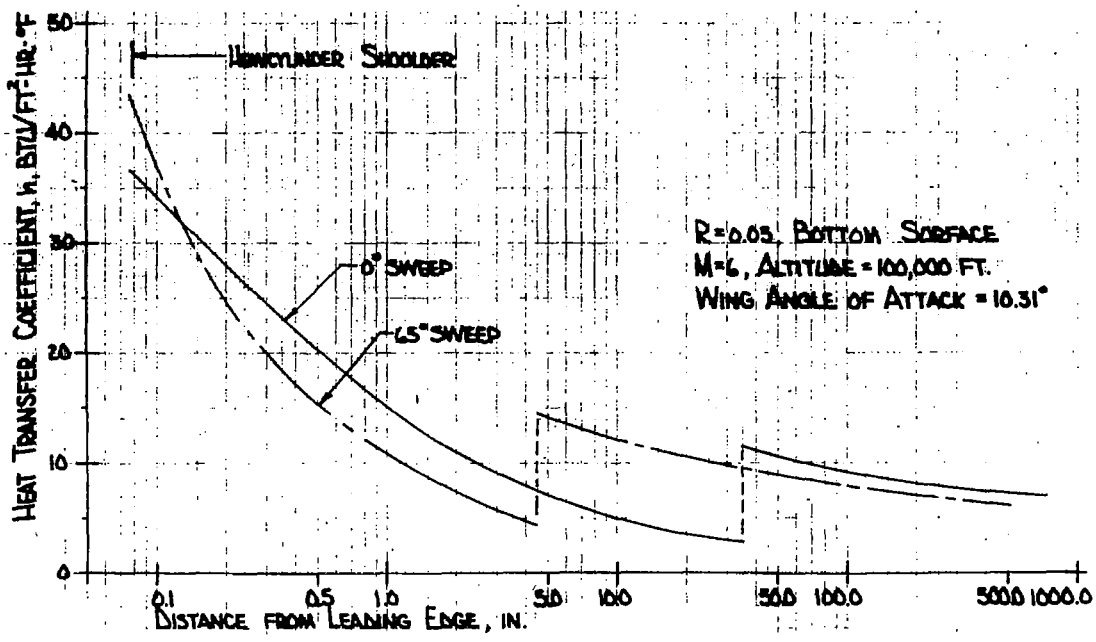

Figure 16. Heat Transfer Coefficients on the Bottom Suffface for a 0.05 in. Leading Edge Radius M = 6.0, α = 10.31°, Altitude = 100,000 ft

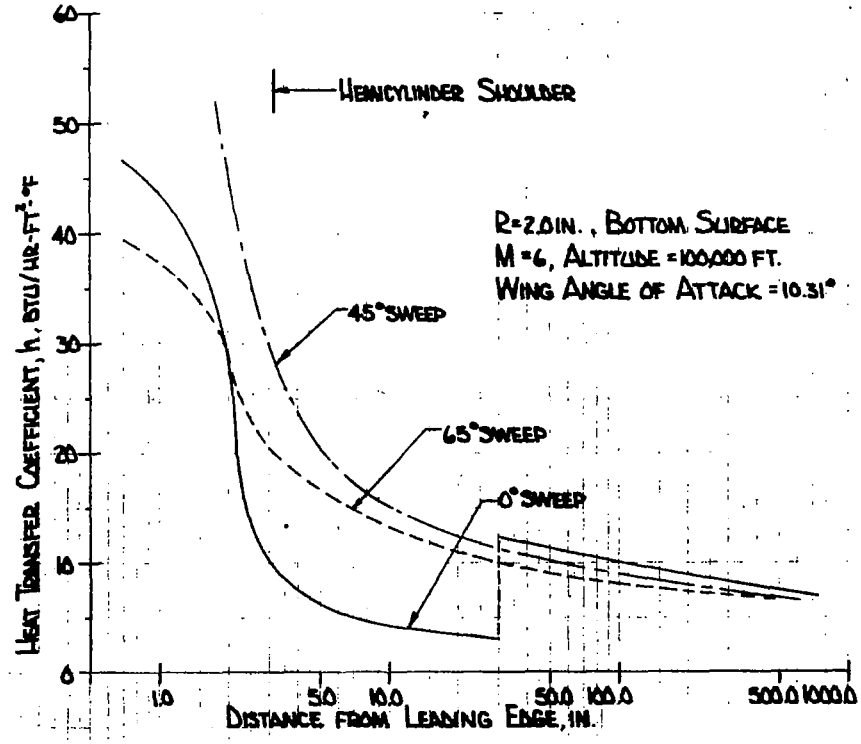

Figure 17. Heat Transfer Coefficients on the Bottom Surface for a 2.0 in. Leading Edge Radius, M = 6.0, α= 10.31°, Altitude = 100,000 ft

turbulent leading edge is evident for sweep angles of 45° or greater for a 2.0 inch leading edge radius. The lack of a transition discontinuity for 45° and 65° sweep cases is due to the fact that the entire wing is in a turbulent flow regime.

Figures 16 and 17 show the much more pronounced laminar to turbulent flow transition and higher heat transfer coefficients that occur on the lower wing surface. For a 0.05 inch leading edge radius flow over the leading edge is laminar for all sweep angles and a transition to turbulent flow occurs on the flat bottom surface only for low sweep angles. For sweep angles of 45° or greater the leading edge is turbulent and no transition occurs on the lower surface. The heat transfer coefficient data presented in Figures 14 through 17 were used to estimate cooling system heat loads for the convective systems studied in Section 7.

C. PRESSURE DISTRIBUTIONS

Local pressures on the wing surface were determined using different theories for the hemicylindrical leading edge and for the flat surfaces. On the leading edge hemicylinder pressures were found using a modified Newtonian theory while on the flat wedge surfaces pressures were determined by a superposition of the wedge pressure due to an oblique shock and blast overpressures due to the blunt leading edge as given by Creager, Reference 11. In the region just aft of the leading edge hemicylinder matching of the two theories mentioned above was done by using a polynomial curve fit. A detailed discussion of the methods used to determine pressure distributions is given in the Appendix.

Figures 18 through 20 summarize pressure data generated using the methods mentioned above. For modified Newtonian flow, as assumed for the leading edge hemicylinder, pressures are a function of S/R and if plotted in the form of Figure 18, one plot is sufficient for all radii. Appropriate factors for determining S given n and R are listed for R = 2.0 inch and R = 0.05 inch. Pressure values for sweep angles between those given can be approximated by assuming a cosine variation of pressure with sweep angle. Examination of Figure 18 indicates a rapid decrease of pressure with sweep. In the region of the stagnation point pressures decrease by a factor of five as the sweep angle changes from 0° to 65°. A rapid decrease of pressure with increasing distance from the stagnation point is also noticed. For the 0° sweep case pressures decrease from 1000 psf at the stagnation point to 40 psf at the top hemicylinder shoulder and 290 psf at the bottom hemicylinder shoulder.

Figure 19 shows pressure data for the flat top surface. On the top surface pressures decrease rapidly with increasing distance from the leading edge. For the 0.05 inch radius leading edge pressures drop below free stream pressures beyond 1.0 inch from the leading edge hemicylinder centerline. For the 2.0 inch radius leading edge, free stream pressures are reached 20.0 inches aft of the leading edge. Pressures on the top surface aft of the maximum wing thickness line are not shown on Figure 19 but are below 1.0 psf.

Pressures shown in Figure 20 are important from the standpoint of determining potential aircraft lift. More than 20.0 inches aft of the leading edge pressures are about 100.0 psf for leading edge radii from 0.05 inch to 2.0 inches. Ignoring leading edge effects and assuming the top surface reaches free stream pressure a pressure difference across

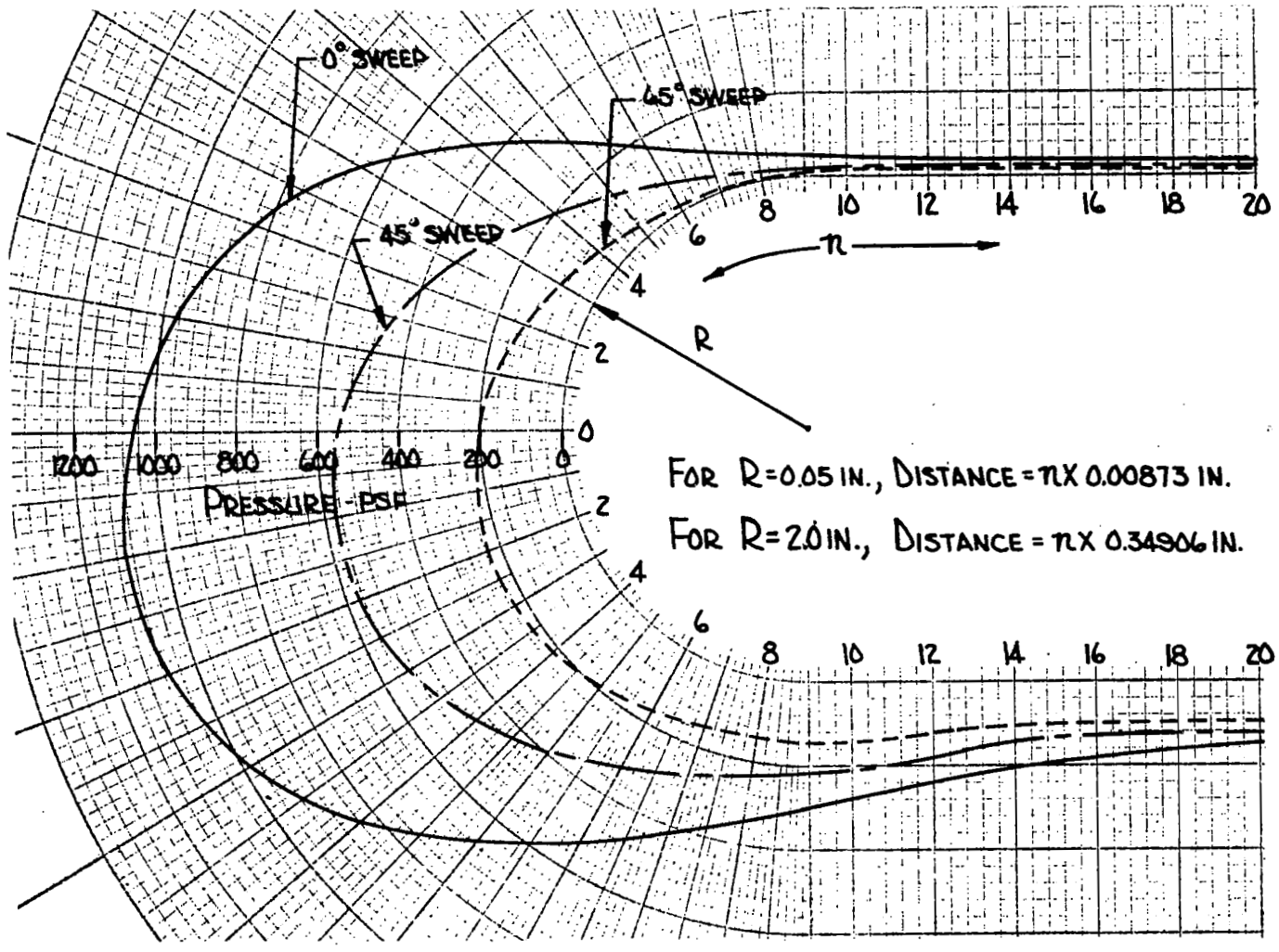

Figure 18. Pressure Distributions on the Leading Edge, M = 6.0, α = 10.31°, Altitude = 100,000 ft

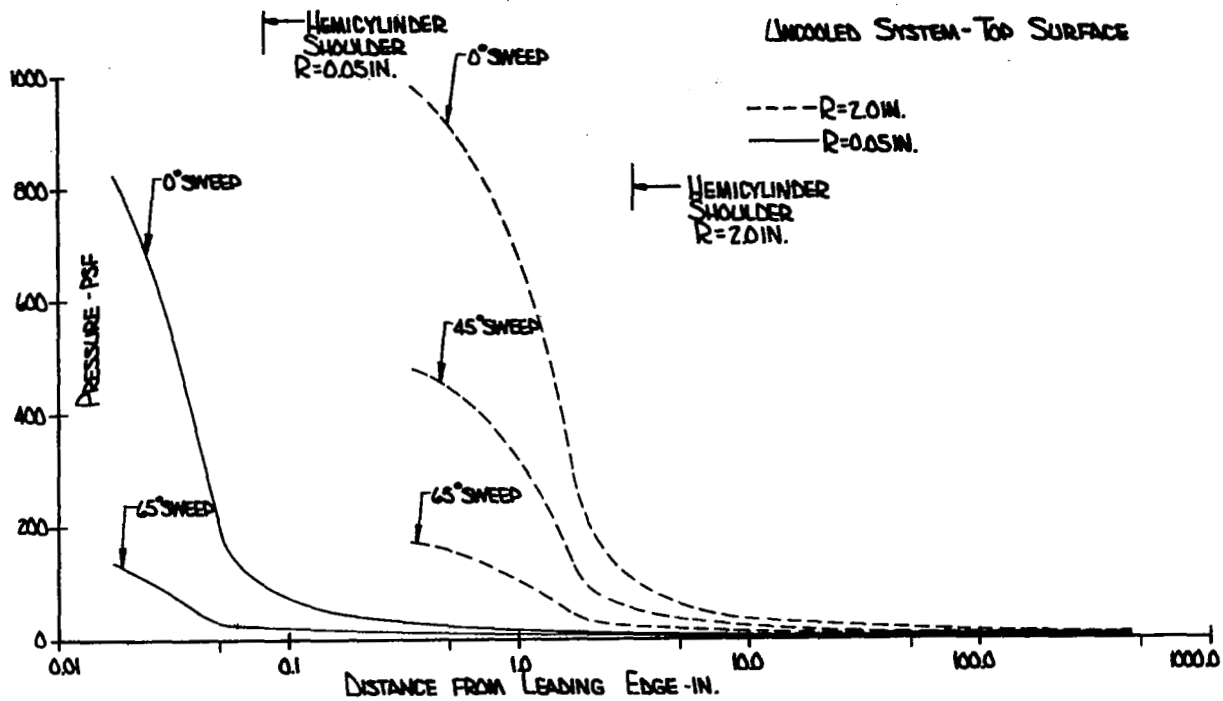

Figure 19. Pressure Distributions on the Top Surface, M = 6.0, α = 10.31°, Altitude = 100,000 ft

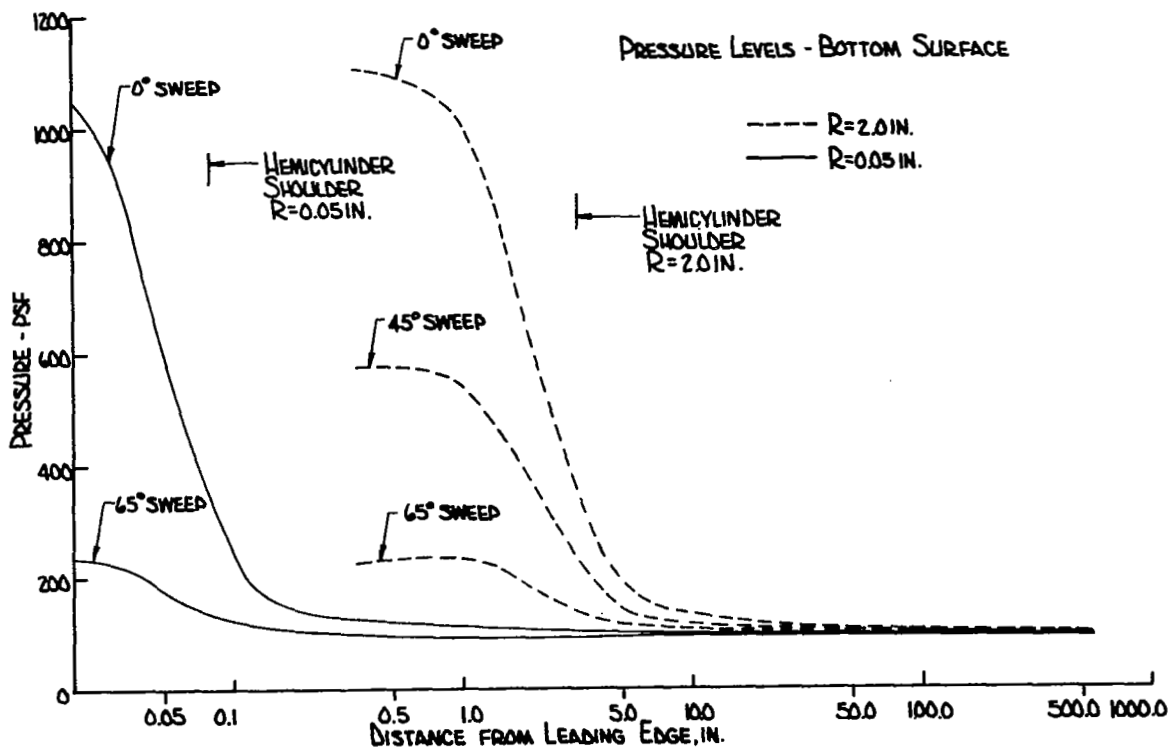

Figure 20. Pressure Distributions of the Bottom Surface, M = 6.0, α = 10.31°, Altitude = 100,000 ft

the wing of about 80.0 psf exists. This pressure differential applied to 6954 ft^2 is sufficient to lift a 556,000 lb aircraft. This is about 20% above the expected weight at 100,000 ft as given in Figure 9. This would indicate that the aircraft is still climbing rapidly when it reaches Mach 6 at 100,000 ft. Since the choice of the 100,000 ft altitude, Mach 6 and 10.31° angle of attack conditions was made to allow cooling system sizing to meet peak heat loads and not solely from aerodynamic considerations, no effort was made to reconcile this excess lift capability.

D. RADIATION EQUILIBRIUM WALL TEMPERATURES

Temperatures on the surface of an uncooled wing were determined using a radiation equilibrium wall assumption which implies that any heat convected to the wall must be radiated away. A heat balance for this radiation equilibrium wall assumption yields the following equation:

$$h\,(T_R - T_W) = \sigma\,\epsilon\,T_W^4$$

where:

T_W, wall temperature, °R

ϵ = 0.8, assumed surface emittance

σ = Stefan-Boltzmann constant

h = heat transfer coefficient, Btu/hr-ft^2-°R

T_R = adiabatic wall temperature, °R

The heat transfer coefficient h is that presented in Section 3B. The method of calculating T_R, the adiabatic wall temperature, is described in the Appendix. Since values of T_R were not plotted a short list of values is given in Table I. The value of T_R listed for the hemicylinder is that for S = 0 in. and is not the maximum value on the hemicylinder. Maximum values occur at the stagnation point.

Figures 21 through 24 present radiation equilibrium wall temperature data for the leading edge and flat wing surfaces. For the 0.05 inch leading edge radius, as shown in Figure 21, uncooled surface temperatures on the leading edge hemicylinder vary from about 1300°F to 2400°F. Variations around the hemicylinder are not as large as previously seen for the heat transfer coefficient due to the fourth power variation of wall temperature. Increasing the edge radius from 0.05 inch to 2.0 inches decreases leading edge hemicylinder temperatures about 25% (i.e., from 2400°F to 1850°F for the 0° sweep stagnation point). For large leading edge radii and sweep angles of 45°, or greater, the leading edge is in turbulent flow and changing to a 2.0 inch radius does not decrease wall temperatures more than 5%.

Figures 23 and 24 present data for the wedge surfaces with dashed lines indicating the 2.0 inch leading edge radius case and solid lines indicating the 0.05 inch leading edge radius case. For the top surface, as shown in Figure 23, the change from a compression to an expansion surface on the leading edge hemicylinder is shown by a sharp change in slope of the temperature curve forward of the hemicylinder shoulder. Comparing data

TABLE I

ADIABATIC WALL TEMPERATURE, T_R

Sweep Angle (deg)	Leading Edge Radius (in.)	S (in.)	T_R (°F)	Location
0	0.05	550	2487	Bottom
	2.0	501	2488	
	0.05	0	2670	Hemicylinder
	2.0	0	2670	
	0.05	450	2405	Top
	2.0	301	2407	
45	0.05	550	2487	Bottom
	2.0	501	2488	
	0.05	0	2581	Hemicylinder
	2.0	0	2581	
	0.05	450	2405	Top
	2.0	301	2406	
65	0.05	550	2487	Bottom
	2.0	501	2487	
	0.05	0	2479	Hemicylinder
	2.0	0	2478	
	0.05	450	2405	Top
	2.0	301	2405	

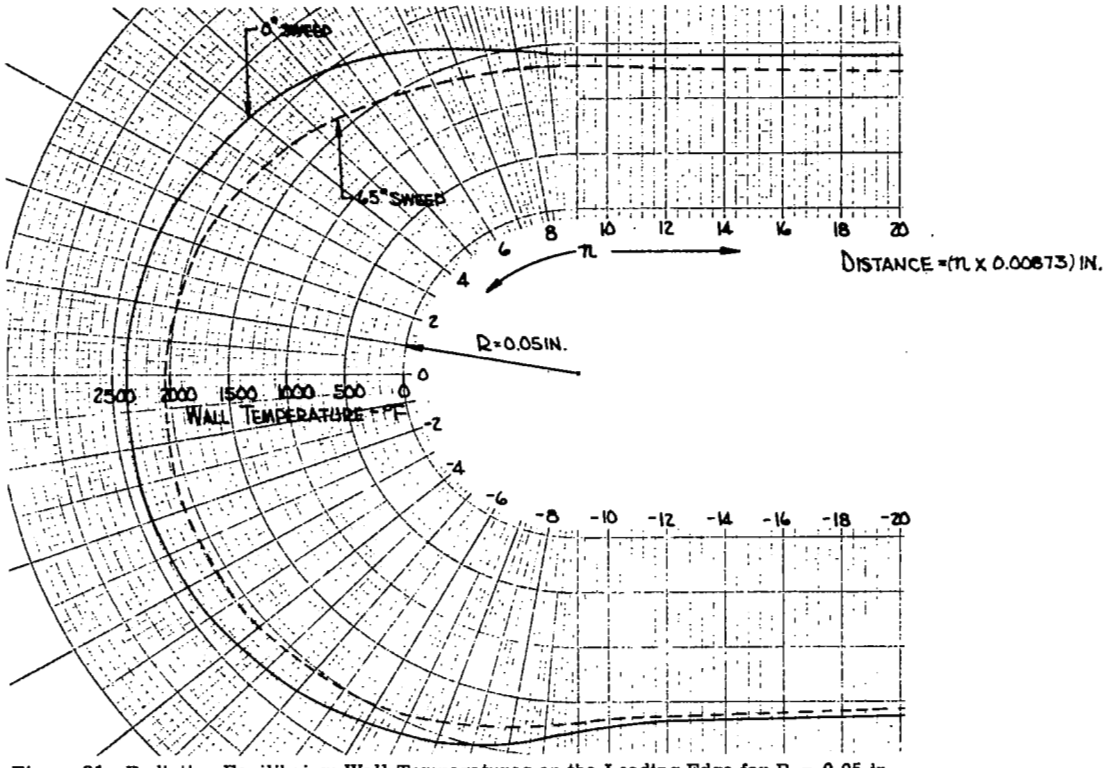

Figure 21. Radiation Equilibrium Wall Temperatures on the Leading Edge for R = 0.05 in., M = 6.0, α = 10.31°, Altitude = 100,000 ft

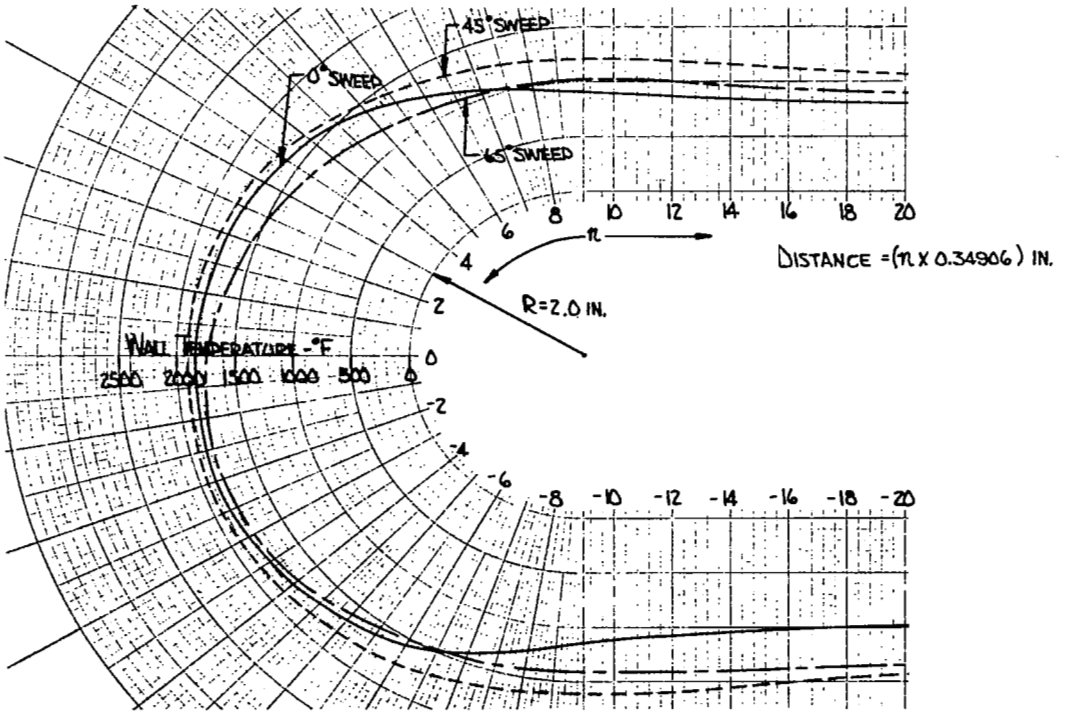

Figure 22. Radiation Equilibrium Wall Temperatures on the Leading Edge for 2.0 in.,[1] M = 6.0, α = 10.31°, Altitude = 100,000 ft

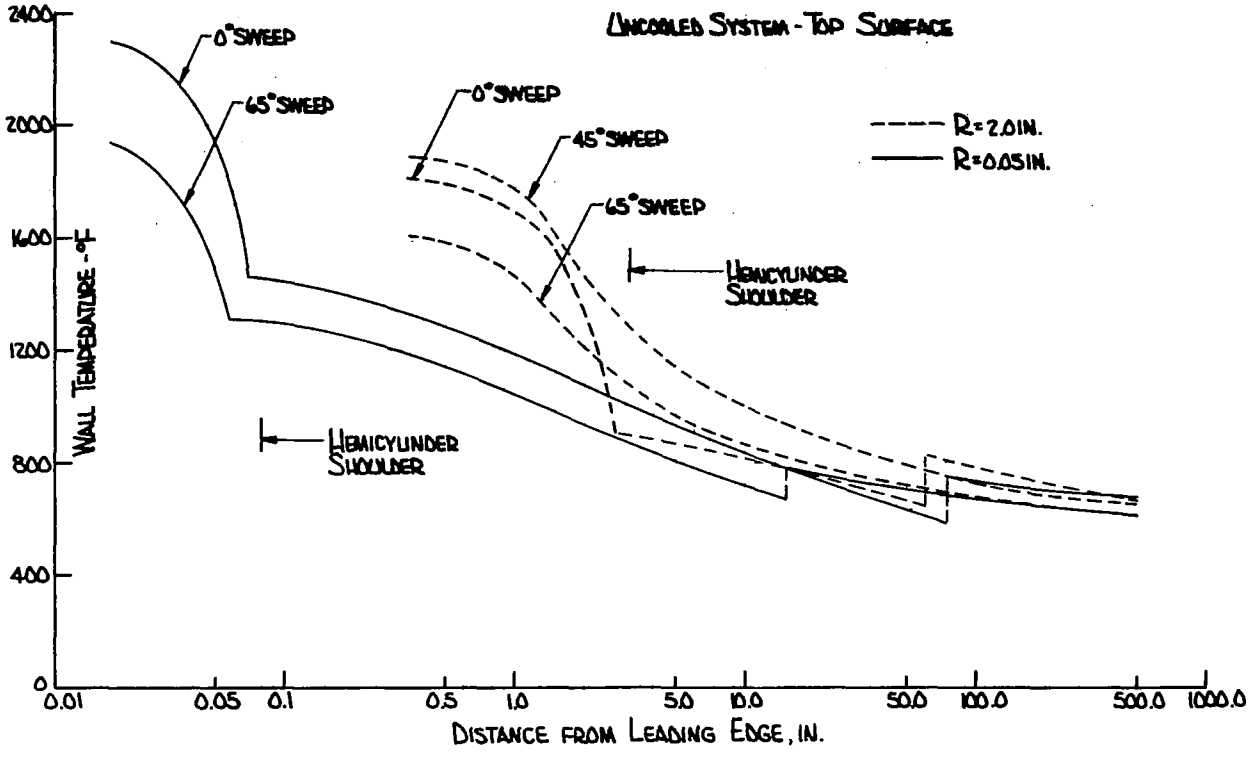

Figure 23. Radiation Equilibrium Wall Temperatures on the Top Surface, M = 6.0, α = 10.31°, Altitude = 100,000 ft

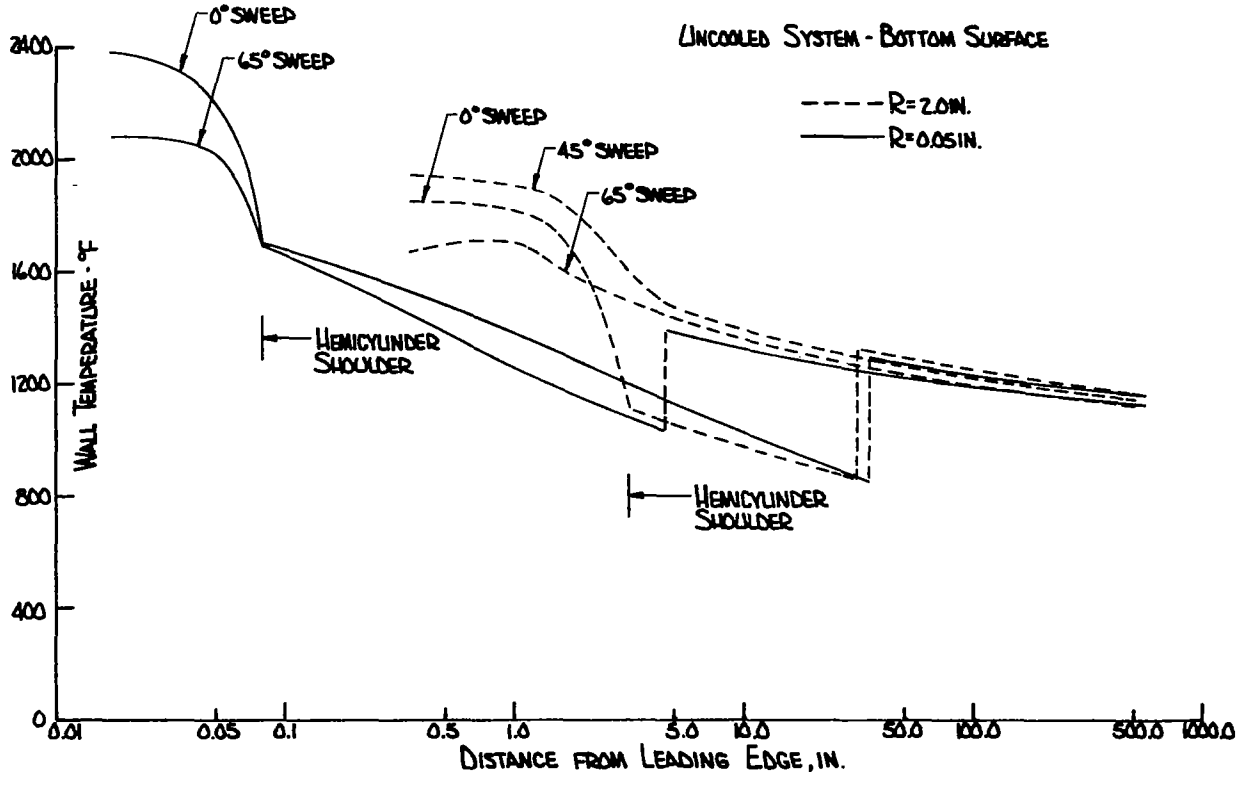

Figure 24. Radiation Equilibrium Wall Temperatures on the Bottom Surface, M = 6.0, α = 10.31°, Altitude = 100,000 ft

for the two leading edge radii it is noticed that beyond 50.0 inches top surface temperatures are between about 600°F and 800°F. For the 0.05 inch radius, laminar flow exists on the leading edge and for the first 10.0 inches on the flat plate. Between 10.0 and 100.0 inches a transition to turbulent flow occurs with the vertical line indicating the onset of transition. The 2.0 inch leading edge is laminar only for 0° sweep and it is only for this sweep that the transition to turbulent flow is noticed at 60.0 inches aft of the leading edge. For sweep angles 45° or greater both the leading edge and flat regions are in turbulent flow. An interesting result of this turbulent leading edge is the higher temperatures for 45° sweep when compared to 0° sweep in the first 60.0 inches.

The bottom surface shows many of the trends evident on the top surface. As shown in Figure 24 the laminar to turbulent transition is evident for the 0.05 inch leading edge radius. A movement of this transition point forward on the wing is also evident as sweep angle is increased. Beyond 40.0 inches, temperatures on the flat surfaces are clustered about 1200°F. Temperatures for the 45° sweep case, 2.0 inch radius, are again above those for the 0° sweep, 2.0 inch radius case in the first 30.0 inches. Comparing Figures 23 and 24 a forward movement of all transition points is evident on the bottom surface. Because of the higher pressures on the bottom surface the critical Reynolds number is reached at a point nearer the leading edge.

E. LIFT AND DRAG COEFFICIENTS

Lift and drag coefficients generated for dry uncooled wings are presented in Figures 25 and 26. Lift coefficients are a result of an integration of the pressure and friction forces in a direction perpendicular to the free stream velocity vector while drag coefficients result from an integration of the pressure and friction forces parallel to the free stream velocity vector. Both the lift and drag coefficients are based on free stream density and velocity and referenced to the wing planform area of 6954 ft^2. Therefore,

$$\begin{pmatrix} \text{Lift} \\ \text{or} \\ \text{Drag} \end{pmatrix} = \left(\frac{1}{2} \rho_\infty S V_\infty^2 \right) \begin{pmatrix} C_L \\ \text{or} \\ C_D \end{pmatrix}$$

For both radii lift and drag coefficients decrease with increasing sweep angle with greater percentage changes in drag than in lift. Results for the two radii show an increase in lift and drag as leading edge radius is increased. Figure 26 shows the effect of radius and sweep on the lift to drag ratio. This ratio increases with increasing sweep angle and decreases with increasing leading edge radius. Dashed lines on Figures 25 and 26 indicate a discontinuity in the data between 65° and 75° sweep. As mentioned previously the wing span was reduced for the 75° sweep case and this effect is seen in the lift and drag data. The effect of transpiration cooling on lift and drag coefficients is discussed in Section 6.

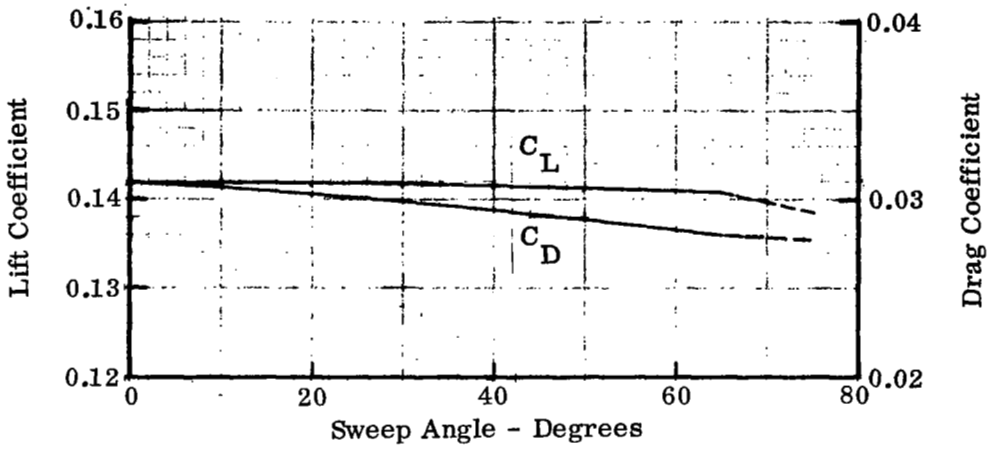

Figure 25. Lift and Drag Coefficients for a 0.05 in. Leading Edge

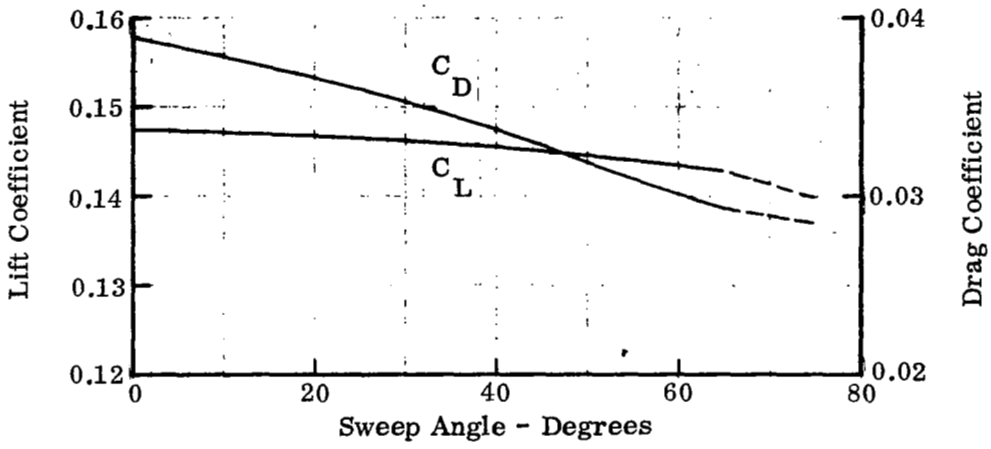

Figure 26. Lift and Drag Coefficients for a 2.0 in. Leading Edge

SECTION 4

IDENTIFICATION OF COOLING SYSTEMS

Extensive past experience with active cooling of hypersonic aircraft indicated the desirability of examining a large number of cooling system - coolant combinations which might be used for the particular application to allow selection of a small number of promising systems for detailed studies. While the most efficient coolants can be selected easily on the basis of total heat capacity, these do not necessarily result in the optimum cooled structural system. The design of cooled structures involves many considerations in addition to the coolant heat capicity, such as, operating temperature levels, structural cooling system weight, weight and volume requirements for the coolant storage tank, distribution system weight and location, pump or pressurization system weight, power source if a pump is used, controls, redundancy for high reliability, possible intermediate heat exchange loops, and heat exchange surfaces. Design of the surface being cooled is strongly influenced by the peak incident heat flux; coolant requirements by the integrated heat load-time parameters; and cooling system sizing by the peak heat load. Since the functional relationships vary for different systems and coolants it is necessary to study various combinations with respect to the particular application of interest in order to define not only the cooling system details but also the influence on overall structural weight.

Representative systems and coolants are discussed in this section. In general, the active cooling systems of interest can be classified as either transpiration and film cooling systems or convective cooling systems. In this section transpiration and film cooling concepts are discussed followed by a discussion of coolants and coolant selection. Convective cooling concepts are then discussed by classification of convective cooling systems into direct and indirect systems. Following this discussion of convective cooling concepts coolants are selected for the concepts of interest. Based on the semi-quantitative comparisons in this section promising cooling system-coolant combinations were selected for further study.

A. TRANSPIRATION AND FILM COOLING SYSTEMS

A surface exposed to an external flow of hot gases can be effectively cooled by exuding a fluid through the surface into the hot gas stream. In transpiration cooling the coolant is forced through a porous media with pore sizing so small that the coolant issues forth as a continuous mass and not in individual jets. For film cooling the coolant is forced through a discrete number of slots or holes and the flow pattern is that of a large number of individual jets. For both transpiration and film cooling the coolant both absorbs heat and changes the distribution of temperature in the boundary layer in such a way that the rate of heat transfer to the surface is altered. The coolant may be solid, liquid, or gaseous material and it may either be inert or chemically active.

In the simplest sense transpiration is reserved for the case of a gaseous coolant having essentially the same properties as the gas flowing in the external hot stream. Transpiration in this restricted sense has been studied extensively, both theoretically and experimentally. In addition, other systems have been examined in which light and heavy gases and liquid water have been injected into the hot gas stream. Very little experimental work has been done with chemically active systems, although some theoretical treatment has been accomplished. A review of transpiration and film cooling theorectical and experimental work is given in Reference 12.

While transpiration and film cooling have been shown to provide considerable promise as high intensity cooling systems, the major problem remains the practical difficulty of fabricating a satisfactory porous or perforated surface structure. Surfaces with continuous porosity are desirable for transpiration systems, but material strength is usually reduced as porosity is increased. If properly accomplished, film cooling may permit simplifications in component structure and plumbing which could offset the increased coolant weight requirement as compared to transpiration cooling. Concepts applicable to transpiration cooling are basically suitable for film cooling if the porous media is replaced by a perforated media. Experience with rocket engine film cooling has indicated the superiority of gaseous coolants over liquids because of flow distribution considerations. A prime requirement is the ability to provide many small discrete outlets. Extensive rocket engine injector development provides the ability to produce controlled hole diameters as small as 3 mils, which, when coupled with available integral tube sheet technology, offers promise of producing the type of structural skin required for efficient film cooling. Since the strength of perforated sheet is much higher than for porous sheet, the structural weight for a film cooled structure might be lighter than that of a transpiration cooled structure.

1. Transpiration and Film Cooling Concepts

Schematic diagrams of typical transpiration or film cooling systems are presented in Figures 27 and 28. The system shown in Figure 27 uses a stored coolant which may be either liquid or gaseous. Figure 28 presents a schematic of a system employing ram air as the coolant. Both figures show possible locations for flowmeters, valves, and filters in relation to the major system components. A recirculating arrangement, illustrated by dashed lines, can minimize the depth of the plenum chamber needed to distribute the transpirant, but at the expense of more complicated plumbing including return lines and a venturi (aspirator). Flow control may also be achieved by means of internal baffling, different supply pressures to each plenum chamber and variable pressure drop through the porous media.

A variety of concepts for transpiration or film cooling of leading edges and wing surfaces are shown in Figures 29 and 30. The defining features of each concept are presented on the figures. The major consideration in all cases is the attainment of a prescribed distribution of the injected fluid consistent with the external heat flux distribution. Unless the local rate of injection is matched to coolant requirements significant weight penalities result. The leading edge and wing surfaces would probably employ sheets of material with different porosities in different regions.

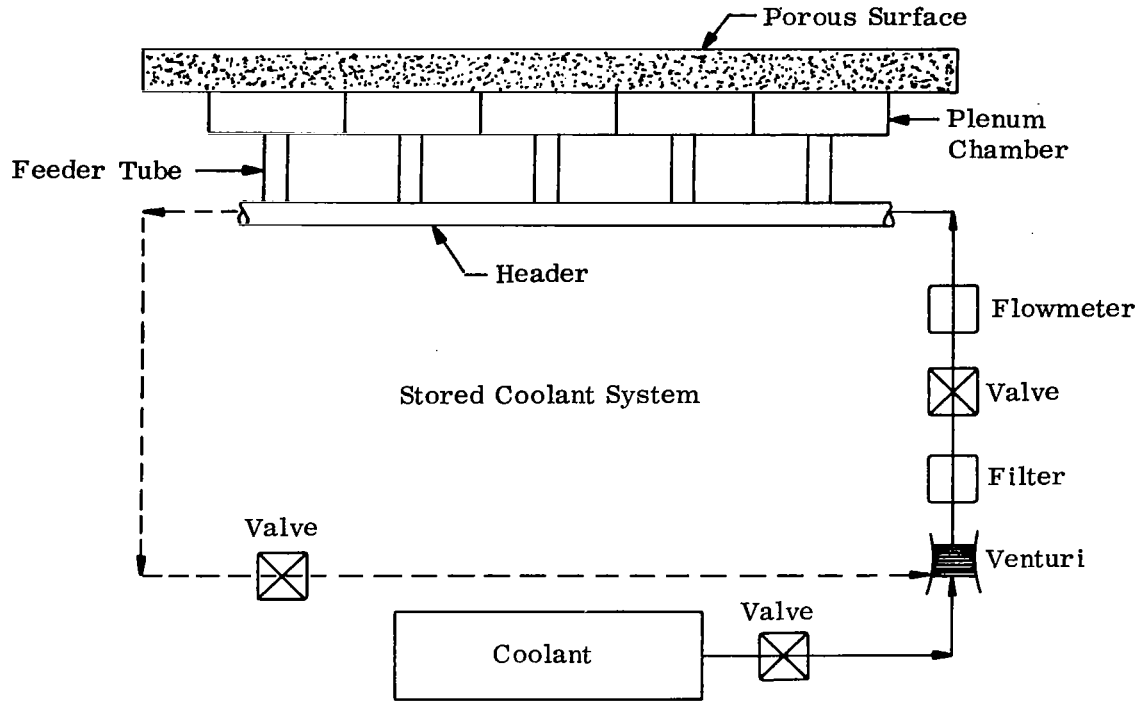

Figure 27. Schematic of Typical Transpiration or Film Cooling Systems Using a Stored Coolant

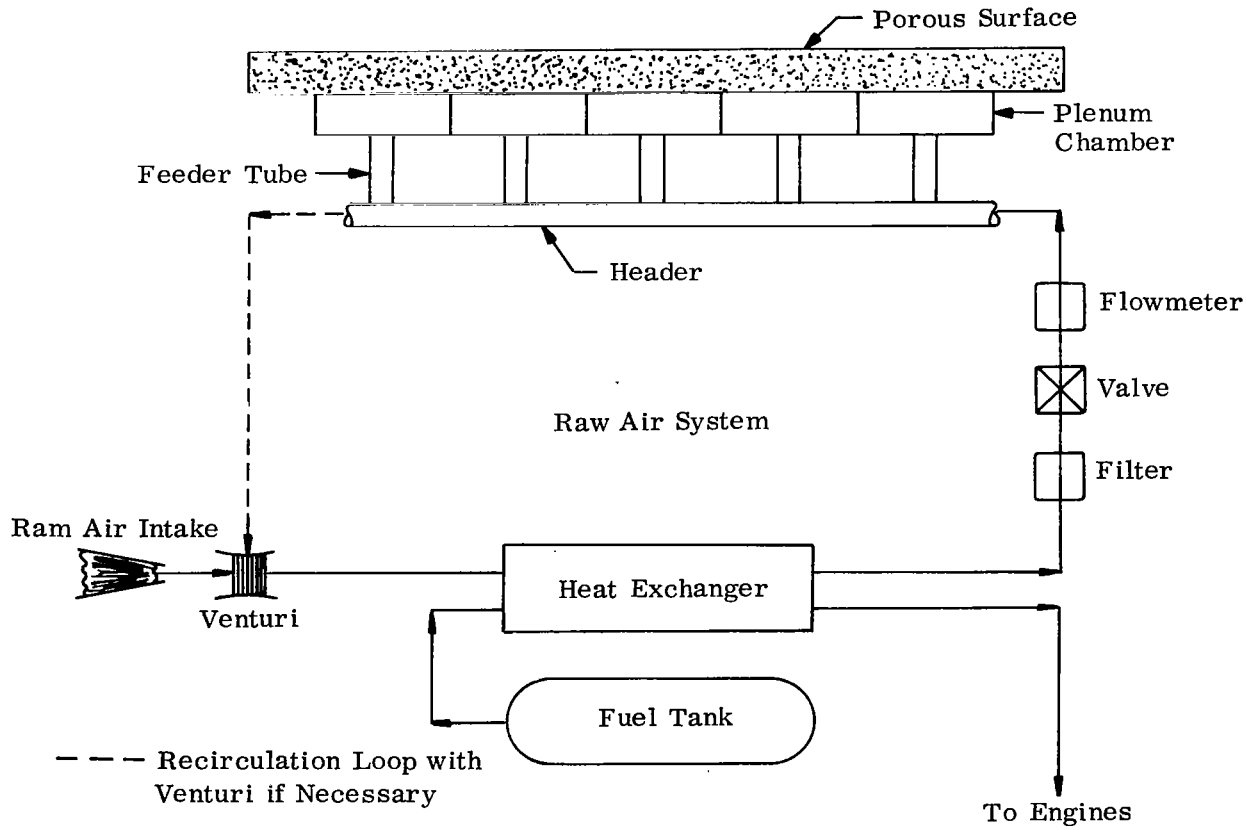

Figure 28. Schematics of Typical Transpiration or Film Cooling Systems, Using Ram Air Coolant

A

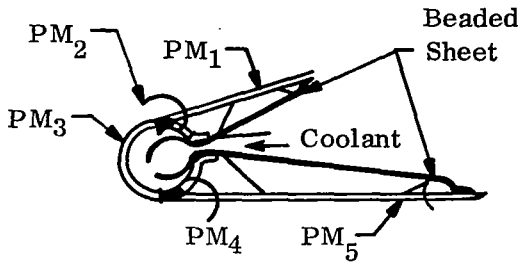

Coolant is supplied through a single set of ports into the leading edge cavity region and flows through porous material to the external boundary layer and into plenum chambers on the upper and lower surfaces. The porous material between the leading edge region and the surface plenum chambers has a tailored pressure drop such that the flow rates are properly balanced.

B

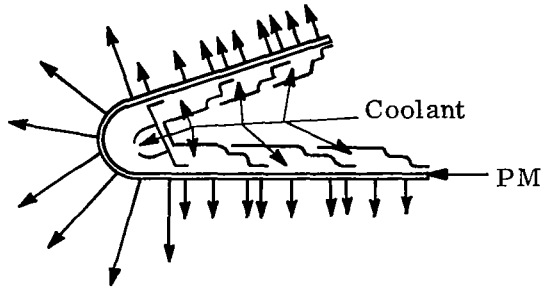

Porous material or slots of fixed size are used and plenum chambers of various sizes distribute the coolant.

C

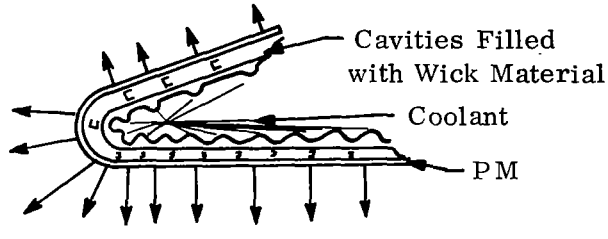

Coolant is supplied through discrete holes in integrally tubed sheet into plenum chambers from which it is distributed into the boundary layer through a porous material or slots. Wick material may be used in the pelnum chambers as an aide in distributing the coolant. Flow may be controlled by proper selection of the porous media, plenum chamber geometry, and coolant line sizing and hole sizing in the beaded sheet.

D

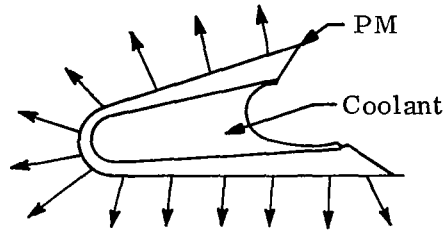

Porous material or slots distribute coolant delivered to a plenum chamber by varying porous material thickness or slot size.

Figure 29. Transpiration or Film Cooling Concepts for the Leading Edge

A

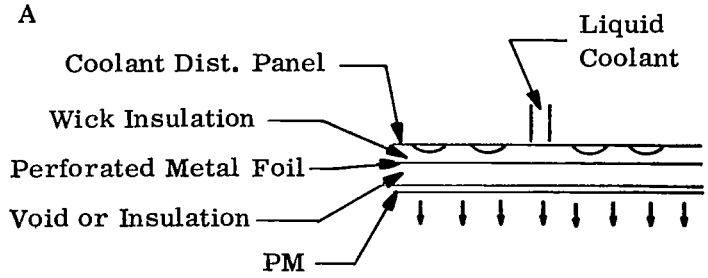

Coolant is distributed by wick held in place by perforated metal foil.

Coolant boils, fills void or insulation with gas which passes through porous material or slots.

B

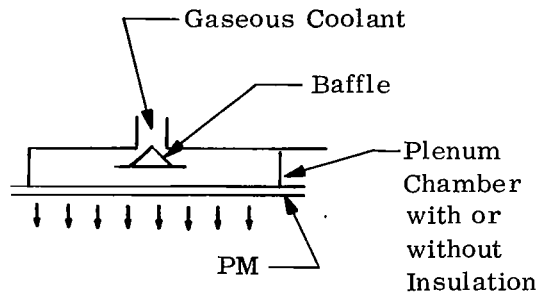

Coolant is distributed by baffle and plenum chamber. Insulation could be used to reduce coolant requirements, flow is controlled by porosity or slot size.

C

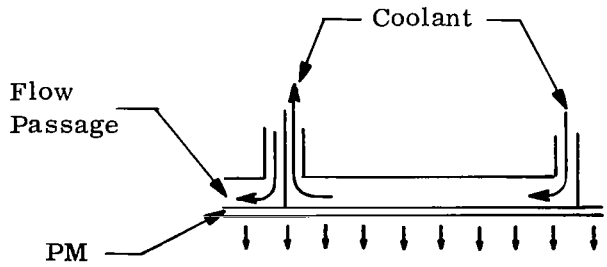

Coolant is circulated by pump and flow rate overboard is controlled by porosity or slot sizing.

Figure 30. Transpiration or Film Cooling Concepts for Wing Surfaces

2. Coolant Selection

Coolants available for use in transpiration or film cooling systems can be classified as either gases or liquids based on their state when they are delivered to the area to be cooled. No matter which type of coolant is chosen, the problems of time-wise and spatial distribution, nonclogging of the porous surface, and reasonable strength of the surface for reasonable weight, continue to be the major practical problem with transpiration systems; the precision of supply in relation to demand is the key to attainment of an efficient system.

A gaseous coolant has one major advantage over a liquid coolant in a transpiration system in that experience has shown that the gaseous coolants are less likely to clog the pores of porous surface material. A major disadvantage of a gaseous system, however, is the large volume, with its resulting large weight, required to store the gas. The primary considerations for the selection of a gas to be used in a transpiration or film cooling system are a high specific heat and a low storage weight. When a comparison is made on this basis hydrogen is by far the best gaseous coolant with helium, nitrogen and air following in descending order of cooling efficiency. Nitrogen and air are very close in this type of comparison and the availability and lower cost of obtaining air might rule out the use of nitrogen. For this study hydrogen, helium, and air were considered the potential coolants for gaseous transpiration or film cooling. The problem of coolant storage is considerably simplified when a liquid is used. For this aircraft application the coolants considered applicable for liquid-vapor transpiration or film cooling are liquid hydrogen, liquid helium and water. Studies using hydrogen, helium, and water allowed system selection studies to be carried out and system applicability to be determined. Before proceeding to more specific discussion it is worth noting that, according to present very limited theories, efficiency of the transpiration or film cooling process is not affected by the time (or location) of the coolant's phase change from liquid to vapor, as long as the location of the phase change is chosen properly so as to cool the surface in question.

B. CONVECTIVE COOLING SYSTEMS

The term "convective cooling" indentified cooling methods which are based on the removal of heat from a wall by a moving fluid which absorbs heat either through a phase change or through a sensible temperature rise. Cooling systems may be classified as direct and indirect types. Direct systems are those which pass the expendable coolant directly through the surface to be cooled. Indirect systems employ one or more intermediate heat transport loops between the item being cooled and the ultimate heat sink.

1. Convective Cooling Concepts

Figure 31 illustrates three direct cooling concepts. The water wall approach, Sketch A, accomplishes cooling by the evaporation of water stored directly in contact with the surface to be kept cool. The water may be in a jellied form or contained within a wick material. As heat penetrates the structure, the water is vaporized and exhausted. A vapor barrier is required if saturation of the insulation by the water vapor is to be avoided. The advantages of this system are simplicity and very small in-plane temperature gradients. Disadvantages, however, appear to outweight the advantages. For both variations

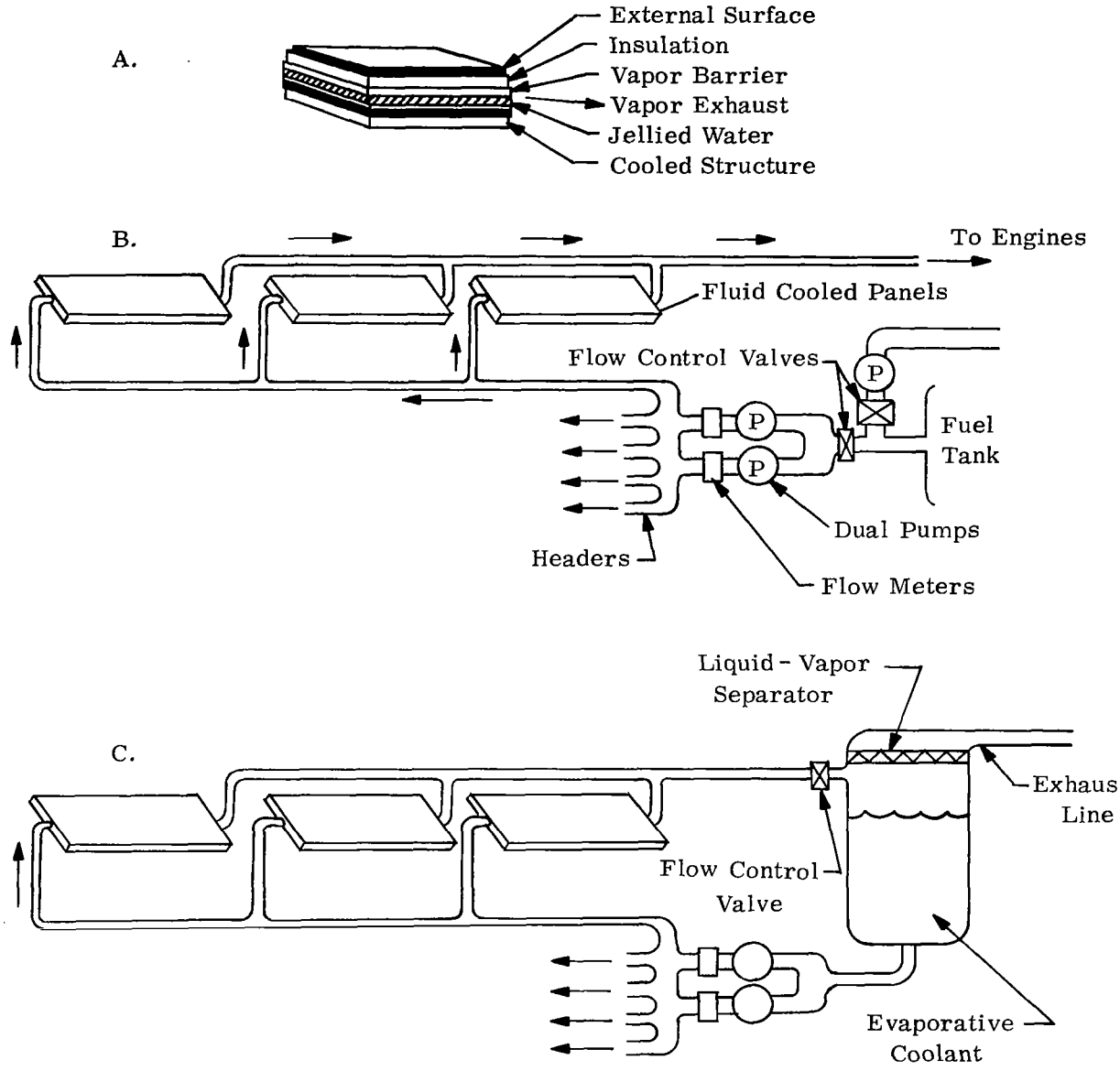

Figure 31. Schematics of Direct Cooling Systems

of this concept thorough knowledge of the internal heat flow distribution is required so that coolant can be properly distributed and local dry-out avoided. Refurbishment of a water-wick system may be accomplished simply by recharging, but for the prepackaged jellied water concept, refurbishment requires removal of much of the external structure. Another major disadvantage of wick systems is their sensitivity to gravitational forces. Experiments with various wick materials have indicated that capillary action will draw water only about two inches above an inlet when the wick is in a vertical position and acted on by a force of 1 g. It is also extremely difficult to avoid runoff on vertical surfaces when wicks are used. Gelling agents added to the water charged into a wick system will eliminate runoff problems, but at the expense of decreased capillary action and increased refurbishment problems.

A second type of direct cooling system is illustrated in Sketch B of Figure 31. Here it is assumed that fuel is used for cooling the structural panels. Beginning at the fuel tank, a portion of the fuel flow is diverted to the cooling system where dual pumps are used to maximize reliability. Under normal conditions, buth pumps would operate at reduced capacity, thereby prolonging their life and minimized maintenance. Failure of either pump would be detected by the flowmeter and manual or automatic control of the other pump could increase its delivery rate to the total required. After leaving the pumps, the coolant would be distributed to manifolds, to feeder lines and, hence to the cooled structure. After absorbing heat in the panels, the coolant would flow to the propulsion system. An obvious advantage of this approach is the fact that there is no weight penalty attributable to the coolant fluid. Disadvantages include the relatively low heat absorbing capability of most fuels, with the exception of hydrogen, and the potentially dangerous situation which could result from leakage of the fuel since the cooled panels would cover a large portion of the vehicle surface. In addition, the total coolant requirement can well exceed the propulsion system requirement for hypersonic vehicles. In such cases, it may be desirable to use an expendable coolant other than fuel for absorbing heat from the cooled panels, and/or to insulate the actively cooled panels from the hot boundary layer.

A direct cooling system employing an evaporative coolant is illustrated in Sketch C, of Figure 31. Coolant from a reservoir is pumped through the cooled panels in much the same manner as was done for the nonevaporative coolant. The upper portion of the reservoir is used as a flash chamber for the hot coolant leaving the panels. A flow control valve is provided just prior to the flash chamber in order to maintain sufficient pressure in the lines to avoid two-phase flow. A liquid-vapor separator is provided between the flash chamber and the exhaust line to minimize liquid carryover. During previous studies flash boiling experiments with sodium indicated that liquid carry over could be limited to about 5% of exhausted vapor flow by using a simple wire mesh liquid-vapor separator. The major disadvantage of this cooling system concept is cavitation in the pumps. Since the coolant reservoir is vented to the atmosphere, the net positive suction head on the pump is essentially the head of the coolant in the reservoir when the vehicle is flying at high altitudes. Near the end of flight, this goes to practically zero, and even when the reservoir is full the head may be quite small.

For this study, the applicable cooling systems are those shown in Sketches B and C, of Figure 31. In general, for such systems the applicable coolants are those with the largest heat capacity within a band of acceptable operating temperature. Considerations of vapor pressure, density, storage temperature, chemical reactivity, safety

and handling are important in the detailed design of the cooling system and influence weight, but they are generally of secondary importance in making selections based upon minimum weight.

With either of the direct convective systems considered applicable, high internal heat transfer coefficients could be realized if boiling is permitted within the coolant passages. Such two phase flow systems were rejected, however, because heat transfer characteristics are difficult to control. These difficulties are associated with the large volume changes which occur as vapor is formed and an uncertainty that the passage walls are entirely wet with liquid. Since the boiling phenomenon, results in very high rates of heat transfer a spray concept may be considered since it eliminates the questionable aspects of two-phase flow as well as pumps and heat exchangers. Figure 32 illustrates a spray cooled nose cap or leading edge. Coolant is forced from a reservoir by gas pressure, is atomized by a spray nozzle, and strikes the heated structure. After vaporization the coolant leaves through an exhaust line and then is either condensed or rejected from the vehicle. Because of the velocity of the droplets in the coolant spray, liquid contacts the heated structure and despite vapor generation a wet wall is assured. Deceleration of the droplets which impact on the hot wall provides heat transfer and vapor separation characteristics which are superior to pool boiling.

Feasibility of the spray cooling concept was demonstrated at Bell Aerosystems using a water spray to cool a flat faced nose cap structure which was subjected to heat fluxes of up to 60 Btu/ft^2-sec. A design such as the one shown in Figure 32 was built and tested under a contract for study of a lithium spray cooling structural concept, Reference 13, which demonstrated the feasibility of lithium spray cooling. Lithium was vaporized in a closed container and three coated columbium alloy nose cap models were cooled using a fine mist spray. System internal pressure was varied to permit vaporization of the lithium droplets at temperatures between 1500°F and 1700°F. External surface temperatures were held below 2200°F by the spray cooling under heat fluxes of up to 610 Btu/ft^2 - sec, corresponding to a radiation equilibrium temperature without cooling of 5800°F. Although instrumentation difficulties precluded experimental determination of the maximum heat flux capability, a conservative analytical extrapolation of test results indicated the limit to be at least 1200 Btu/ft^2 - sec. In addition to its high heat flux capability, the heat capacity of lithium, about 10,000 Btu/lb, as compared to water, about 1000 Btu/lb, greatly reduces coolant weight and storage volume requirements. This advantage is gained at the expense of a higher operating temperature of about 1700°F for lithium as compared to about 200°F for water.

A number of indirect convective cooling system concepts are illustrated in Figure 33. In general, indirect systems offer greater flexibility than direct systems with regard to choice of coolants, operating temperature levels, and insensitivity to gravitational effects. The simplest form of indirect cooling system is illustrated in Sketch A of Figure 33. A closed heat transport loop transfers heat from the panels to be cooled to the heat exchangers. In addition to containing the transport fluid, the closed loop would also contain a pump for circulating the transport fluid, a flowmeter, and an expansion tank which would contain a quantity of transport fluid for makeup purposes should minor leakage occur. Heat absorbed from the panels may be rejected to an expendable coolant or to the fuel. If an expendable coolant is used, a pressurized reservoir may be adequate for supply purposes.

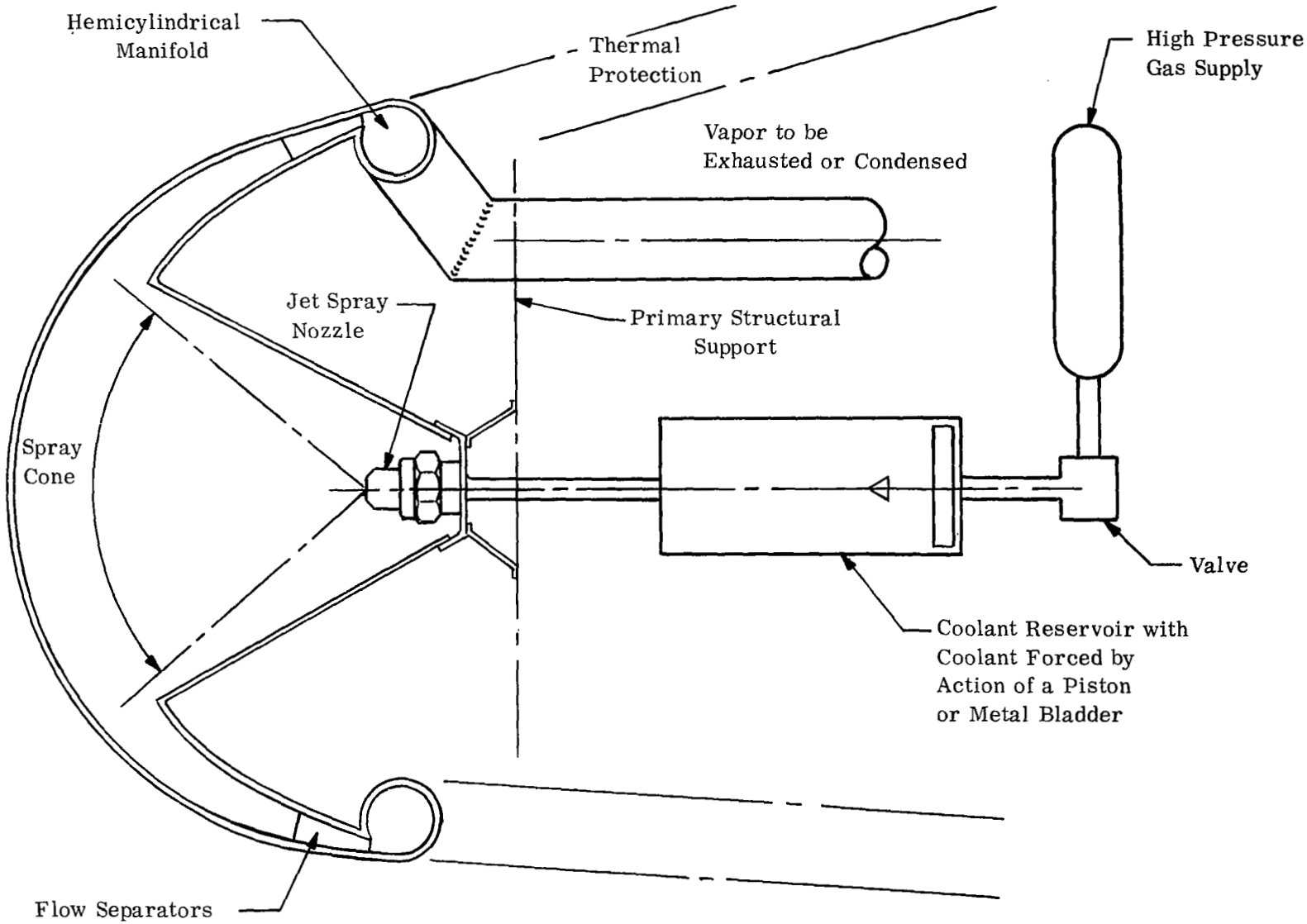

Figure 32. Typical Design for a Water or Lithium Spray Cooled Leading Edge

The use of fuel might require a pump so that there is sufficient pressure in the exhaust line from the heat exchanger to deliver the fuel to the propulsion system. In any case, a flow control valve would be contained between the reservoir for the heat sink coolant and the heat exchanger.

If a heat sink other than hydrogen fuel is used,the temperature drop in the transport fluid may not be adequate to maintain the desired structural temperature. For example, water might be chosen as a heat sink because of its high heat of vaporization. However, difficulties are encountered if one attempts to boil large quantities of water at low temperatures. To decrease the temperature of the transport fluid an axuiliary coolant and a second heat exchanger might be employed as illustrated in Sketch B, of Figure 33. Ammonia is a particularly attractive auxiliary coolant.

Another technique for reducing the temperature of the transport fluid would be to introduce a refrigeration cycle, as shown schematically in Sketch C of Figure 33. After being compressed, the refrigerant would be cooled by the same coolant used to absorb the major portion of heat from the transport fluid. Expansion of the refrigerant through a turbine would reduce its temperature and thereby provide auxiliary cooling of the refrigerant. Because of the relative inefficiency of a refrigeration cycle, as compared to direct heat rejection through a single heat exchanger, it is preferable to remove most of the heat from the transport fluid by rejecting it directly to the heat sink. This reduces the size of the refrigeration cycle equipment and hence the weight penalty associated with auxiliary machinery.

Heat transport loops of minimum weight and maximum efficiency would use liquid transport fluids. If the heat sink is hydrogen fuel, freezing problems might be encountered. One way to avoid such problems is to introduce an intermediate loop between the primary heat transport loop and the heat sink. An arrangement of this type is shown in Sketch D of Figure 33. The ideal fluid for the intermediate loop would be helium because of its good heat transfer characteristics and high safety, as compared to other gases. Such a transport loop would contain a blower for circulating the helium.

Since the heat capacity of hydrogen depends primarily upon sensible temperature rise, an intermediate refrigeration cycle might provide advantages over the circulatory intermediate loop. With the refrigeration cycle, Sketch E, it would be possible to raise the temperature of the refrigerant and thereby increase the outlet temperature of the hydrogen coolant. This would reduce the quantity of hydrogen required for cooling purposes. A tradeoff study is necessary to determine the weight trends of the refrigeration cycle as its compression ratio is increased as compared to the decrease in coolant requirement.

Studies have been conducted in past years (i.e., Reference 14) which have demonstrated the effectiveness of liquid metals for cooling the most highly heated portions of hypersonic airframe structures. Extensive analysis and design work has been carried out using sodium, potassium, Nak, lithium, and lithium hydride. These studies led to the complete design of a liquid metal cooling system for the nose and leading edges of a typical reentry vehicle. Tests of this system are described in Reference 14. A maximum circulating coolant temperature of 1632°F was reached during the course of the test program. In the test loop Nak served as the heat transport fluid, while sodium was used as the

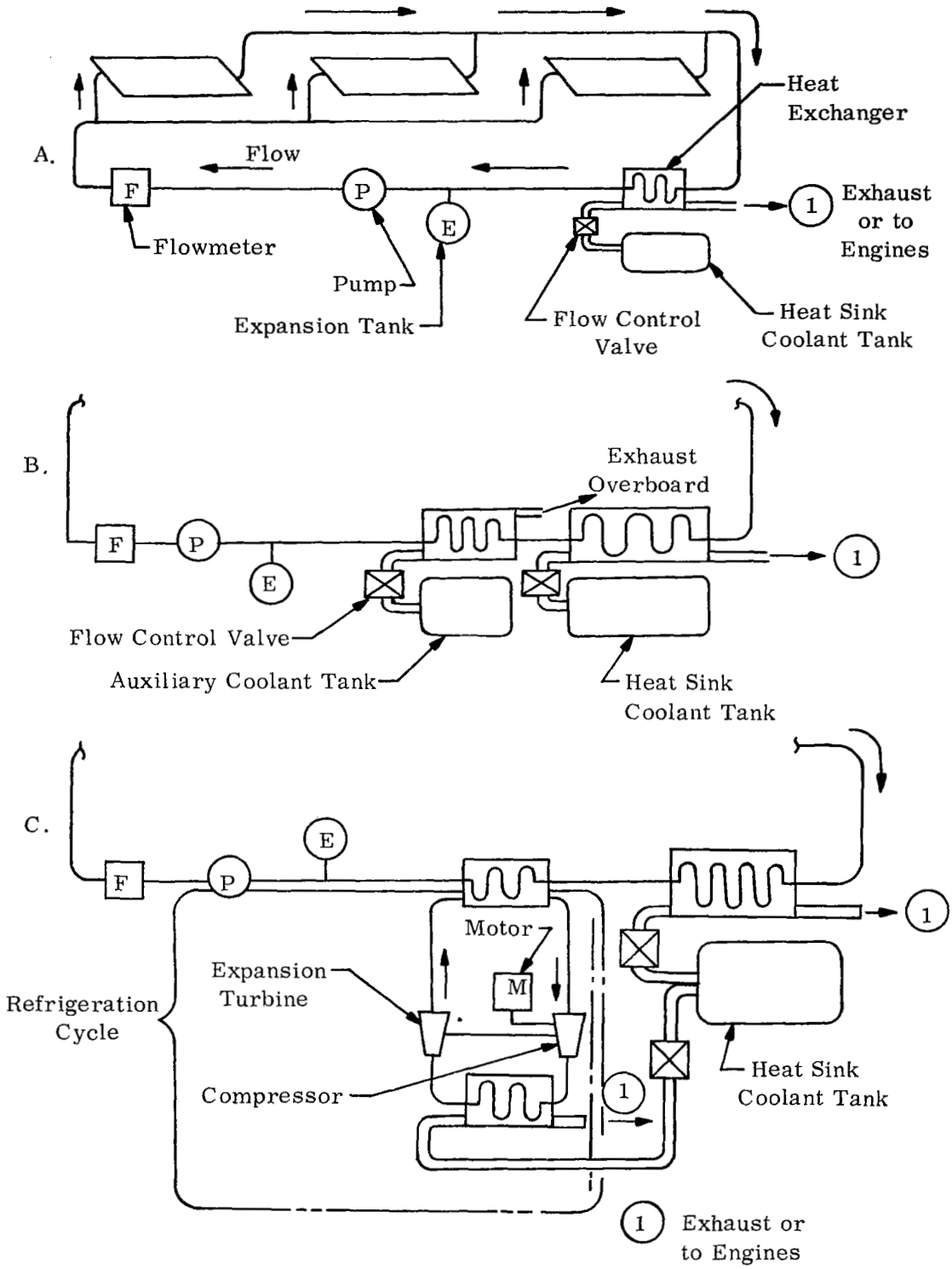

Figure 33. Schematics of Indirect Cooling Systems

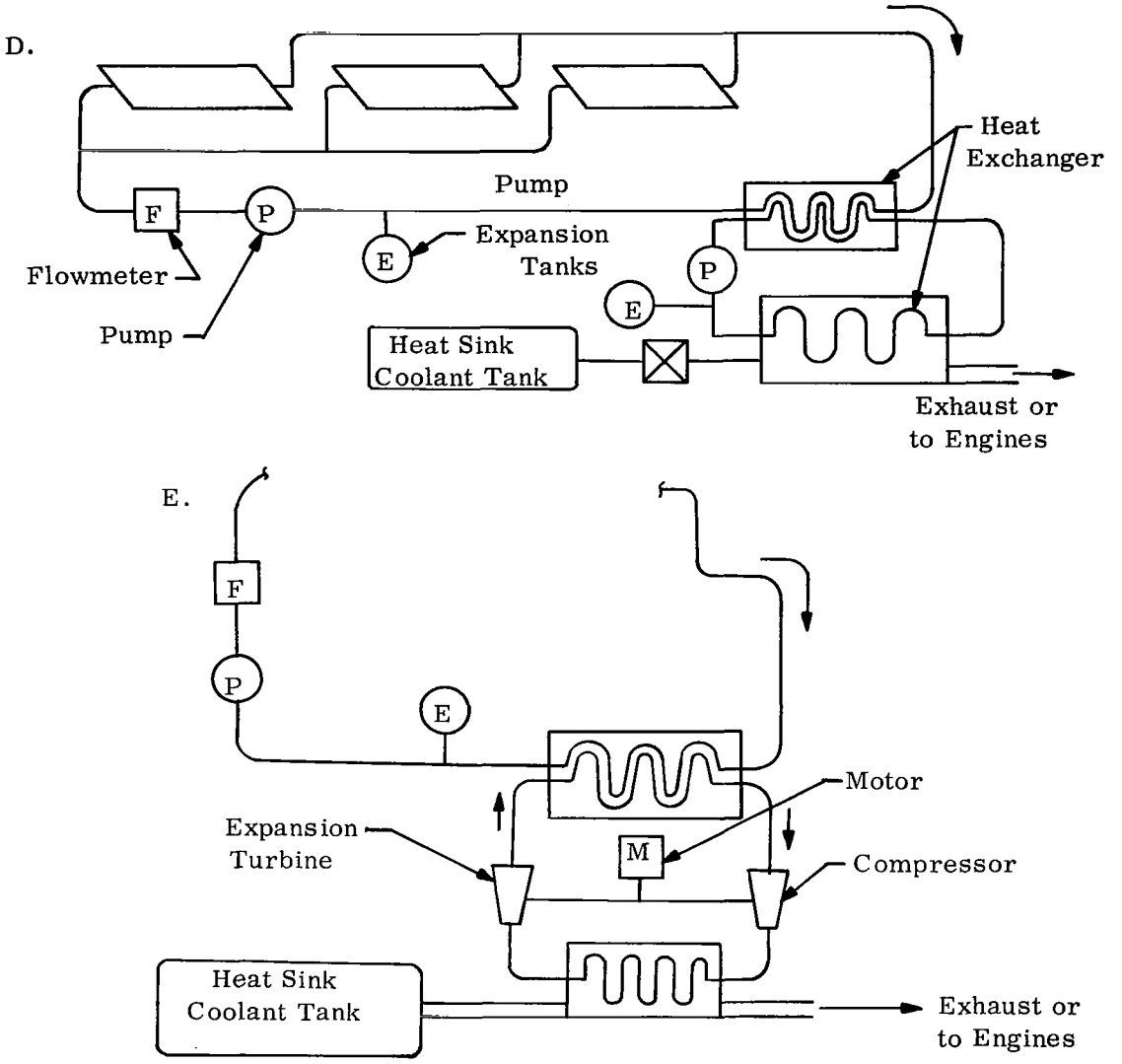

Figure 33. (Cont)

evaporative coolant. A total of 284 hours of operating time were accumulated with this closed cycle system, 71 hours of which were above 1300°F.

Convective cooling by means of gases, such as hydrogen, stored as liquids has been studied extensively and is being successfully practiced in rocket engine thrust chambers. Rocket nozzle cooling is done with the materials at hand, i.e., one of the propellants, chosen for reasons other than cooling capability. For a gas the limitation to the rate of heat transfer is the ability of the structural wall to withstand the high temperature at high heat flux rates resulting from low heat transfer coefficients. Heat transfer coefficients will be maximized by choosing hydrogen as the gaseous coolant, but the best attainable heat transfer coefficients in conjunction with the structural material properties will still limit the heat absorbing capability of the system.

Another indirect system worth mention is the radiative system. For a hypersonic wing the area on the top surface behind the maximum thickness line would be an ideal radiator surface because of the small aerodynamic heat load in this area predicted using conventional theories . Figure 34 shows a typical closed cycle radiative system employing a coolant loop which absorbs heat from the leading edge surface by means of a temperature rise and then rejects this heat from a shallow compartment of large surface area, in a cooler portion of the airframe, by means of radiation, (for example, the rear portion of the top wing surface). The radiative system is exceedingly simple, including only a pump, distribution lines, temperature controller, connectors, and a radiator, in addition to the heated surface itself, and it uses a familiar coolant, either a gas or a liquid for the heat transport fluid. No coolant is consumed as in the other systems described above, so that the radiative system becomes more and more effective as the total vehicle heat load increases. A temperature sensor which actuates the pump drive is the only control required. The inherent disadvantage of a radiative cooling system is the large surface area required for the rejection of the heat if a reasonable surface temperature is to be used for the radiator. For a cooled wing design, the rear upper surface offers the most attractive radiator location, but questions as to the real aerodynamic heat input (as influenced by flow separation, vorticity, etc.) to this region make radiator design, and hence overall system design, impossible at the present time.

2. Coolant Selection

Where cooling is the primary consideration, the choice of coolant is based on both the ability of the material to store heat, and the ability to transfer heat. The first depends primarily on heat capacity, the second on specific heat, viscosity, thermal conductivity and density.

The heat capacity of any particular coolant is the sum of the heat of fusion, the heat of vaporization, the sensible heat due to temperature rise of the solid and/or liquid phases, and the heat requirements of endothermic and exothermic chemical reactions. The relative importance of various components of heat capacity is a function of the particular coolant, but certain trends may be noted. In general, the heat of vaporization is much larger than the heat of fusion. The relative magnitude of the heat of vaporization and the sensible heat due to temperature rise also shows an approximate relationship for various classes of coolants. For materials which are gaseous at standard temperature and pressure conditions, heats of vaporization range from about 10 to 700 Btu/lb, while

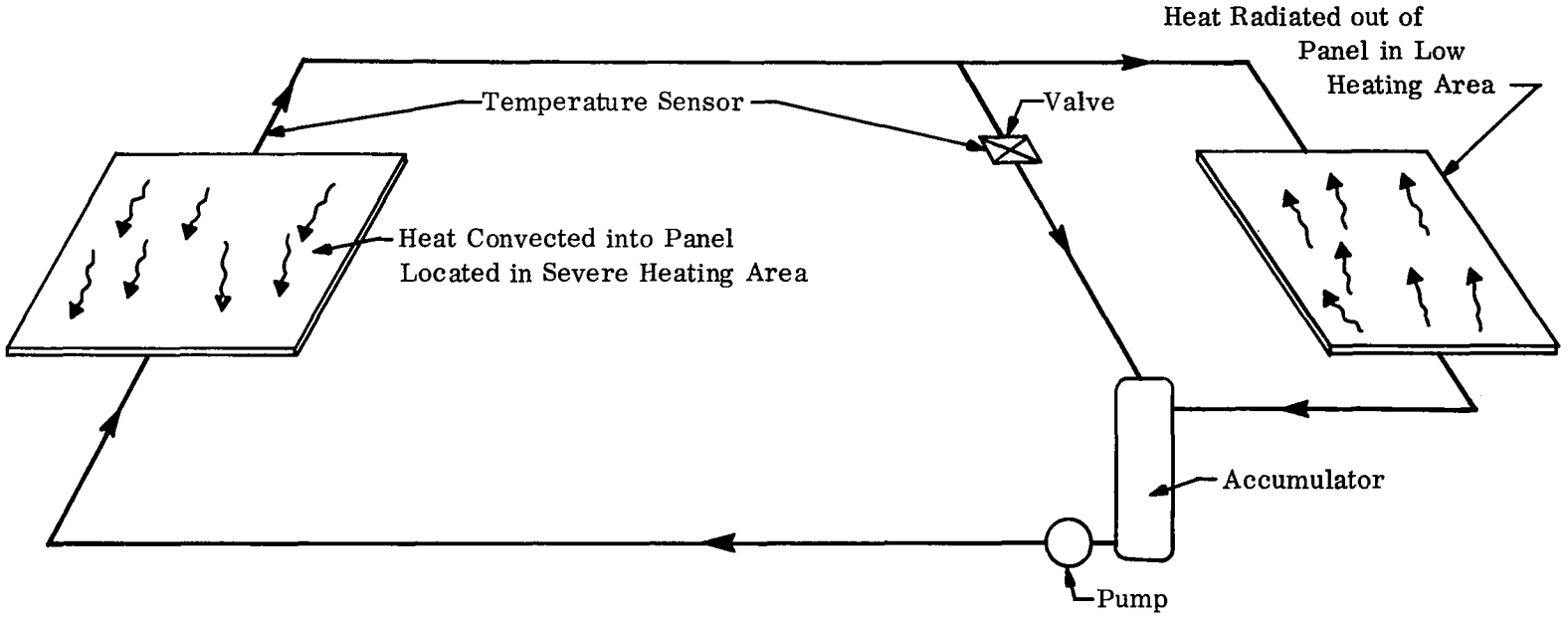

Figure 34. Schematic of a Closed Cycle Radiative System

specific heat values are generally above 1.0 Btu/lb°F. In this group,only hydrogen with its specific heat of approximately 3.5 Btu/lb°F, helium with its specific heat of 1.24 Btu/lb°F, and ammonia with its heat of vaporization of approximately 650 Btu/lb are potential candidates as expendable coolants. Among the more common fluids which are liquid at standard temperature and pressure, heats of vaporization range from about 100 to 1000 Btu/lb with specific heat values generally below 1.0 Btu/lb°F. In this particular category, water has no equal because of its high heat of vaporization of about 1000 Btu/lb and its specific heat, 1.0 Btu/lb°F.

When heat loads impose a need for very large heat capacities a number of exotic alternatives to the above mentioned coolants are available. If liquid metals are to be used, lithium and its compounds are the most practical choices because of their very large heat capacities. In addition, the evaporation of lithium, the decomposition of lithium hydride or lithium borohydride will yield a large capacity heat sink while other compounds are inferior.

These reactions can be taken further by boiling the residual lithium and thus substantially increasing the heat capacity. Lithium hydride has a potential heat absorbing capability of over 15,000 Btu/lb. Lithium borohydride has a somewhat smaller heat capacity, about 12,000 Btu/lb, but the initial reaction takes place at lower temperature. Recent studies sponsored by the Air Force, Reference 15, have shown the potential of endothermically decomposing fuels such as methyl cyclohexane. The sum of sensible, latent, and reaction heat capacities approach 2000 Btu/lb, an attractive heat sink capability. However, the reaction heat capacity (about 900 Btu/lb) is only obtainable at elevated temperatures, 600°F -1000°F. For any heat sink it is necessary to carefully consider the practicality of heat rejection at a high sink temperature. A summary of the high heat capacity coolants is given in Table II.

When the ability of a coolant to transfer heat is of primary concern then coolant specific heat, viscosity, thermal conductivity and density must be considered. A comparison of the fluids was made on the basis of a performance parameter which is the ratio of pumping power to heat transfer conductance. This parameter can be developed for either turbulent or laminar flow, Reference 16. In Figures 35 and 36, the turbulent and laminar performance parameters are given for four silicone fluids and an ethylene glycol solution, based on coolant property data obtained primarily from Reference 17. The ethylene glycol solution, a widely used heat transfer fluid, decomposes above 250°F. Since the more severe pumping requirements occur at the lower temperatures, these figures show the performance parameter between -65°F and +100°F. For the lower end of this temperature spectrum FC-75 has the lowest (most favorable) value of this parameter. At the upper end the 60-40 ethylene-glycol solution has the lowest value. The value of this performance parameter assumes considerable importance in system design since low values indicate low pump horsepowers and/or low heat exchanger weights. For the fluids examined, the ranking was approximately the same for either turbulent or laminar flow. Of the fluids which have acceptable operating temperature limits, FC-75 has the most favorable performance parameter. However, the vapor pressure approaches 150 psia at 400°F requiring a hermetic pressurized system. This would add unwarranted cost and complexity to system design. The fluid having the next best performance parameter was DC-331. This silicone base fluid is considerably less expensive than FC-75 and has better libricity.

TABLE II

HIGH HEAT CAPACITY COOLANTS

1. Gaseous at S.T.P.

   a. Hydrogen, C_p = 3.5 Btu/lb°R

   b. Helium, C_p = 1.24 Btu/lb°R

   c. Ammonia, heat of vaporization approximately 650 Btu/lb

2. Liquid at S.T.P.

   a. Water, C_p = 1.0 Btu/lb°R
      heat of vaporization approximately 1000 Btu/lb

3. Exotics

   a. Lithium, heat capacity approximately 10,000 Btu/lb

   b. Lithium Borohydride, heat capacity approximately 12,000 Btu/lb

   c. Lithium Hydride, heat capacity approximately 15,000 Btu/lb

   d. Methyl Cyclohexane, heat capacity approximately 2000 Btu/lb

1 Ethylene Glycol Solution 60-40
2 Dow Corning 331 Fluid
3 Coolanol 45 Monsanto
4 FC-75 3M
5 Oronite - 8200

Note: Dashed lines indicate areas where extrapolation of one or more fluid properties was necessary.

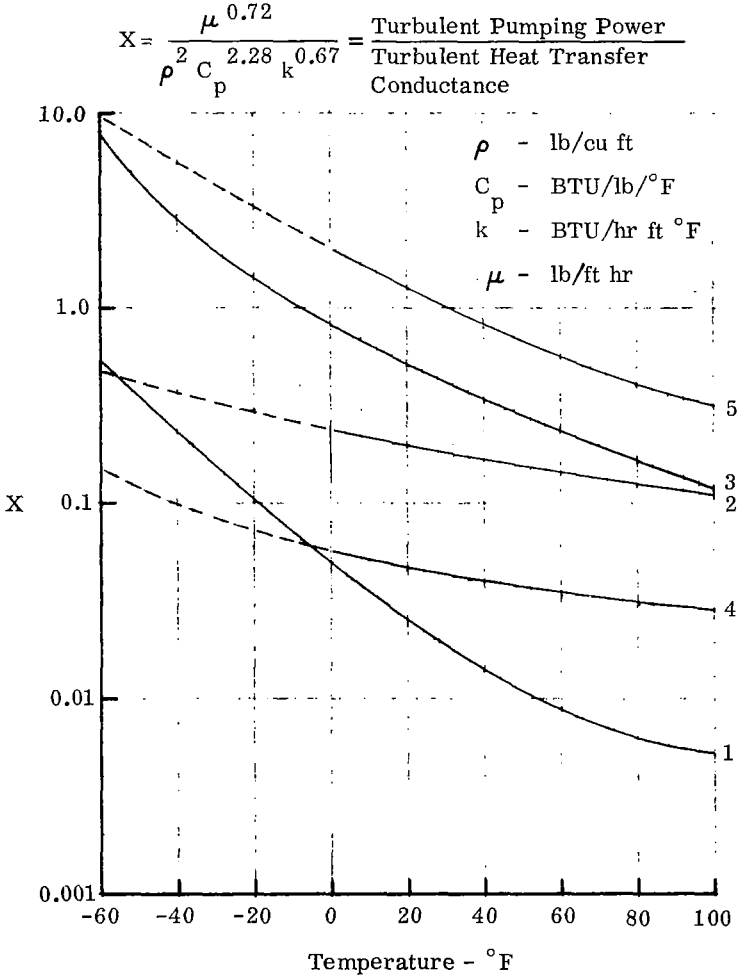

Figure 35. Comparison of Liquid Coolants Turbulent Flow Heat Transfer

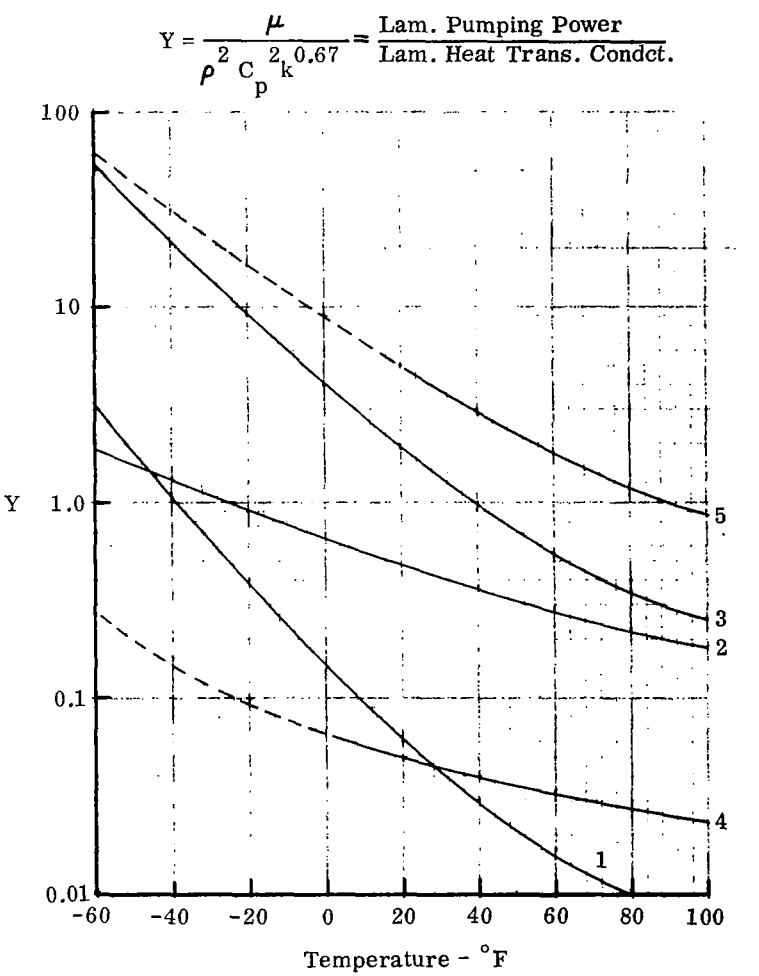

Figure 36. Comparison of Liquid Coolants Laminar Flow Heat Transfer

Based on these considerations, DC-331 was chosen as the best silicone heat transfer fluid. Properties data for DC-331 are given in Figures 37 and 38. DC-331, according to manufacturer's information, has excellent thermal stability up to 480°F in a closed system. However, incipient thermal instability just above 400°F has been indicated in other tests which also yielded viscosity determinations approximately 40 percent higher than the nominal values given by the manufacturer.

Along with a requirement for a favorable value of the above performance parameter other requirements must also be fulfilled for severe aircraft environments. The requirements for a heat transport fluid also include:

a. Compatibility with all systems and components

b. A large operating temperature range (no change of state or chemical decomposition)

c. Negligible toxicity (U.L. Group 5 or better)

d. Availability of property data through the operating temperature range.

Other requirements which tend to be difficult to define precisely, and thus are a matter of judgement are:

a. Good heat transfer and pumping power characteristics (low value of performance parameter)

b. High flash point

c. Low vapor pressure

d. Average dielectric strength

The requirement for an extremely wide operating temperature range eliminates all but a few liquid heat transfer fluids. Most are either too viscous at low temperatures or encounter some chemical decomposition at high temperatures. The most promising liquid coolant candidates are listed in Table III along with a summary of pertinent properties information. If high temperatures and/or high flux levels are encountered and liquids are no longer applicable many alternatives still exist. Gases can be used as heat transfer fluids and the relative merit of gases compared in much the same manner that liquids are compared. Figures 39 and 40 present the turbulent and laminar performance parameters for four gaseous coolants. A comparison of hydrogen, helium, nitrogen and air ranks hydrogen as the best gaseous coolant by far with helium second best. Nitrogen and air are very close in the comparison and for most applications air would probably be favored over nitrogen from cost considerations. Oxidation problems might favor the choice of nitrogen for a gaseous coolant. Helium is not a favorable choice for most applications because of its high cost and its tendency to leak from systems which will contain most other gases.

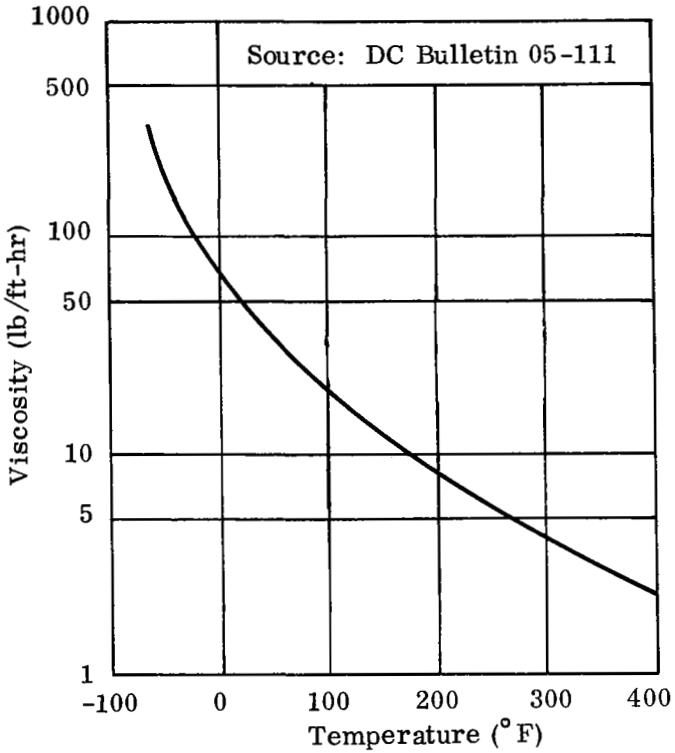

Figure 37. Viscosity-Temperature Characteristic-Dow Corning 331

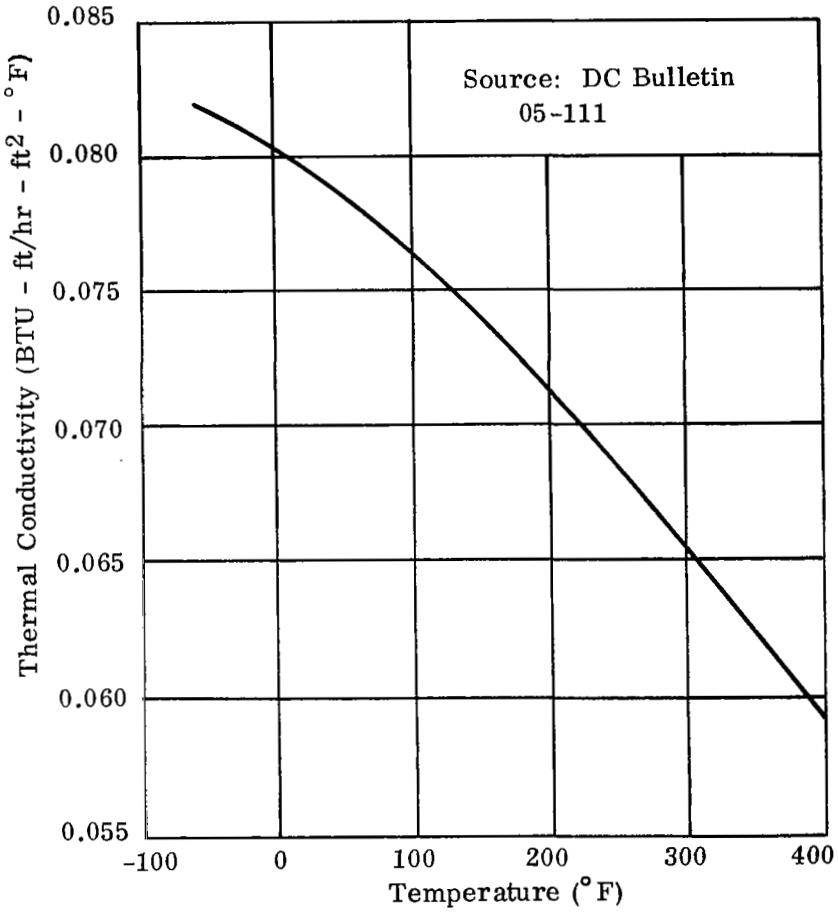

Figure 38. Thermal Conductivity versus Temperature - Dow Corning 331

TABLE III

PROPERTIES OF CANDIDATE HEAT TRANSFER FLUIDS

Property		FC-75 (3M)	Coolanol 45 (Monsanto)	Oronite 8200	Dow Corning 331	Ethylene Glycol (60-40)
Operating Temperature,	°F min.	-80	-65	-65	-130	-65
	max.	440	400	500	400	250
Flash Point, °F		None	370	390	400	240
Density lb/ft^3	at -65°F	122.3	59.3	61.2	63.2	69.2
	at 100°F	107.5	54.5	46.4	57.8	66.2
Viscosity lb/ft-hr	at -65°F	32	5520	5430	308	996
	at 100°F	2.78	27.5	71.6	18.1	7.25
Specific Heat Btu/lb°F	at -65°F	0.21	0.38	0.29	0.40	0.60
	at 100°F	0.25	0.46	0.39	0.43	0.77
Thermal Conductivity Btu/hr-°F-ft	at -65°F	0.088	0.062	-	0.082	-
	at 100°F	0.077	0.075	0.080	0.076	0.22
Approx. Vapor Press. psia	at 400°F	150	0.08	-	23.2	14.5 (250°F)
Toxicity		Nil	Nil	Nil	N.A.	Nil

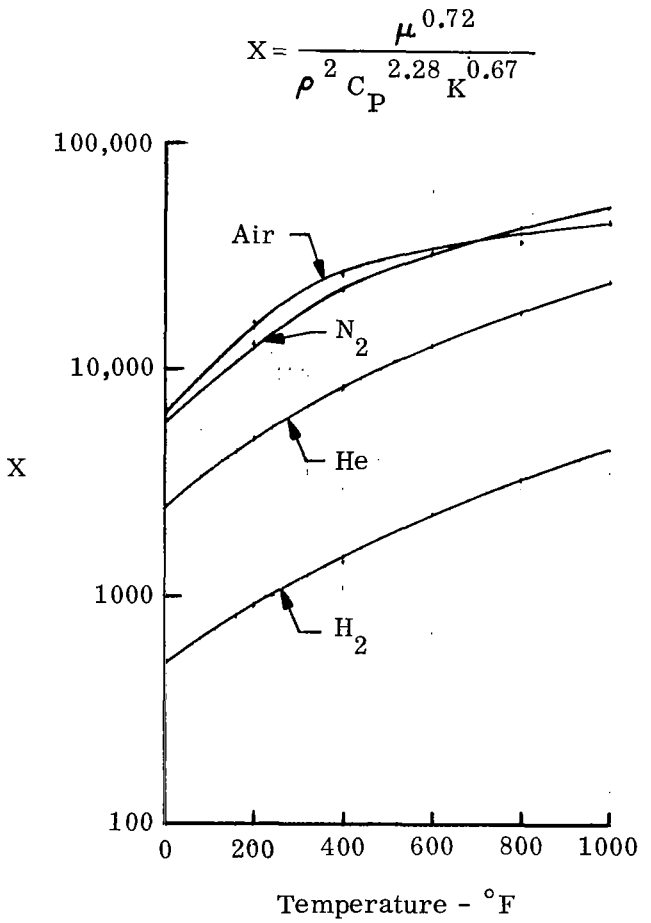

Figure 39. Comparison of Gaseous Coolants - Turbulent Flow Heat Transfer

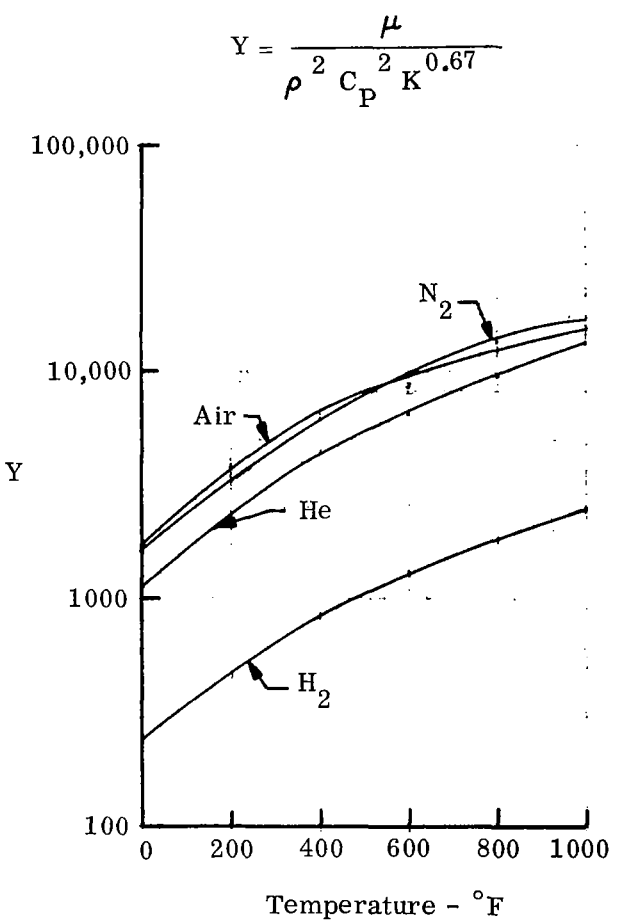

Figure 40. Comparison of Gaseous Coolants - Laminar Flow Heat Transfer

Comparing Figures 39 and 40 with earlier data on liquid coolants dramatically demonstrates the advantage of a liquid coolant over a gaseous coolant if temperatures permit the use of a liquid coolant. Values of both performance parameters at temperatures of 200°F indicate that to obtain the same heat transfer conductance in a gas as in a liquid requires a pumping power about 1000 times greater for the gas. For aircraft application a pumping power penalty of 1000 times will probably eliminate the use of gases whenever liquids can be used. Also, because of the higher specific volume of gasses relative to liquids, the size and weight of the mechanical components will be greater when gaseous systems are used.

3. Convective Coolant - Cooling Systems Combinations

Table IV presents a summary of many possible combinations of coolants and convective cooling systems using the concepts previously discussed. A variety of direct systems are listed in the table for the sake of completeness. However, for purposes of this study the questionable performance of systems with two-phase flow in the coolant passages limited direct system studies to consideration of gaseous coolants or liquids which are sprayed onto the heated surface. In the direct system, the use of low density water vapor dictated larger diameter passages, larger pumps, and higher weight than for the indirect system. Spray systems using water or lithium offer an attractive direct system alternative to two-phase passage flow while using the heat capacity of a liquid-vapor phase change. Both water and lithium spray systems have been studied extensively and their use was considered for the present application. For indirect systems both liquid and gaseous transport fluids can be considered along with many heat sink possibilities. Applicable liquid transport fluids include both silicone and water-glycol. Gaseous transport fluids include hydrogen, helium, nitrogen or air.

Structural materials are not listed in Table IV because the choice is dependent on many factors other than the cooling system operating temperature range. Applicable materials include aluminum, titanium, superalloys or refractory metals.

C. SELECTED SYSTEMS

A large number of cooling system-coolant combinations were discussed and semiquantitatively compared in Sections 4A and 4B. It was not considered necessary to undertake detailed studies of all cooling system-coolant combinations because a careful review of the characteristics of each combination, in light of vehicle application requirements, permitted the choice of a few most promising combinations for more detailed study. The selections, which will be discussed, still encompass a variety of system-coolant combinations from which the most promising cooling concepts were most likely to be identified.

For transpiration and film cooling, the selection of a concept, with its associated system details, is dominated by the choice of a coolant. It was considered necessary to examine both gases and liquids so that the coolants chosen included hydrogen, helium, air, and water. In the case of the air coolant, both stored and ram supplies were chosen for investigation. For the ram air supply it was considered necessary to examine the air scoop to be used and techniques for cooling ram air to usable temperature levels. Nitrogen was not considered for a transpiration or film cooling system because of its similarity to air. If stored

TABLE IV

CONVECTIVE COOLING CONCEPTS

System Classification	Convective Heat Transfer Mode	Description	Heat Transport System	Heat Sink	Approximate Useful Temperature Range
Direct Systems	Liquid	Pressurized coolant flows through passages then flash boils in a chamber and is expended	(1)	Water	70°F to 250°F
			(1)	Lithium	1500°F to 2600°F(2)
	Two-phase Flow Liquid to Vapor	Pressurized coolant flows, boils in passages in structure and is expended.	(1)	Water	70°F to 250°F
			(1)	Lithium	400°F to 2600°F(2)
	Two-phase Flow, Liquid to Vapor, or Single Phase Flow of a Gas	Pressurized coolant flows through passages in structure and is expended. Boiling might be allowed in structure by introducing liquid coolant	(1)	Hydrogen	-420°F to 2600°F(2)
			(1)	Helium	-450°F to 2600°F(2)
			(1)	Nitrogen	-300°F to 2600°F(2)
	Spray Boiling	Pressurized coolant flows through nozzles causing liquid droplets to impinge on hot structure and vaporize	(1)	Water	70°F to 400°F
			(1)	Lithium	1500°F to 2600°F(2)
Indirect Systems	Liquid Transport Fluid	Liquid transport fluid is pumped through item to be cooled and heat exchanger where it is cooled by heat sink coolant	Silicone Fluid	Water	70°F to 400°F
				Hydrogen	
			Water-glycol	Water	70°F to 200°F
				Hydrogen	
			NaK	$LiBH_4$	70°F to 500°F(3)
				LiH	70°F to 1500°F(3)
				Li	70°F to 2600°F(2)
	Gaseous Transport Fluid	Gaseous transport fluid is pumped through item to be cooled and heat exchanger where it is cooled by heat sink coolant	Hydrogen Helium, Nitrogen or Air	Water	70°F to 2600°F(2)
				Hydrogen	-420°F to 2600°F(2)
	Closed-cycle Radiative	Employs a gas or liquid transport loop with a radiator for a heat sink	Gas: Hydrogen, Helium, Nitrogen, or Air Liquid: Water-glycol or Silicone	Radiator	70°F(4) to 2600°F(2) 70°F to { 200°F (water-glycol) / 400°F (Silicone)
Other	Direct Air Convection and Transpiration	Ram air taken on board, cooled by hydrogen fuel or water and then used as a convective coolant and transpirant.	(1)	Hydrogen and Air	-200°F to 2600°F(2)

NOTES:

(1) No heat transport system as such. Heat sink coolant is passed directly through structure to cooled.

(2) Maximum temperature is material controlled and will probably be as high as possible while still retaining the advantages of a cooling system.

(3) Higher heat capacities can be obtained if residual lithium is vaporized.

(4) Minimum temperature is established by radiator design.

air is a feasible transpirant or film coolant then stored nitrogen is an alternate coolant for application where oxidation is a problem.

For the direct and indirect convective cooling concepts, emphasis was placed on using the hydrogen fuel of the vehicle as the ultimate heat sink. While many direct cooling system concepts might be considered, those which appear most promising on the basis of previous discussions included direct convective cooling with the hydrogen fuel and spray cooling with water or lithium. In addition, direct convective cooling with ram air was selected since the air could be transpired after having cooled a portion of the airframe. Direct cooling with hydrogen is potentially attractive from a weight standpoint since both storage and coolant weights might be charged to the propulsion system without a direct influence on total cooled system weight. Water and lithium spray cooling concepts were considered worthy of further study because of their high heats of vaporization and relatively high densities which would reduce storage volume requirements. Although lithium has an 8 to 1 advantage over water with respect to heat capacity and can provide cooling at much higher heat fluxes, water is more easily handled and yields systems having lower distribution line weights.

Several detailed analytical studies of indirect cooling systems led to the conclusion that liquid heat transport fluids are always superior to gaseous fluids if the operating temperature limits were such that liquids could be used. On this basis water-glycol and silicone transport fluid systems were selected for examination where the hydrogen fuel was used as the ultimate heat sink. For comparative purposes limited studies of an indirect cooling system with a gaseous heat transport fluid were also carried out.

Table V summarizes the convection and spray cooling concepts chosen for study. One potentially useful concept, the closed cycle radiative indirect cooling system was not chosen for continued study. System weights are expected to be comparable to those of the transport loops in other types of indirect systems. This particular concept might be considered for application if the available fuel supply is inadequate for cooling purposes.

TABLE V

SELECTED COOLING SYSTEM COOLANT COMBINATIONS

A. Transpiration or Film Cooling Systems

1. Hydrogen (gas)
2. Helium (gas)
3. Air (gas)
4. Water (liquid or vapor)

B. Convective Systems

1. Direct Systems
   a. Hydrogen (gas)
   b. Water (liquid-vapor spray)
   c. Lithium (liquid-vapor spray)
   d. Air (gas)
2. Indirect Systems
   a. Water-glycol (liquid)
   b. Silicone (liquid)
   c. Helium (gas)

SECTION 5

RADIATION AUGMENTED ACTIVE COOLING

Estimates of the total heat load on the baseline wing indicate that large quantities of coolant might be required to cool the wing structure to temperatures which allow the use of aluminum or titanium. Before proceeding to active cooling system selection studies, an investigation of classical methods of thermal protection was conducted. The methods used for this investigation are general and results were applied to both transpiration (or film) cooling and convective cooling systems. The two types of thermal protection studied are an air gap/radiation shield system and an insulation system.

Because of the low thermal conductivity of gases the most efficient methods of insulating involve the use of a blanket of air with arrangements for minimizing heat transmission by convection and radiation. The kinectic theory shows that the thermal conductivity of a gas is proportional both to the density of the gas and to the mean free path of its molecules. The density is directly proportional to pressure, and the mean free path is inversely proportional to pressure so that the conductivity remains constant until the pressure is so low that the mean free path of the molecules is of the same order as the air space in question. This air space could be fiber spacing or pore size in an insulation or plate spacing in air gap. Further reductions in pressure effect thermal conductivity only through the density, so that conductivity decreases proportionately. Introduction of an insulating material into the air space breaks up the air space into small cells so that convection is prevented, and, if the fill is carefully chosen most of the radiation is blocked. Since the heat transfer through such a material is complex, an overall conductivity is usually determined experimentally and the material is treated theoretically as if it had only conduction characteristics.

An attractive method of using the low conductivity of air is to omit the fill material, with a consequent saving in weight, and to provide the two parallel walls bounding the air space with highly reflective (low emittance) surfaces to minimize radiant heat transfer. For this system convection effects must be considered and the system will be effective only if an environment is available which minimizes convection. The quantity of heat transferred by natural convection between horizontal plates is proportional to the ratio between the coefficient of cubic expansion and the square of kinematic viscosity. The heat transferred by natural convection increases as the cube or fourth root of this ratio increases depending upon turbulent or laminar conditions. The ratio increases rapidly with decreasing pressure and with increasing temperature. These changes are large, but for this application pressure and temperature conditions minimize the heat transferred by natural convection. Application in this instance involves an aircraft which cruises at high altitude where pressures are low (below 10 mm of Hg), and at high speed involving high temperature. Conditions are correct, therefore, for minimizing natural convection in air gaps used as insulation provided that dynamic pressure can be kept out of the air gap. From the above discussion both the complexity and advantages of

thermal protection are evident. If properly augmented by a thermal protection arrangement such as an air gap, radiation shielding, insulation, or combinations of these, the heat input to an active cooling system can be considerably reduced thereby reducing the quantity of hydrogen or other heat sink coolant required.

The results of many prior studies, for example References 2, 3 and 18 have resulted in a well founded belief that for thermally protected active cooling systems using insulation the minimum system weight is obtained when insulation weight equals heat sink coolant weight. This is only true if heat leakage through the insulation is expressed solely in terms of the apparent thermal conductivity of the insulation and effects such as conduction through supports or radiation through gaps in the insulation are neglected. A second and much more important stipulation incorporated in the above conclusion is that the entire weight of the heat sink coolant is charged to the cooling system. For the present application the hydrogen fuel is the primary heat sink coolant and its weight is not charged to the cooling system, therefore, the conclusions of prior optimization studies, such as those presented in References 2, 3 and 18, are not entirely valid for this aircraft application. Great care must be exercised to remove old prejudices established by these prior insulated active cooling system studies.

In this study the most thermally efficient system is the one which raises the hydrogen fuel to the highest possible temperature before it is consumed by the engines. The optimum system from a weight point of view minimizes the total vehicle weight taking into consideration the restriction that if hydrogen requirements for cooling exceed hydrogen requirements for propulsion then the cooling system must be penalized for the additional heat sink coolant weight. If additional coolant is required the ultimate heat sink might be one of the exotics listed in Table II used to supplement the hydrogen fuel.

In the next two subsections of this report an air gap/radiation shield system and insulation system are analyzed and their effectiveness compared. Methods of analysis are simple, yet sufficiently accurate for preliminary design purposes. Moreover, some of the results presented in this section have been checked using the more sophisticated techniques given in Reference 19 and are in good agreement.

A. AIR GAP AND RADIATION SHIELD SYSTEMS

As mentioned earlier, an attractive method of using the low conductivity of air is to omit the fill material in an air gap, with a consequent saving in weight, and to provide the two parallel walls bounding the air space with highly reflective (low emittance) surfaces to minimize radiant heat transfer. A discussion of materials and their emittance characteristics is available in both References 18 and 19. Low emittance surfaces are available with aluminum (attractive at low temperatures) and various noble metals (applicable at high temperatures). Reflective materials have emittances below 0.10 and in most cases, these emittances can be maintained for very long times at their respective operating temperatures.

A schematic of the mathematical model used to evaluate air gap radiation shield systems is shown in Figure 41. It consists of an outer surface heat shield with an emittance of 0.8, a series of equally spaced radiation shields with an emittance of 0.2, and

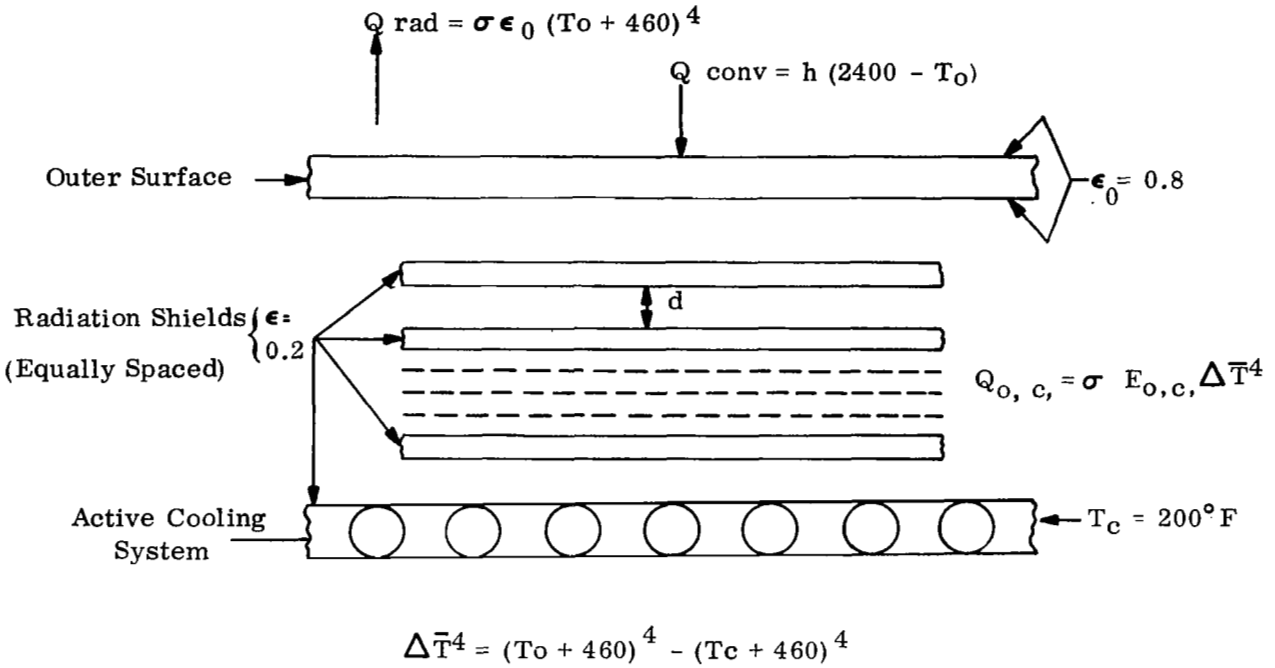

Figure 41. Schematic of Air Gap Radiation Shield System

an inner structure with an emittance of 0.2 whose temperature is maintained at 200°F by an active cooling system. Because of the uncertainties associated with analytical treatment of conduction and convection, it was assumed that a simple radiation relationship could be used for analyses with the assumed emittances adjusted to account for all heat transfer terms. The choice of effective emittances was made by referring to the results of Reference 19, wherein conduction and convection heat transfer are considered in addition to radiation effects. No heat leaks through supports were included in the mathematical model.

Equations governing the steady state performance of such a system are given in Figure 41. The effective emittance of a group of radiation shields, $E_{o,c}$ is given by

$$E_{o,c} = ABC/(AC + BC + AB)$$

$$A = \epsilon/(2 - \epsilon)$$

$$B = \epsilon/(2 - \epsilon)\,(n - 1)$$

$$C = \epsilon_o\,\epsilon/(\epsilon_o + \epsilon - \epsilon_o\,\epsilon)$$

NOTE

For n = o $\qquad E_{o,c} = C$

For n = 1 $\qquad E_{o,c} = AC/(A + C)$

Solutions of the given system of equations yielded the data shown in Figures 42 and 43. The number of radiation shields n describes the following systems,

n = o Air gap system, no radiation shields, the system consists of an outer heat shield surface and an inner actively cooled structure,

n = 1, 2, . . . n signifies the number of shields evenly spaced between the outer surface and the inner surface.

The heat transfer coefficient, h, covers the range of values presented in Figures 12 through 17. The calculations for the radiation shield systems were done only for the flat regions because space limitations will probably prevent such a system from being used in the neighborhood of the leading edge. Therefore values of heat transfer coefficient range from about 1.0 Btu/ft^2 hr°F to values above 10.0 Btu/ft^2 hr°F.

In Figure 42 the heat input to the cooling system is plotted as a function of the number of radiation shields and the convective heat transfer coefficient at the outer surface. As expected, increasing the number of radiation barriers increases the effectiveness of the barrier system but at a decreasing rate. Figure 43 gives the outer surface temperature for the parameters presented in Figure 42. It is noticed that the outer surface temperature is not a strong function of the number of radiation shields. When there is no radiation barrier between the outer and inner surfaces the outer surface temperature is from 20°F to 50°F below the outer surface temperatures with radiation barriers. The data presented in Figures 42 and 43 was used to compare protected versus unprotected active cooling systems, Table VI.

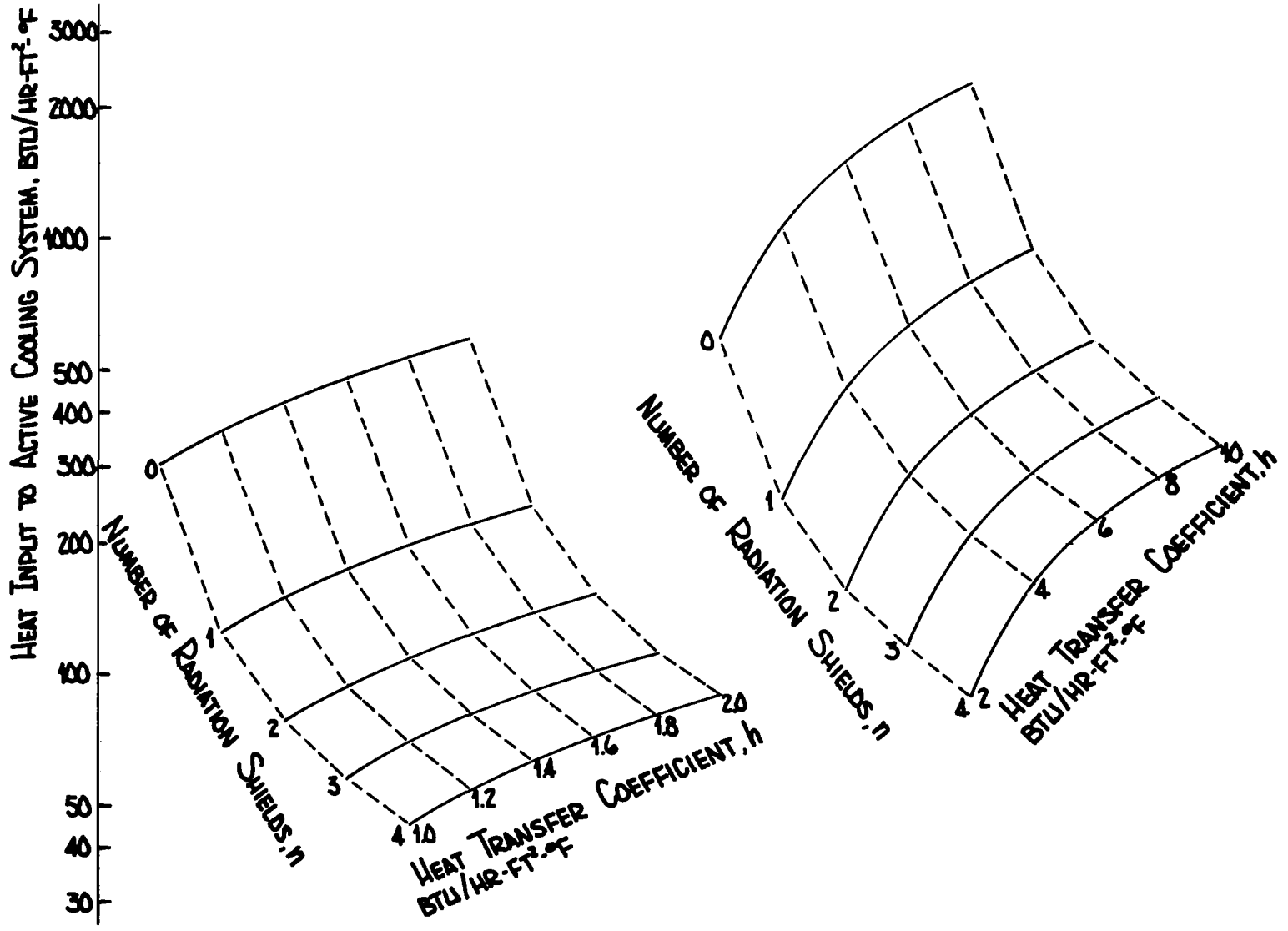

Figure 42. Heat Input to Active Cooling System for an Air Gap - Radiation Shield System

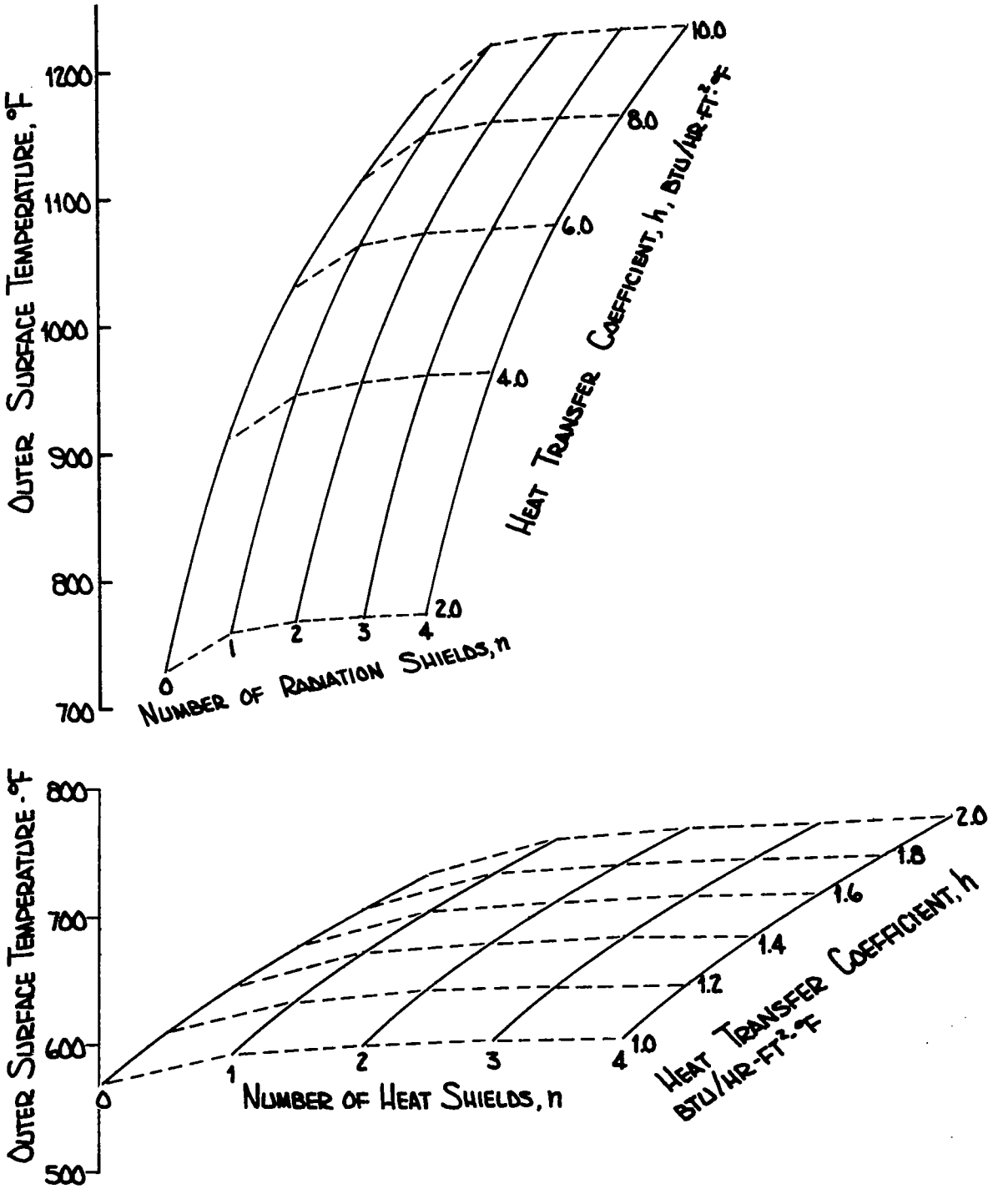

Figure 43. Outer Surface Temperatures of an Air-Gap Radiation Shield System

TABLE VI

AIR GAP RADIATION SHIELDED ACTIVE COOLING SYSTEM COMPARISON

	Unprotected Active Cooling System		Protected System n = 0		Protected System n = 4		Head Load Reduction Factor, Q_R (3)	
							n = 0	n = 4
h (Btu/ft^2-hr-°F)	Q (1) (Btu/ft^2-hr)	T_o (2) (°F)	Q (1) (Btu/ft^2-hr)	T_o (2) (°F)	Q (1) (Btu/ft^2-hr)	T_o (2) (°F)		
1.0	2300	200	300	570	44	600	7.7	52.3
2.0	4600	200	590	730	87	770	7.8	52.9
4.0	9200	200	1050	910	160	960	8.76	57.5
8.0	18,400	200	1900	1110	285	1160	9.68	64.56
10.0	23,000	200	2250	1180	335	1230	10.22	68.7

NOTES:

(1) Q is the heat input to the cooling system

(2) T_o is the temperature of the outermost surface

(3) Q_R is the ratio of the unprotected system heat input to the protected system heat input

If the radiation system is not used then the active cooling system is exposed directly to boundary layer heating. Heat flow into an unprotected active cooling system is given by $Q_{in} = h\ (T_R - T_W)$. For the bottom surface $T_R \approx 2500$ F, thus for $T_W = 200^\circ$F the above equation becomes $Q_{in} = 2300\ h$ as shown in Table VI for the unprotected systems for various values of h.

The heat reduction factor, Q_R, given in Table VI emphasizes the reduction in heat flow which can be obtained by the use of a well designed air gap radiation shield system. With just an outer surface protecting the active cooling system from the hot boundary layer, simple air gap system heat inputs can be reduced by a factor of about 10. When four radiation shields are used between the inner and outer surfaces the heat flow to the cooling system could be reduced by a factor of about 60. The outer surface temperatures listed in Table VI for protected systems are within the capability of titanium or superalloy materials, particularly if they are used for lightly loaded heat shields. Weights were obtained for a radiation shield system by conservatively estimating expected support requirements and handling characteristics of state-of-the-art materials, and for two thicknesses of radiation shielding. As shown below:

	Component	Weight, lb/ft^2
1.	1 mil rhodium foil	0.065
2.	5 mil rhodium foil	0.325
3.	1 mil aluminum foil	0.0144
4.	5 mil aluminum foil	0.072
5.	Attachments and spacers for foils	0.035 (for each rhodium foil) 0.015 (for each aluminum foil)
6.	Superalloy outer surface 0.020 inch thick (equivalent)	1.00
7.	Titanium outer surface 0.025 inch thick (equivalent)	0.57
8.	Attachments for outer surface	0.10

Table VII presents weight estimates for various systems based on the element weights listed above. These weight estimates are used in later sections to estimate total cooled system weights.

B. INSULATED ACTIVE COOLING SYSTEMS

Current uses of thermal protection systems have focused upon insulated systems because of advantages such as availability of efficient low density insulation materials, ease of fabrication, and low cost. When compared to radiation shielded systems, insulation concepts display a few significant disadvantages. The most obvious of the problems associated with insulation is that of moisture pickup and retention if the vehicle is subjected

TABLE VII

AIR GAP RADIATION SHIELD SYSTEM WEIGHT ESTIMATES

	High Temperature Systems Superalloy Outer Surface Rhodium Shields		Moderate Temperature Systems Superalloy Outer Surface Aluminum Shields		Low Temperature Systems Titanium Outer Surface Aluminum Shields	
n	1 Mil foil (lb/ft^2)	5 Mil foil (lb/ft^2)	1 Mil foil (lb/ft^2)	5 Mil foil (lb/ft^2)	1 Mil foil (lb/ft^2)	5 Mil foil (lb/ft^2)
0	1.10	1.10	1.10	1.10	0.67	0.67
1	1.20	1.49	1.13	1.19	0.70	0.76
2	1.30	1.88	1.16	1.27	0.73	0.85
3	1.40	2.27	1.19	1.36	0.76	0.94
4	1.50	2.66	1.22	1.45	0.79	1.03

to rain or cooling system temperatures below the dew point. Careful control can probably eliminate problems associated with cooling below the dew point, but rain protection may be a major problem. Any wing that employs an insulated structural concept will use heat shields. To minimize thermal stresses expansion joints will be required and it will be impossible to completely seal the outer surface of the vehicle. Therefore, considerable water pickup will be difficult to avoid. Other problems include vibration resistance, shrinkage and general degradation of the thermal properties of the insulation under long term operation. In the following paragraphs degrading factors such as those mentioned are not considered and an insulated system evaluation is made solely on the basis of mathematical predictions using thermal property data from Reference 20.

Figure 44 presents a schematic of the ideal insulation system studied. Dynaquartz*, a heat treated silica fiber insulation was chosen as a typical high temperature insulation, although a variety of other insulations might be considered. Figures 45 and 46 present density and thermal conductivity data for Dynaquartz. The idealized insulation system chosen for study is made up of an active cooling system, at 200° F, which is protected by x_i inches of Dynaquartz insulation and a nonstructural outer surface designed to transmit pressure loads to the actively cooled structure. The mathematical relations governing the heat transfer in the ideal system are given in Figure 44. Supports or other forms of heat leakage through the insulation are assumed negligible. The apparent thermal conductivity as given in Figure 46 accounts for radiation and convection effects in the insulation as described in Reference 20. Analysis results for the insulation system are presented in Figures 47 and 48.

In Figure 47 the heat input to the cooling system is plotted as a function of the insulation thickness and the convective heat transfer coefficient to the outer surface. Increasing the insulation thickness decreases heat input to the active cooling system for values of constant heat transfer coefficient. Figure 48 gives outer surface temperatures for the parameters in Figure 47. It is noticed that the outer surface temperature is strongly dependent on the convective heat transfer coefficient but shows a weak dependence on the insulation thickness. Weights for the insulation system are a function of insulation thickness and insulation density and are estimated in Table VIII. Outer surface attachment weights are included at 0.10 lb/ft^2 . The titanium and superalloy outer surface weights are 0.67 lb/ft^2 and 1.00 lb/ft^2, respectively.

Table IX presents a comparison of a protected vs an unprotected active cooling system assuming insulation protection is used. Reductions of heat input by factors of 5 to 60 can be achieved with insulation over the range of convective heat transfer coefficients listed. Comparing Table VI and Table IX, radiation shielding versus insulation, the effect of convection and conduction losses can be partially evaluated. In Table VI for h = 1 and n = o the heat reduction ratio, Q_R , is 7.7. In Table IX for h = 1 and x_i = 0.2 inch, Q_R , is 4.6. At first glance this effect may seem strange, but it must be remembered that computed values of heat flow for an insulation take into account all modes of heat transfer in the insulation through the use of an effective thermal conductivity. For low values of h (small temperature difference across the insulation), convection and conduction heat transfer are a significant part of the total heat transfer through the insulation.

* Registered trademark of the Johns-Manville Co.

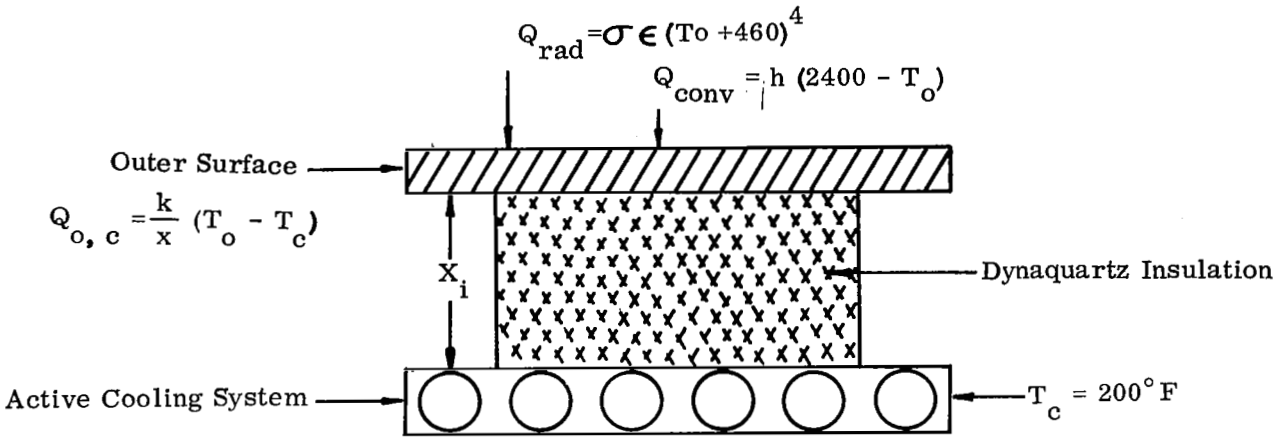

Figure 44 Schematic of Insulation System

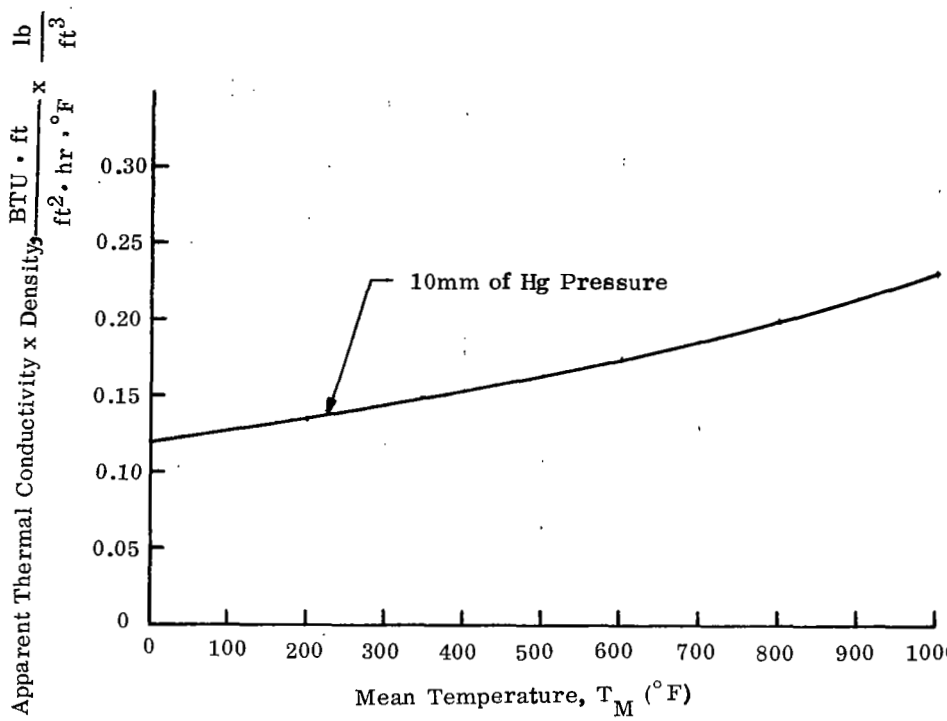

Figure 45. Apparent Thermal Conductivity x Density for Dynaquartz

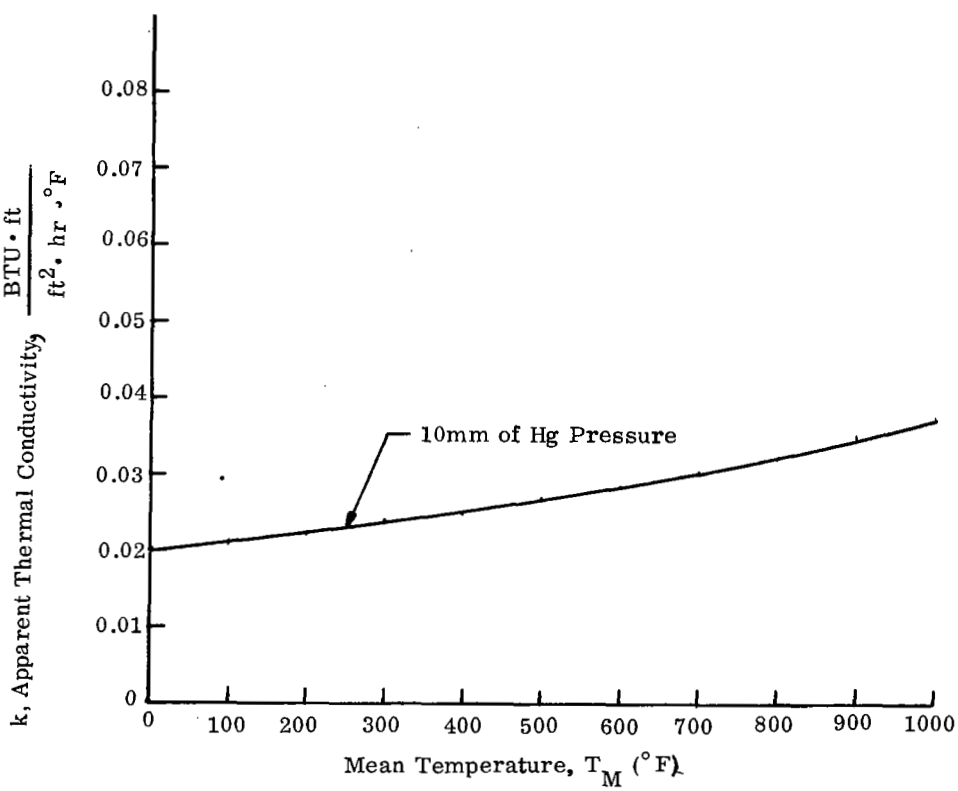

Figure 46. Apparent Thermal Conductivity of Dynaquartz

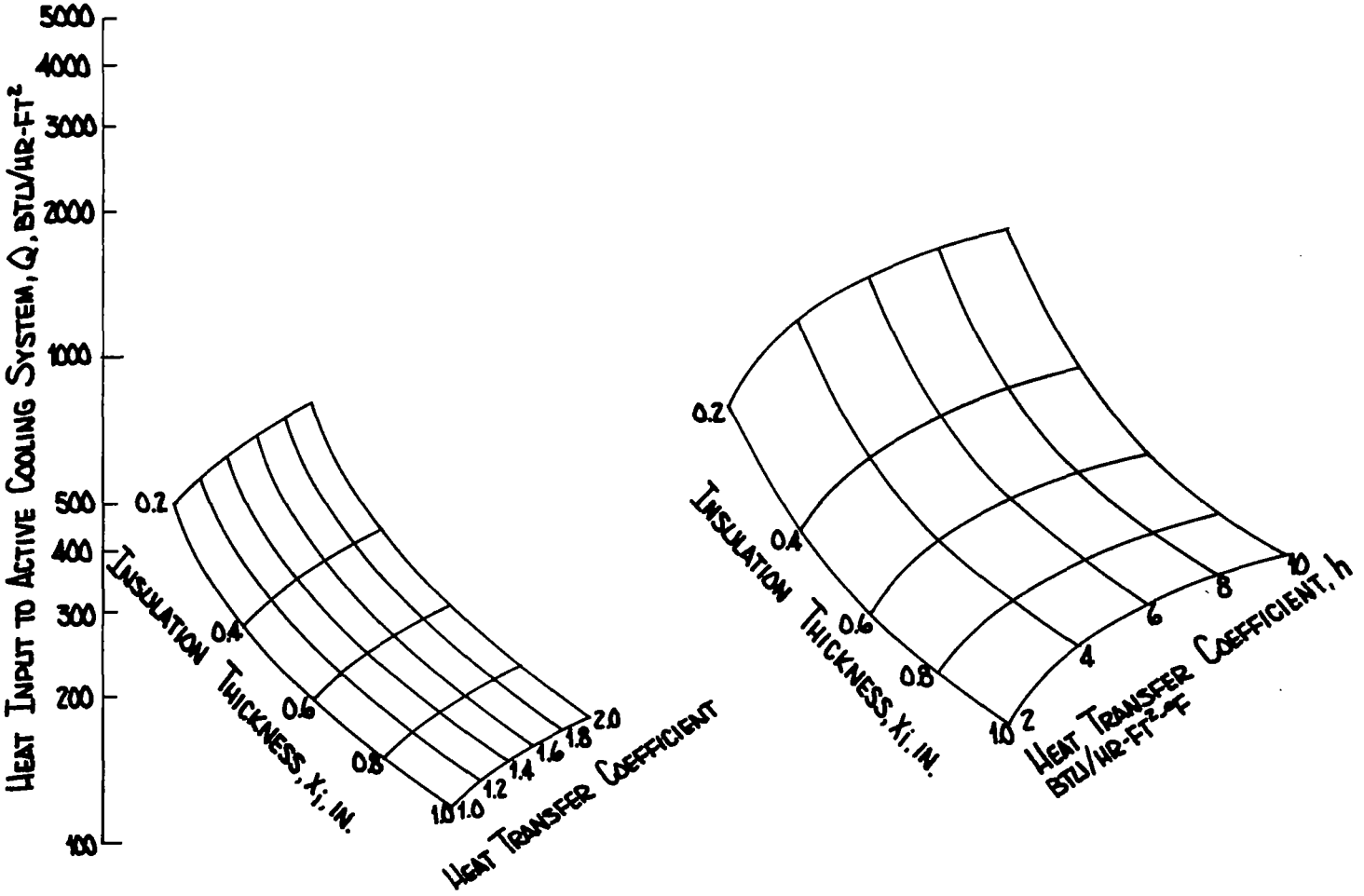

Figure 47. Heat Input to an Insulated Active Cooling System

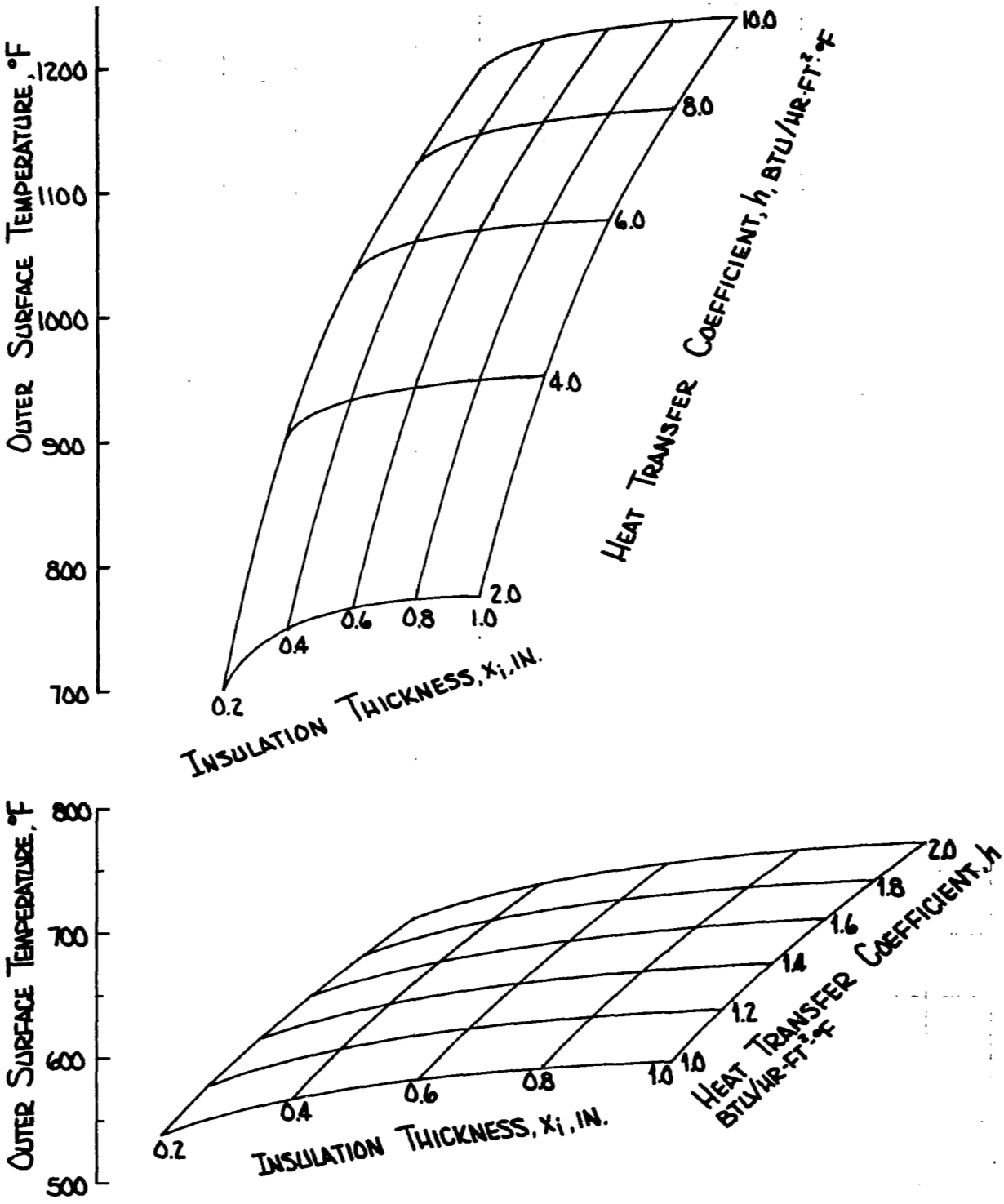

Figure 48. Outer Surface Temperatures of an Insulated Active Cooling System

TABLE VIII
INSULATION SYSTEM WEIGHT ESTIMATES

Insulation Thickness (in.)	High Temperature Systems Superalloy Outer Surface (lb/ft^2)	Low Temperature Systems Titanium Outer Surface (lb/ft^2)
0	1.10	0.67
0.2	1.20	0.77
0.4	1.36	0.89
0.6	1.46	0.99
0.8	1.56	1.10
1.0	1.67	1.20

TABLE IX

INSULATION PROTECTED ACTIVE COOLING SYSTEM COMPARISON

	Unprotected Active Cooling System		Protected System X_i=0.2 in.		Protected System X_i=1.0 in.		Heat Load Reduction Factor, Q_R (3)	
							X_i = 0.2 in.	X_i = 1.0 in.
h (Btu/ft^2-hr-°F)	Q (1) (Btu/ft^2-hr)	T_o (2) (°F)	Q (1) (Btu/ft^2-hr)	T_o (2) (°F)	Q (1) (Btu/ft^2-hr)	T_o (2) (°F)		
1.0	2300	200	500	540	120	595	4.6	19.2
2.0	4600	200	800	710	175	775	5.75	26.3
4.0	9200	200	1180	900	250	950	7.8	36.8
8.0	18,400	200	1650	1125	350	1165	11.15	52.6
10.0	23,000	200	1800	1200	385	1240	12.8	59.7

NOTES:

(1) Q is the heat input to the cooling system

(2) T_o is the temperature of the outermost surface

(3) Q_R is the ratio of the unprotected system heat input to the protected system heat input

The conclusion which can be drawn from the above is important for aircraft design. In low heating regions, a well evacuated thin gap between two surfaces is as good if not better at reducing heat loads than the equivalent gap filled with insulation. In fact it might be concluded that insulation should not be used. For higher heating rates, (larger temperature differences) the above trend is not noticed and a small thickness of insulation is better than the equivalent gap.

To compare a radiation system and an insulation system, equivalent k_ρ values for radiation shielding were determined as functions of the number of barriers (shields) and the external and internal surface temperatures. Referring to Figure 41 the equivalent thermal conductivity times density of a radiation barrier system is calculated as follows:

$$k_{eff} = E_{o,c} \ (\sigma) \ (T_o^4 - T_c^4) \ (n + 1) \ d / \ (T_o - T_c)$$

and

$$\rho_{eff} = (1728) \ (t) \ (\rho) \ (n) \ / \ (n + 1) \ d$$

so that,

$$(k_\rho)_{eff} = \frac{E_{o,c} \ \sigma \ (T_o^4 - T_c^4)}{(T_o - T_c)} \ (1728) \ (n) \ (t) \ (\rho)$$

$$(k_\rho)_{eff} \ , \ \frac{\text{Btu - in.}}{\text{ft}^2 \text{ - hr - } ^\circ\text{F}} \times \frac{\text{lb}}{\text{ft}^3}$$

Table X lists effectiveness values for rhodium and aluminum radiation barriers for both 1 mil and 5 mil foil. As mentioned in Reference 21 aluminum foils can withstand temperatures up to 1000°F.

Comparing effectiveness values from Table X with values in Figure 45 the weight problems of radiation shield systems become evident. Although one 1.0 mil aluminum foil shield is better than an insulation system up to a mean temperature of 600°F, radiation shields are generally heavier than the comparable insulation in the moderate temperature range. As shown in Reference 18 radiation shields are very effective for extreme high temperature application where ceramic foams are the only insulation available.

TABLE X

EFFECTIVENESS OF RADIATION SHIELDS, EQUIVALENT $K\rho$, $\frac{\text{Btu - in.}}{\text{ft}^2\text{ - hr - }^\circ\text{F}} \times \frac{\text{lb}}{\text{ft}^3}$

Rhodium Shields, $\rho = 0.4495$ lb/in.^{3}

Aluminum Shields, $\rho = 0.10$ lb/in.^{3}

$T_c = 200^\circ\text{F}\ (660^\circ\text{R})$, $T_M = \frac{1}{2}(T_o + T_c)$

			1 Mil Rhodium Foil		5 Mil Rhodium Foil		1 Mil Aluminum Foil		5 Mil Aluminum Foil	
T_M		T_o	n		n		n		n	
($^\circ$F)	($^\circ$R)	($^\circ$F)	1	4	1	4	1	4	1	4
300	760	400	0.168	1.88	0.84	9.4	0.037	0.42	0.187	2.09
400	860	600	0.249	2.82	1.25	14.1	0.055	0.63	0.278	3.14
500	960	800	0.360	4.09	1.80	20.45	0.080	0.91	0.40	4.55
600	1060	1000	0.505	5.73	2.53	28.65	0.112	1.27	0.564	6.38
700	1160	1200	0.687	7.79	3.44	38.95	–	–	–	–
800	1260	1400	0.910	10.33	4.55	51.65	–	–	–	–
900	1360	1600	1.180	13.39	5.90	66.90	–	–	–	–

SECTION 6

TRANSPIRATION AND FILM COOLING SYSTEM SELECTION STUDIES

The injection of a cool fluid into a hot boundary layer is an effective way of reducing the temperature of a surface over which the boundary layer flows. Depending upon the specific details of coolant injection the process may be identified as transpiration or film cooling. In both cases the surface is cooled by heat transfer to the coolant and by a blocking of the heat transfer from the hot gas to the surface. This blocking effect is due to the modifications of temperature and velocity profiles as a result of fluid injection. When the coolant is injected into the boundary layer through a porous media the process is called transpiration cooling whereas injection through discrete slots or holes in such a manner as to create a protective layer of coolant on the surface is called film cooling. Except in the immediate region of the surface to be cooled the equipment required for transpiration or film cooling is essentially the same. Potentially useful coolants are also the same.

As discussed in Reference 12, there are three reasons for the superior effectiveness of transpiration or film cooling over the conventional techniques of convective cooling. For transpiration cooling a porous material with a large surface area is used as the injector. The coolant and injector are in intimate contact making them an extremely efficient heat exchanger. For both transpiration and film cooling the coolant acts as an insulator between the surface and the free stream gas, and in addition, injection alters the velocity and temperature distributions across the boundary layer in a manner conducive to a much lower heat flux.

In this section the results of transpiration and film cooling system selection studies are presented and discussed. For transpiration and film cooling, the selection of a concept, with its associated system details, is dominated by the choice of a coolant. Coolant choice is primarily flow rate dependent and determination of coolant flow rates can be accomplished without knowing system details, hence this section concentrates upon determination of coolant flow rates. Possible system details are suggested and system weight estimates are made.

A. TRANSPIRATION COOLING

Many theoretical and experimental investigations of the problem of transpiration cooling are available and a summary of these works is presented in Reference 12. A study of the theories of transpiration cooling presented in Reference 12 reveals two major problems concerning present knowledge of the subject. First, there is considerable uncertainty as to which of the various theories gives the best prediction. Each theory contains fairly drastic simplifications and experimental data to check the theories are too few in number and in many cases of doubtful accuracy. Secondly, the methods of prediction are difficult to apply to a design problem.

For this project a method outlined by D. B. Spalding, D. M. Auslander and T. R. Sundaram (Reference 27), which is recommended in Reference 12, was chosen for predicting coolant flow rates. The Appendix contains a summary of this method and the modifications necessary to allow calculation of transpiration flow rates for the wing configurations presented in Figures 4 through 8.

Figure 28 presented schematics of two typical transpiration cooling models. Since the approach to the solution of the heat and mass transfer problem as presented by Spalding, et al, was to obtain empirical correlations which fit the heat transfer data, a review of the governing equations was not presented herein, rather the data generated by the use of this empirical correlation is presented and discussed.

Figures 49 through 67 present selected data from the transpiration cooling flow rate analyses for a 200°F outer surface temperature (T_{wall} = 200°F). Data for hydrogen, helium, air and water are presented and discussed. Following the data for a 200°F outer surface temperature a discussion of outer surface temperature variations is presented.

The choice of T_{wall} = 200° F was predicated by the ability to employ aluminum alloy construction for the load carrying structure and as a convenience to enable the generation of transpiration cooling data without concern for radiation equilibrium wall temperature variations along the wing. As the data in Figures 21 through 24 shows, radiation equilibrium wall temperatures range from near 600°F on top surface just forward of the maximum thickness line to 2500°F on the 0.05 inch leading edge hemicylinder. At this point in the study it was not obvious which areas should be cooled to what temperature so a temperature below the radiation equilibrium temperatures for the wing was chosen. If a higher wall temperature is assumed the relative merit of coolants as established at the 200°F wall temperature does not change even though the flow rates are reduced.

As a result of the adiabatic assumption incorporated in the theory, the backface temperature of the porous material is the same as the coolant inlet temperature indicated on Figures 49 through 67 by $T_{ref.}$ As implied by the equations given in the Appendix coolant flow rates are reduced as the temperature difference $T_{wall} - T_{ref}$, is increased. At first glance this would seem to be very beneficial, but the heat flux reduction factor is dependent on the coolant flow rate and as flow rate is reduced the heat the coolant must absorb is increased. Tradeoffs involved in this effect are not easily seen by a study of the governing equations so analyses were conducted for two reference temperatures for both hydrogen and helium.

1. Hydrogen Injection

A ranking of gaseous transpirants in order of cooling effectiveness yields hydrogen with its specific heat of approximately 3.5 Btu/lb°R, as the most effective. For the present application, hydrogen transpiration is feasible as long as the wall temperature is sufficiently low to prevent combustion of the hydrogen as it is injected (below approximately 1500°F). Since hydrogen was expected to yield the lowest flow rates of any gaseous transpirant it was studied first to establish a comparative base. Figures 49 through 53 present selected data from the hydrogen transpiration analyses for a 200°F outer

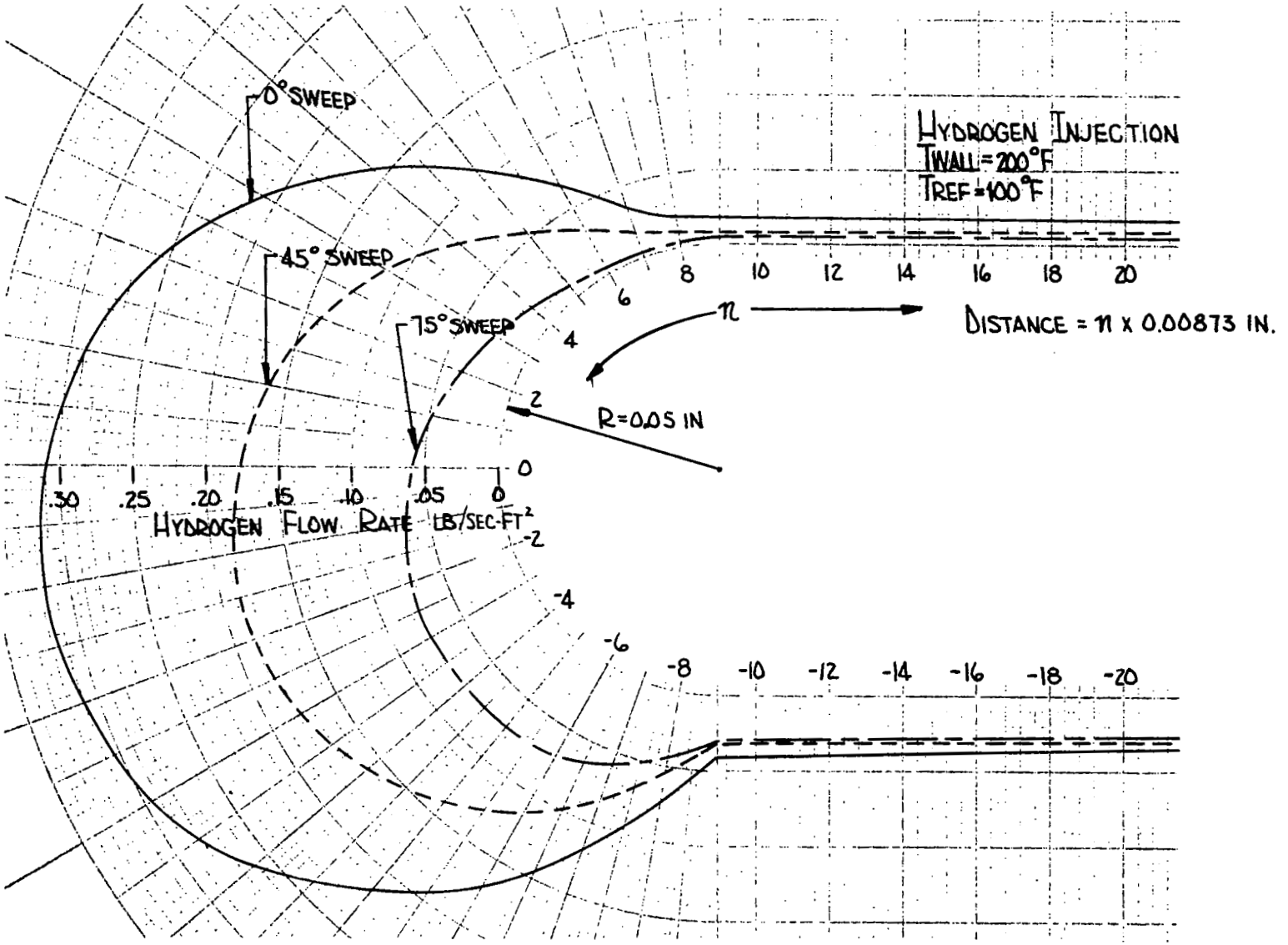

Figure 49. Hydrogen Flow Rates for a 200°F, 0.05 in. Radius, Transpiration Cooled Leading Edge for a 100°F Hydrogen Inlet Temperature, M = 6.0, α = 10.31°, Altitude = 100,000 ft

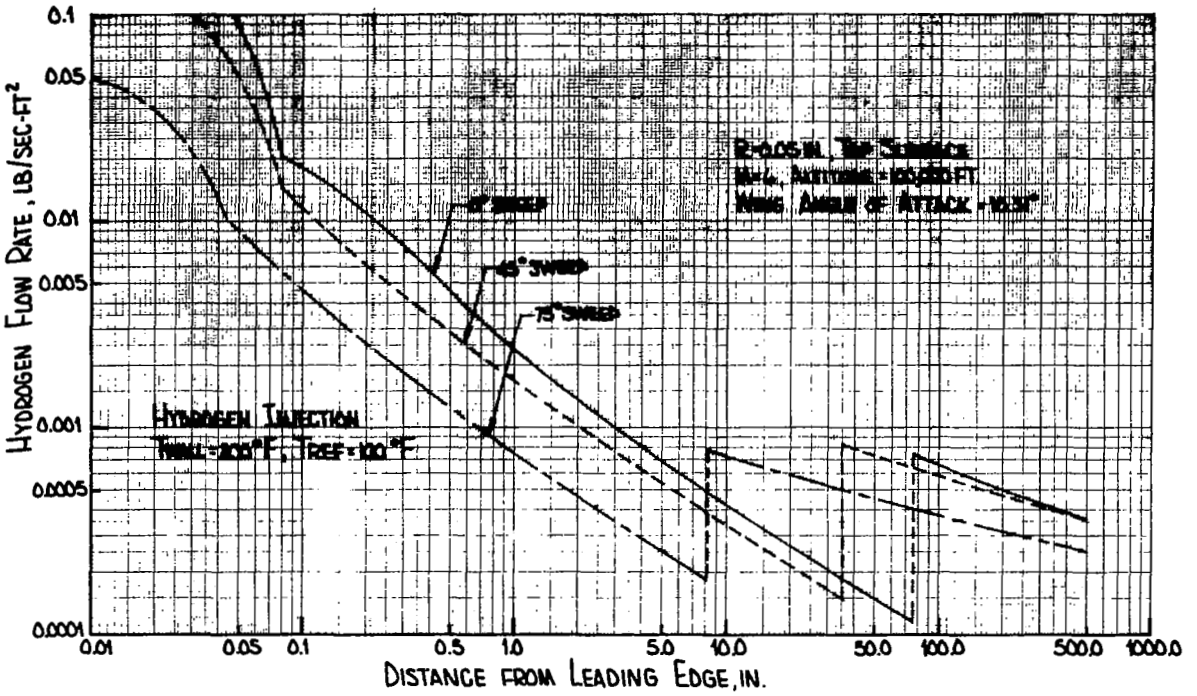

Figure 50. Hydrogen Flow Rates for a 200°F Transpiration Cooled Top Surface for a 0.05 in. Leading Edge Radius and a 100°F Hydrogen Inlet Temperature, M = 6.0, α = 10.31°, Altitude 100,000 ft

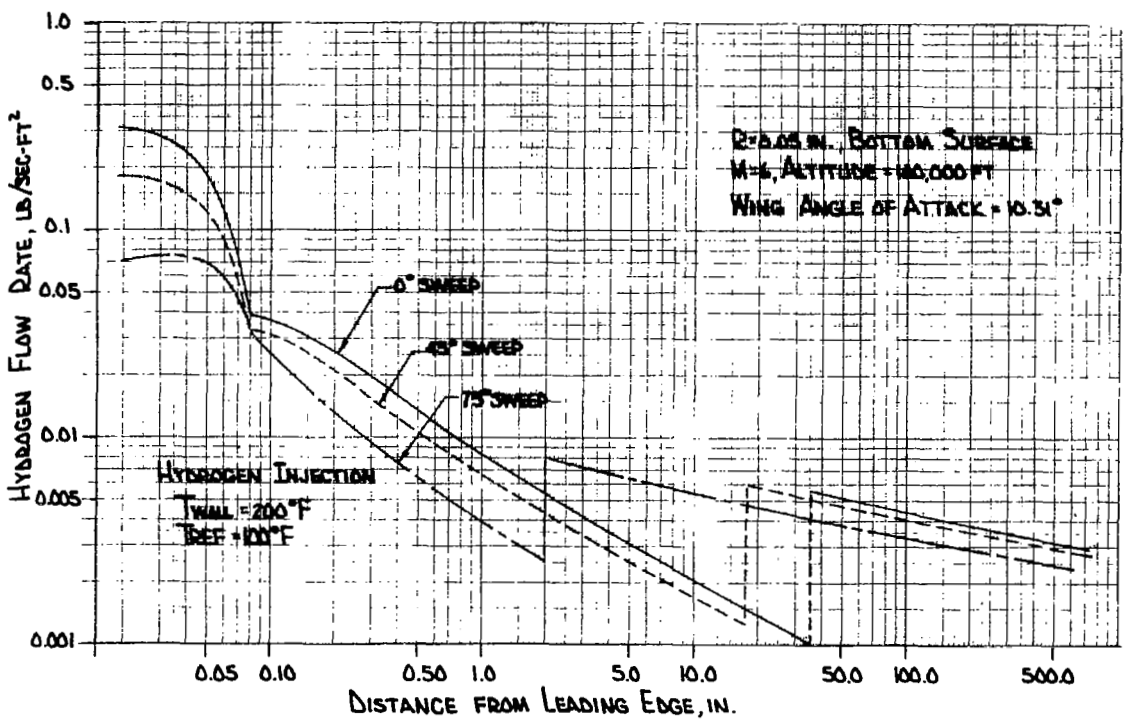

Figure 51. Hydrogen Flow Rates for a 200°F Transpiration Cooled Bottom Surface for a 0.05 in. Leading Edge Radius and a 100°F Hydrogen Inlet Temperature, M = 6.0, α = 10.31°, Altitude = 100,000 ft

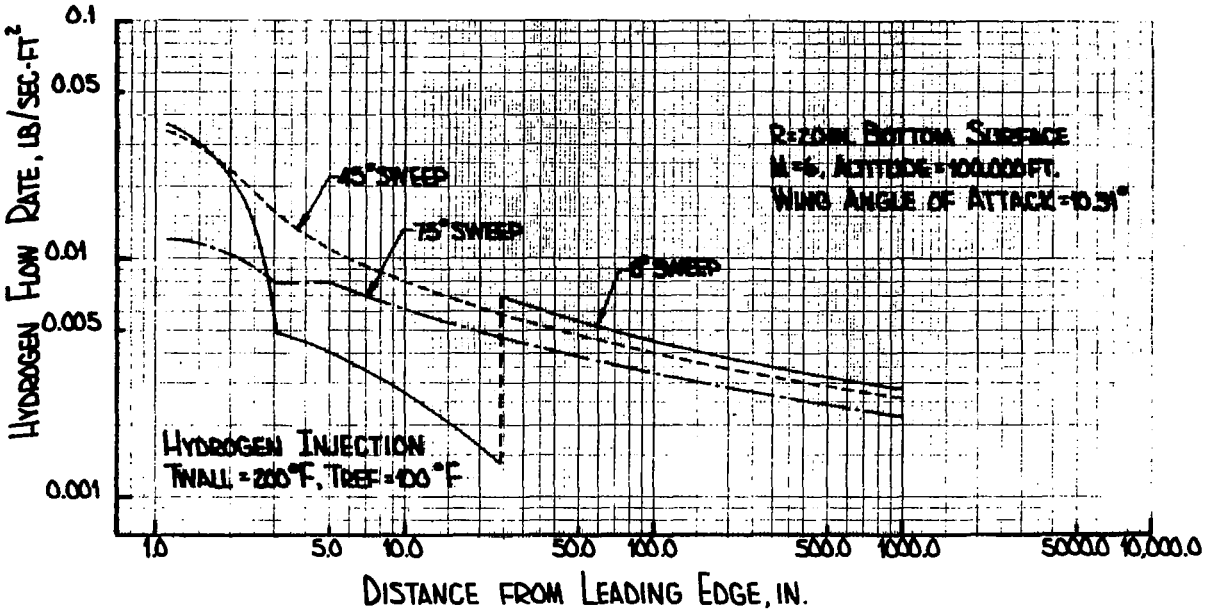

Figure 52. Hydrogen Flow Rates for a 200°F Transpiration Cooled Bottom Surface for a 0.05 in. Leading Edge Radius and a 100°F Hydrogen Inlet Temperature, M = 6.0, α = 10.31°, Altitude = 100,000 ft

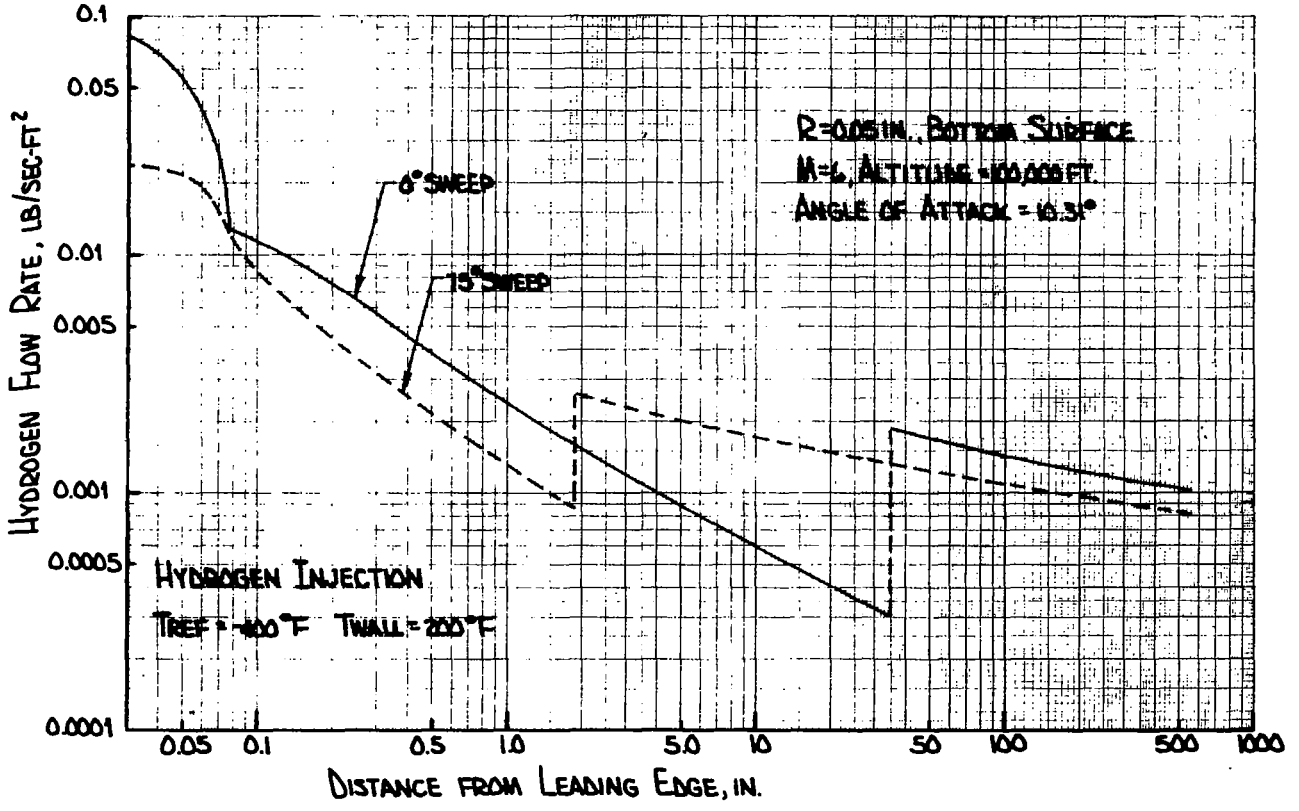

Figure 53. Hydrogen Flow Rates for a 200°F Transpiration Cooled Bottom Surface for a 2.0 in. Leading Edge Radius and a -400°F Hydrogen Inlet Temperature, M = 6.0, α = 10.31°, Altitude = 100,000 ft

surface temperature. Figures 49, 50, and 51 are for a 100°F hydrogen inlet temperature and a 0.05-inch leading edge radius. Figure 52 presents data for the bottom surface of a 2.0-inch leading edge radius wing for a hydrogen inlet temperature of 100°F. Figure 53 again presents data for the bottom surface, but for a 0.05-inch leading edge radius wing and a hydrogen inlet temperature of -400°F.

Figure 49 shows the distribution of hydrogen flow rate around the leading edge hemicylinder. The maximum flow rate occurs at the stagnation point and varies from 0.33 lb/sec-ft^2 for a 0° swept wing to 0.075 lb/sec-ft^2 for a 75° sweep wing. For all sweep angles flow rates decrease rapidly from the stagnation point to the hemicylinder shoulder. For the 0° sweep case this flow rate change is about a factor of 10 reduction while for 75° sweep it is approximately a factor of 2 reduction.

Figures 50, 51, and 53 show the effect of laminar to turbulent transition for all sweep angles for a 0.05-inch leading edge radius. Figure 52, a 2.0-inch leading radius edge case, shows this laminar to turbulent transition only for the 0° sweep wing. For sweep angles of 45° or greater, turbulent flow exists over the entire wing. The horizontal line from approximately 3.0 inches to 6.0 inches indicates a mismatch between the hemicylinder and flat plate turbulent flow theories. Data for the 2.0-inch radius is presented only to demonstrate that leading edge radius effects are of second order when the wing is considered as a whole. Perturbations on radius are included in the section on air injection to verify this conclusion.

Table XI summarizes the data for hydrogen injection for a 200°F outer surface temperature by tabulating the integrated flow rates for three portions of the wing for both the 100°F and -400°F reference temperatures. At this point it is worth repeating that this reference temperature is both hydrogen inlet temperature and the porous material backface temperature. For purposes of integration of the transpiration flow rate data and for presentation of convective cooling system data the wing was broken into three sections to be cooled; a leading edge, a top surface, and a bottom surface. The leading edge section extends over the first 60.0 inches (5.0 ft) of the foremost portion of the wing. This includes two surfaces, the bottom leading edge surface from 60.0 inches back of the leading edge to the zero point on the leading edge hemicylinder and the top leading edge surface extending from the same zero point rearward, 60.0 inches along the top surface. These distances are measured perpendicular to the leading edge. The top flat surface extends from 60.0 inches aft of the leading edge on the top surface to the maximum thickness line on the top surface. The bottom surface extends from 60.0 inches aft of the leading edge on the bottom surface to the rearmost portion of the wing. The top rear edge surface is not cooled. In Section 7, Figures 80 and 81 locate these areas on the respective wing configurations. Table XIX lists the variation of these areas with sweep angle. The data presented through Sections 6 and 7 is very sensitive to the choice of wing division and a thorough familiarity with the area variations with sweep is necessary for proper interpretation of the results.

As shown in Table XI, leading edge flow rates vary from approximately 9,000 lb/hr to 30,000 lb/hr and from approximately 2800 lb/hr to 9,000 lb/hr as sweep angle is varied from 0 degrees to 75 degrees for the 100°F and -400°F reference temperatures respectively. At this point two significant effects must be noted. First, the hydrogen

TABLE XI

HYDROGEN TRANSPIRATION FLOW RATES, 200°F OUTER SURFACE TEMPERATURE, 0.05-INCH LEADING EDGE RADIUS

-100°F Reference Temperature				-400°F Reference Temperature		
Wing Region	Sweep Angles			Sweep Angles		
	0°	45°	75°	0°	45°	75°
Leading Edge	9140	17,400	29,900	2810	5360	9190
Top	5830	4820	2380	1790	1480	730
Bottom	78,800	74,700	57,700	24,300	23,000	17,800
Total (lb/hr)	93,800	97,100	90,000	28,900	29,900	27,700

flow rate for a 200°F outer surface would seem to be high enough to preclude transpiration cooling the entire wing to this temperature. For this reason other wall temperatures were examined and the flow rates for wall temperature variations are presented later in this section. Secondly, when the reference temperature was reduced to -400°F to yield a 600°F temperature rise in the hydrogen as compared to the previous 100°F temperature rise, flow rate reductions were not 6 times as expected but only 3.25 times. The possibility of this happening was mentioned earlier and is a result of a reduction in the "blocking effect" when flow rate is reduced.

2. Helium Injection

In order of transpiration cooling effectiveness helium with its specific heat of approximately 1.25 Btu/lb°R, ranks second only to hydrogen. Selected data for helium is given in Figures 54 through 57 for 0° and 75° sweep angles and for 0.05-inch leading edge radius. A perturbation on the leading edge radius was omitted for the helium data presentation. Examination of Figure 54 reveals the same trends as observed for hydrogen injection. Flow rates are greatest at the stagnation point decreasing with sweep angle approximately as the cosine of the sweep angle. Flow rates decrease with increasing distance from the leading edge with approximately an order of magnitude decrease for 0° sweep from the stagnation point to the hemicylinder shoulder and a factor of 2 reduction in flow rate from the stagnation point to the hemicylinder shoulder for 75° sweep.

Table XII summarizes the helium transpiration flow rate data in integrated form for a 200°F outer surface temperature and a 0.05-inch leading edge radius. As in the hydrogen case, reduction of the reference temperature to increase the helium ΔT from 100°F to 650°F did not result in a proportional reduction in flow rate. For helium this increase in ΔT of 6.5 times only lowered the helium flow rates by slightly more than 3 times. This is less than the corresponding gain for hydrogen and this difference can be attributed indirectly to the 2.8 times lower specific heat of helium when compared to hydrogen. This specific heat effect can also be seen by comparing Tables XI and XII. Helium flow rates are about 2.4 times greater than the corresponding hydrogen flow rates and this effect is almost wholely a result of the specific heat difference between hydrogen and helium. The helium flow rates listed in Table XII are high enough to preclude choice of a 200°F outer surface temperature for the entire wing using helium as the transpirant.

3. Air Injection

Although results presented for hydrogen and helium were conclusive as far as ruling out a 200°F outer surface temperature for the entire wing using a stored gas, the possibility of transpiration cooling portions of the wing or possibly the entire wing with ram air was investigated. For this study, data is presented for both 0.05-inch and 2.0-inch radii because leading edge effects become significant if transpiration cooling is considered only for discrete portions of the wing. Figures 58 through 63 present data for the 0.05-inch and 2.0-inch leading edge hemicylinder, top surface, and bottom surface. The data is presented for the 0°, 45°, and 75° sweep angle configurations. Integrated data is summarized in Table XIII.

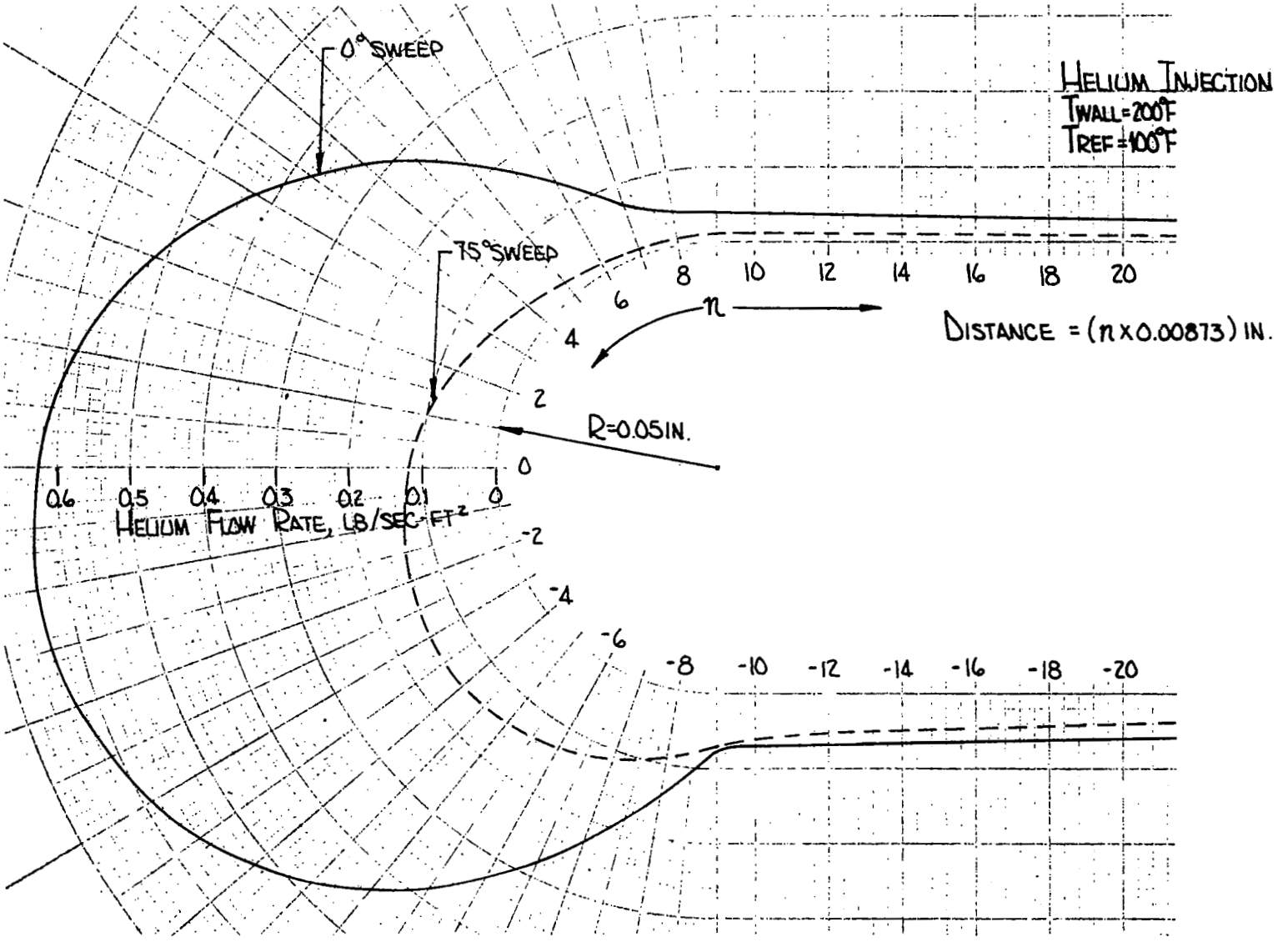

Figure 54. Helium Flow Rates for a 200°F 0.05 in. Radius, Transpiration Cooled Leading Edge for a 100°F Helium Inlet Temperature, M = 6.0, α = 10.31° Altitude = 100,000 ft.

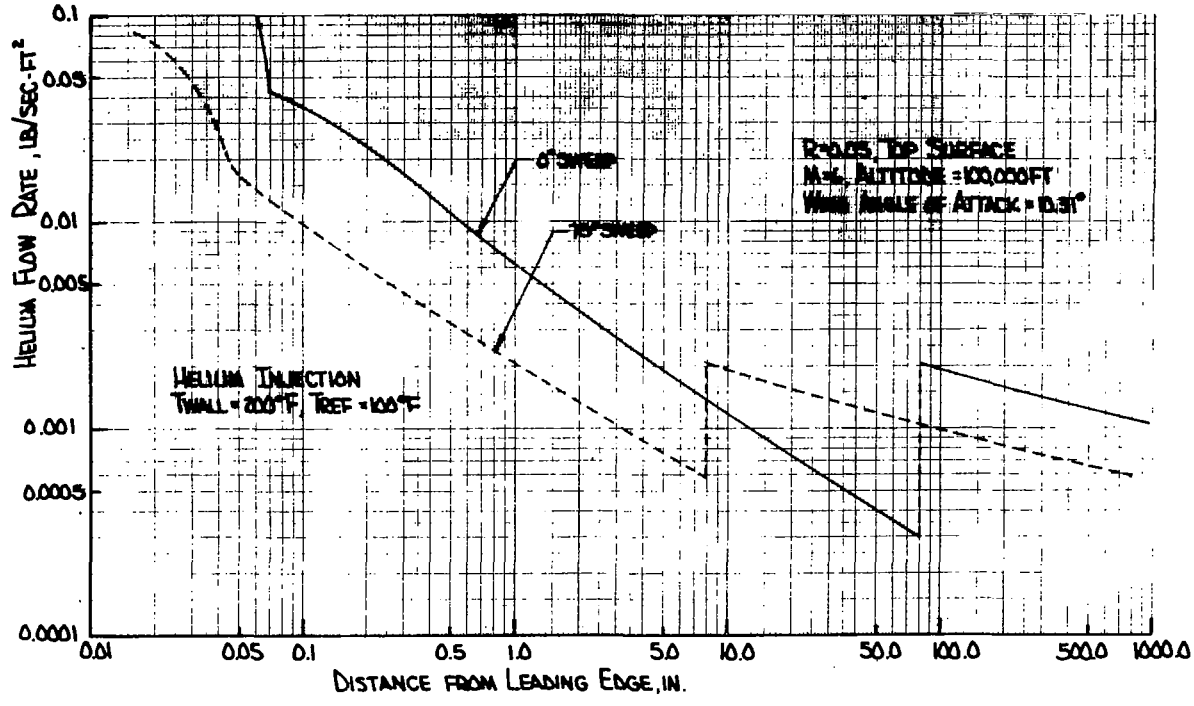

Figure 55. Helium Flow Rates for a 200°F Transpiration Cooled Top Surface for a 0.05 in. Leading Edge Radius and a 100°F Helium Inlet Temperature, M = 6.0, α = 10.31°, Altitude = 100,000 ft

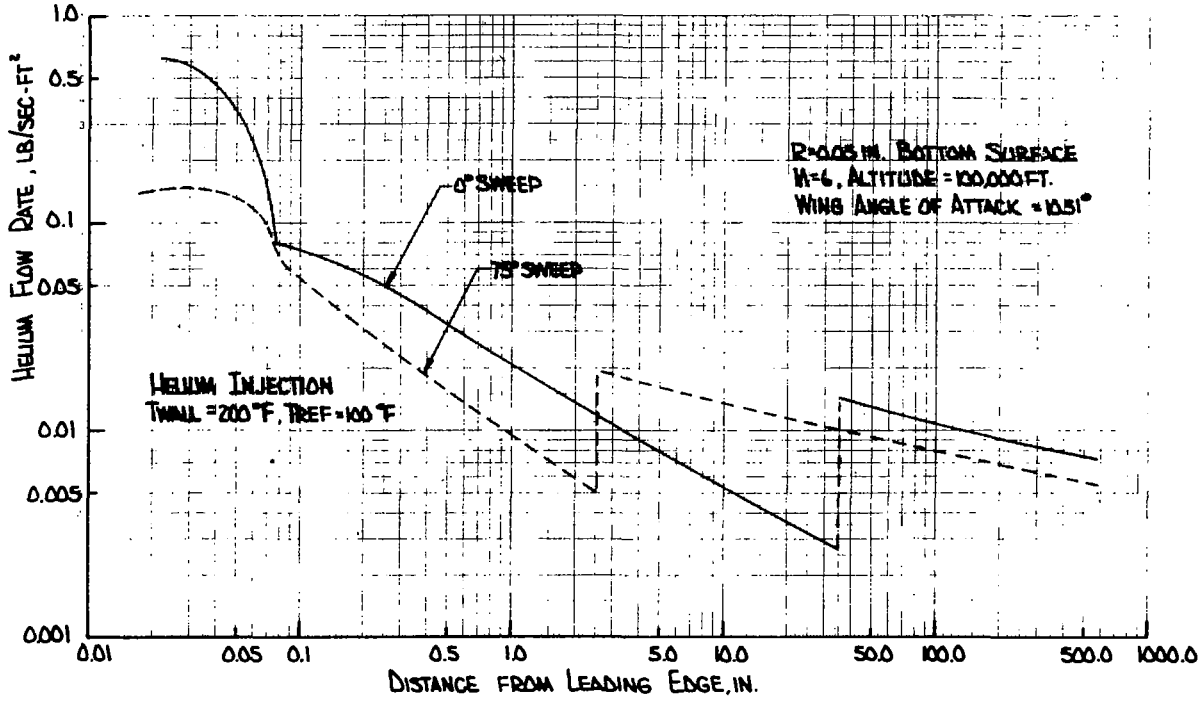

Figure 56. Helium Flow Rates for a 200°F Transpiration Cooled Bottom Surface for a 0.05 in. Leading Edge Radius and a 100°F Helium Inlet Temperature, M = 6.0, α = 10.31°, Altitude = 100,000 ft

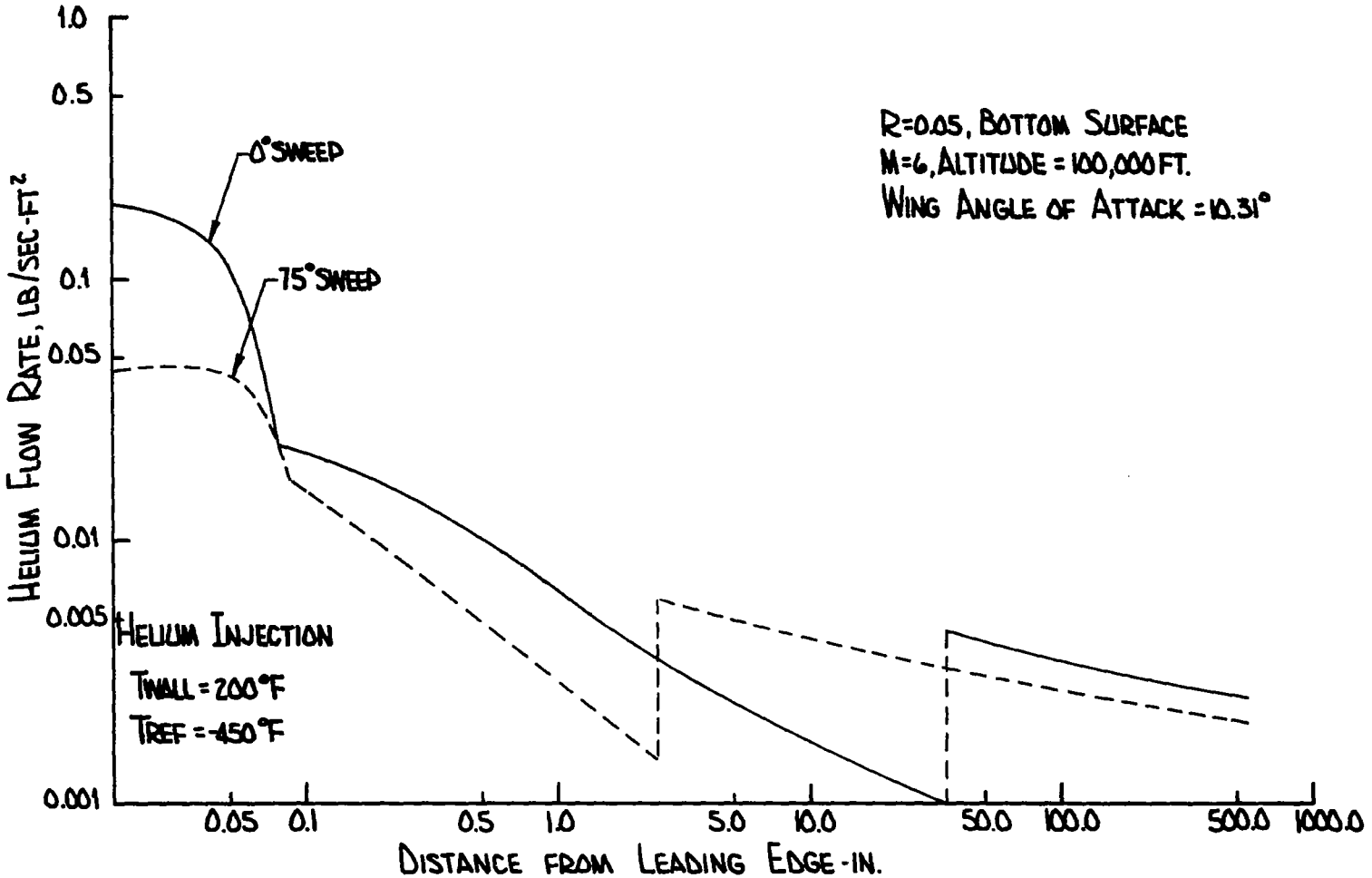

Figure 57. Helium Flow Rates for a 200°F Transpiration Cooled Bottom Surface for a 0.05 in. Leading Edge Radius and a -450°F Helium Inlet Temperature, M = 6.0, α = 10.31°, Altitude = 100,000 ft

TABLE XII

HELIUM TRANSPIRATION FLOW RATES, 200°F OUTER SURFACE TEMPERATURE, 0.05-INCH LEADING EDGE RADIUS

	100° Reference Temperature			-450°F Reference Temperature		
	Sweep Angles			Sweep Angles		
Wing Region	0°	45°	75°	0°	45°	75°
Leading Edge	21,700	37,900	72,700	6570	11,500	22,000
Top	17,300	13,600	6190	5760	4540	2060
Bottom	185,000	169,000	128,000	61,700	56,400	42,700
Total (lb/hr)	224,000	221,000	207,000	74,000	72,400	66,800

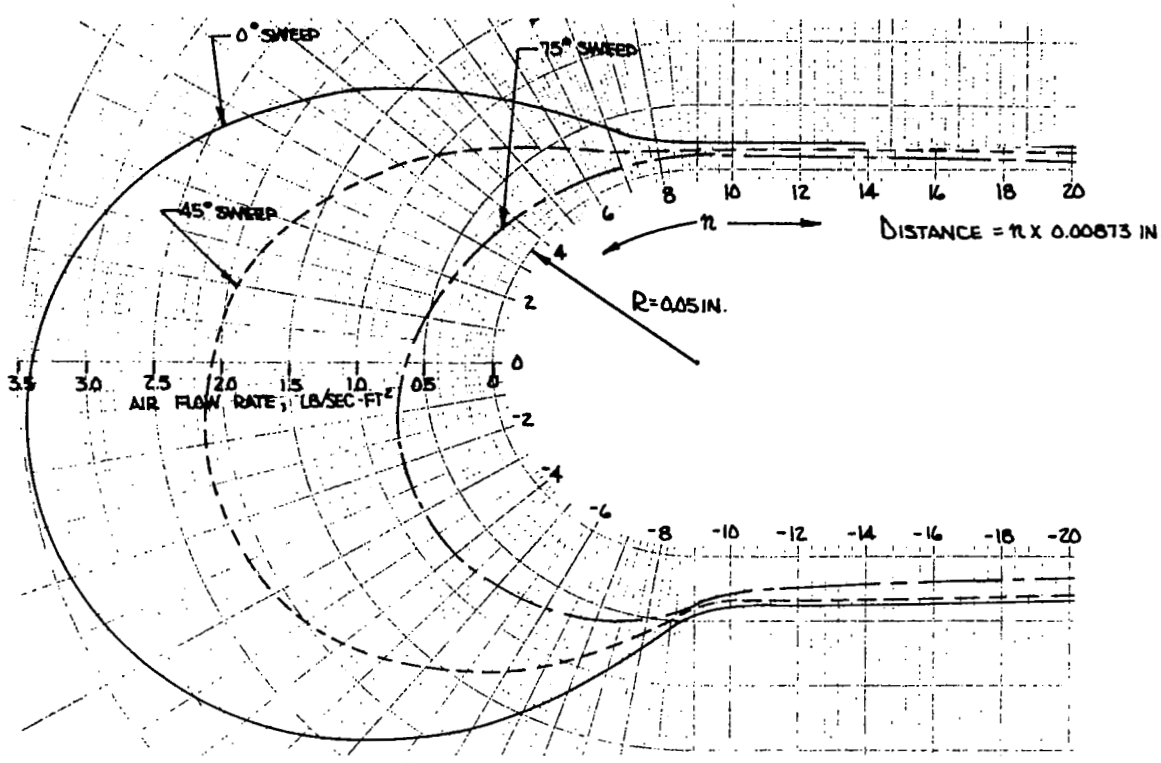

Figure 58. Air Flow Rates for a 200°F, 0.05 in. Radius, Transpiration Cooled Leading Edge for a 100°F Air Inlet Temperature, M = 6.0, α = 10.31°, Altitude = 100,000 ft

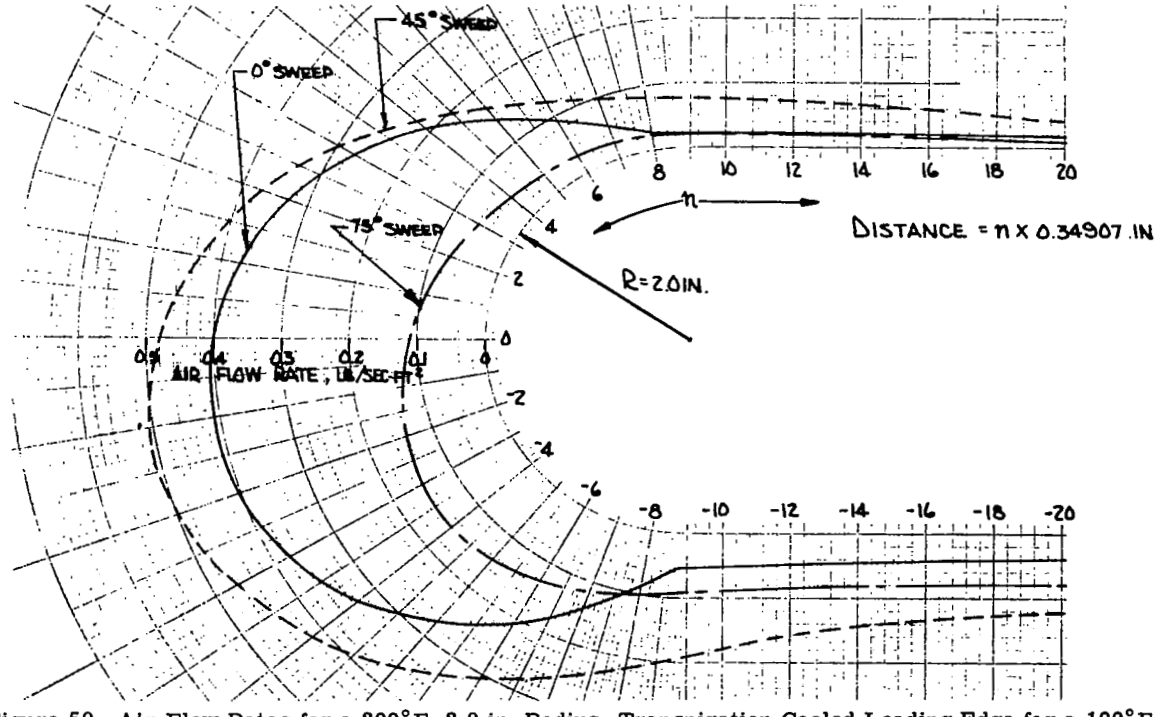

Figure 59. Air Flow Rates for a 200°F, 2.0 in. Radius, Transpiration Cooled Leading Edge for a 100°F Air Inlet Temperature, M = 6.0, α = 10.31°, Altitude = 100,000 ft

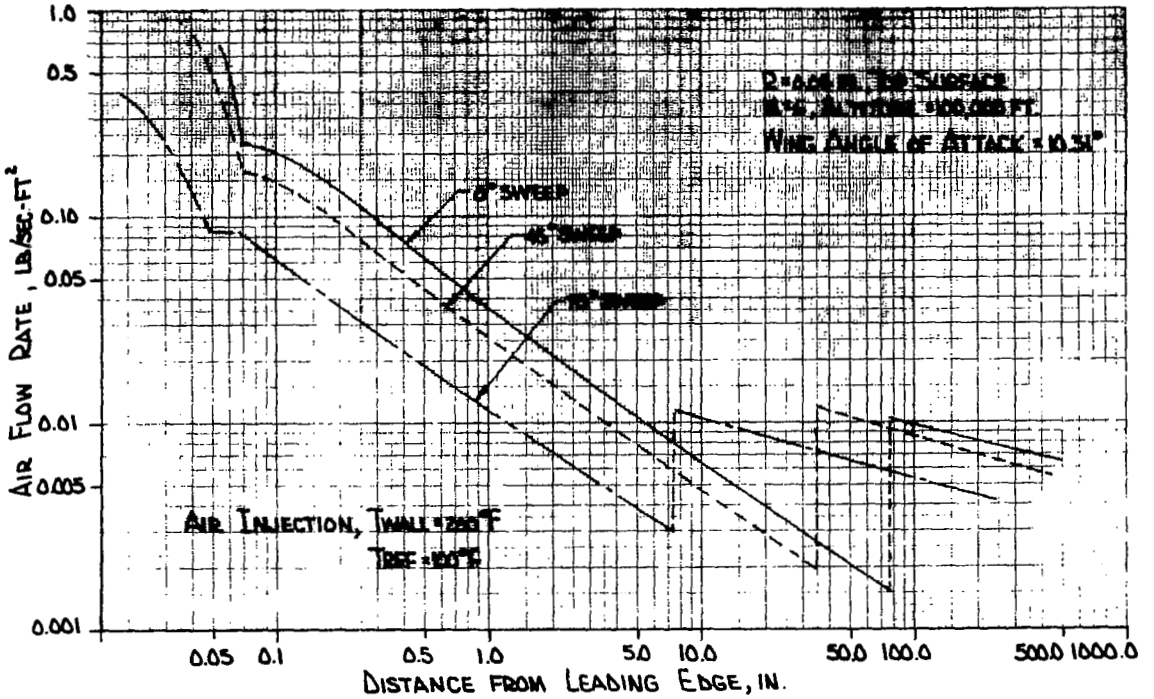

Figure 60. Air Flow Rates for a 200°F Transpiration Cooled Top Surface for a 0.05 in. Leading Edge Radius and a 100°F Air Inlet Temperature, M = 6.0, α = 10.31°, Altitude = 100,000 ft

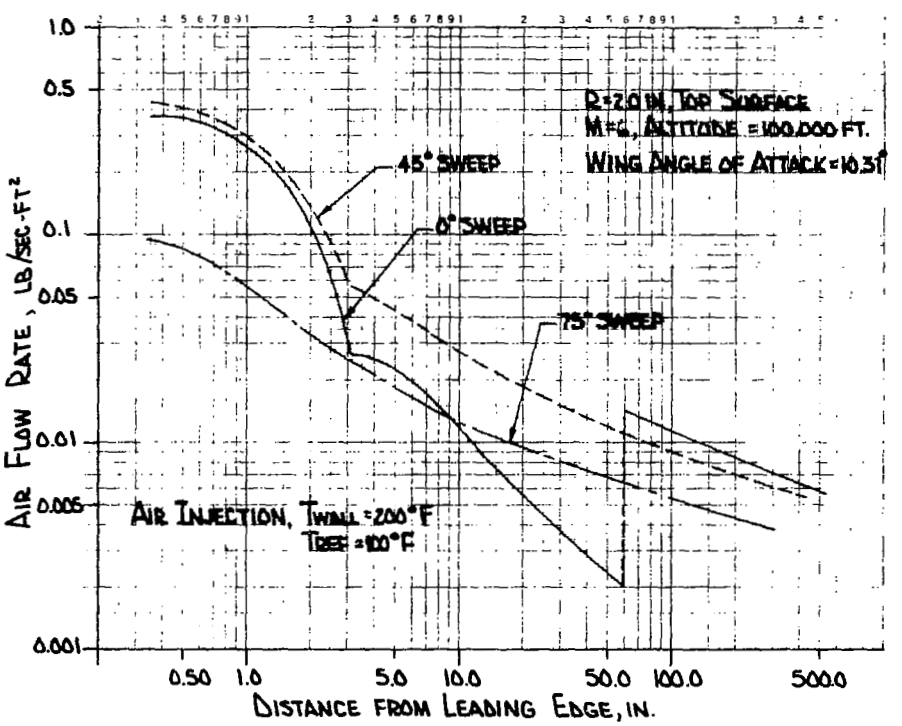

Figure 61. Air Flow Rates for a 200°F Transpiration Cooled Top Surface for a 2.0 in. Leading Edge Radius and a 100°F Air Inlet Temperature, M = 6.0, α = 10.31°, Altitude = 100,000 ft

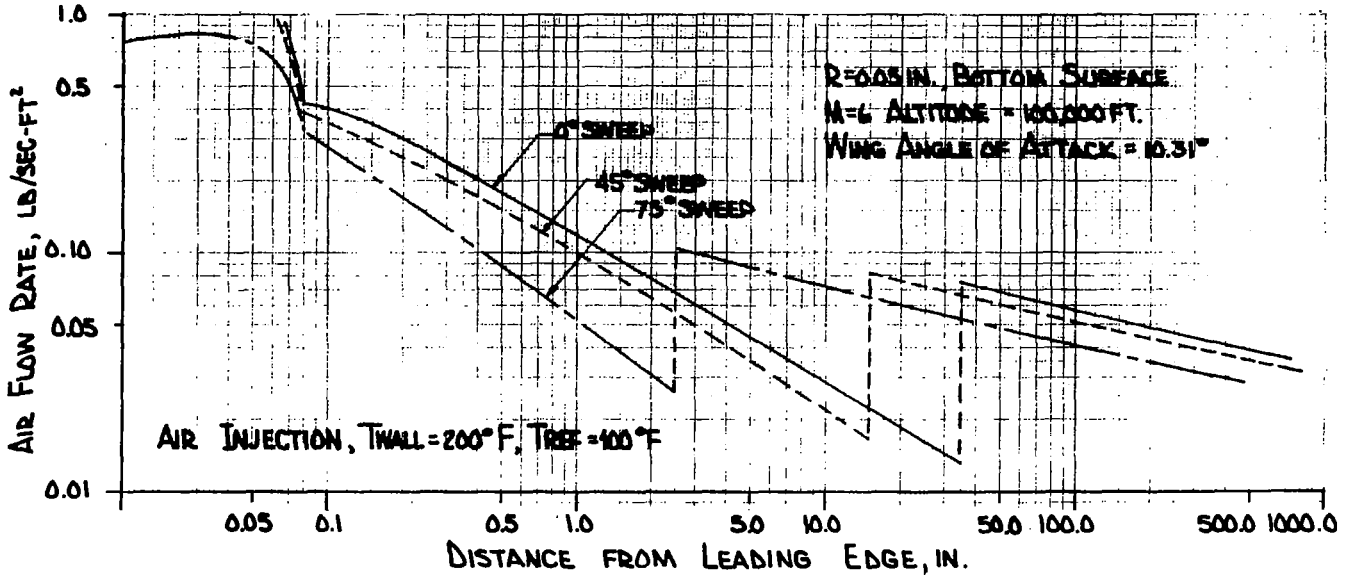

Figure 62. Air Flow Rates for a 200°F Transpiration Cooled Bottom Surface for a 0.05 in. Leading Edge Radius and a 100°F Air Inlet Temperature, M = 6.0, α = 10.31°, Altitude = 100,000 ft

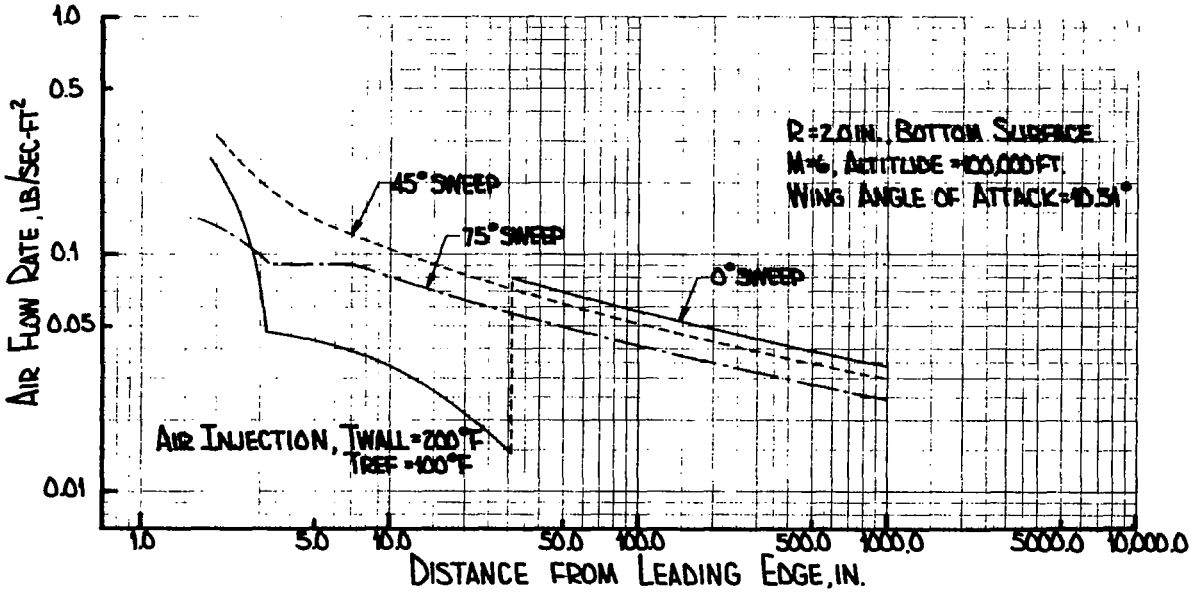

Figure 63. Air Flow Rates for a 200°F Transpiration Cooled Bottom Surface for a 2.0 in. Leading Edge Radius and a 100°F Air Inlet Temperature, M = 6.0, α = 10.31°, Altitude = 100,000 ft

TABLE XIII

AIR TRANSPIRATION FLOW RATES, 200°F OUTER SURFACE TEMPERATURE, 100°F REFERENCE TEMPERATURE

Wing Region	Flow Rate (lb/hr)	0.05-inch Leading Edge Radius			2.0-inch Leading Edge Radius		
		Sweep Angles			Sweep Angles		
		0°	45°	75°	0°	45°	75°
Leading Edge	Air	117,000	205,000	395,000	151,000	338,000	435,000
	Hydrogen	53,000	92,700	179,000	68,200	153,000	197,000
Top Surface	Air	93,500	73,400	33,600	97,300	67,100	33,900
	Hydrogen	42,300	33,200	15,200	44,100	30,400	15,300
Bottom Surface	Air	999,000	913,000	694,000	999,000	898,000	705,000
	Hydrogen	452,000	413,000	314,000	452,000	406,000	319,000
Totals (lb/hr)	Air	1,210,000	1,190,000	1,120,000	1,250,000	1,300,000	1,180,000
	Hydrogen	547,000	539,000	508,000	564,000	590,000	531,000

Note: Air Temperature Change = 2640°R
Hydrogen Temperature Change = 400°R

Figures 58 and 59 present leading edge hemicylinder air flow rate data for the minimum and maximum radii, 0.05-inch and 2.0-inch respectively. For a 0.05-inch radius, the leading edge is in a laminar flow regime for all sweep angles. For a fixed location on a leading edge hemicylinder flow rates decrease approximately with the cosine of the sweep angle as sweep angle increases from 0° to 75°. When the leading edge radius is increased to 2.0 inches turbulent leading edge effects cause noticeable changes in the data. For 0° sweep the leading edge is in a laminar flow regime while for 45° or greater sweep angles the leading edge is in a turbulent flow regime. Due to turbulent leading edge effects flow rates for a 45° sweep are above those for 0° sweep on the leading edge hemicylinder. This effect must be remembered if transpiration cooling is to be considered for the leading edge hemicylinder only.

Transpiration flow rate data for air on the top surface is presented in Figures 60 and 61. The 0.05-inch leading edge radius case is presented in Figure 60 and shows the expected laminar to turbulent transition on the flat surface with transition moving forward as sweep angle increases. For a 2.0-inch leading edge radius the turbulent leading edge effects are carried onto the top flat surface with 45° sweep flow rates above 0° sweep flow rates until the 0° sweep case makes a laminar to turbulent transition approximately 60.0 inches aft of the leading edge. The bottom surface transpiration flow rate data for 0.05 and 2.0-inch leading edge radii is presented in Figures 62 and 63 respectively. Transition effects are much the same on the bottom surface as on the top surface. For the 2.0-inch leading edge however, as seen in Figure 63, the transition point on the bottom surface is at approximately 30.0 inches from the leading edge as compared to 60.0 inches for the top surface. Again, comparing top and bottom surfaces, an order of magnitude difference in flow rates is seen with the higher flow rates on the highly heated bottom surface.

Table XII summarizes the air injection transpiration flow rate data for the 0.05 inch and 2.0-inch leading edge radii. A cursory examination of the results reveals flow rate variations from 33,600 lb/hr to 1,000,000 lb/hr as sweep angle and radius are varied. In Section 7 the feasibility of bringing ram air on board is investigated under a section on ram air convective cooling. In that section it is shown that 100,000 lb/hr of ram air could be taken on board with a large capture area scoop with reasonable drag penalties. As the air flow rates in Table XIII show, 100,000 lb/hr of ram air will transpiration cool only a small portion of the wing. Another major problem associated with this ram air system is the quantity of hydrogen necessary to cool the air. An estimate of the hydrogen flow rates required for the various radius-sweep angle perturbations is given in Table XIII. Considering that a hydrogen fuel load of approximately 200,000 lb is on board the aircraft, and that many other portions of the aircraft must be cooled, it becomes obvious that if the ram air transpiration system is practical for a 200°F outer surface temperature it is only applicable over a very limited area of the wing. It should again be emphasized that these conclusions have been based on calculations for a 200°F outer surface temperature and when wall temperature variations are presented later in this section this system in particular will appear more attractive.

The effect of leading edge radius on transpiration flow rates can be seen in Table XIII. In a gross sense leading edge radius does not affect system selection results significantly although it will play an important part in detailed system designs.

As a final point under air transpiration system studies, mention must be made of the similarity in properties between air and nitrogen. The air flow rates presented in Table XIII are very close to those which would be calculated for a nitrogen transpiration system. Although air was considered as a possible transpirant because it could be brought on board through a ram air scoop, nitrogen might be considered as an inert alternative to a stored air system. However, both the stored air and stored nitrogen systems would be inferior to a stored helium system.

4. Steam Injection

As an alternative to the use of cryogenic or ram air coolants an investigation of the feasibility of transpiration cooling with water was conducted. For water transpiration three alternatives exist. A water evaporator remote from the transpiration system could be cooling the electronic equipment, the landing gear bay, etc, and then supplying the transpiration system with steam at about 100°F which is subsequently transpired. The transpiration cooling system could boil the water with the latent heat of vaporization of water absorbing a large percentage of the aerodynamic heat load. Again water vapor would be transpired. The third alternative would be a liquid water transpiration cooling system.

In this section the first of the above systems is investigated. Transpiration flow rates for steam injection for a 100°F inlet temperature and a 200°F outer surface temperature are presented in Figures 64, 65 and 66. These figures present local flow rates over the wing surface for the 0.05-inch leading edge configuration for a 200°F outer surface temperature. It has been assumed that the water has boiled in a location remote from the transpiration system and is introduced at the backface of the porous material at 100°F. Since the plotted results are very similar to those previously presented they need not be discussed.

Table XIV presents the integrated flow rates for the three wing divisions previously chosen and it is again seen that for a 200°F transpiration cooled outer surface only a very small portion of the wing could be cooled using steam injection. For such a system it does not appear feasible to cool more than a very small portion of the leading edge.

5. Water Injection

Although the transpiration cooling theories incorporated into the computer program described in the Appendix are strictly for gas injection, it was felt that they could be adapted for calculations involving water if appropriate corrections were made to account for the heat capacity associated with a liquid-vapor phase change. Figure 67 and Table XV show the results of a calculation of water flow rates done by lowering the steam reference temperature to a level low enough to account for the increased heat capacity from the liquid-vapor phase change. The data in Table XV shows almost an order of magnitude improvement over that in Table XIV for steam injection. To support the results of this brief investigation a more detailed series of analyses were conducted and are described in the following paragraphs.

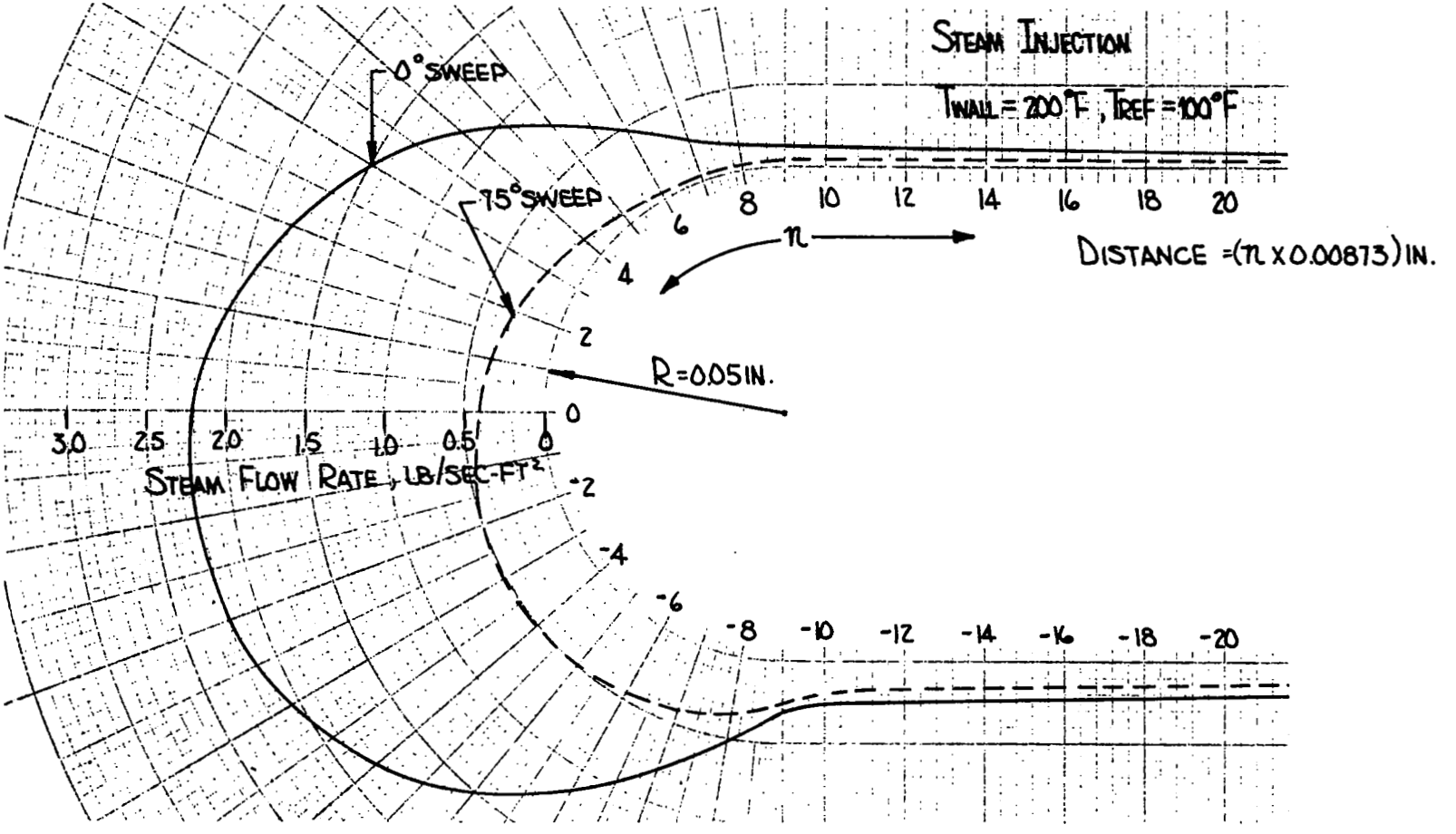

Figure 64. Steam Flow Rates for a 200°F, 0.05 in. Radius, Transpiration Cooled Leading Edge for a 100°F Steam Inlet Temperature, M = 6.0, α = 10.31°, Altitude = 100,000 ft

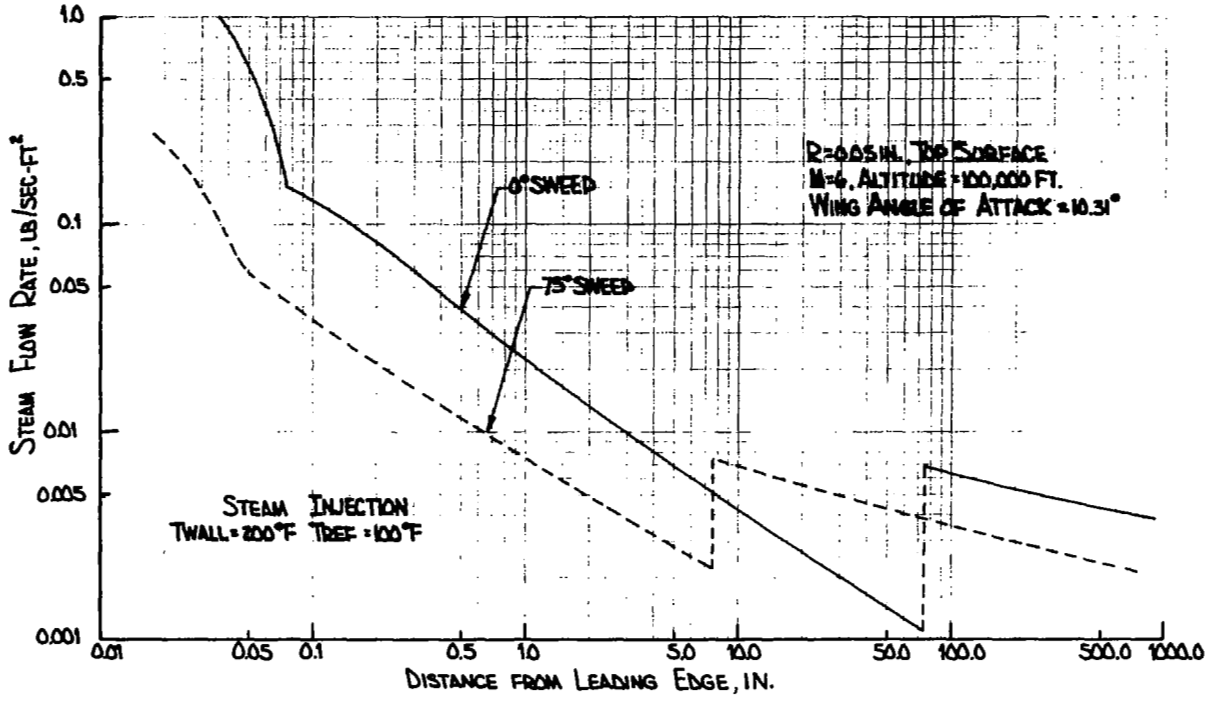

Figure 65. Steam Flow Rates for a 200°F Transpiration Cooled Top Surface for a 0.05 in. Leading Edge Radius and a 100°F Steam Inlet Temperature, M = 6.0, α = 10.31°, Altitude = 100,000 ft

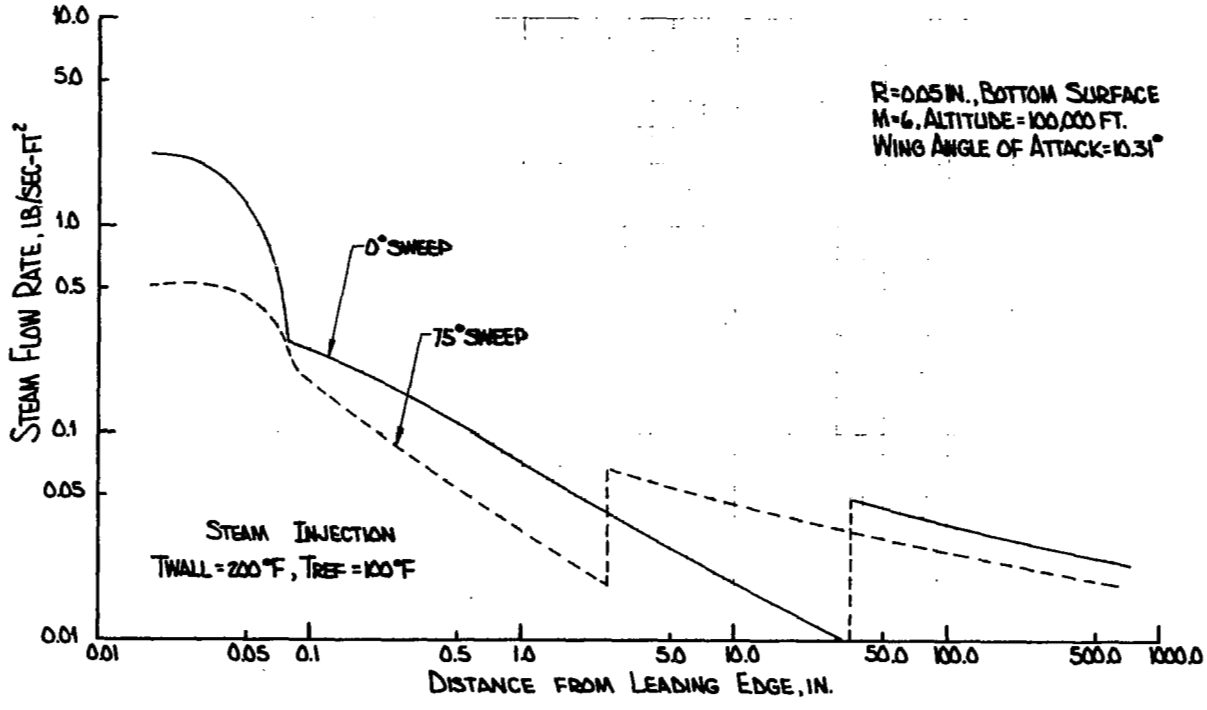

Figure 66. Steam Flow Rates for a 200°F Transpiration Cooled Bottom Surface for a 0.05 in. Leading Edge Radius and a 100°F Steam Inlet Temperature, M = 6.0, α = 10.31°, Altitude 100,000 ft

TABLE XIV

STEAM TRANSPIRATION FLOW RATES, 200°F OUTER SURFACE TEMPERATURE, 0.05-INCH LEADING EDGE RADIUS

100°F Reference Temperature

	Sweep Angles		
Wing Region	0°	45°	75°
Leading Edge	74,900	131,000	253,000
Top	59,800	47,000	21,600
Bottom	640,000	585,000	445,000
Total (lb/hr)	775,000	763,000	719,000

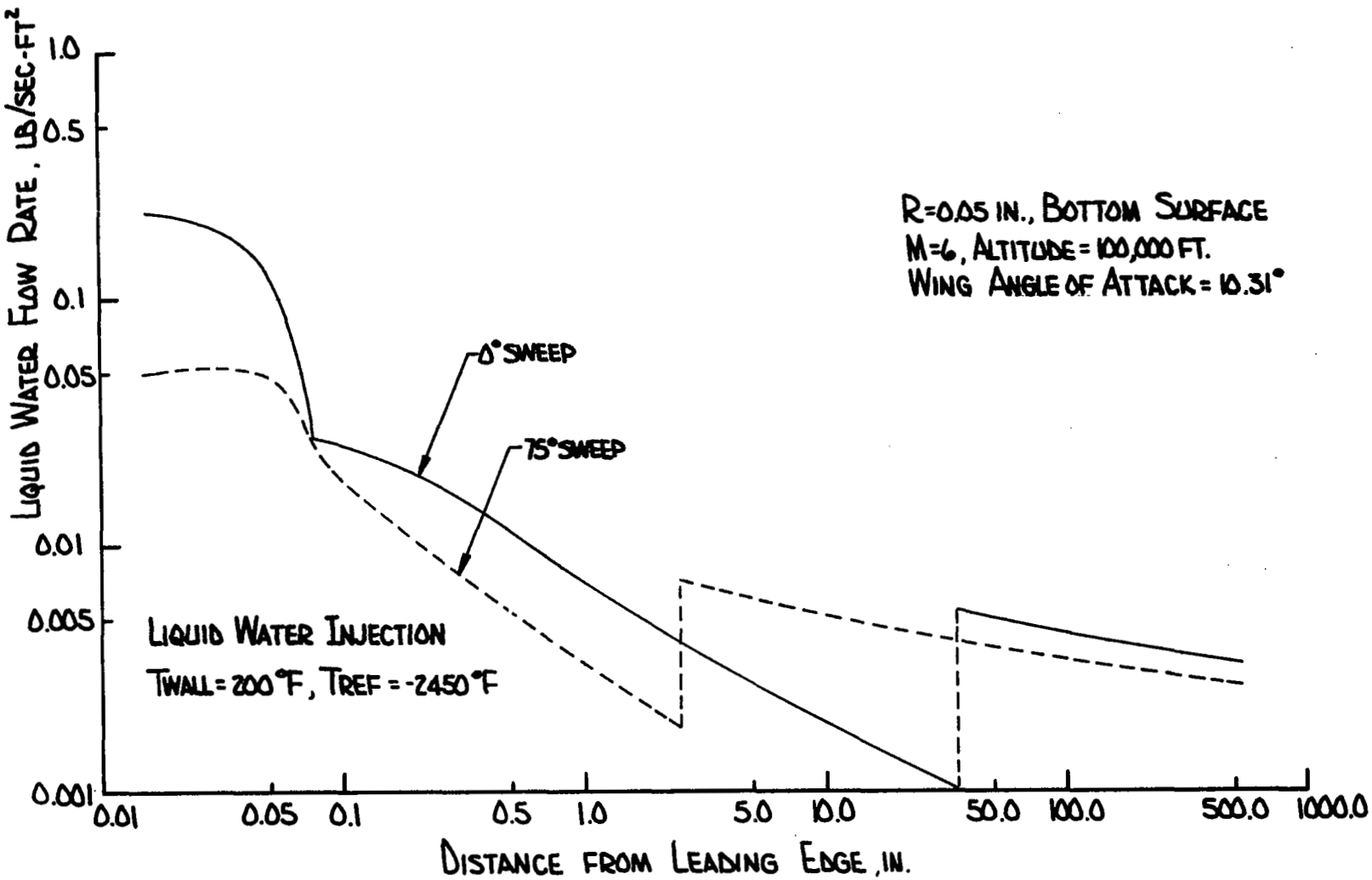

Figure 67. Water Flow Rates for a 200°F Transpiration Cooled Bottom Surface for a 0.05 in. Leading Edge Radius, M = 6.0, α = 10.31°, Altitude = 100,000 ft

TABLE XV

WATER TRANSPIRATION FLOW RATES, 200°F OUTER SURFACE TEMPERATURE
0.05-INCH LEADING EDGE RADIUS

-2450°F Reference Temperature

	Sweep Angles		
Wing Region	0°	45°	75°
Leading Edge	7500	13,100	25,300
Top	7470	5880	2700
Bottom	80,000	73,200	55,600
Total (lb/hr)	95,000	92,200	83,600

Suppose that instead of assuming the water turns to steam before leaving the porous surface, as was assumed above, it is assumed that the surface will be kept cool by forcing water through at a sufficient rate to maintain the surface wet. The solution to this problem can be expressed in terms of the variables in the Appendix and a familiarity with that development is now assumed.

A mass transfer driving force B can be defined as follows in terms of an enthalpy, i .

$$B = \frac{i_\infty - i_o}{i_o - i_{ref} + (q_{rad/m}'')}$$

There are a number of different ways to express the enthalpy of an air-water-vapor mixture and the following scheme is suggested as being adequate for this application. The scheme is that presented in Reference 28.

Air: Express t in °F, and let 0°F be the datum. Then,

$$i_\infty = C_P \left(t_\infty + \frac{r V_\infty^2}{2\, g_c\, J\, C_P} \right) = C_P\, t_R$$

$$i_o = C_P\, t_o$$

NOTE: t_R is the recovery temperature, °F

Water Vapor: Let the datum be liquid water at 32°F, then for water vapor,

$$i_{H_2O} = i_{fg,\,32} + C_{P_{H_2O}} (t - 32) = 1076 + 0.45\, t - 14$$

$$i_o = 0.45\, t_o + 1062$$

Air-Water-Vapor-Mixture: m_o is the mass concentration of water vapor at the air-water interface.

$$i_o = m_{air}\, i_{air} + m_o\, i_{H_2O} = (1 - m_o)\, i_{air} + m_o\, i_{H_2O}$$

$$i_o = (0.24 + 0.21\, m_o)\, t_o + 1062\, m_o$$

Pure Liquid Water:

$$i_{ref} = C_P\, (t_{ref} - 32) = t_{ref} - 32$$

In Reference 28 an alternate expression for B in terms of the concentration of water-vapor at the air-water interface, m_o, is developed and is,

$$B = \frac{m_o}{1 - m_o}$$

For an air-water-vapor mixture the mass concentration of water vapor in the mixture can be expressed in terms of the total pressure of the mixture P and the partial pressure of the water vapor P_o. If in the boundary layer there is an interface between liquid water and an air-water-vapor mixture, and if thermodynamic equilibrium exists at the interface, then P_o is the saturated vapor pressure of water at the interface temperature. Given t_R and P the mass transfer driving force B, can be uniquely determined, as well as the interface temperature t_o, which is also the surface temperature. The solution is an iterative one but is easily handled by a computer.

Values of t_R, the recovery temperature, are given in Table I. The local surface pressure P is a constant over much of the wing and since solutions for B can be used to determine the water flow rate parametric data was generated. Figure 68 presents a plot of B versus t_R and P for a range of pressures as found on the bottom surface of the wing.

To obtain the mass flow rate rigorously is a tedious calculation and not amenable to parametric studies. As a fair and conservative approximation to a turbulent boundary layer problem a mass flow rate expression can be developed assuming a Couette flow, constant property model. The resulting equation is given below in terms of: h, the uncooled heat transfer coefficient; C_P, the specific heat at constant pressure of the free stream; and B, the mass transfer driving force.

$$m'' = \frac{h}{C_{P\infty}} \ln (1 + B)$$

This expression yields flow rates above the rigorous solution by only partially accounting for the blocking effect. For zero blocking effect the ln(1 + B) term degenerates to B, thus, the blocking effect can be estimated as follows:

B	ln(1 + B)	Blocking Effect
0.6	0.470	22%
0.5	0.405	19%
0.4	0.336	16%
0.3	0.262	13%
0.2	0.182	9%
0.1	0.095	5%

As can be seen the blocking effect approaches zero as B approaches zero which is the expected trend. Figure 69 presents water flow rates versus B and h for this Couette flow, constant property model.

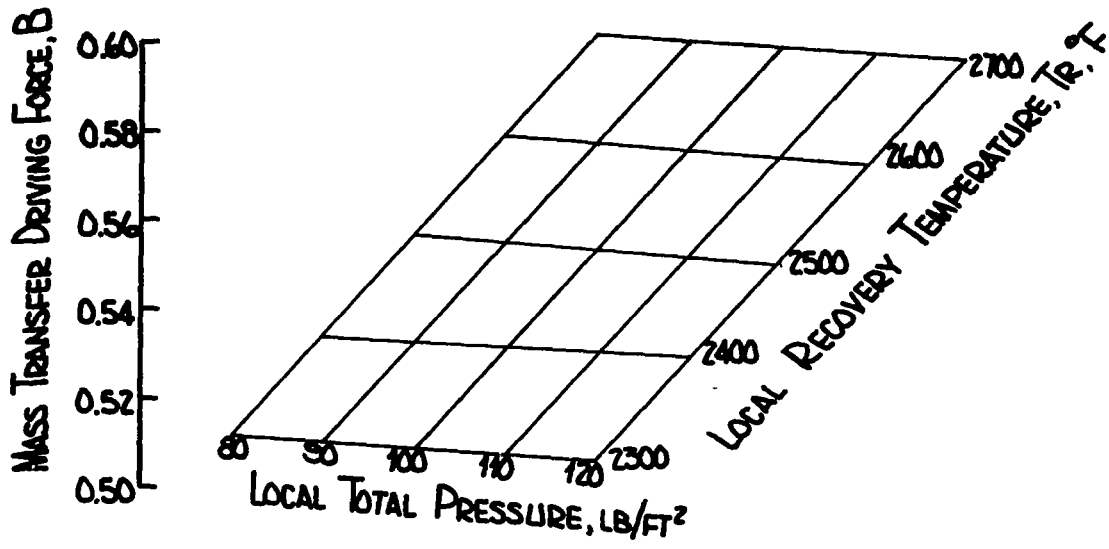

Figure 68. Mass Transfer Driving Force, B for Liquid Water Injection versus Local Total Pressure, P and Local Recovery Temperature, T_R

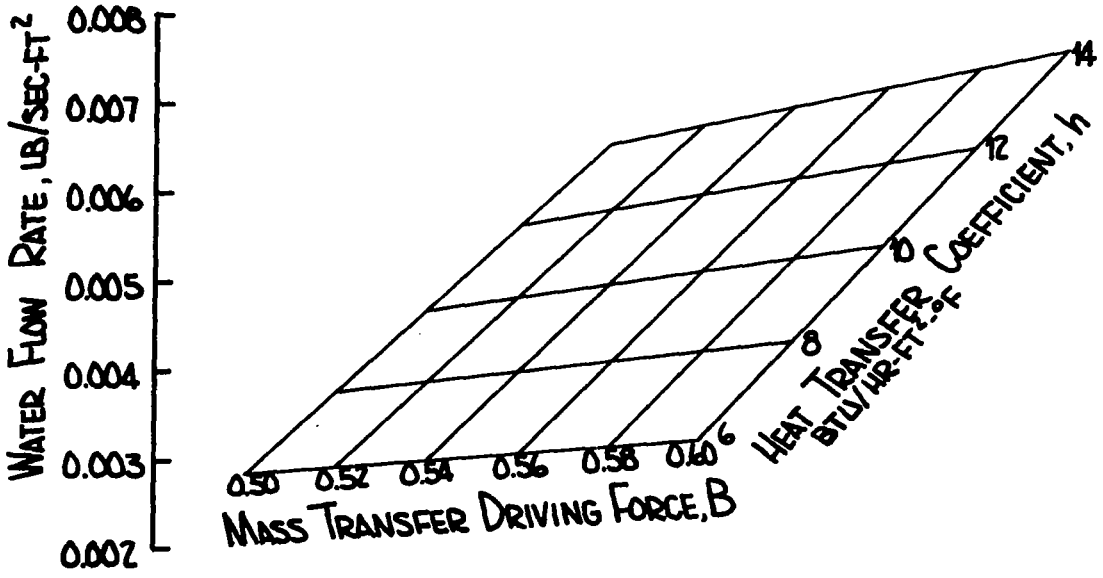

Figure 69. Water Flow Rates versus Mass Transfer Driving Force, B and Heat Transfer Coefficient, h

Data for water injection is presented in Figures 68 and 69 and the results are unexpectedly linear. Although these plots appear linear, extrapolation much beyond the range of the variables presented is not recommended. One variable in the problem solution is not given in Figures 68 and 69. The wet surface temperature is between 50°F and 70°F for the range of variables presented in these figures.

Using typical values of the defining parameters, a comparison with results in Figure 67 can be made. The local pressure and recovery temperature on the bottom wing surface are approximately 100 psf and 2500°F respectively. For these values of pressure and temperature the corresponding value of B from Figure 68 is 0.554. For a 0° sweep wing, 0.05-inch leading edge radius, 60.0 inches back on the bottom surface the heat transfer coefficient is 10.0 Btu/hr-ft^2-°F (Figure 16). Using these values of B and heat transfer coefficient the corresponding water flow rate from Figure 69 is 0.005 lb/sec-ft^2. This checks very well with the value predicted on Figure 67 for the 0° sweep wing. With the above presentation as verification of the T_{ref} = -2450.0°F method used in Figure 67 the water flow rates tabulated in Table XV were used for water injection. The reference temperature method was also used for outer surface temperature variations using liquid water.

6. Wall Temperature Variations

As mentioned earlier, data was generated for a number of different wall temperatures (outer surface temperatures). Referring to the radiation equilibrium wall temperature data presented earlier it is apparent that the range of applicable wall temperatures is dependent on the location on the wing surface. For the 0.05-inch leading edge radius hemicylinder, uniform wall temperatures up to 1400°F are feasible. On the top surface uniform temperatures up to 600°F could be attained while on the bottom surface uniform temperatures up to about 1100°F could be attained. In this section estimates of transpiration flow rates are made for various wall temperatures within the applicable range for each surface.

Examination of computer results for the transpirants under consideration revealed that the variation of flow rate with outer surface temperature could be summarized by the curves given in Figure 70. These curves are plotted on semi-logarithmic graph paper and are nearly straight implying that flow rates decrease exponentially as outer surface temperature is increased. It was also noticed that this relationship was valid for the range of reference temperatures studied. Figures 71 through 76 show the numerical values of flow rate for specific outer surface temperatures and reference temperatures for hydrogen, helium, air and water transpiration. Selected data from Figures 71 through 76 are summarized in Tables XVI and XVII. In these tables the minimum flow rates for transpiration cooling the entire wing are presented.

In Table XVI the use of a 100°F structure is incorporated into the title to again emphasize that the coolant inlet temperature and the porous material backface temperature are equal and that an aluminum structure and plumbing could be used. The boiling water temperature of 80°F is an estimate of the temperature at which the water would boil with sufficient pressure to drive the steam through the porous material into the boundary layer. Examination of the total flow rates in Table XVI reveals that about

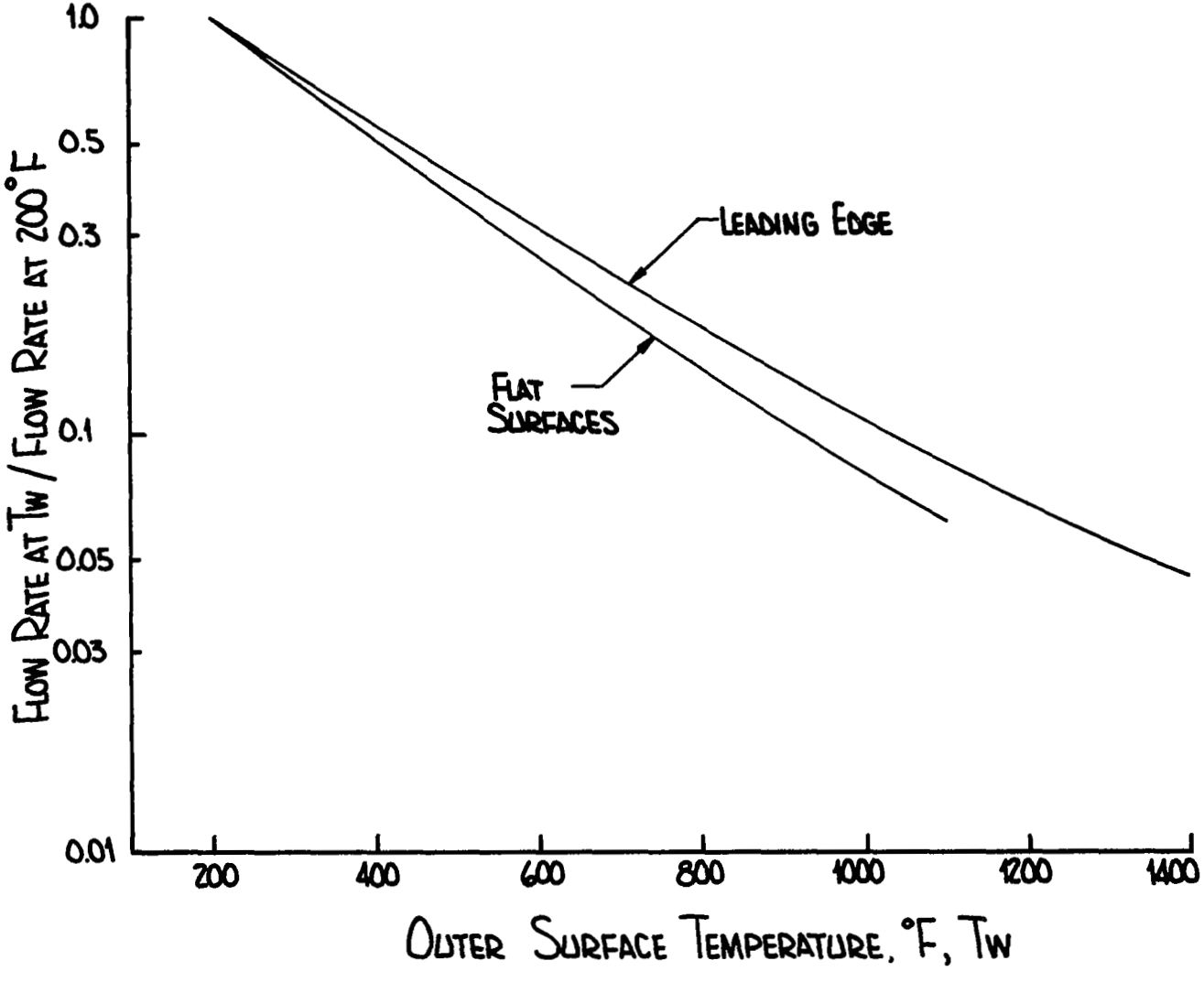

Figure 70. Flow Rate Variation versus Outer Surface Temperature

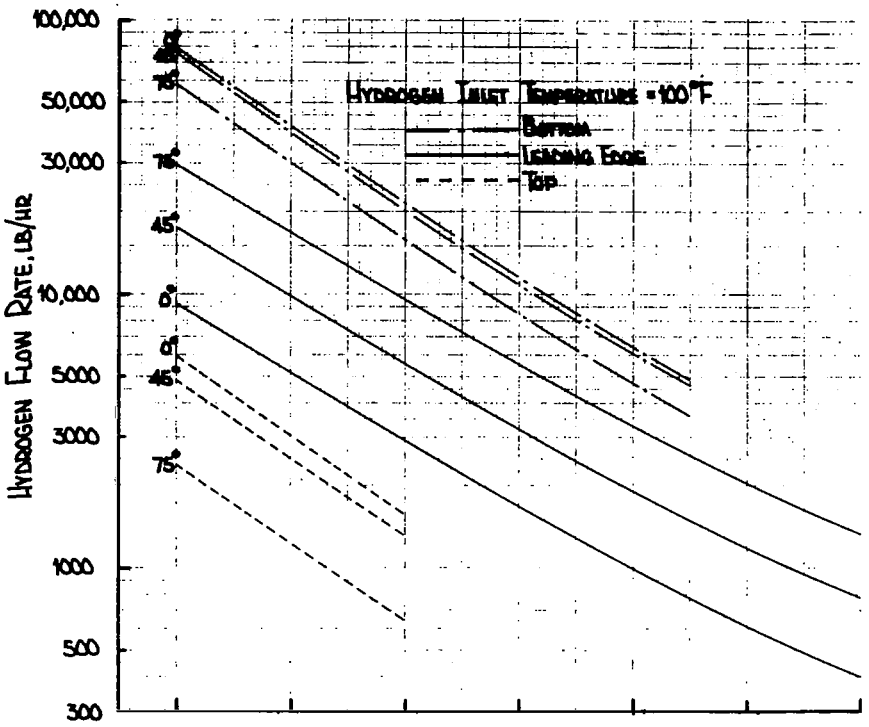

Figure 71. Hydrogen Flow Rate versus Outer Surface Temperature for a Hydrogen Inlet Temperature of 100°F and a 0.05 in. Leading Edge Radius, M = 6.0, α = 10.31°, Altitude=100,000 ft

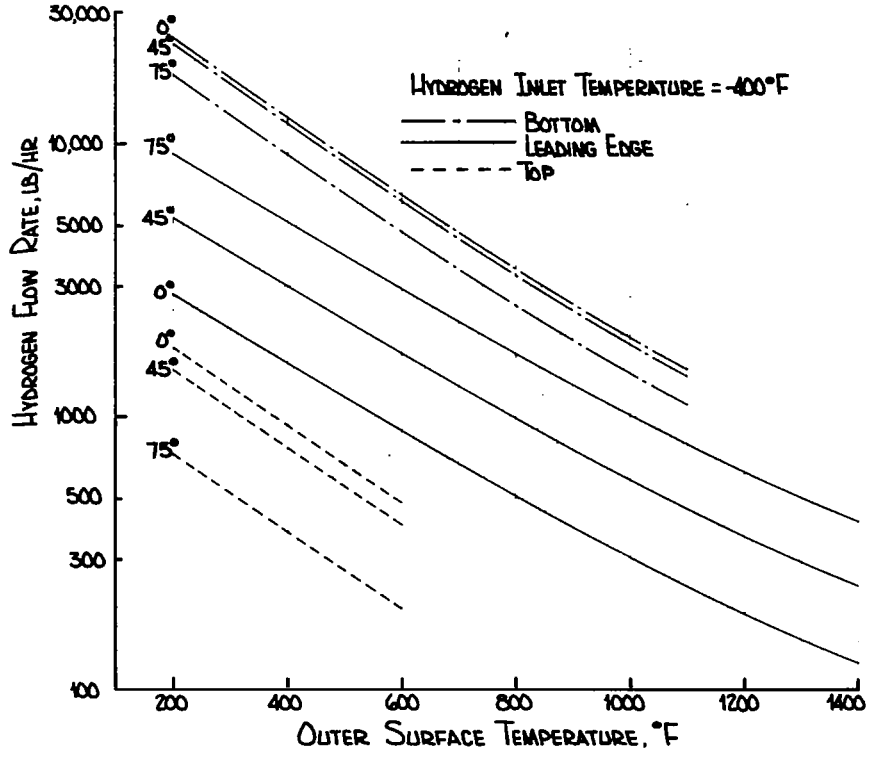

Figure 72. Hydrogen Flow Rate versus Outer Surface Temperature for a Hydrogen Inlet Temperature of -400°F and a 0.05 in. Leading Edge Radius, M = 6.0, α = 10.31°, Altitude = 100,000 ft

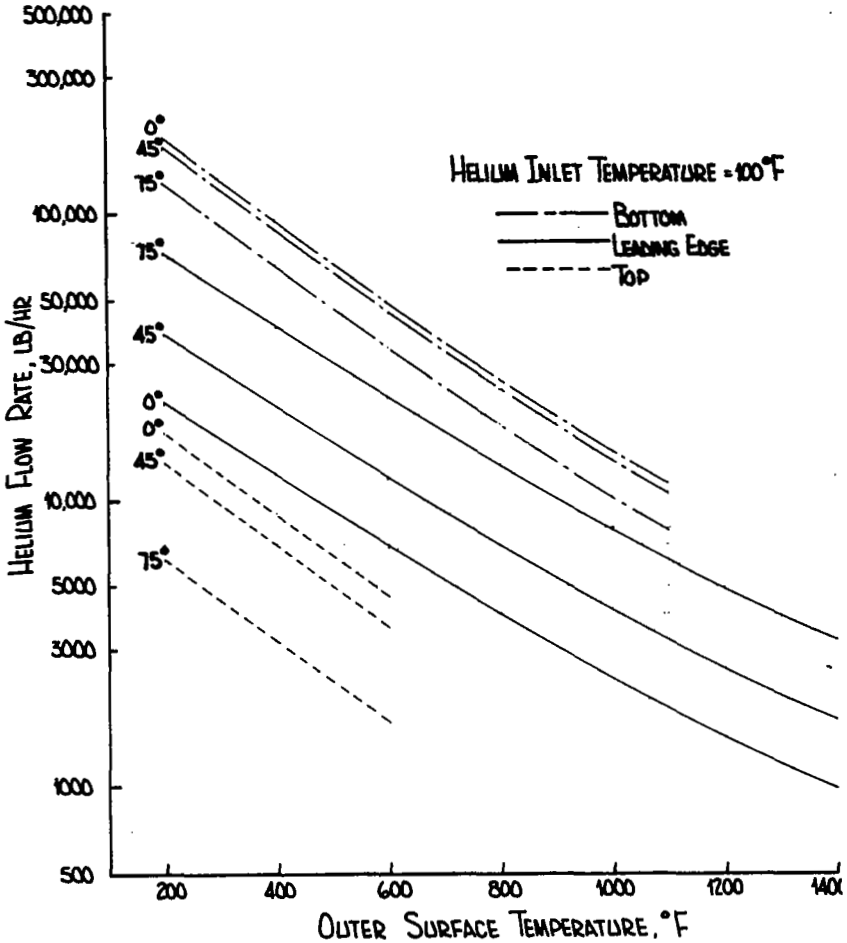

Figure 73. Helium Flow Rate versus Outer Surface Temperature for a Helium Inlet Temperature of 100°F and a 0.05 in. Leading Edge Radius, M = 6.0, α = 10.31°, Altitude = 100,000 ft

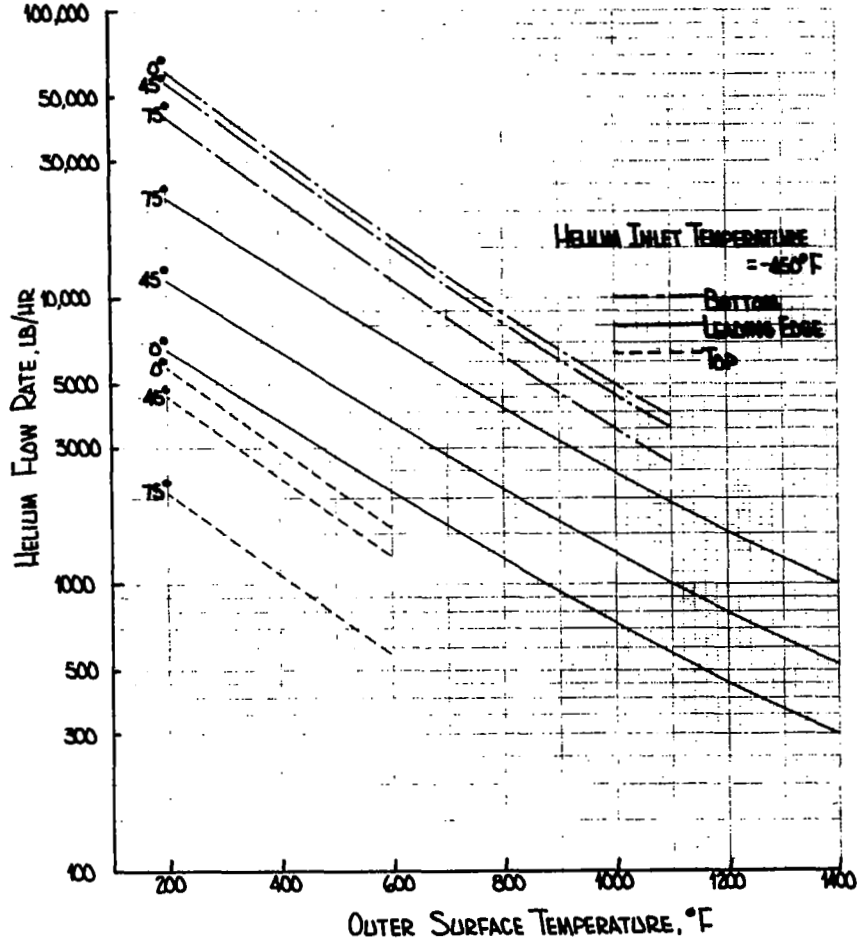

Figure 74. Helium Flow Rate versus Outer Surface Temperature for a Helium Inlet Temperature of -450°F and a 0.05 in. Leading Edge Radius, M = 6.0, α = 10.31°, Altitude = 100,000 ft

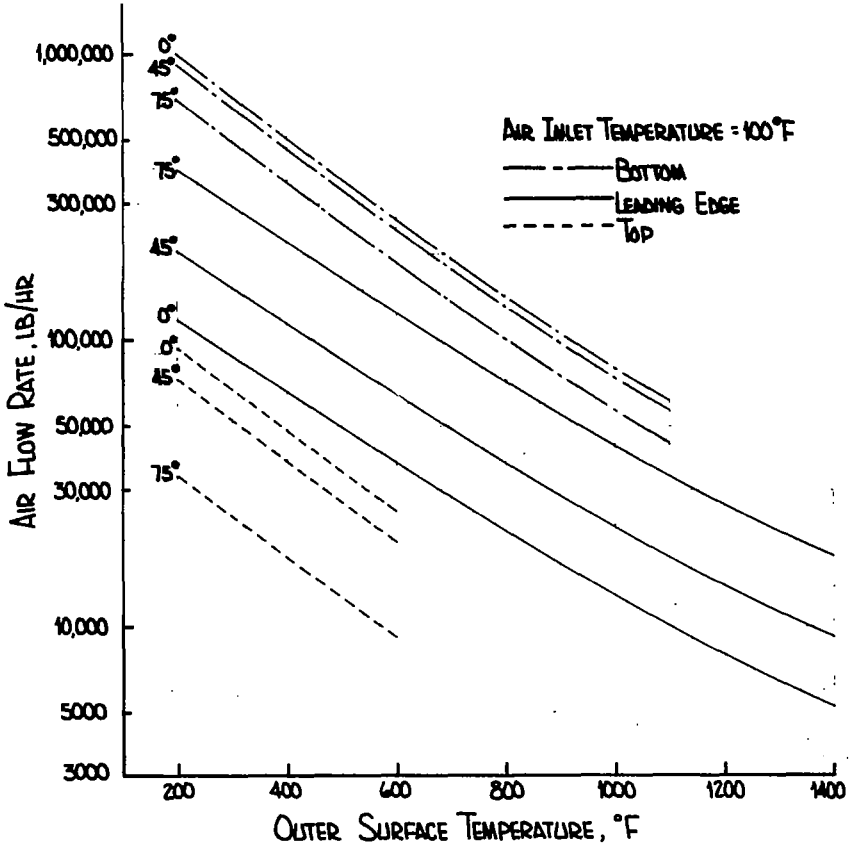

Figure 75. Air Flow Rate versus Outer Surface Temperature for an Air Inlet Temperature of 100°F and a 0.05 in. Leading Edge Radius, M = 6.0, α = 10.31°, Altitude = 100,000 ft

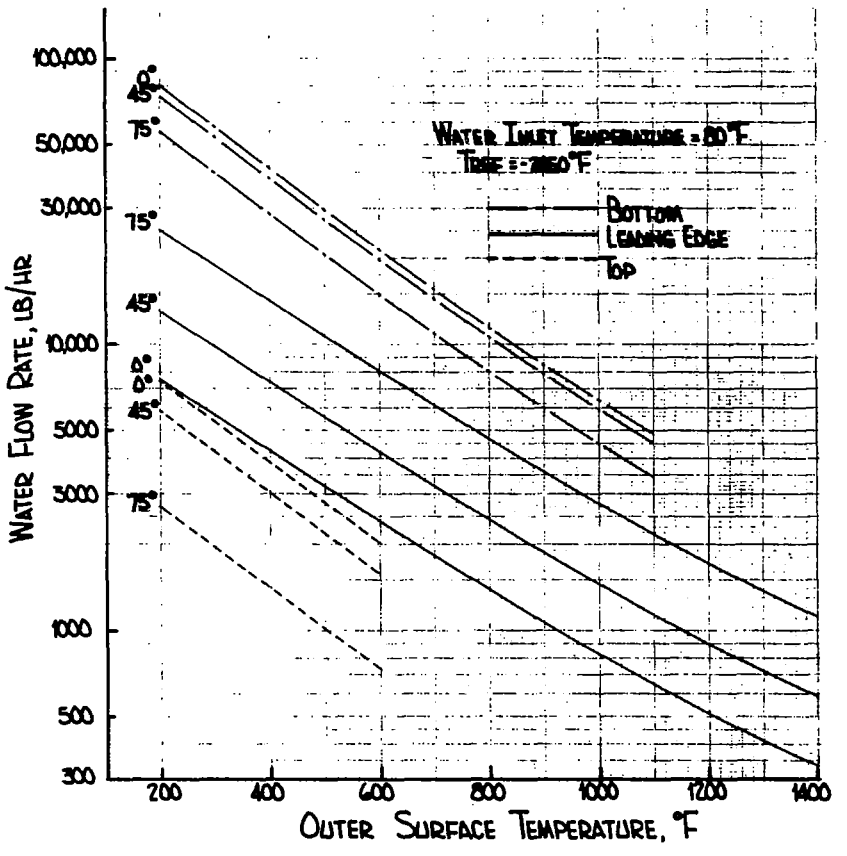

Figure 76. Liquid Water Flow Rate versus Outer Surface Temperature for Water Boiling at 80°F and a 0.05 in. Leading Edge Radius, M = 6.0, α= 10.31°, Altitude = 100,000 ft

TABLE XVI

MINIMUM FLOW RATES FOR TRANSPIRATION COOLING
THE ENTIRE WING; 100°F STRUCTURE(2)(3)
WITH HIGH TEMPERATURE POROUS MEDIA

Wing Region	Outer Surface Temperature(1) (°F)	Mass Flow Rate, lb/hr											
		Hydrogen Injection (2)			Helium Injection (2)			Air Injection (2)			Liquid Water Injection (3)		
		Sweep Angle			Sweep Angle			Sweep Angle			Sweep Angle		
		0°	45°	75°	0°	45°	75°	0°	45°	75°	0°	45°	75°
Leading Edge	1400	411	784	1340	979	1710	3270	5270	9210	17,800	337	590	1140
Top Surface	600	1570	1300	642	4670	3670	1670	25,200	19,800	9080	2020	1590	729
Bottom Surface	1100	4890	4630	3580	11,500	10,500	7950	61,900	56,600	43,000	4960	4540	3450
Total (lb/hr)	--	6870	6720	5570	17,100	15,900	12,900	92,400	85,700	69,800	7300	6710	5320

NOTES: (1) Outer surface of non-structural porous material
(2) Structure temperature is equal to the transpirant inlet temperature of 100°F
(3) Structure temperature is equal to the boiling water temperature of 80°F

TABLE XVII

MINIMUM FLOW RATES FOR TRANSPIRATION COOLING THE ENTIRE WING WITH CRYOGENIC COOLANT

Wing Region	Outer (1) Surface Temperature °F	Mass Flow Rate, lb/hr					
		Hydrogen Injection (2)			Helium Injection (3)		
		Sweep Angle			Sweep Angle		
		0°	45°	75°	0°	45°	75°
Leading Edge	1400	126	241	413	295	517	991
Top Surface	600	484	400	197	1560	1220	557
Bottom Surface	1100	1500	1430	1100	3800	3500	2650
Total (lb/hr)	–	2110	2070	1710	5670	5240	4200

NOTES:

(1) Outer Surface of Non-Structural Porous Material
(2) Hydrogen Inlet Temperature = -400°F
(3) Helium Inlet Temperature = -450°F
(4) Nominal Structural Operating Temperature = 100°F

6000 lb/hr of hydrogen or water would be needed to cool the wing for a hydrogen inlet temperature of 100°F or a boiling water temperature of 80°F. As will be seen later in this section, this quantity of water or hydrogen could be carried on board for approximately the same weight penalty. The flow rates of helium and air required, approximately 15,000 lb/hr and 85,000 lb/hr respectively, appear too high to enable these transpirants to be considered for cooling the entire wing. It should be mentioned however, that it is conceivable to ingest an air flow rate of 85,000 lb/hr. The main reason for rejecting the air system for the entire wing is that the quantity of hydrogen required to cool the incoming air is more than the quantity of hydrogen available on board the aircraft.

Table XVII tabulates data for the two cryogenic coolants examined, hydrogen and helium. The total flow rates for helium are approximately 2.5 times those for hydrogen. For helium entering at -450°F approximately 5000 lb/hr would be needed while only 2000 lb/hr of -400°F hydrogen is needed. A structure temperature was not listed for these cryogenic coolants because the exact number is a complex function of cooling system detailed design. However, the problem is not one of the structure exceeding 100°F or the permissible use temperature of aluminum, but one of the structure becoming too cold. An elaborate (and heavy) insulation system would be needed to prevent the structure from being cooled below the dew point.

System weights for the transpiration systems presented in Tables XVI and XVII are discussed later in this section. The details of a transpiration system were not considered until film cooling flow rates were estimated and the feasibility of film cooling investigated.

B. FILM COOLING

The predominant boundary layer mechanism for the baseline wing is turbulent flow. Since the standard compressible turbulent boundary layer has not yielded to a rigorous analytical treatment, little in the way of theoretical predictions exists in the area of film cooling for the present application. A comparison of convection, transpiration and film cooling techniques was first discussed by Eckert and Livingood (Reference 30) in 1954. Their conclusion was that over the range of parameters of interest $10^3 \leq Re_X \leq 10^9, P_R = 0.7$, transpiration cooling was clearly superior. Experimental verification of this conclusion is available in the literature, but analytical techniques for prediction of flow rates for film cooling degenerate to correlations such as that proposed by Hatch-Papell, Reference 29.

For purposes of this project a method of obtaining film cooling flow rates based on the Hatch-Papell correlation (Reference 29) was used for initial investigations. Using this correlation film cooling flow rates were found to be about 2.5 times greater than the corresponding transpiration flow rates, due to an estimate of small blocking effects for film cooling. If blocking effects are totally neglected, film cooling flow rates would be about 3.0 times the transpiration flow rates presented earlier. For the present application the blocking effect for gases in film cooling is small resulting in the conclusion that transpiration cooling is clearly superior to film cooling as noted in Reference 30. However, for liquids such as water, the analyses presented earlier for transpiration cooling still are applicable for film cooling and suggest that flow rates are independent of the method of injection as long as the injection technique can maintain the surface wet. If

this is true a liquid film cooling system would probably be superior to a transpiration system because of the somewhat lighter distribution system, better structural efficiency of perforated sheet as compared to porous sheet, and a smaller probability of clogging.

To design a film cooling system information concerning the effect of the slot is necessary in addition to a flow rate per unit area for the system. For laminar flows there have been reported many analyses concerning the effectiveness of film cooling. Eckert, using the results obtained by Wieghardt (Reference 31) found that for single slots, when $X/a > 100$ the slot effectiveness η is given by,

$$\eta = \frac{T_W - T_C}{T_E - T_C} = 1 - 21.8 \left(\frac{\rho_C \, u_C}{\rho_E \, u_E} \right)^{0.8} \left(\frac{X}{a} \right)^{-0.8}$$

where T_W is the wall temperature, X is the streamwise distance, T_C, T_E, u_C, u_E, and ρ_C ρ_E are the temperatures, velocities, and densities of the coolant and external flow field respectively (See Figure 77). Eckert considered a value of $\eta \geq 0.2$ as yielding "sufficient cooling".

To obtain results for $(X/a) < 100$ is a problem that is not easily resolved. The only effectiveness correlation available is that presented in Reference 32 and must be used very cautiously in the present application. As presented in this reference the effectiveness, η_o, was found to be correlated by the relation

$$\eta_o = 1 - 16.9 \left(\frac{\rho_C \, u_C}{\rho_E \, u_E} \right)^{0.8} \left(\frac{X}{a} \right)^{-0.8}$$

when $$\left(\frac{X}{a} \right) \Big/ \left(\frac{\rho_C \, u_C}{\rho_E \, u_E} \right) \geq 60$$

Because of the similarity between the above equation and Eckert's results and by comparison with very limited data from compressible experiments, very cautious use of the above equation may be justified.

Studies of compressible flow fields and film cooling have been presented in References 33, 34, and 35 and lead to the conclusion that the most desirable configuration is one such as that shown in Figure 77 with laminar flow in the slot. A laminar slot should allow a laminar film of coolant to completely cover the surface of the skin, substantially reducing both skin friction and convective heating. Convective heating which penetrates the laminar barrier must be absorbed by the coolant temperature change. Turbulent flow in the slots is considered unacceptable. A turbulent emission will induce turbulence in a laminar external flow field, increasing heating rates and possibly increasing drag. Emitting a turbulent coolant into a turbulent flow field reduces the possibility of a cool film in contact with the surface and makes prediction of wall temperatures almost impossible within the bounds of present theories and experiments. A supersonic experiment carried

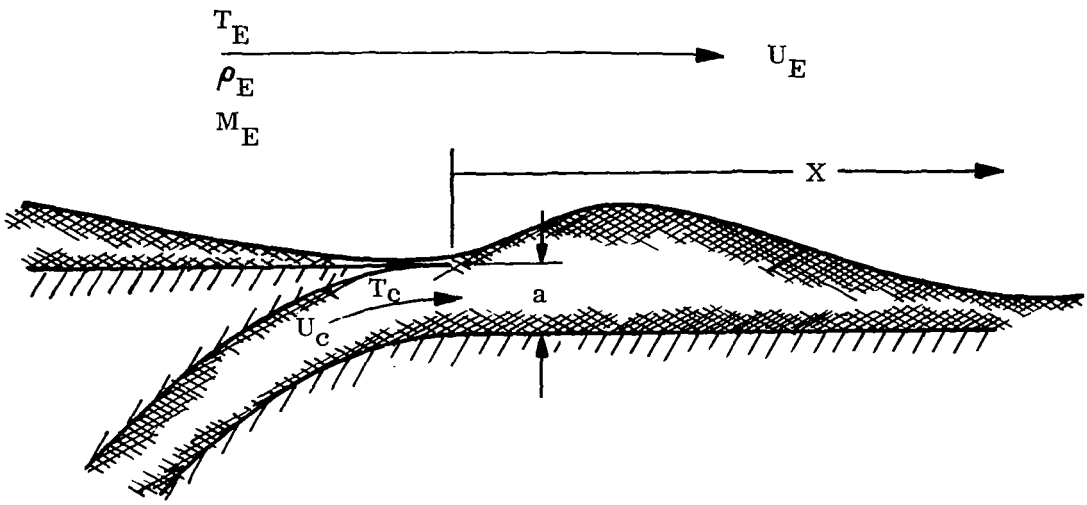

A. Suggested Slot Configuration

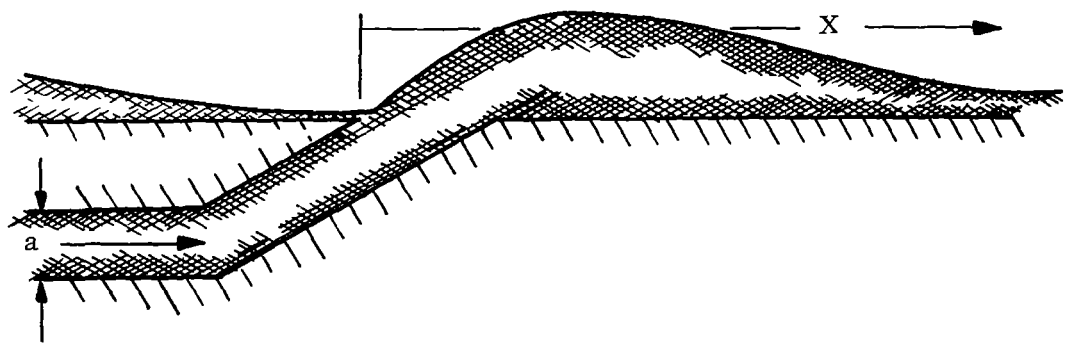

B. Alternate Slot Configuration

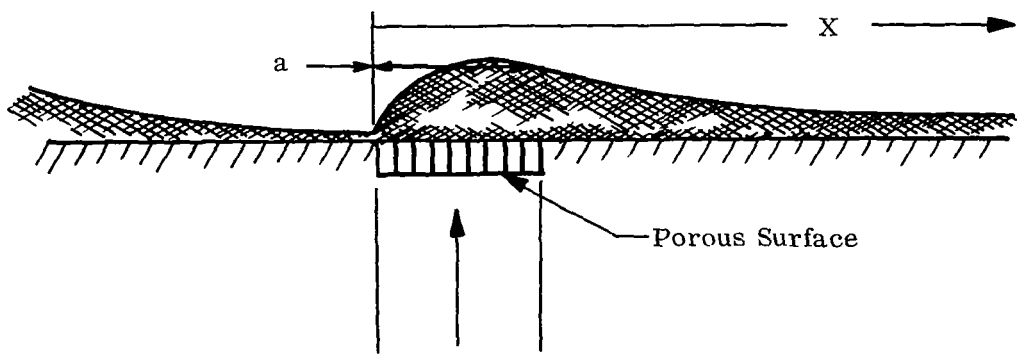

C. Porous Slot Configuration

Figure 77. Typical Film Cooling Inlet Configurations

out at Mach 3 is described in Reference 35 and concludes that the most effective slot configuration is a narrow slot with $a = 0.018$ inches. All slots with large, a, which were investigated produced an increase in skin friction (drag increase) apparently caused by an undesirable distortion of the external velocity profile.

The set of equations just presented can be used to size slots for the gaseous coolants under consideration. Calculations were carried out for hydrogen gas injection on the bottom surface of a 45° swept wing for a surface temperature of 200°F and a hydrogen inlet temperature of -400°F. One such calculation is outlined below.

For the bottom surface of a 45° swept wing at 100,000 ft, Mach 6, and 10.31° angle of attack, the external flow pressure, temperature, density and velocity are approximately 93 psf, 1212°F, 0.00104 pcf and 4560 fps over most of the flat region of the wing (From $S = 60$ inches to the rear of the wing).

Using the above data and a hydrogen inlet temperature of -400°F the cooling effectiveness is 0.372 and the following expression for (X/a) is obtained.

$$(X/a) = 60.5 \left(\rho_C \, u_C / \rho_E \, u_E \right)$$

Assuming a rectangular slot of width "b" and height "a" and defining a slot Reynolds number, the following relationship is obtained.

$$X = 153.0 \left(\mu_C \right) \left(Re_{slot} \right) (a + b/2b)$$

where: X = distance between slots, inches

μ_C = viscosity, lb/ft-sec.

Re_{slot} = slot Reynolds number, $\rho \, u_C \, D_h / \mu_C$

D_h = slot hydraulic diameter, $2ab/(a + b)$

Hatch-Papell's correlation assumes the hydrogen coolant is injected into the boundary layer at -400°F and the viscosity of hydrogen is evaluated at the inlet conditions. For these conditions the above expression becomes,

$$X = (1.0) \left(Re_{slot} \right) \left(\frac{a}{b} + 1 \right) \times 10^{-4}$$

Since slot heights of approximately 0.02 inches are desirable the slot width is fixed by the need for a Reynolds number between 1500 and 2000.

For the problem previously stated and at a position 450 inches from the leading edge the film cooling flow rate is 0.0024 lb/sec-ft^2 from Hatch-Papell's correlation. Assuming a slot width of 0.10 inches the resulting Reynolds number is approximately

500 for slots that are about 2.0 inches apart. The above calculation is typical of film cooling results for the baseline vehicle. It appears that reasonable slot separations are obtainable.

A similar set of equations is not available for liquid water injection with subsequent boiling and an experimental approach would have to be used to design such a system. At this point reasonable slot spacings were assumed to exist with justification for this assumption resting with experiments to be run at some future time.

Using the above discussion as a reference, a decision was made to eliminate film cooling with gases from further consideration on the basis of flow rate comparisons with transpiration cooling. Film cooling studies using water should be considered until a choice can be made between transpiration or film cooling using water injection. In the following section cooling system component weight estimates are made for both transpiration and film cooling systems.

C. COOLING SYSTEM COMPONENT WEIGHT ESTIMATES

The governing factor in designing either a transpiration or film cooling system is the attainment of a distribution of the injected fluid consistent with the external heat flux distribution. Simultaneous studies of typical wing structures led to the conclusion that the weight of the basic structural component is much greater than anticipated cooling system hardware weights. Therefore, the most desirable structural operating temperature levels are those which permit the use of low density structural alloys such as aluminum or titanium. Since coolant flow rate restrictions indicate that the coolant temperature rise must be maximized, coolant inlet temperatures will be 100°F or below, and the coolant will be able to maintain the structure at 200°F or below permitting the use of aluminum or titanium.

In Section 8 structural weights are presented for both cooled aluminum and cooled titanium wing structures. The skin thicknesses in these structures were assumed large enough to incorporate cooling passages for distributing the coolant. In this section weight estimates are made for those cooling system components which would be needed in addition to the wing structural weights presented in Section 8.

The possibility of designing a water transpiration cooling system using the liquid-vapor phase change appeared good based upon the flow rates presented earlier (Table XVI). When system details were investigated however, some important disadvantages of such a system were brought to light. Some accounting must be made for residual water in a water transpiration system. A water film below the porous outer surface of at least 1/16 inch thickness is needed to properly distribute the water and prevent local hot spots during boiling. The weight of a 1/16 inch thick water film is approximately 0.325 lb/ft^2 of wetted (cooled) surface area. This adds about 3300 lb to the weight of water required to cool the wing. It appears possible to use a water evaporating system taking into account the above weight penalty and remembering that the sensitivity of liquid water to changes in aircraft orientation must be accounted for with a complex distribution system.

Referring to Tables XVI and XVII weight determination schemes are now discussed for transpiration systems employing hydrogen, helium, air, and water. System weights are the sum of the weight of the following components.

Coolant weight: The weight of coolant required was determined by multiplying the flow rate in lb/hr from either Table XVI or XVII by the equivalent steady state time of 1.5 hours.

Tankage, tank insulation, tank support weight: The weights of coolant tankage, tank insulation and tank supports required was estimated as follows:

1. Hydrogen: The additional weight of hydrogen to be carried for a transpiration system was assumed to be added to the fuel tankage system. From Reference 1, approximately 0.14 lb of insulation, tankage and supports were needed per pound of hydrogen stored. This weight factor was assumed for the hydrogen transpiration systems.
2. Helium: Since the helium must be carried on board as an additional item it was assumed to be carried in the wings. From Reference 36 it was determined that helium could be efficiently stored in 100-lb quantities in one-foot radius spherical tanks at 50°R at a pressure of 3500 psi. These tanks with their associated insulation and supports yield a weight factor for helium storage of approximately 0.25 lb of insulation, tankage and supports per pound of stored helium.
3. Air: Only a ram air system was considered for weight determination.
4. Water: Water can be stored in 1000-lb quantities under 100 psi pressure for approximately 0.02 lb of tankage and supports per pound of stored water.

Plumbing Weight: The plumbing weight estimate accounts for such items as line weights, header weights, valve weights and line and header insulation weights. These weights are a function of the inlet temperatures and were estimated as follows:

Hydrogen, Helium and Air

Inlet Temperature	Leading Edge Area	Flat Areas
-400°F or -450°F	0.50 lb/ft^2	1.0 lb/ft^2
+100°F	0.25 lb/ft^2	0.5 lb/ft^2

Liquid Water

Inlet Temperature	Leading Edge Area	Flat Areas
70°F	0.15 lb/ft^2	0.15 lb/ft^2

The choice of the above weight factors was based on information from References 2, 3, 18, 19, and 20, and decisions regarding coolant distribution techniques as shown schematically in Figure 80, Section 7. The flat areas are supplied from separate inlet headers for each area. The leading edge area would be supplied by one inlet line for gaseous transpiration. The same weight factors listed above were used for the convective systems in Section 7 with the plenum chamber allowance in the above numbers applied to an outlet header allowance in the case of the convective systems.

Porous Material Weight: Porous material weight estimates were made using the models given in Figure 78. Since these weight estimates were large they are included as a separate item in Table XVIII. For transpiration cooling systems to compete weightwise with the convective concepts discussed in the next section these porous material weights must be reduced to less than 0.5 lb/ft^2. A summary of the porous material weights is given below.

Top Surface	0.71 lb/ft^2
Bottom Surface	0.77 lb/ft^2
Leading Edge	0.75 lb/ft^2

NOTE: per ft^2 of surface area.

Total System Weight: Using the weight factors discussed in the above paragraphs weights were determined for the promising transpiration and film cooling systems. These weight estimates are summarized in Table XVIII. For hydrogen transpiration systems with the hydrogen entering at 100°F and -400°F, the cooling system component weights, exclusive of the porous material weights, are approximately 16,000 lb and 13,000 lb respectively. When a porous material weight of approximately 0.75 lb/ft^2 is added to the component weight estimates the resulting system unit weights are over 3.0 lb/ft^2 of planform area (6954 ft^2). The best transpiration cooling system based on the weight estimates from Table XVIII are listed below.

(1) Hydrogen transpiration, -400°F inlet temperature
(2) Liquid water transpiration, water boiling at 80°F
(3) Helium transpiration, -450°F inlet temperature
(4) Hydrogen transpiration, +100°F inlet temperature

Also included in Table XVIII is a weight estimate for the most promising film cooling system. For this system slots could be cut in the aluminum skin of the wing structure thus eliminating the porous matrix. Figure 79 shows a schematic of the film cooling system used to determine these weights. For the above weight estimation scheme a liquid water film cooling system as tabulated in Table XVIII weighs about 140,000 lb or about 6.0 times a comparable transpiration cooling system. Based on the above weight estimates film cooling with water is not considered feasible for any large area of the wing.

TABLE XVIII
WEIGHT ESTIMATES FOR PROMISING TRANSPIRATION AND FILM COOLING SYSTEMS

	Units	0° Sweep	45° Sweep	75° Sweep
Porous Material Weight (see Figure 78)	lb lb/ft^2	8,060 1.15	7,830 1.13	7,660 1.10
Hydrogen Transpiration 100°F Inlet Temperature	lb* lb/ft^2	2,500 3.59	24,100 3.47	21,600 3.10
Hydrogen Transpiration -400°F Inlet Temperature	lb* lb/ft^2	21,900 3.14	21,000 3.02	19,300 2.77
Helium Transpiration -450°F Inlet Temperature	lb* lb/ft^2	28,900 4.16	27,300 4.08	24,200 3.49
Air Transpiration 100°F Inlet Temperature	(Weight estimates for stored air and hydrogen requirements for cooling ram air were excessive for cooling entire wing)			
Liquid Water Transpiration Water Boiling at 80°F	lb* lb/ft^2	24,400 3.50	23,000 3.31	20,600 2.97
Liquid Water Film Cooling Water Boiling at 60°F	lb* lb/ft^2	147,000 21.1	143,600 20.5	129,500 18.6

NOTES: 1. *Include porous material, coolant, distribution system, and tank weights
2. Weights in lb/ft^2 are based on a wing planform area of 6954 ft^2

Figure 78A Actual Size

Figure 78B Ten(10) Times Actual Size

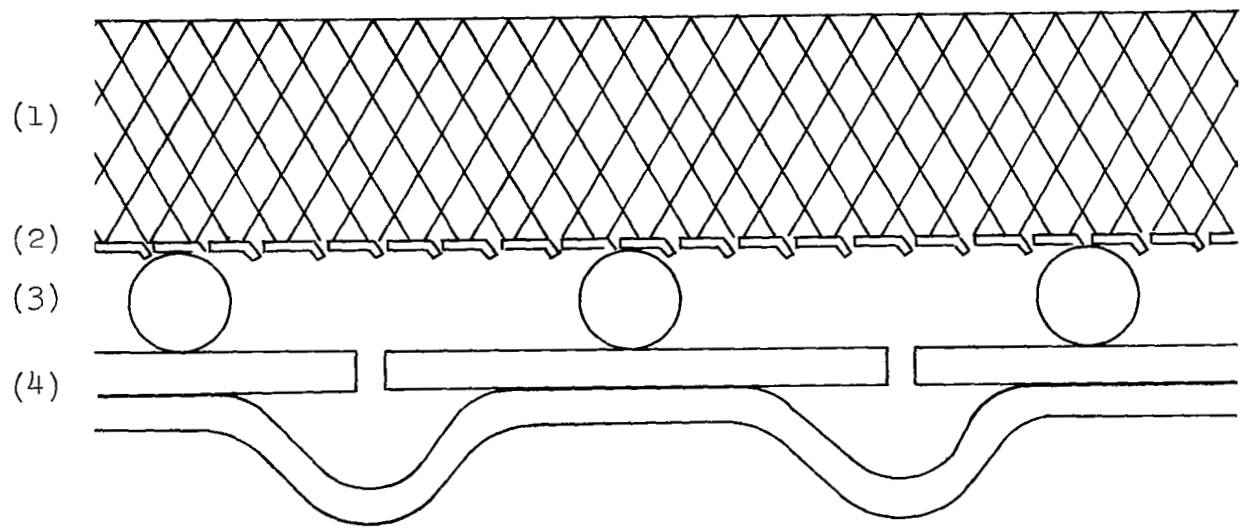

(1) Porous Material: 50% porosity

Top Surface: 316 stainless steel rigimesh

Bottom Surface
Leading Edge : L-605 rigimesh

(2) Radiation Shield: effective emittance of porous material plus radiation shield is 0.8

Top Surface: 5 mil thick slotted aluminum foil

Bottom Surface
Leading Edge : 3 mil thick slotted stainless steel foil

(3) Wire Mesh Separators: 1/16 inch diameter wire in 1/4 x 1/4 inch grid

Top Surface: aluminum, 0.35 lb/ft^2

Bottom Surface
Leading Edge : stainless steel, 1.0 lb/ft^2

(4) Primary Structure: weight of this component not included in transpiration cooling system weight estimates (structural weights are calculated in Section VIII)

Figure 78. Schematic of Transpiration Cooling System for Weight Estimates

Ten(10) Times Actual Size

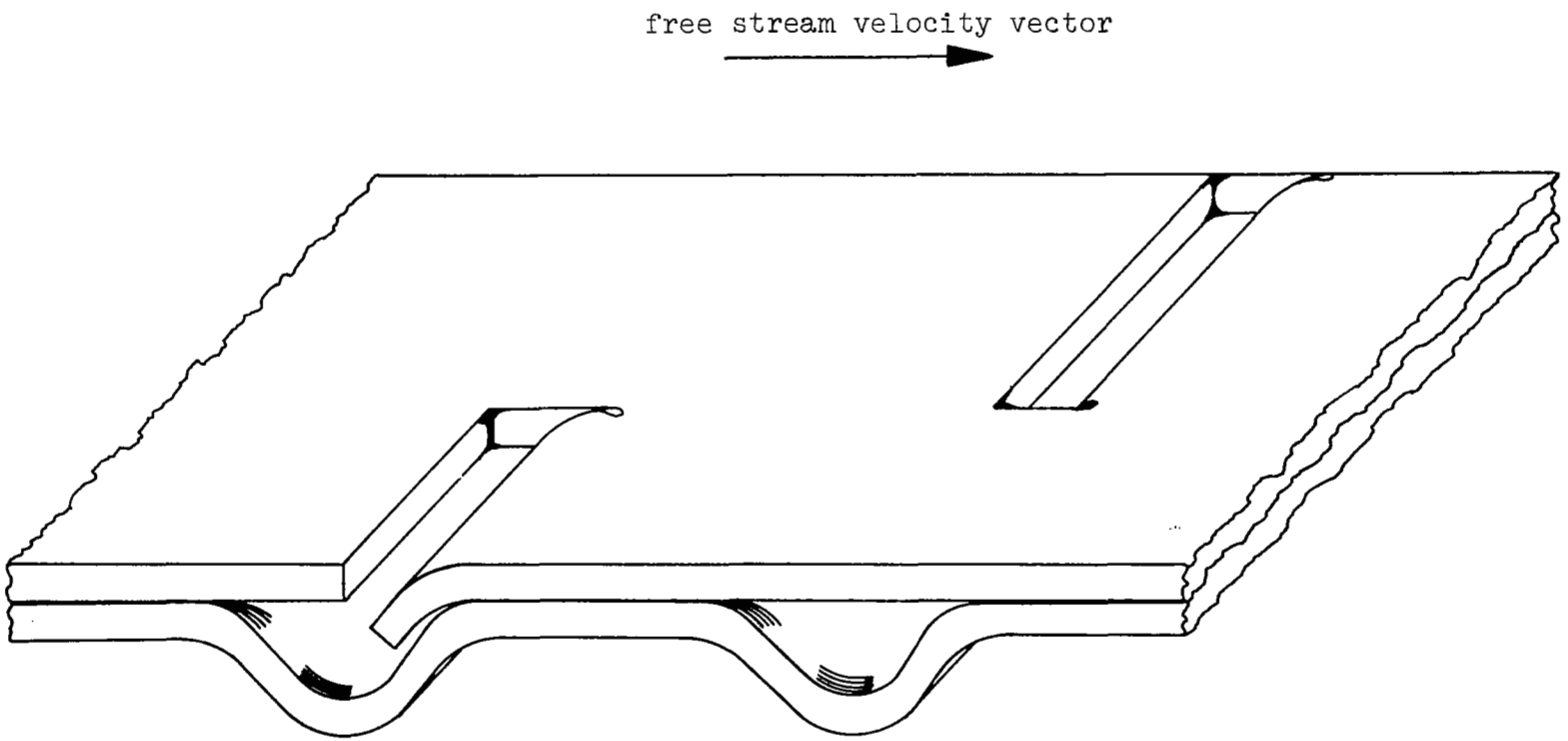

NOTE: passages which are integral with the structural skin feed an alternating arrangement of slots

Figure 79 Schematic of Water Film Cooling System for Weight Determination

SECTION 7

CONVECTIVE AND SPRAY COOLING SYSTEM SELECTION STUDIES

This section presents the results of analytical studies of direct (including spray boiling) and indirect convective cooling systems as selected from cooling system concept - coolant combinations reviewed in Section 4. Hydrogen and air were considered as coolants for the direct convective systems while water and lithium were selected coolants for the direct spray cooling approaches. For the indirect systems, water-glycol and silicone fluids were studied in closed loops to transport heat from the structure to be cooled to a heat exchanger where heat is rejected to the hydrogen fuel. For the direct hydrogen and air systems and for the indirect water-glycol and silicone systems it was assumed that a portion of the heat capacity of the fuel supply could be used for structural cooling without adversely influencing the total vehicle fuel load. That is, the weight of hydrogen required to cool these particular types of systems was not considered to be part of the cooling system weight. Since this may be an optimistic assumption its implications will be discussed in a subsequent section, along with techniques for reducing the percentage of fuel heat capacity required for structural cooling purposes.

With this as a basis the purpose of the convective and spray cooling system analyses was to define coolant flow rates as a function of structural operating temperature and wing sweep angle. Coolant flow rate data was used to establish weights for the coolant distribution systems. The data generated provides a basis for trade-off studies between cooling system and structural weight considerations. Since wing structural weight is a function of wing sweep angle and operating temperature level the effects of these parameters on cooling system flow rates and weights were investigated.

It should be noted that when fuel is used as the coolant and coolant weight is not charged to the cooling system the normal type of thermal protection system optimization which trades-off expendable coolant weight and insulation system weight, such as described in Ref. 2, 3, and 18, is inappropriate. Rather, the minimum weight of the structural component is achieved when all forms of external insulation are eliminated and the external surface of the component which is exposed to aerodynamic heating is cooled directly. Weight tradeoffs are then made between the structural weight of the component and the hardware items of the cooling system such as distribution lines, heat exchangers, pumps, controls, etc. Since the weight of the basic structural component is much greater than that of the cooling system hardware, the most desirable operating temperature levels are those which permit the use of low density structural alloys such as aluminum or titanium. Only when the heat capacity of the fuel is insufficient to absorb the structural cooling load is it necessary to consider insulation systems external to the cooled structure.

Figure 80 presents the assumed distribution system schematic for the convective cooling system (excluding spray boiling) selection studies. For the convective studies each

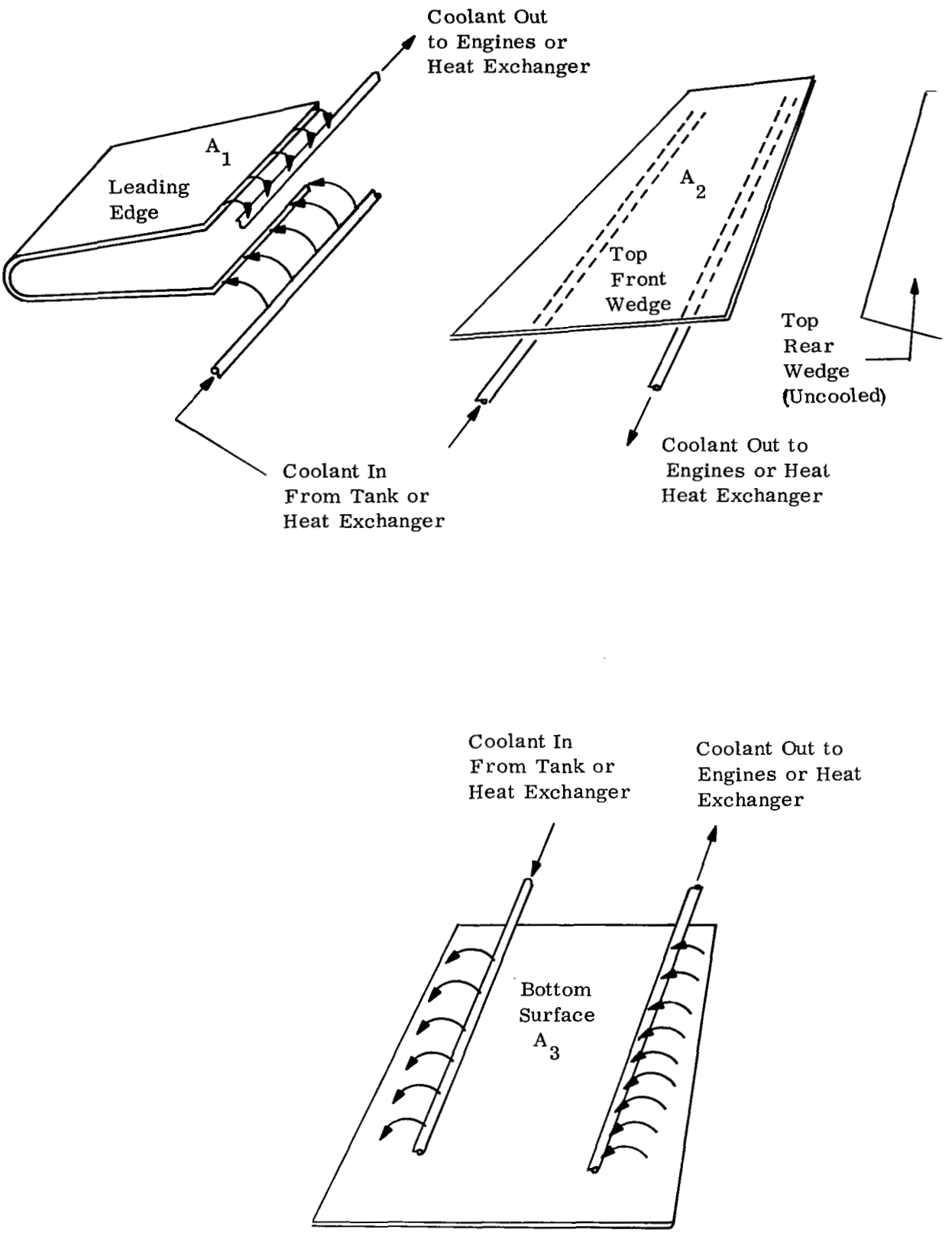

Figure 80. Coolant Distribution to Wing Sections for Convective Systems

half of the wing was broken into three sections to be cooled. The bottom flat surface area extended from S = -60.0 inches to the rear of the wing. The leading edge area extended from S = -60.0 inches to S = + 60.0 inches, and the top flat surface area extended from S = + 60.0 inches to the maximum thickness line. The bottom, leading edge, and top surface areas each have their respective inlet and outlet headers. For the top and bottom flat surfaces the coolant flows in the direction of decreasing heat transfer coefficient.

Figure 81 and Table XIX present a breakdown of the heat transfer data for the convective cooling system selection studies. Shown in Figure 81 is the section breakdown for one half the wing for the 0° and 65° sweep configurations. The average heat transfer coefficient listed was determined by an incremental integration over the surface in question. For example,

$$h_l = \sum_{A_1} \frac{A_i h_i}{A_1}$$

The heat input to any surface was estimated by using the equation given below.

$$Q = h_{avg} A (T_R - T_w) - \sigma \epsilon (T_w + 460.0)^4$$

where: A and h_{avg} are given in Table XIX
values of T_R are given in Table I
ϵ is assumed as 0.8.

The data listed in Table XIX cannot be used to check results in this section exactly. If such a check is made differences in the order of 5 to 10 percent will be noted especially in the neighborhood of the leading edge where the laminar to turbulent transition occurs. These small differences are due to the integration increments used and do not affect system weights noticeably.

A. DIRECT HYDROGEN SYSTEM

A schematic of the direct hydrogen system is given in Figure 82 and indicates the assumed temperatures and operating conditions. A liquid hydrogen pump is used to pump fuel from the tanks through the wing cooling panels and then to the engines. The hydrogen pump raises the hydrogen to supercritical pressures so that the liquid fuel does not undergo a phase change from liquid to vapor. The fuel temperature is -420°F entering the cooling passages and 50°F below the mean wall temperature when it leaves the cooling passages. The feasibility of designing such a cooling system was investigated during studies summarized in Reference 22.

Table XX outlines the method used here to determine hydrogen flow rates and hydrogen convective cooling system component weights for a direct hydrogen system. The pertinent parameters for direct hydrogen convective system calculations are the hydrogen flow rates, hydrogen inlet and outlet temperatures and system weights. Weight elements of the direct hydrogen cooling system are limited to the

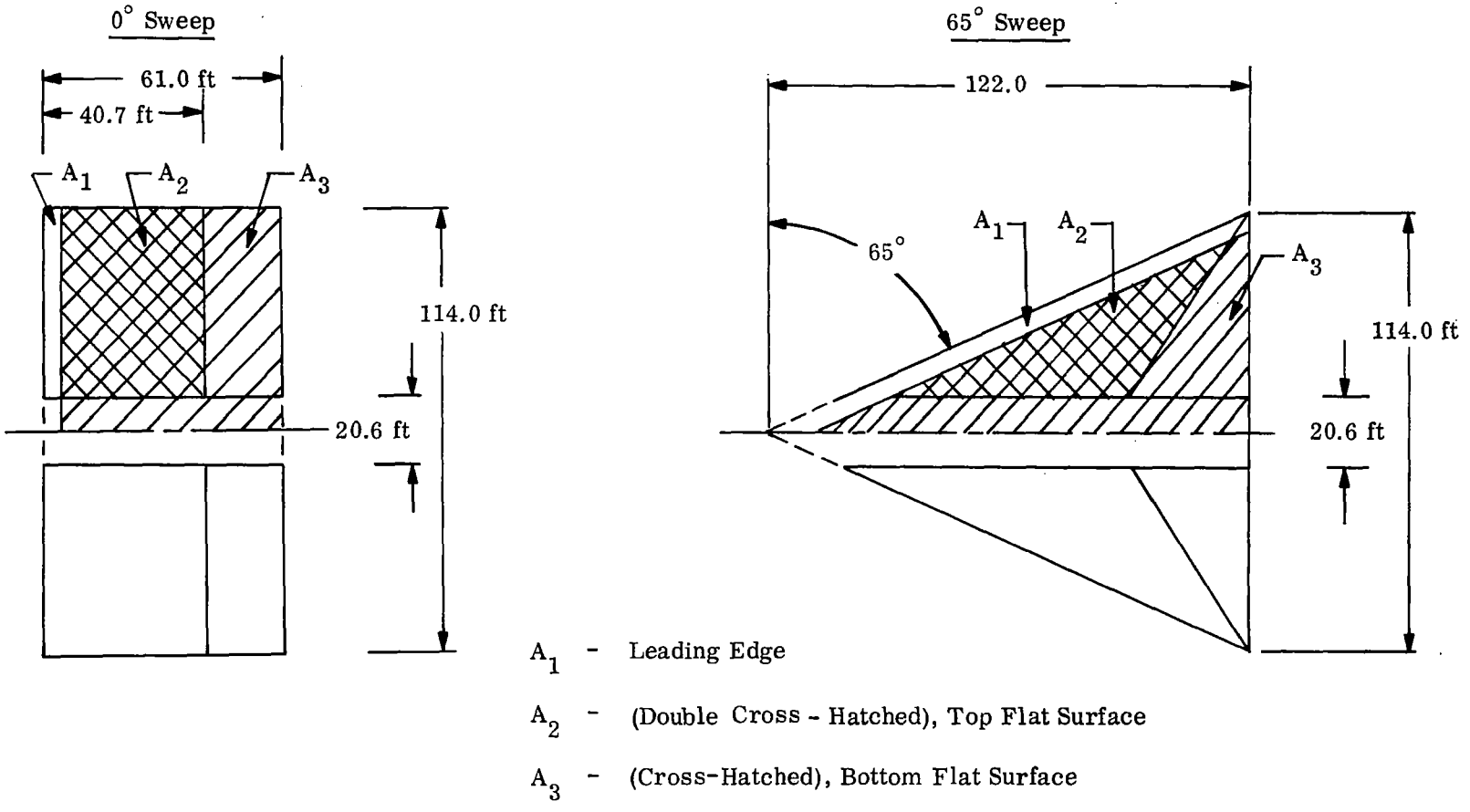

A_1 - Leading Edge

A_2 - (Double Cross - Hatched), Top Flat Surface

A_3 - (Cross-Hatched), Bottom Flat Surface

Figure 81. Wing Area Divisions for Cooling System Studies

TABLE XIX

AREAS, AVERAGE HEAT TRANSFER COEFFICIENTS AND HEAT LOADS FROM CONVECTIVE COOLING SYSTEM STUDIES (1) (2)

Sweep Angle	A_1	h_1	Q_1	A_2	h_2	Q_2	A_3	h_3	Q_3
degrees	ft^2	Btu/hr-ft^2-°F	Btu/hr x 10^{-6}	ft^2	Btu/hr-ft^2-°F	Btu/hr x 10^{-6}	ft^2	Btu/hr-ft^2-°F	Btu/hr x 10^{-6}
0	518	5.23	5.97	1667	1.44	5.28	3192	7.70	56.2
30	599	5.70	7.50	1533	1.43	4.82	3145	7.66	55.1
45	733	6.44	10.4	1407	1.37	4.25	3074	7.56	53.1
65	1237	6.59	18.5	1220	1.23	3.31	2836	7.18	46.6
75	1467	6.21	20.7	925	1.14	2.32	2693	6.83	42.1

NOTES: (1) Areas and heat loads are for one-half the wing only and for a 0.05 inch leading edge radius

(2) Heat loads are for a 200°F outer surface temperature

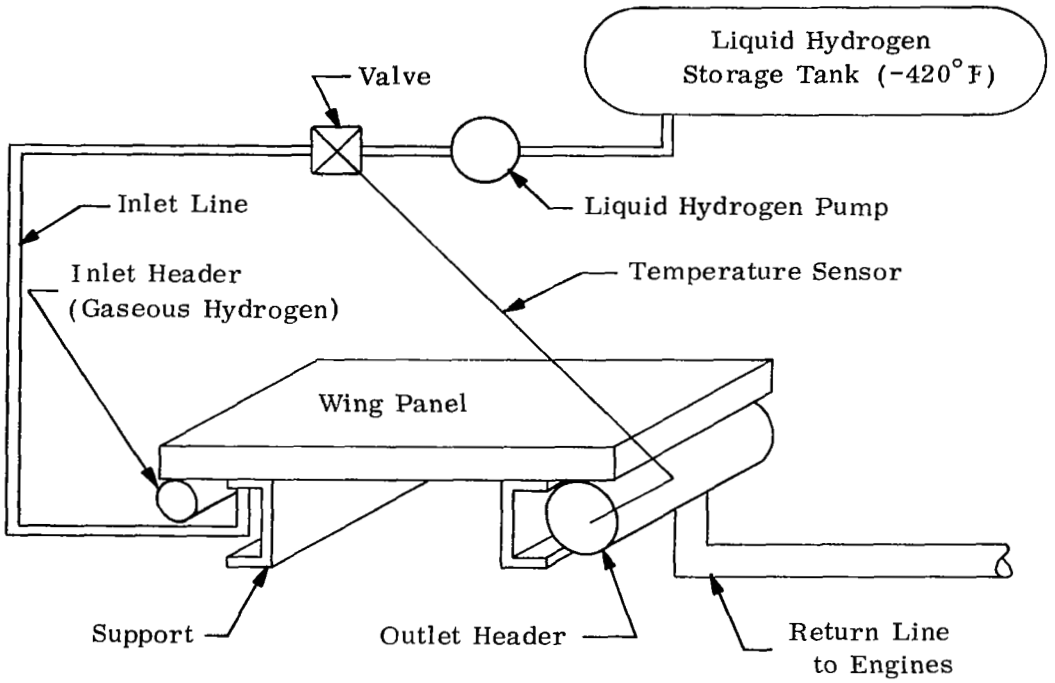

Figure 82. Direct Hydrogen Convective Cooling System Schematic

TABLE XX

DIRECT HYDROGEN SYSTEM PARAMETERS

A. HYDROGEN FLOW RATE, LB/HR

Flow rate (lb/hr) = heat input (Btu/hr)/heat capacity (Btu/lb)

where:

heat input = $h\,(T_R - T_w)(A) - \sigma\epsilon T_w^4 A$

heat capacity of hydrogen = $c_p\,((T_w - 50) - T_s)$

h	convective heat transfer coefficient
T_R	recovery temperature
T_w	wall temperature
A	area of hemicylindrical leading edge
c_p	hydrogen specific heat (3.5 Btu/lb°F)
T_s	hydrogen inlet temperature (-420°F)
ϵ	emittance (0.8)
σ	Boltzmann's constant (0.173×10^{-8} Btu/hr-ft^2-°R^4)

B. HYDROGEN PUMP AND MOTOR WEIGHT (LIQUID HYDROGEN)(taken from Reference 2)
Pump and motor weight (lb) = 8.0 (hydrogen flow rate/2000) + 8.0

C. APU FUEL WEIGHT
APU fuel weight (lb) = (0.25 lb/hr ft^2)(A)θ
where θ is the steady state equivalent time = 1.5 hr.

D. DISTRIBUTION SYSTEM WEIGHT
Leading edge plumbing weight (lb) = (0.5 lb/ft^2)A
Flat areas plumbing weight (lb) = (1.0 lb/ft^2)A
The plumbing weight estimate accounts for such items as line weights, header weights, valve weights and line and header insulation weights.

NOTE:
Cooling passages are in the skin and skin weight is included as a structural weight item in Section 8.

distribution system since the hydrogen tank and hydrogen fuel weight are considered to be part of the fuel system rather than the cooling system. Since the wing structure is considered to be part of the vehicle airframe rather than part of the cooling system, weights for coolant passages in the wing structural skin were included as part of the structural studies in Section 8.

Hydrogen flow rates are obtained by a heat balance assuming the hydrogen absorbs all heat input to the wing. The convective heat input is obtained using the radiation equilibrium values of heat transfer coefficients. Wall temperatures were assumed to have a mean value equal to 50° above the assumed hydrogen outlet temperature. Figures 83 through 90 present hydrogen flow rates and hydrogen convective cooling system weights vs maximum hydrogen temperature and sweep angle. Sweep angles identify wing configurations as shown in Figures 4 through 8. Figures 83 through 86 show results for the 0.05 inch and 2.0 inch radii leading edges respectively. While Figures 87 and 89 and Figures 88 and 90 present data for the top and bottom surfaces respectively. Examination of Figures 83 and 90 reveals the following trends. Because pump and motor weight allowances are small compared to total system weights the system weight estimate is weakly dependent on maximum hydrogen temperature. The maximum hydrogen temperature controls hydrogen flow rate requirement which in turn determines pump and motor weights.

As seen in Figures 83 through 86 leading edge radius effects are not of primary importance, rather, for the leading edge, the area of the leading edge increasing with increasing sweep angle is the dominant parameter. Differences in results for the two radii presented can be attributed to the laminar to turbulent transition on the leading edge as the radius is increased. Weights for the leading edge vary from about 900 lb to 2640 lb as sweep angle varies from 0° to 75°. The 75° sweep wing case is somewhat distorted because of the change in wing span as shown in Figure 8. Hydrogen flow rates increase with increasing sweep as shown in Figures 84 and 86 because leading edge area increases faster than heat transfer coefficients decrease with increasing sweep angle. Hydrogen flow rates decrease as the hydrogen is heated to higher temperatures. For the flat surfaces hydrogen system weights and hydrogen flow rates are presented in Figures 87 through 90. Both system weights and hydrogen flow rates decrease with increasing sweep angle because both area and heat transfer coefficients decrease with increasing sweep angle. For the top flat surface hydrogen distribution system weights vary from 4,640 lb to 2,560 lb, decreasing as sweep angle increases from 0° to 75°, while for the bottom flat surface system weights vary from 9,000 lb to 7,500 lb, as the sweep angle increases. For a 150°F maximum hydrogen temperature and 0° and 75° sweep angles hydrogen flow rates for the top surface vary from 5300 lb/hr to 2300 lb/hr while for the bottom surface the hydrogen flow rates vary from 56,000 lb/hr to 42,000 lb/hr.

Table XXI summarizes the direct hydrogen system data presented in Figures 83 through 90. As shown in this table the average cooled surface temperature is 50°F above the maximum hydrogen temperature. Although these two parameters are indirectly related (the assumed surface temperature determining heat input and the assumed hydrogen outlet temperature determining hydrogen flow rates) they should be interpreted as merely representative numbers for determining hydrogen system weight estimates and not as rigorously fixed. The maximum hydrogen flow rate in Table XXI occurs for the lowest hydrogen outlet temperature of 150°F and is approximately 68,000 lb/hr. For this hydrogen

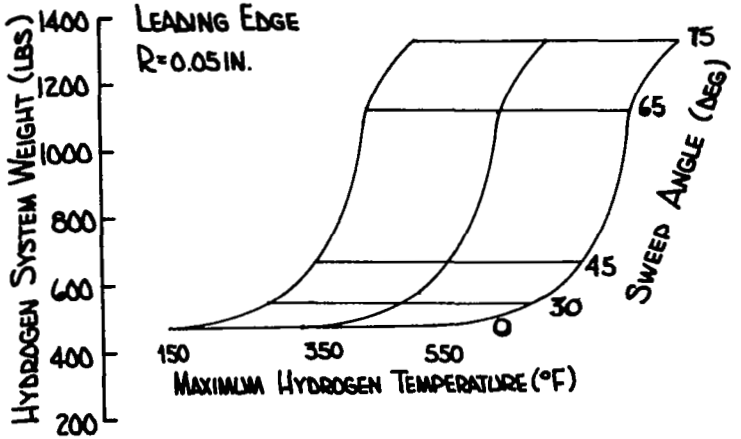

Figure 83. Cooling System Component Weights for One-Half the Wing for a Direct Hydrogen Leading Edge Cooling System for a 0.05 inch Leading Edge Radius for M = 6.0, α = 10.31°, Altitude = 100,000 ft

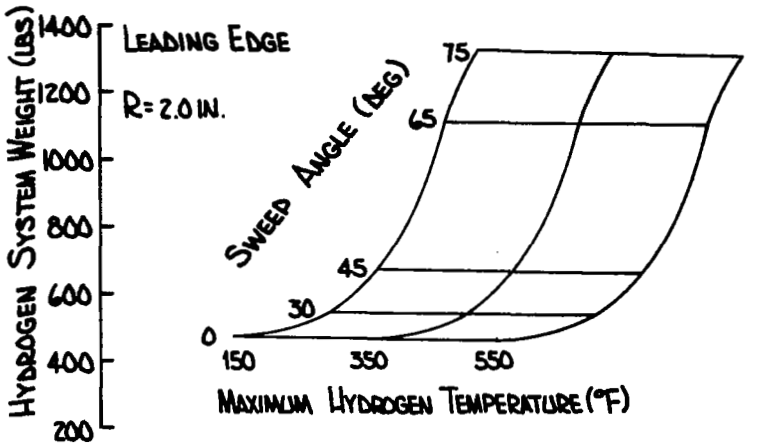

Figure 85. Cooling System Component Weights for One-Half the Wing for a Direct Hydrogen Leading Edge Cooling System for a 2.0 inch Leading Edge Radius for M = 6.0, α = 10.31°, Altitude = 100,000 ft

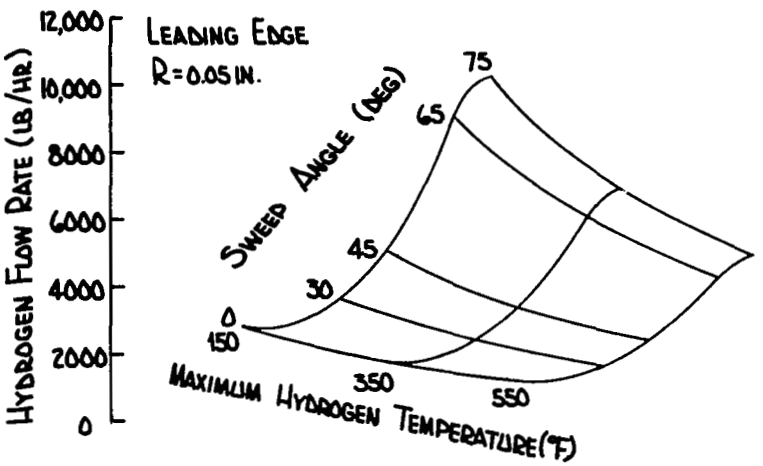

Figure 84. Hydrogen Flow Rates for One-Half the Wing for a Direct Hydrogen Leading Edge Cooling System for a 0.05 inch Leading Edge Radius for M = 6.0, α = 10.31°, Altitude = 100,000 ft

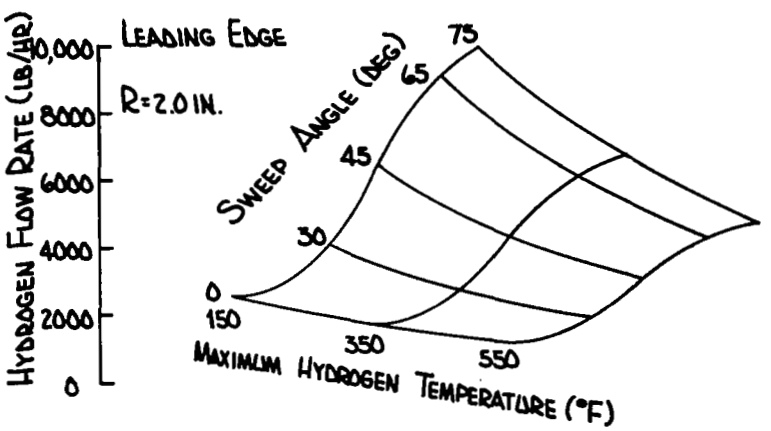

Figure 86. Hydrogen Flow Rates for One-Half the Wing for a Direct Hydrogen Leading Edge Cooling System for a 2.0 inch Leading Edge Radius for M = 6.0, α = 10.31°, Altitude = 100,000 ft

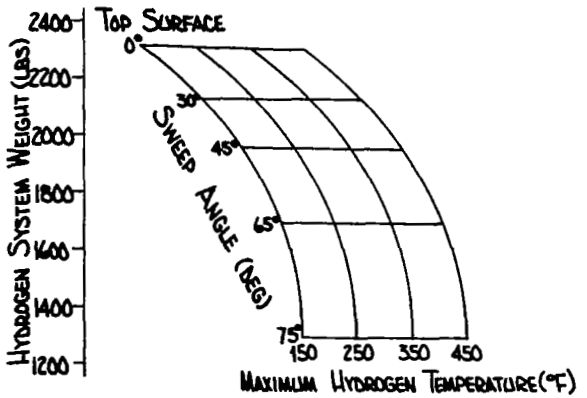

Figure 87. Cooling System Component Weights for a Direct Hydrogen Cooling System for One-Half the Top Surface of the Wing for a 0.05 inch Leading Edge Radius for M = 6.0, α = 10.31°, Altitude = 100,000 ft

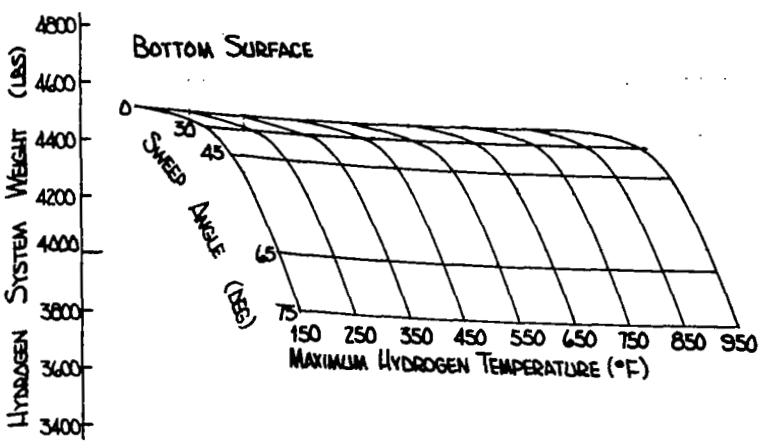

Figure 88. Cooling System Component Weights for a Direct Hydrogen Cooling System for One-Half the Bottom Surface of the Wing for a 0.05 inch Leading Edge Radius for M = 6.0, α=10.31°, Altitude = 100,000 ft

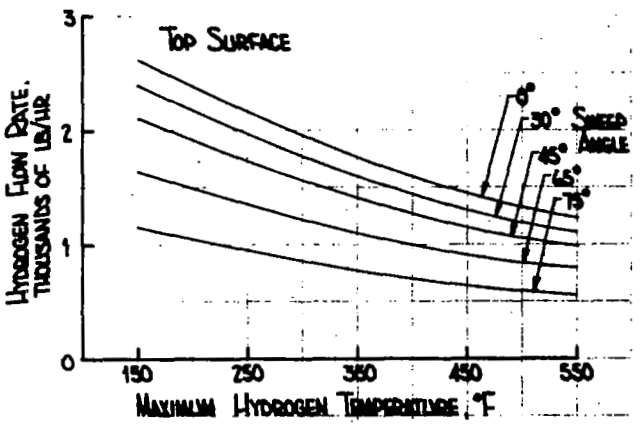

Figure 89. Hydrogen Flow Rates for a Direct Hydrogen Cooling System for One-Half the Top Surface of the Wing for a 0.05 inch Leading Edge Radius for M = 6.0, α = 10.31°, Altitude = 100,000 ft

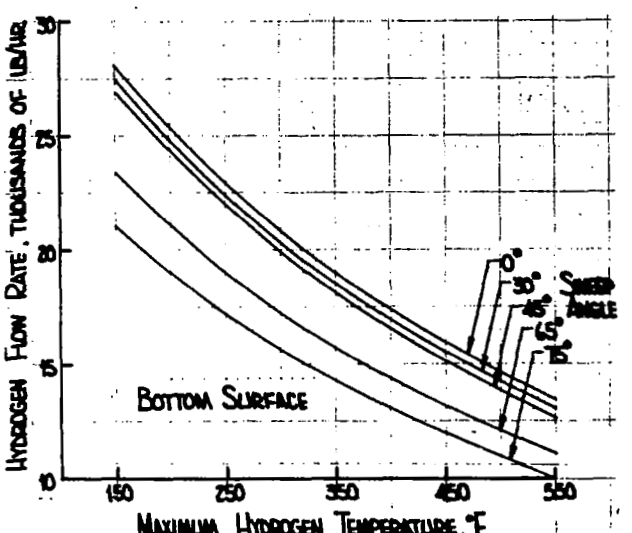

Figure 90. Hydrogen Flow Rates for a Direct Hydrogen Cooling System for One-Half the Bottom Surface of the Wing for a 0.05 inch Leading Edge Radius for M = 6.0, α = 10.31°, Altitude-100,000 ft

TABLE XXI
DIRECT HYDROGEN SYSTEM SUMMARY
(0.05 inch Leading Edge Radius)

Average Cooled Surface Temperature (°F)	Maximum Hydrogen Temperature (°F)	Total Hydrogen Flow Rate (lb/hr)					Total Hydrogen System Component Weight (lb)				
		Sweep Angle					Sweep Angle				
		0°	30°	45°	65°	75°	0°	30°	45°	65°	75°
200	150	66,900	67,200	67,400	68,000	64,500	14,600	14,200	13,900	13,600	12,800
300	250	54,900	54,700	55,200	55,500	53,300	14,600	14,200	13,900	13,600	12,800
400	350	44,900	44,800	45,600	45,400	44,100	14,500	14,100	13,800	13,500	12,700
500	450	37,500	37,400	37,900	38,400	37,300	14,500	14,100	13,800	13,500	12,700
600	550	31,800	31,800	32,200	32,500	31,300	14,400	14,100	13,800	13,400	12,700

*NOTE: The above numbers are for the total wing area

outlet temperature and average cool surface temperature, and aluminum outer skin could be used resulting in very low cooled wing weights. A hydrogen flow rate of 40,000 to 50,000 lb/hr is estimated for each of the four (4) engines on the aircraft of interest. So as can be seen from Table XXI it appears possible to fabricate a cooled aluminum wing with a cooling system component weight of approximately 14,000 lb using a hydrogen flow rate slightly above that required for 1 engine.

As shown in Table XXI sweep angle effects cancel out for a cooled wing study. Although the heat transfer coefficients on the leading edge decrease with sweep the area increases and as shown in Table XIX the heat load increases. This effect is negated by the decreasing heat load on the bottom surface. Hydrogen flow rate and hydrogen system component weight are almost independent of a choice of sweep angle with the exception of 75° sweep angle for which the original span assumption is violated making the tabulated flow rates and component weights lower than the values which would have otherwise been expected.

B. LIQUID CONVECTIVE SYSTEMS

In Section 4 two liquid transport fluids were selected for use in an indirect convective cooling system with the fuel as a heat sink. For operating temperatures below 200°F a water-ethelene glycol solution was selected as the best transport fluid, while if temperatures exceeded 200°F but remained below 400°F a silicone fluid (Dow Corning 331) was selected for use. In this section analysis results for systems employing the above fluids are presented and discussed.

A schematic for either a water-glycol or silicone system is given in Figure 91. In this system either transport fluid is pumped through the wing skin entering at a sink temperature, T_S, and leaving at an outlet temperature, T_O. The transport fluid temperature could be controlled by bypassing the hydrogen heat exchanger. Hydrogen fuel is pumped from the tanks through a heat exchanger to the engine installation area. Hydrogen is assumed to enter the heat exchanger at -400°F and leave at 100°F below the transport fluid sink temperature (T_S - 100°F). The hydrogen flow rate may be controlled by the engine requirements thus eliminating complex and heavy control valves and bypass lines.

For systems which employ liquid transport loops the headers for distribution of fluid to the integral coolant passages are also integral with the structural skin. This is possible because of the relatively low flow volumes as compared to gaseous transport fluids where header size would probably preclude the use of integral headers. The weights for the direct hydrogen system, Table XX, included headers as part of the plumbing weight.

Table XXII summarizes system parameters for both the water-glycol and silicone systems. For a water glycol system a maximum outlet temperature of about 200°F is necessary to insure that local boiling does not occur, while for a silicone system a maximum outlet temperature of 400°F is necessary to insure that fluid instabilities are avoided. These temperatures and the specific heats of the respective coolants are the controlling system parameters since they dictate flow rates.

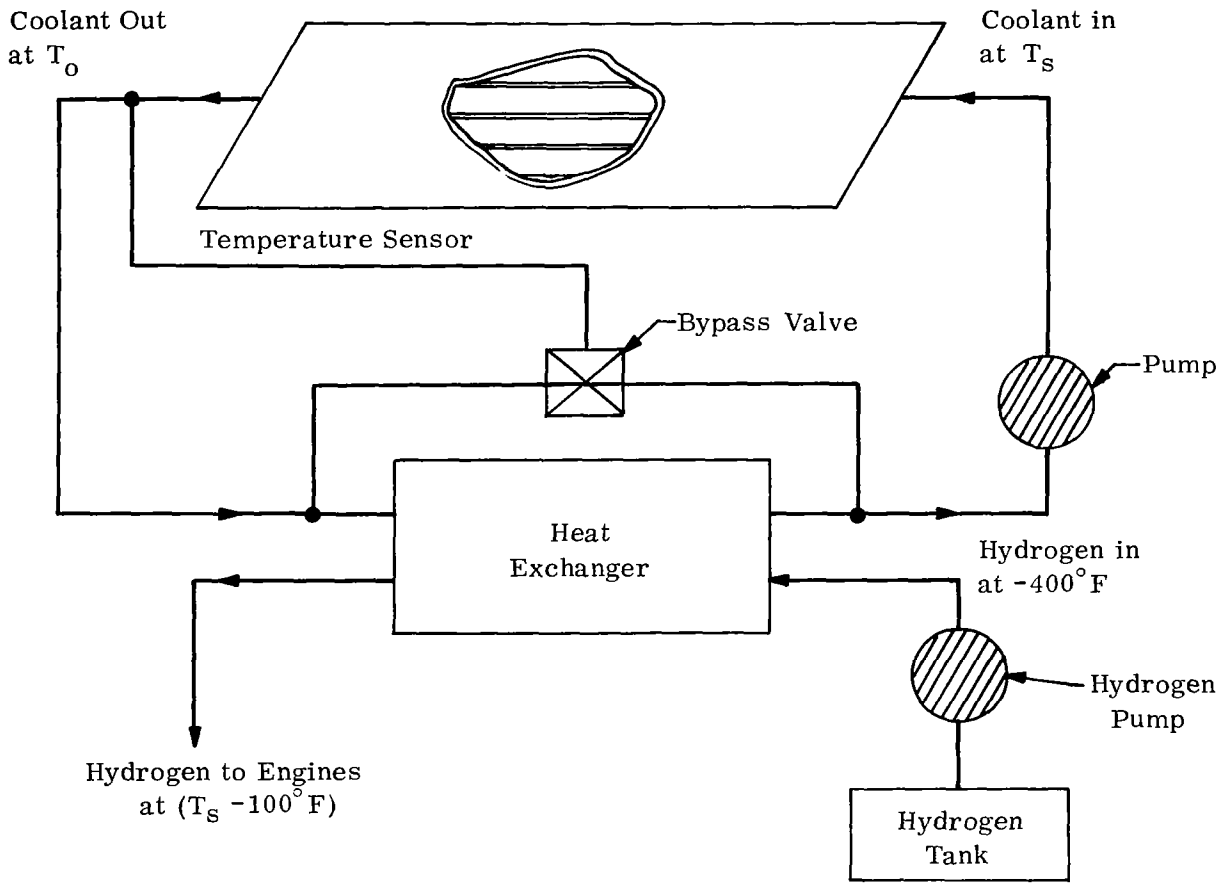

Figure 91. Indirect Liquid Convective Cooling System Schematic

TABLE XXII

LIQUID CONVECTIVE SYSTEM PARAMETERS

A. FLUID FLOW RATE

Flow rate (lb/hr) = heat input (Btu/hr)/heat capacity of fluid coolant (Btu/lb)

where:

heat input = $h (T_R - T_W) (A) - \sigma \epsilon T_W^4 A$

heat capacity of coolant = $c_p (T_o - T_s)$

h	convective heat transfer coefficient
T_R	recovery temperature
T_W	Average surface temperature
A	area
c_p	specific heat { 0.77 Btu/lb°F for water glycol; 0.43 Btu/lb°F for silicone
T_s	minimum transport fluid temperature
T_o	maximum transport fluid temperature = T_W

B. HEAT EXCHANGER WEIGHT

Weight (lb) = (5.75×10^{-5})(Flow rate)$(c_p)(T_o - T_s)$

C. HYDROGEN FLOW RATE

$$\text{Hydrogen Flow Rate} = \frac{\text{(coolant flow rate)(coolant heat capacity)}}{3.5\ [(T_s - 100) + 400°F]}$$

D. COOLANT FLUID PUMP AND MOTOR WEIGHT

This is taken from Figure 29, Reference 2.

E. APU FUEL WEIGHT

APU fuel weight (lb) = $(0.10\ lb/hr\text{-}ft^2)(A)(1.5\ hr)$

F. DISTRIBUTION SYSTEM WEIGHT

Distribution system weight (lb) = $(0.15\ lb/ft^2)(A)$

NOTE:

Cooling passages are in the structural skin and do not contribute to cooling system weight.

At this point it should be emphasized that the temperatures chosen are merely representive temperatures used to obtain estimates of cooling system weights and typical performance characteristics. Past experience has shown that system weights are not sensitive to the exact values of these temperatures as long as the temperatures are close to the actual temperatures which will be used in the final system design. Variations of these parameters will be investigated later in this report.

1. Indirect Water-Glycol Cooling System Studies

Results for the indirect water-glycol cooling system are presented in Figures 92 through 100. In these figures water-glycol system weights, water-glycol flow rates and hydrogen flow rates are presented as functions of the sink temperature (T_S) and wing sweep angle. Wing sweep angles identify the wing configurations presented in Figures 4 through 8. Preliminary investigations of both the water-glycol and silicone systems indicated that as the sink temperature increases hydrogen flow rates will decrease and transport fluid flow rates will increase. Decreasing hydrogen flow rates may be desirable from the standpoint of matching engine fuel flow rate requirements. Since transport fluid pumping requirements are a function of transport fluid flow rate, it is necessary to investigate a range of transport fluid flow rates. Three representative sink temperatures were chosen for each transport fluid studied. For the water-glycol transport fluid sink temperatures of -50°F, 0°F, and +50°F were chosen. This range of sink temperatures was sufficient to identify the tradeoffs involved in these studies. Before discussing the data presented in Figures 92 through 100 in detail it should be emphasized again that system weights, water-glycol flow rates, and hydrogen flow rates presented in these figures are for one-half the wing only. No distortion of the results due to the change in span for the 75° case is evident in Figures 92 through 100 because carpet plots were not used for the data presentation. Although it may be sufficient for the present study to tabulate the data as in Table XXI the possibility of hybrid systems was visualized, thus, for the three-wing area breakdown data was presented in graphical form to allow combinations of systems to be evaluated at a later time.

Figures 92 through 94 present water-glycol system weights, water-glycol flow rates and hydrogen flow rates for the maximum and minimum radii studied. A strong dependence of system weight on sink temperature is not seen because water-glycol flow rates are moderate (as will be shown later) and the resulting pump and motor weights are small compared to distribution system weight estimates. Heat exchanger weights are a function of the heat input to the transport fluid which is not a function of sink temperature. The wall temperature of 200°F noted on all figures in this section again denote the mean wall temperature used to determine heating rates and should not be interpreted as a constant wall temperature. A comparison of these figures indicates again that leading edge radius is not a strong variable. The laminar-turbulent transition does not appear to affect the results except when the entire leading edge makes a transition from laminar to turbulent flow as is shown in the 45° sweep case.

Water-glycol system weights for the leading edge vary from approximately 1,000 lb for the 0° sweep case to 3,300 lbs for the 75° sweep case. Water-glycol flow rates are generally in the 100,000 to 300,000 lb/hr range. Hydrogen flow rates for the leading edge are in the 10,000 to 40,000 lb/hr range. The expected trend of water-glycol

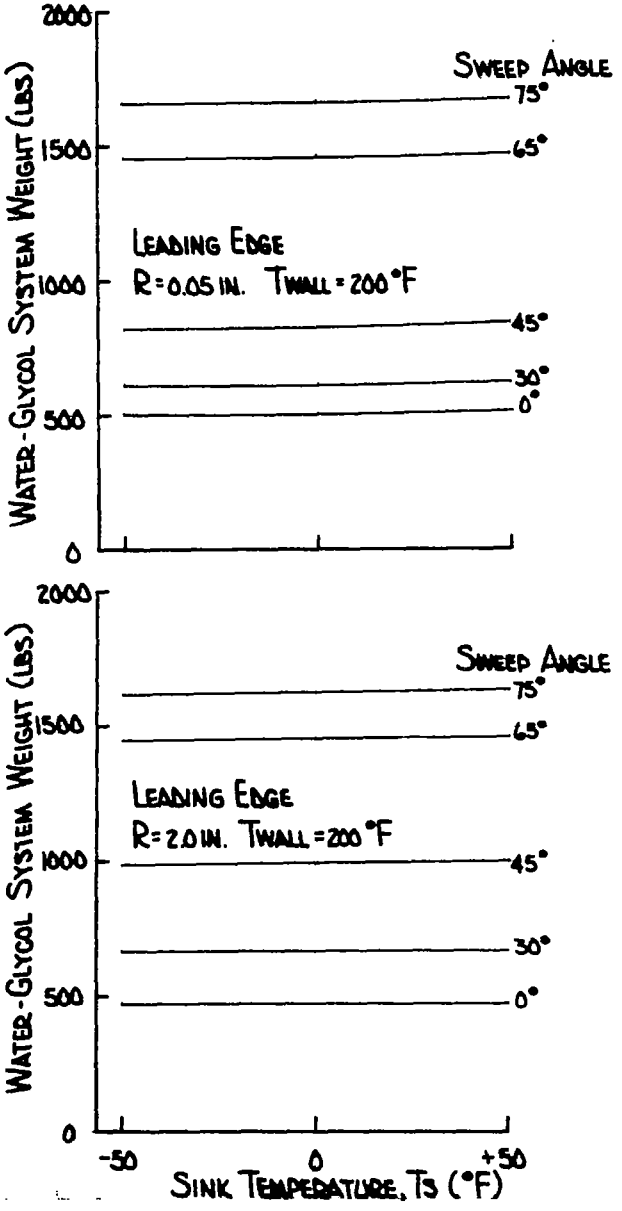

Figure 92. Cooling System Component Weights for an Indirect Water-Glycol Cooling System for One-Half of the Wing for 0.05 and 2.0 inch Leading Edge Radii for M = 6.0, α = 10.31°, Altitude = 100,000 ft

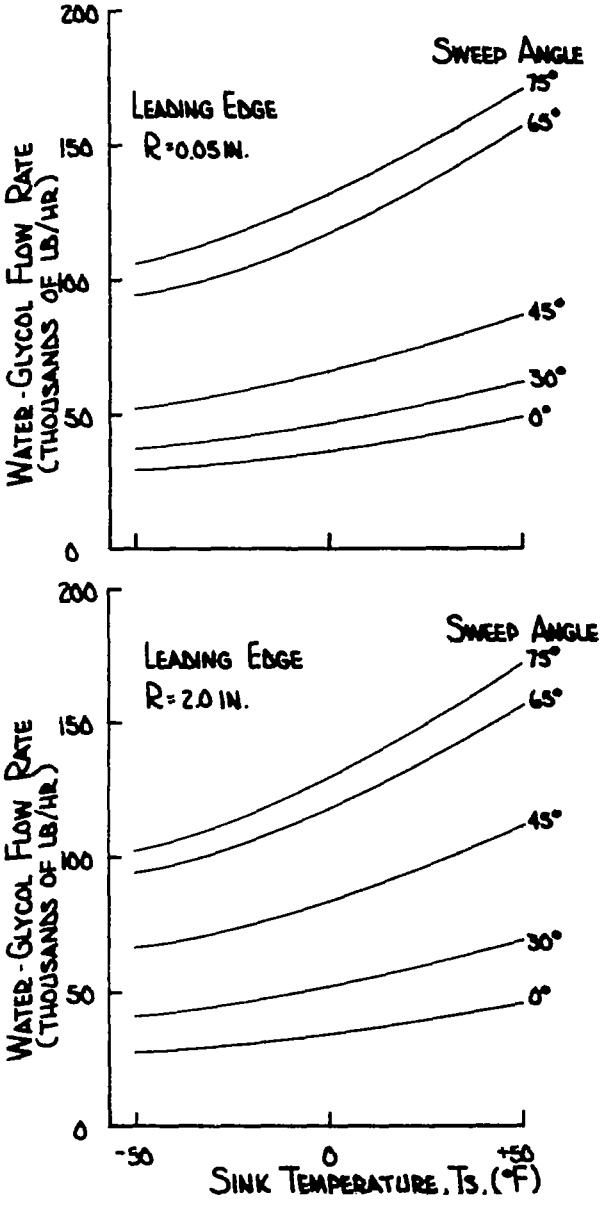

Figure 93. Water-Glycol Flow Rates for an Indirect Water-Glycol Cooling System for One-Half of the Wing for 0.05 and 2.0 inch Leading Edge Radii for M = 6.0, α = 10.31°, Altitude = 100,000 ft

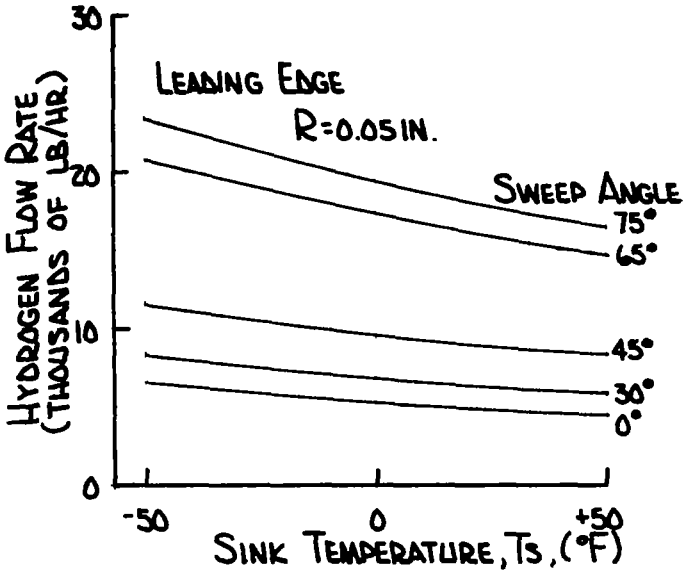

Figure 94. Hydrogen Flow Rates for an Indirect Water-Glycol Cooling System for One-Half of the Wing for 0.05 and 2.0 inch Leading Edge Radii for M = 6.0, α = 10.31°, Altitude = 100,000 ft

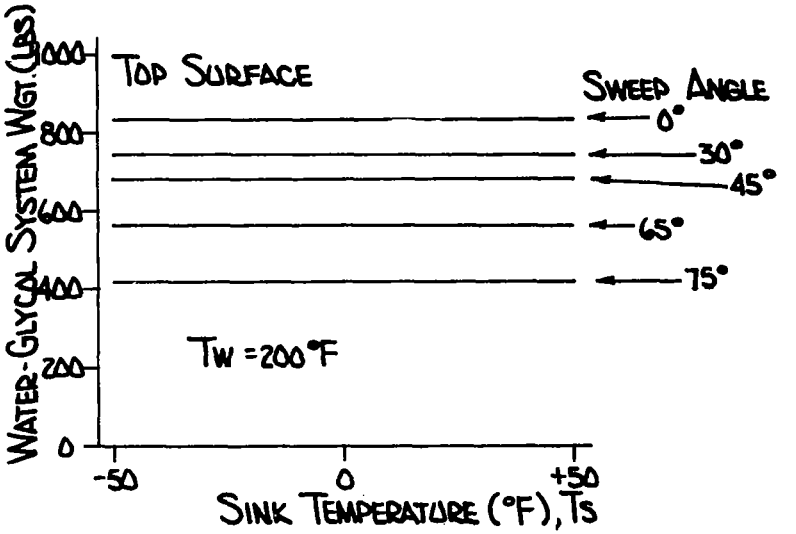

Figure 95. Cooling System Component Weights for an Indirect Water-Glycol Cooling System for One-Half of the Surface of the Wing for a 0.05 inch Lead ing Edge Radius for M = 6.0, α = 10,31°, Altitude = 100,000 ft

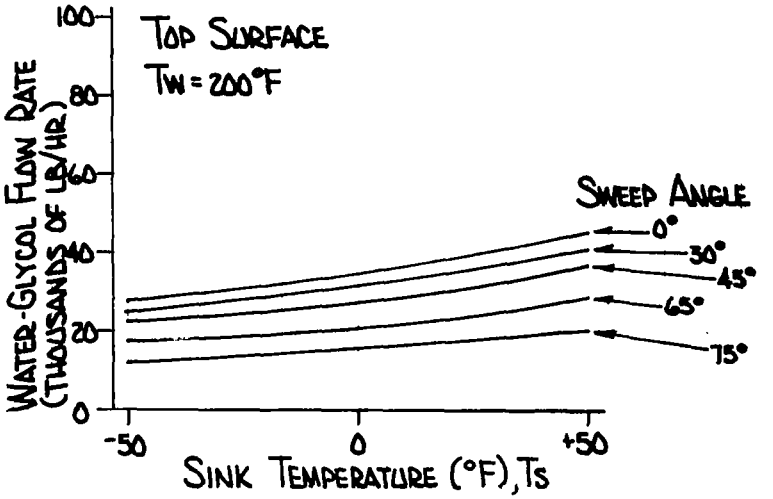

Figure 96. Water-Glycol Flow Rates for an Indirect Water-Glycol Cooling System for One-Half of the Top Surface of the Wing for a 0.05 inch Leading Edge Radius for M = 6.0, α = 10.31°, Altitude = 100,000 ft

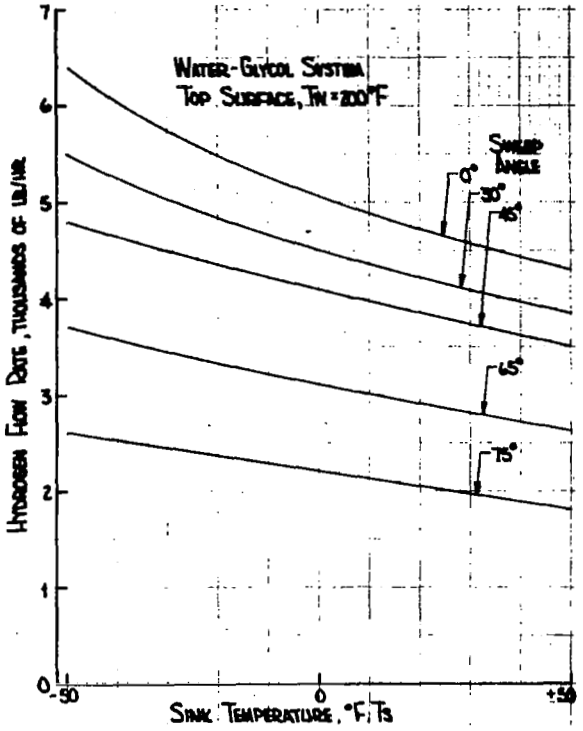

Figure 97. Hydrogen Flow Rates for an Indirect Water-Glycol Cooling System for One-Half of the Top Surface of the Wing for a 0.05 inch Leading Edge Radius for M = 6.0, α = 10.31°, Altitude = 100,000 ft

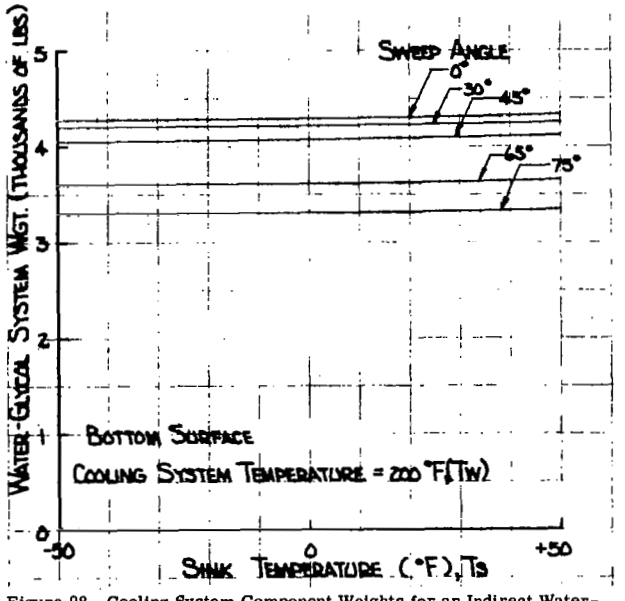

Figure 98. Cooling System Component Weights for an Indirect Water-Glycol Cooling System for One-Half of the Bottom Surface of the Wing for a 0.05 inch Leading Edge Radius for Radius for M = 6.0, α = 10.31°, Altitude = 100,000 ft

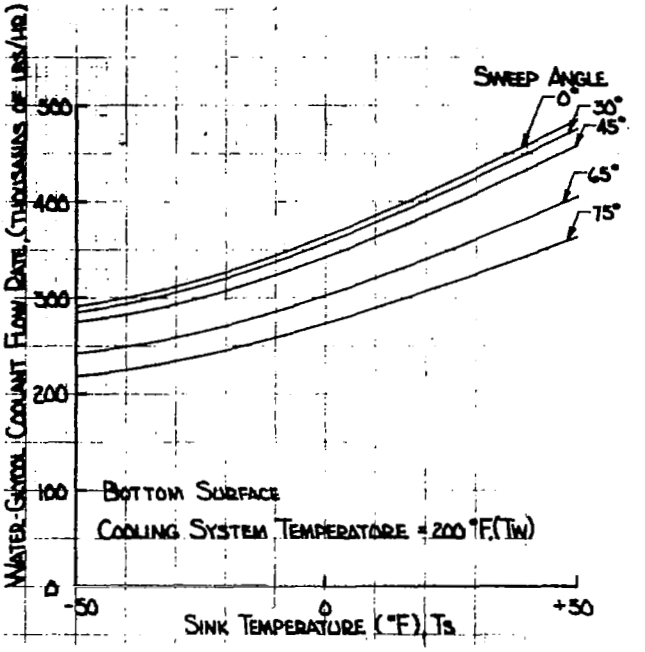

Figure 99. Water-Glycol Flow Rates for an Indirect Water-Glycol Cooling System for One-Half of the Bottom Surface of the Wing for a 0.05 inch Leading Edge Radius for M = 6.0, α = 10.31°, Altitude = 100,000 ft

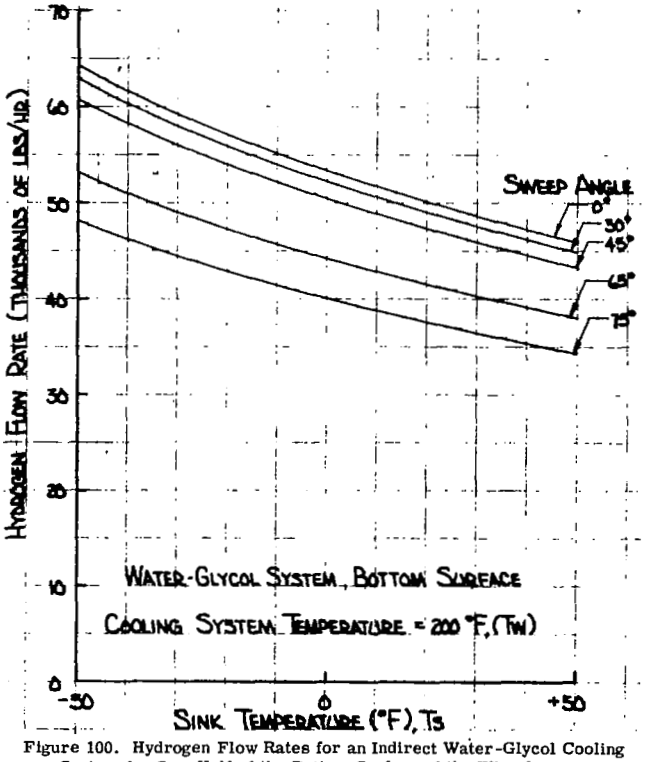

Figure 100. Hydrogen Flow Rates for an Indirect Water-Glycol Cooling System for One-Half of the Bottom Surface of the Wing for a 0.05 inch Leading Edge Radius for M = 6.0, α = 10.31°, Altitude = 100,000 ft

flow rate increasing with increasing sink temperature and hydrogen flow-rate decreasing with increasing sink temperature is evident in Figures 93 and 94. System weights, water-glycol flow rates and hydrogen flow rates increase with increasing sweep angle because the leading edge area is increasing faster than heating rates on the leading edge decrease with increasing sweep angle.

Figures 95 through 97 and Figures 98 through 100 present water-glycol system data for flat top and bottom surfaces respectively. For these surfaces the trend with sweep angle is reversed from that noticed for the leading edge areas with water-glycol system weights, water-glycol flow rates and hydrogen flow rates decreasing with increasing sweep angle because both the area in question and the heat transfer coefficients are decreasing with increasing sweep angle. For the top surface water-glycol system weights range from approximately 800 to 1600 lb while for the bottom surface system weights range from approximately 6,600 to 8,600 lb. Water-glycol flow rates for the top surface are in the 40,000 lb/hr range, while water-glycol flow rates for the bottom surface are in the 700,000 lb/hr range. Hydrogen flow rates for the top surface are in the 4,000 lb/hr range while hydrogen flow rates for the bottom surface are in the 100,000 lb/hr range. A summary of this data is presented following a discussion of the indirect silicone cooling systems.

2. Indirect Silicone Cooling System Studies

Results for the indirect silicone cooling system are presented in Figures 101 through 109. In these figures silicone system weights, silicone flow rates, and hydrogen flow rates are presented as functions of the sink temperature and wing sweep angle. The value of the wing sweep angle defines the wing configurations shown in Figures 4 through 8. As shown in Figures 101 through 109 the average wall temperature for the silicone system is 400°F which is 200°F higher than for the water-glycol system. This assumed wall temperature of 400°F results in significantly lower heat loads for the silicone system as compared to the water-glycol system and will result in lower hydrogen flow rates.

Leading edge silicone system weight, silicone flow rate, and hydrogen flow rate variations for radii of 0.05 inch and 2.0 inches are presented in Figures 101 through 103. Silicone system weights range from approximately 960 lb for the 0°sweep case to 3200 lb for the 75° sweep case. Leading edge radius is not a strong variable with the most significant effect occurring for 45° where a transition from an entirely laminar leading edge for the 0.05 inch radius to an entirely turbulent leading edge for the 2.0 inch radius occurs and the turbulent heat transfer coefficients are above the laminar heat transfer coefficients. This results in higher weights for the 45° sweep case. Silicone flow rates for the leading edge, as shown in Figure 102, increase very rapidly as sink temperature approaches the assumed wall temperature. This is a result of the assumption as noted in Table XXII that the maximum transport fluid temperature is equal to the mean surface temperature. Thus, for a sink temperature of 300°F the silicone fluid has a maximum to minimum temperature range of only 100°F. For sweep angles of 0, 30 and 45° silicone flow rates would be about 100,000 lb/hr. For sweep angles of 65° or 75°silicone flow rates would probably be about 400,000 lb/hr for the leading edge. Hydrogen flow rates for the leading edge are about 10,000 lb/hr for 0, 30, and 45° sweep angles and about 20,000 lb/hr for 65° and 75° sweep angles.

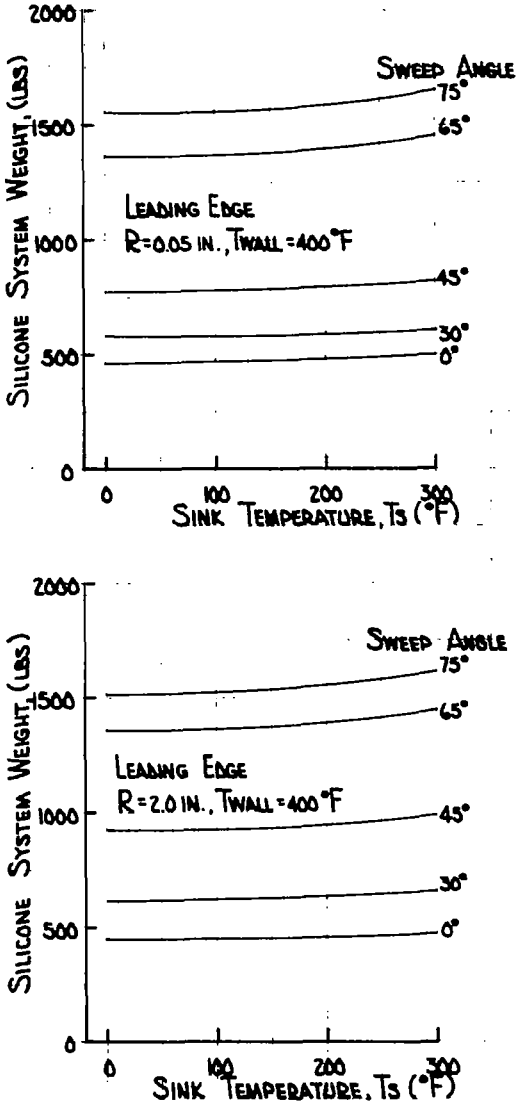

Figure 101. Cooling System Component Weights for an Indirect Silicone Cooling System for One-Half of the Wing for 0.05 and 2.0 inch Leading Radii for M = 6.0, α = 10.31°, Altitude 100,000 ft.

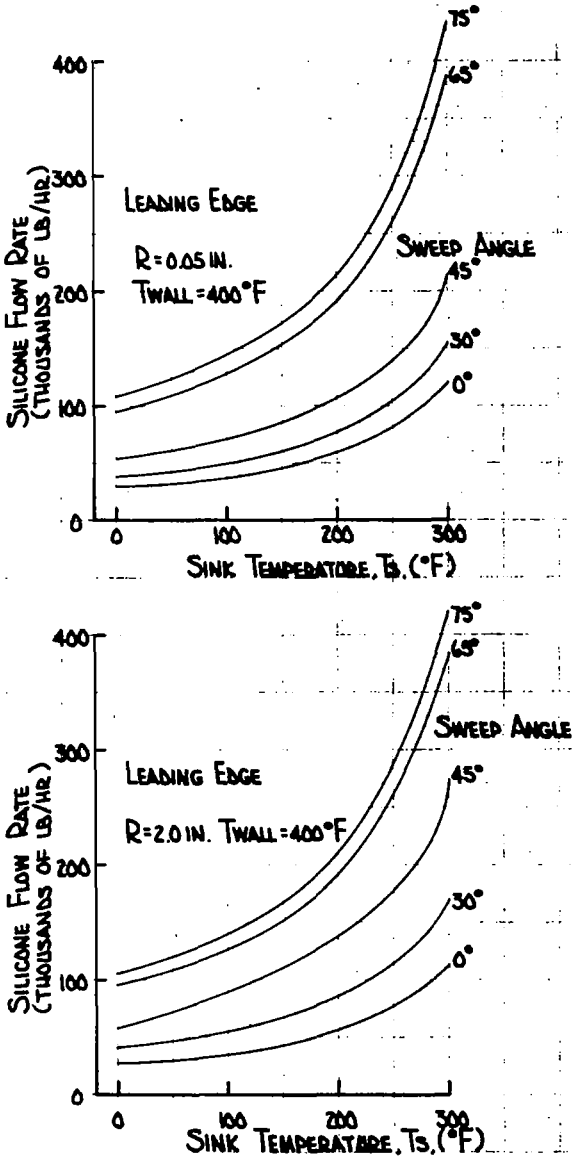

Figure 102. Silicone Flow Rates for an Indirect Silicone System for One-Half of the Wing for 0.05 and 2.0 inch Leading Edge Radii for M = 6.0, α = 10.31°, Altitude = 100,000 ft.

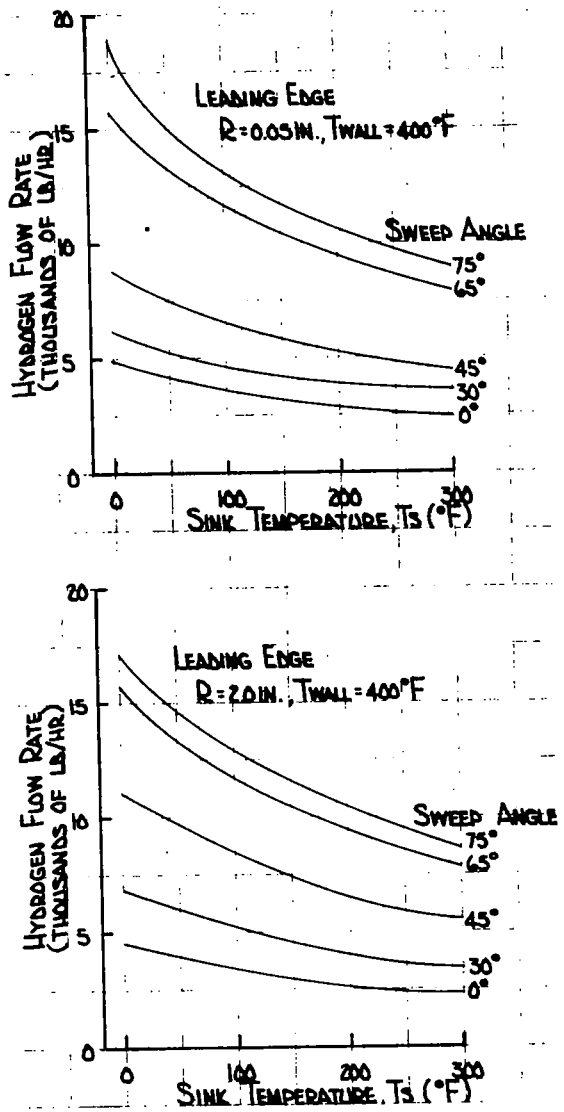

Figure 103. Hydrogen Flow Rates for an Indirect Silicone Cooling System for One-Half of the Wing for 0.05 and 2.0 inch Leading Edge Radii for M = 6.0, α = 10.31°, Altitude = 100,000 ft.

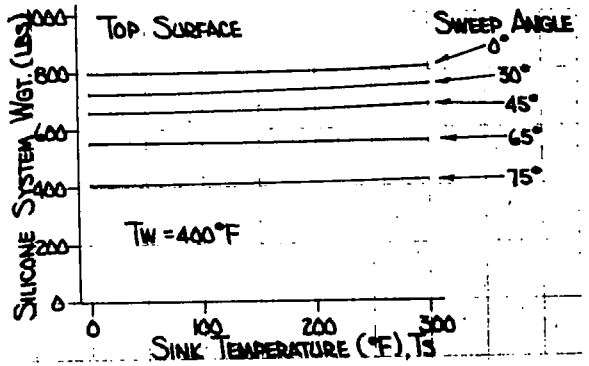

Figure 104. Cooling System Component Weights for an Indirect Silicone Cooling System for One-Half of the Top Surface of the Wing for a 0.05 inch Leading Edge Radius for M = 6.0, α = 10.31°, Altitude = 100,000 ft.

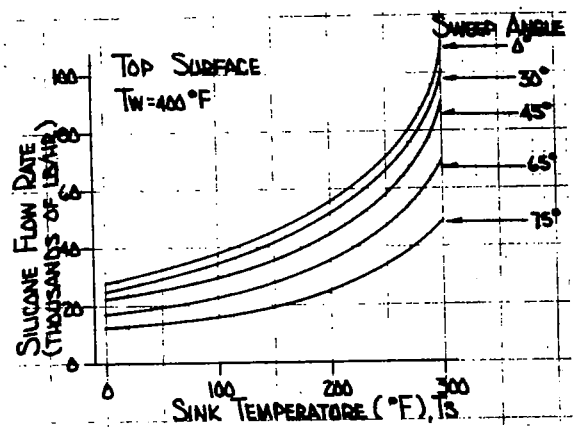

Figure 105. Silicone Flow Rates for an Indirect Silicone Cooling System for One-Half of the Top Surface of the Wing for a 0.05 inch Leading Edge Radius for M = 6.0, α = 10.31°, Altitude = 100,000 ft.

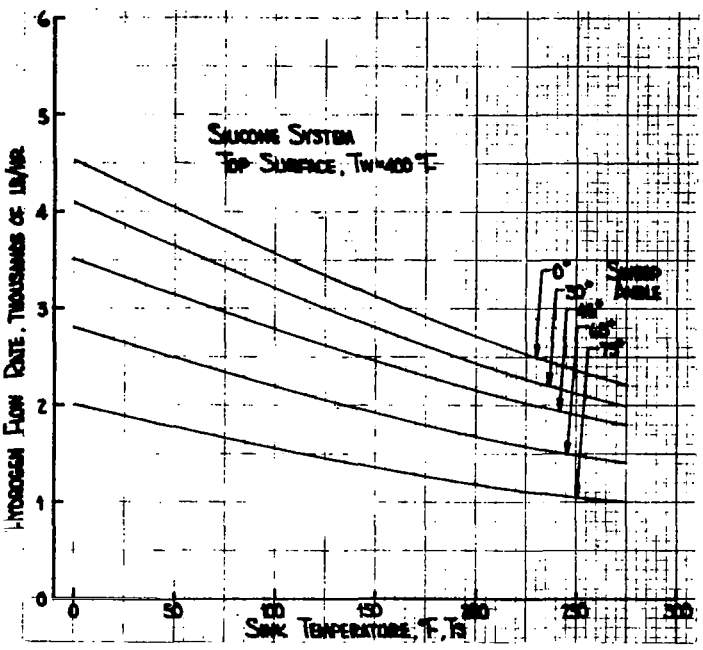

Figure 106. Hydrogen Flow Rates for an Indirect Silicone Cooling System for One-Half of the Top Surface of the Wing for a 0.05 inch Leading Edge Radius for M = 6.0, α = 10.31°, Altitude 100,000 ft.

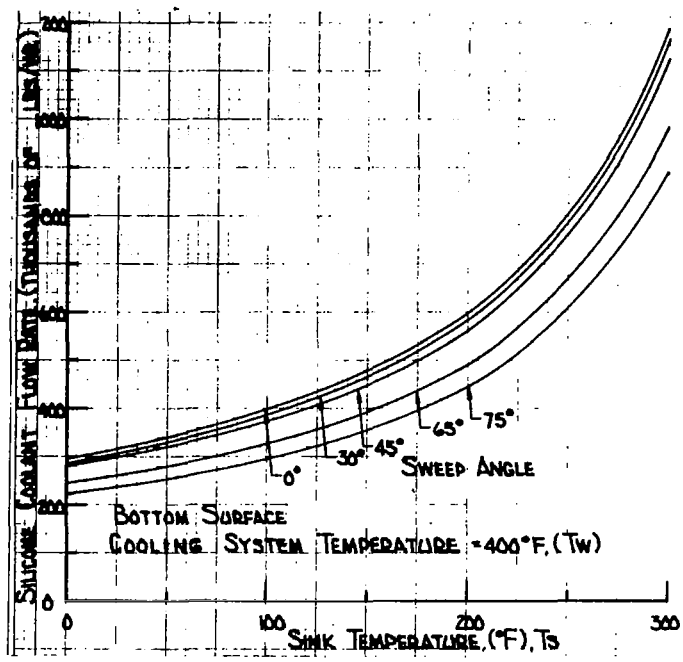

Figure 108. Silicone Flow Rates for an Indirect Silicone Cooling System for One-Half of the Bottom Surface of the Wing for a 0.05 inch Leading Edge Radius for M = 6.0, α = 10.31°, Altitude = 100,000 ft.

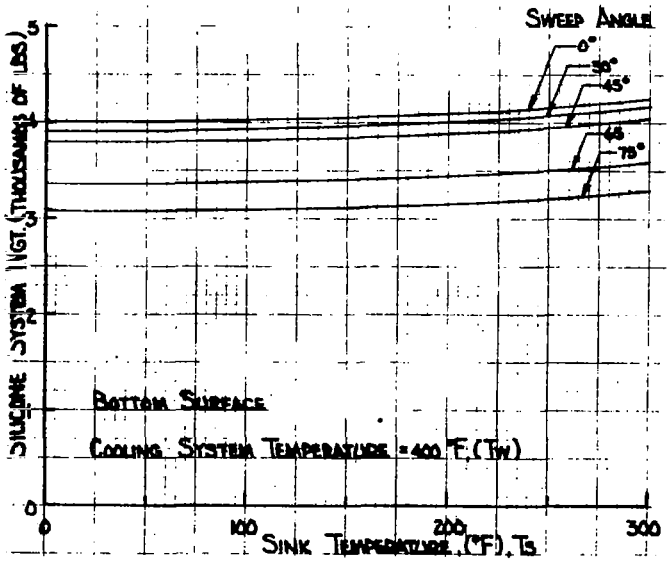

Figure 107. Cooling System Component Weights for an Indirect Silicone Cooling System for One-Half of the Bottom Surface of the Wing for a 0.05 inch Leading Edge Radius for M = 6.0, α = 10.31°, Altitude = 100,000 ft.

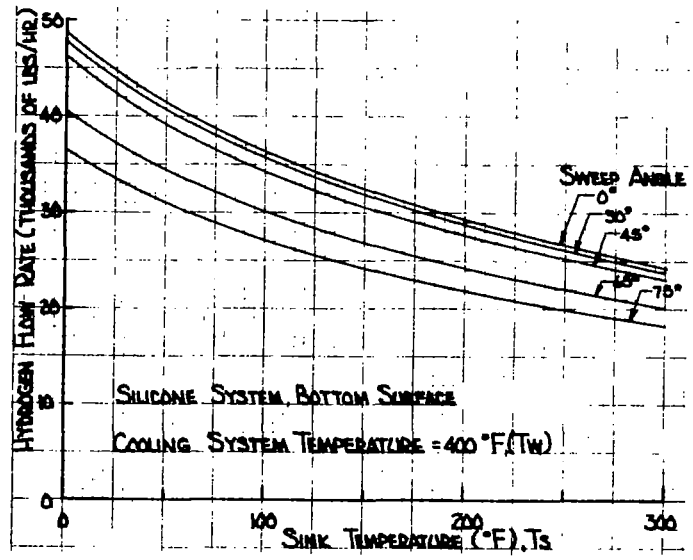

Figure 109. Hydrogen Flow Rates for an Indirect Silicone Cooling System for One-Half of the Bottom Surface of the Wing for a 0.05 inch Leading Edge Radius for M = 6.0, α = 10.31°, Altitude = 100,000 ft.

Data for the top and bottom flat surfaces is presented in Figures 104 through 109. Silicone system weights for the top surface range from 800 to 1600 lb for 75° and 0° sweep angles respectively. For the bottom surface silicone system weights range from 6200 lb to 8,000 lb for the 75 and 0° angles respectively. Silicone flow rates for the top surface are in the 100,000 lb/hr range while silicone flow rates for the bottom surface are in the 1,000,000 lb/hr range. Hydrogen flow rate requirements for the silicone system are approximately 4,000 lb/hr for the top surface and 60,000 lb/hr for the bottom surface. The following section summarizes both the water-glycol and silicone cooling system weights for the range of sweep angles studied.

3. Indirect Liquid Convective Cooling System Summary

Table XXIII summarizes the indirect convective cooling systems using water-glycol and silicone transport fluids, for a wing with a leading edge radius of 0.05 inches. Results for radii up to 2.0 inches would not vary more than a few percent. The data in Table XXIII was obtained by summing cooling system component data for the leading edge, top surface, and bottom surface areas and thus is representative of a cooling system for the complete wing. The most noticeable affect seen in Table XXIII is the small variation of the parameters tabulated with respect to sweep angle. This effect will become very significant when structural weights are calculated in Section VIII. At this point it appears from a cooling system component standpoint that sweep angle effects are again canceled out when the wing is examined in total.

Cooling system component weights for both the water-glycol and silicone systems are very weak functions of sink temperature. This effect will allow tradeoffs between hydrogen flow rate requirements and water-glycol or silicone flow rate requirements without concern for the effect on cooling system component weights. Water-glycol and silicone flow rates are in the range of 1 million pounds per hour. Flow rates of this magnitude are reasonable, but appear large in this table because of the approximately 10,000 sq ft cooled surface area. A flow rate of 1,000,000 lbs/hr for the wing is approximately 100 lb/hr per sq ft of surface area. Of course, flow rates on the bottom surface will be much larger than on the top surface and it is expected that flow rates on the bottom surface will be approximately 200-300 lb/hr per sq ft. A tradeoff between water-glycol flow rate and silicone flow rate and their respective sink temperatures is not felt to be necessary because even flow rates as high as 2 million lb/hr for the wing will still allow a cooling system of the type under consideration to be easily designed.

Hydrogen flow rates, on the other hand, present more of a problem for these systems. For the water-glycol system in particular, hydrogen flow rates are approaching the maximum allowable based on estimates of engine fuel requirements. Roughly, the required flow rate for each of the four engines for the aircraft in question is about 37,000 lb/hr making a total hydrogen flow rate of 147,000 lb/hr available without exceeding fuel flow rate requirements. As can be seen in Table XXIII hydrogen flow rates for the lower sink temperatures for the water glycol system exceed this estimate. However, at this point in the study this is not a point of great concern because these flow rate estimates are approximate estimates which can be reduced as detail studies progress. It should be mentioned that heat exchanger design assumptions are the main cause of the hydrogen

TABLE XXIII
INDIRECT LIQUID CONVECTIVE COOLING SYSTEM SUMMARY

	Water-Glycol System	Sweep Angle					
	200°F Mean Outer Surface Temperature	Sink Temperature (°F)	0°	30°	45°	65°	75°
Water-Glycol System 200°F Mean Outer Surface Temperature	Cooling System	-50	11,200	11,100	11,100	11,200	10,700
	Component Weight	0	11,300	11,200	11,200	11,300	10,800
	(lb)	+50	11,400	11,300	11,300	11,400	10,900
	Water-Glycol	-50	700,000	694,000	698,000	710,000	674,000
	Flow Rate	0	872,000	868,000	870,000	880,000	842,000
	(lb/hr)	+50	1,160,000	1,160,000	1,160,000	1,180,000	1,110,000
	Hydrogen	-50	154,000	153,000	154,000	155,000	148,000
	Flow Rate	0	128,000	127,000	128,000	129,000	123,000
	(lb/hr)	+50	109,000	109,000	110,000	111,000	105,000
Silicone System 400°F Mean Outer Surface Temperature	Cooling System	0	10,500	10,400	10,500	10,600	10,100
	Component Weight	100	10,600	10,500	10,500	10,600	10,100
	(lb)	200	10,800	10,700	10,700	10,800	10,300
	Silicone	0	706,000	698,000	712,000	720,000	688,000
	Flow Rate	100	952,000	938,000	952,000	954,000	912,000
	(lb/hr)	200	1,440,000	1,420,000	1,420,000	1,430,000	1,370,000
	Hydrogen	0	116,000	116,000	117,000	118,000	115,000
	Flow Rate	100	87,000	86,400	87,000	87,600	83,400
	(lb/hr)	200	70,200	70,400	70,400	70,800	67,700

flowrate predictions being above the 147,000 lb/hr baseline. More efficient heat exchangers than the one assumed for preliminary system weight estimates have been designed and built, but it was felt that specification of these types of heat exchangers at this point in the study would unduly complicate the calculations and possibly hinder the proper interpretation of the results. For the silicone system, hydrogen flowrates are in the 100,000 lb/hr range and are significantly below estimated engine fuel flowrate requirements. Again, these flowrates can be reduced by more rigorous specification of heat exchanger design parameters. Examples of this improvement will be given in Section 9.

C. RAM AIR CONVECTIVE SYSTEM

Prior to the examination of air as a transpirant an investigation was conducted to determine the feasibility of using ram air as a convective coolant. Flowrate requirements were higher than those for transpiration cooling, as would be expected. However, the results of the analyses of ram air convective cooling of the upper and lower wing surfaces are presented in this section because of the possible integration of convective air cooling with air transpiration cooling of the leading edges. For a system of this type the critical components with respect to weight and aircraft performance are the inlet air cooling device and the ram air scoop. These are examined in the next two subsections.

1. Ram Air Convective System Weight Determination

Cooling systems using the atmosphere as a heat sink have been in general use since the inception of the airplane. The use of a supersonic air stream for cooling requires either the use of a turbine or a heat exchanger to extract the kinetic energy from the ingested air stream so that its velocity relative to the airframe is lost. This kinetic energy loss must be accomplished in a way that results in an air temperature compatible with the vehicle cooling system.

If a turbine is used, its power output must be converted into heat or work. While some work might be extracted for useful purposes such as electrical power generation, the total quantity of work available from the mass flow of air required to cool the wing will exceed aircraft needs. Recompression of the internal cooling stream, after it has absorbed structural heat, is the usual procedure for rejecting this excess power. Therefore, the atmospheric cooling system consists of an inlet and diffuser, an air turbine, a heat exchanger (structure), a mechanical utilizer (compressor) and an exit. The compressor and exit could be replaced by a transpiration cooling system.

At first glance, open cycle atmoshperic cooling is an attractive cooling system because it requires no weight in heat sink material within the vehicle. This is particularly convenient for long flight times since the cooling system weight will be independent of time. Air is also a convenient fluid to circulate around the structure because it has no particular hazards, ducting leakage is unimportant, there is no system maintenance except for the turbine (and compressor), and no logistic problems are involved.

However, there are serious limitations to this system. The entire inlet duct and the first nozzle stage of the turbine would be subjected to stagnation temperatures and would

operate at these temperatures, unless cooled, since these areas experience worse boundary layer conditions than the external surface. Temperatures are near stagnation because no relief by radiation is possible in an internal duct; each hot wall merely radiates to all others and the effect is canceled.

Recompression, to absorb the work removed from the air stream, means raising the temperature of the stream that already contains the entire net influx of heat to the structure. Thus, it must be expelled at approximately the original velocity, but at a much higher temperature, so that temperatures on some of the compressor blades and along the exit duct exceed those on the inlet side.

Other problems are introduced by the large volumes involved when the air is expanded to a temperature low enough to be useful, and by relatively small heat transfer coefficients that are obtained between the slow-moving internal air and the structure.

The system just described was direct cooling by means of air; the term "direct" signifies that the final coolant (air) is used in contact with the structure to be cooled. An indirect system is possible in which a secondary fluid is circulated, in a closed system, through the structure and a heat exchanger. The air passes only over the heat exchanger.

The indirect system was not considered seriously during the present study because its only advantage lies in overcoming the difficulty of circulating large volumes of air through the structure. Both the turbine and the compressor for the main air flow are still required and the extreme temperature problems of the inlet and exit systems are not reduced.

The size, and therefore the weight, of the turbine-compressor unit is largely a function of the air volume to be handled. The J73-GE-3 turbojet engine weighing 3880 lb, takes a sea-level air flow of 142 lb/sec and has a frontal area of 9.96 ft^2. The mass flow is equivalent to 1850 ft^3/sec. By comparison, it may be expected that the turbine-compressor for open cycle atmospheric cooling at Mach 6 would be somewhat smaller and lighter than the J73, but after allowances are made for cooling, it may be expected that the unit will weigh at least 5000 lb.

Referring to Table XVI air flow rates for transpiration cooling are seen to be about 50,000 lb/hr for the bottom surface of the wing and about another 25,000 to 30,000 lb/hr for cooling the top surface and leading edge. Assuming that an inlet diffuser can yield an air pressure of 1200 psf at the turbine inlet with an inlet temperature of 3200° R this turbine-compressor unit must handle 79 ft^3/sec per 1000 lb/hr of air taken on board. Proportioning this roughly to the J73-GE-3 turbojet engine (with an allowance for cooling), weights for a turbine-compressor would be about 5000 lb per 50,000 lb/hr of intake air. For a turbine only, weights would be roughly half the above or 2500 lb per 2000 lb/hr of intake air.

Although it appears that an expansion turbine system could be built, the complexities of this system discouraged its use. Cooling requirements and the problem of utilization of the power extracted from the ingested airstream were the major reasons for rejection of this system. System weight estimates did not yield unreasonably high weights.

The feasibility of a system incorporating a hydrogen-air heat exchanger cannot be determined until weights and hydrogen flow rate requirements for such a system are es-

timated. In the following paragraphs a heat exchanger weight determination scheme is outlined and weight and hydrogen flow rate requirements are presented for a convective system incorporating a hydrogen-air heat exchanger. It was concluded in Section VI that transpiration cooling the entire wing with air was not feasible. The purpose of studies presented in this section is to investigate the possibility of a hybrid convective-transpiration system using air as the coolant. As will be seen, it is not possible to convectively cool the entire wing using ram air, but convective cooling in conjunction with transpiration cooling should be investigated.

A schematic of the convective portion of such a system is shown in Figure 110 where the major components and the operating parameters are indicated. Ram air is brought on board through an air scoop entering at approximately 80 lb/in^2 pressure and a temperature of 3200°R. This ram air is cooled in a ram air-hydrogen heat exchanger with the cool air leaving the heat exchanger at a sink temperature, T_s. The cool sir is used in a convective system leaving at a temperature denoted by T_o and is then used for transpiration cooling selected portions of the wing. No consideration has been given to the possibility of recirculating the air based on studies of convective cooling with gases as included earlier in this section. The hydrogen fuel used to cool the air enters the ram air-hydrogen heat exchanger at a temperature of -400°F and leaves the heat exchanger at a temperature 100°F below the sink temperature.

As seen from the studies on the air transpiration concept large mass flow rates are expected and it was anticipated that a ram air heat exchanger such as that shown in Figure 110 would be a large cooling system component. To reasonably size such a component a minimum weight heat exchanger configuration must be used. Reference 23 describes in detail the optimization of heat exchangers of the cross-counter-flow type. The heat exchanger and its associated power source are assumed to be the only components in a system to be weight optimized. The characterization of the heat exchanger - power pair consists of developing a set of equations which relate physical properties of the components to their functional characteristics and state points. The basic equation of optimization is an expression for the weight of the heat exchanger plus the weight of the power system required to operate it. The assumptions in the development of this equation are as follows:

a. Header weight directly proportional to core weight

b. Linear power penalty

c. Velocity changes and their effects on pressure losses are neglected

d. Incompressible fluid

e. Fluid properties constant

f. Reynolds number is the primary independent variable

g. Fin effectiveness constant

The final optimized equations for the heat exchanger yield many interesting results the most significant of which are listed below. For a fixed power penalty, a selected core, and selected fluids and for minimum heat exchanger weight:

a. Reynolds numbers are constant (do not change as the design heat load, Q, is changed)

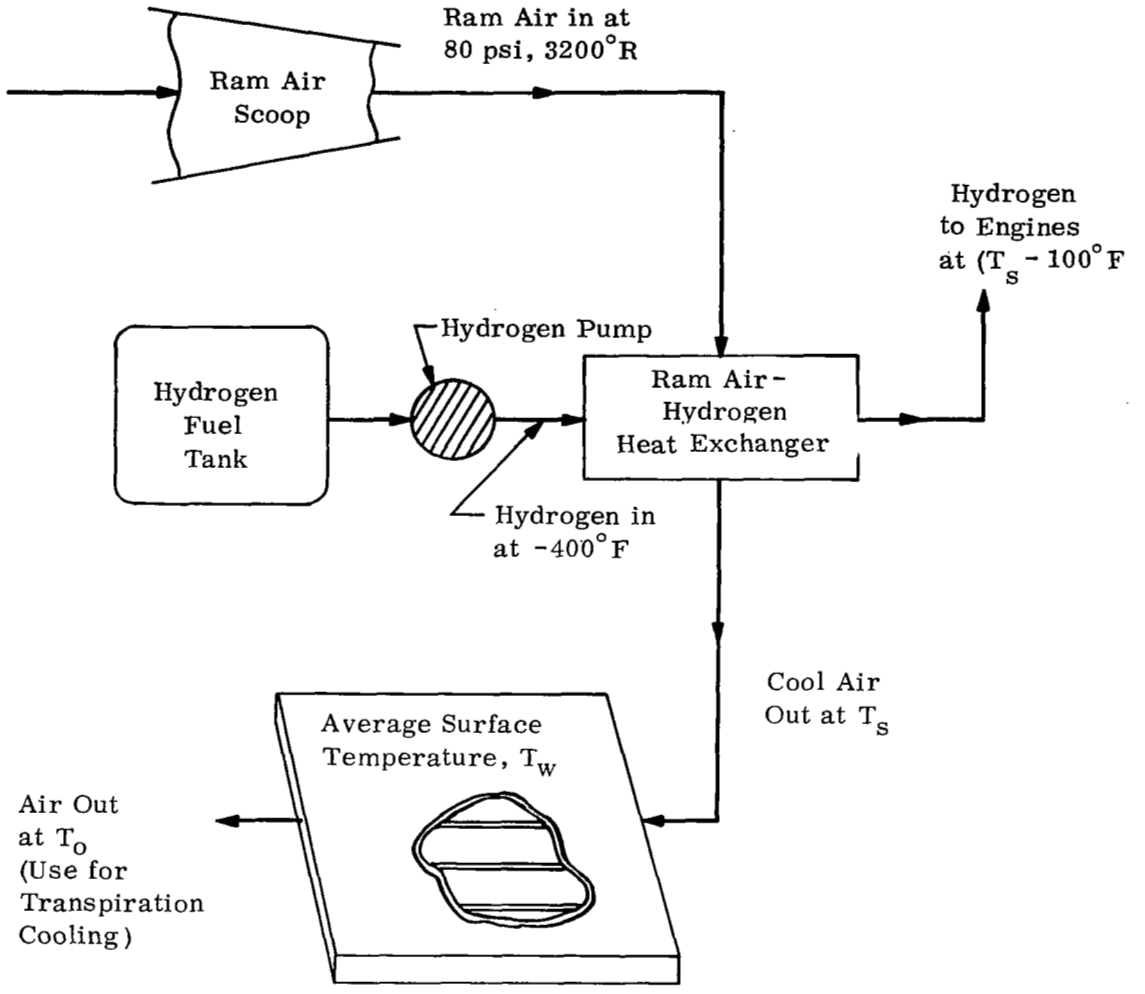

Figure 110. Ram Air Convective Cooling System Schematic

b. Flow dimensions of the heat exchanger are independent of Q

c. Weight, volume, and the no-flow dimension are directly proportional to Q (for constant values of $A\ U_{av}/(Cp\ \Delta T)_{min}$) where:

A, is the total heat transfer area on one side

U_{av}, average overall heat transfer coefficient

Cp, specific heat

ΔT, (T inlet - T outlet)

T, temperature

For the particular problem at hand an iteration on core geometry was not felt necessary. Using past experience on the development of lightweight heat exchangers as found in References 24 and 25, a choice of core geometry was made, assuming the ram air was cooled by supercritical hydrogen. The core geometries chosen are the 11-1 plain fin (hydrogen side) and the 3/8-6.06 louvered fin (air side) shown in Reference 26. Using the above core geometry and a power penalty of 1.1 lb/hp, heat exchanger weights were determined for cooling ram air with supercritical hydrogen. Assuming a header allowance of 15% of the core weight, the following optimization parameters were obtained:

a. Reynolds Number, Air Side = 9300

b. Reynolds Number, Hydrogen Side = 9400

c. Minimum Weight = 35.2 (UA)
Note: $(UA)_{air} = (UA)_{hydrogen}$

The above parameters were incorporated into a computer program to give heat exchanger weight, volume and dimensions for given air flow rates, air and hydrogen temperatures. Results from this computer program were incorporated in the weight determination for the ram air convective cooling system. For the system shown schematically in Figure 110 the controlling operating parameters are summarized in Table XXIV.

Figures 111 through 116 present the convective data for the ram air convective-transpiration system. Since a perturbation on wall temperature was included for the transpiration results it was felt that a perturbation on wall temperature should also be included for the convective systems. As noted in Figures 111, 112 and 113 data was generated for the top surface for average wall temperatures of 200°F and 400°F. For the bottom surface similar data was generated for average wall temperatures of 200°F and 600°F. Since the air being used in a transpiration system must be the air leaving the convective system higher wall temperatures than those studied were not felt necessary.

Hydrogen flow rate data is plotted as a function of sink temperature in both Figures 111 and 114. For a constant sweep angle and constant wall temperature a minimum point occurs. It was observed from a study of data for all five sweep angles that the minimum point did not change significantly with sweep angle for a constant wall temperature. Thus, data is presented only for the 0° sweep angle cases. For a 200°F wall temperature for both the top and bottom surfaces the minimum point occurs at a sink temperature of approximately -50°F. For a wall temperature of 400°F and a wall temperature of 600°F

TABLE XXIV

RAM AIR CONVECTIVE SYSTEM PARAMETERS

A. Air cooled from 2740°F (3200°R) to T_s

B. Hydrogen heated from -400°F (60°R) to (T_s - 100°F)

C. Specific heat:
   Air, 0.23 Btu/lb°R
   Hydrogen, 3.5 But/lb°R

D. Ram air system component weights

1. Heat Exchanger Weight = 35.2 UA

$$UA \cong \frac{\text{heat transferred (Btu/hr)}}{\text{log mean temperature difference (°R)}}$$

2. Distribution system weight = (1.0 lb/ft²)A

Note:
The distribution system weight estimate includes such items as ram air scoop and associated lines, lines for delivering air to wing panels and then to transpiration system with associated control valves, supports, etc.

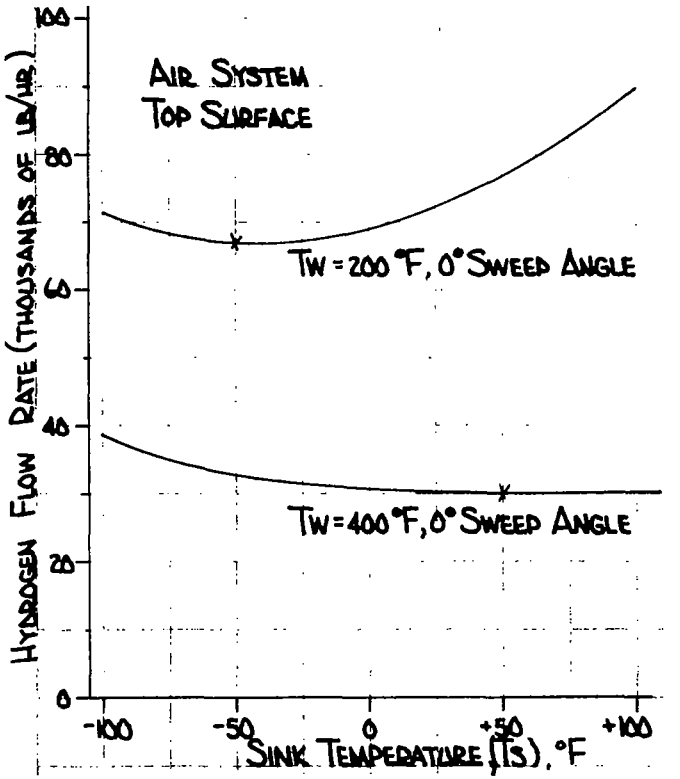

Figure 111. Sink Temperature Determination for 200°F and 400° Outer Surface Temperatures for a Ram Air Convective Cooling System for One-Half of the Top Surface of the Wing for a 0.05 inch Leading Edge Radius for M = 6.0, α = 10.31, Altitude = 100,000 ft

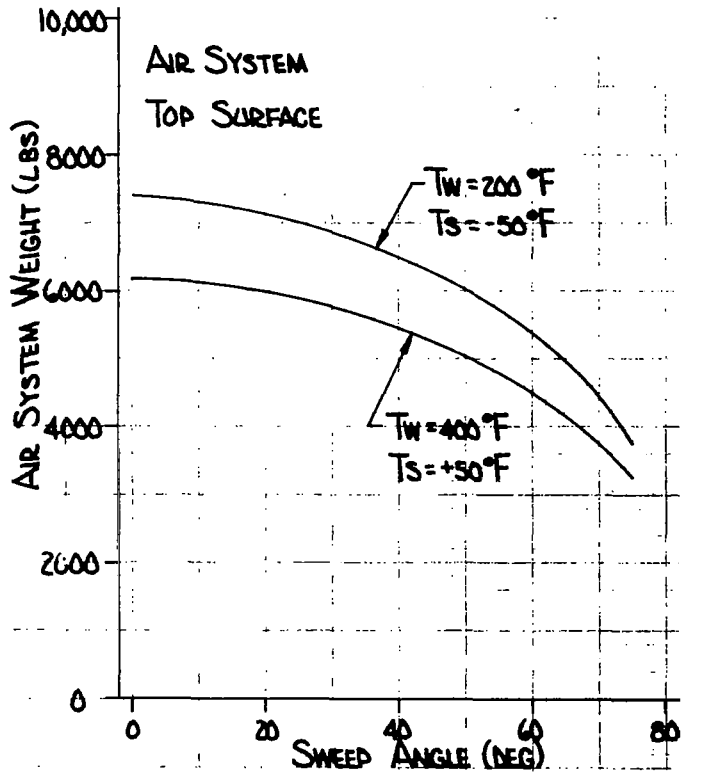

Figure 112. Cooling System Component Weights for a Ram Air Convective Cooling System for One-Half of the Top Surface of the Wing for a 0.05 inch Leading Edge Radius for M = 6.0, α = 10.31°, Altitude = 100,000 ft

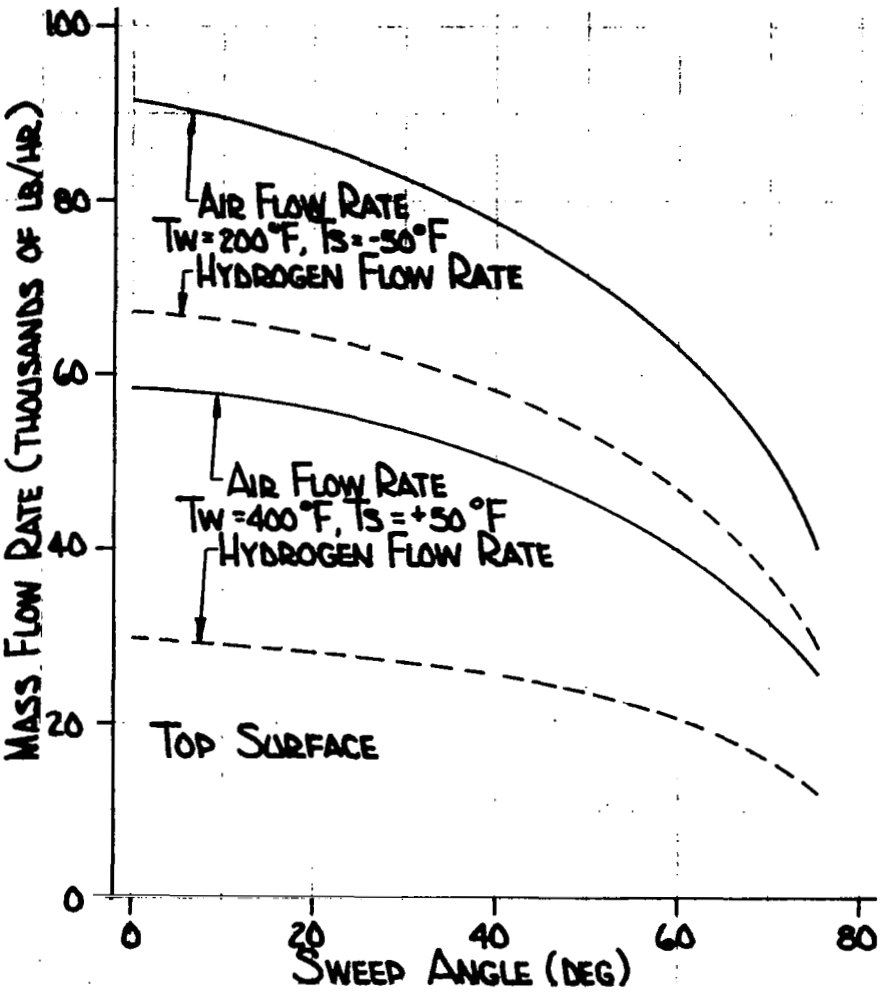

Figure 113. Air and Hydrogen Flow Rates for a Ram Air Convective Cooling System for One-Half of the Top Surface of the Wing for a 0.05 inch Leading Edge Radius for M = 6.0, α = 10.31°, Altitude = 100,000 ft

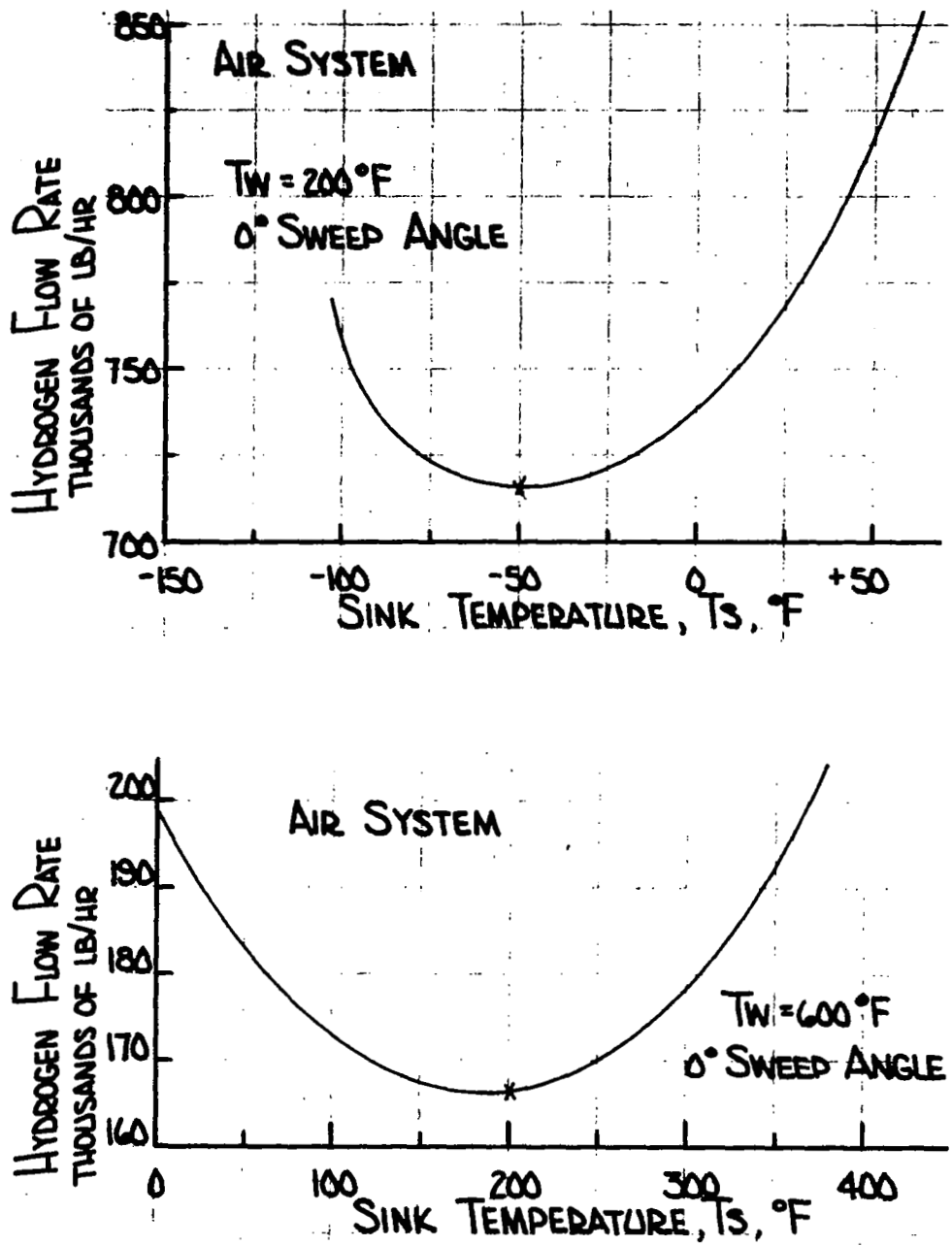

Figure 114. Sink Temperature Determination for 200°F and 600°F Outer Surface Temperatures for a Ram Air Convective Cooling System for One-Half of the Bottom Surface of the Wing for a 0.05 inch Leading Edge Radius for M = 6.0, α = 10.31°, Altitude = 100,000 ft

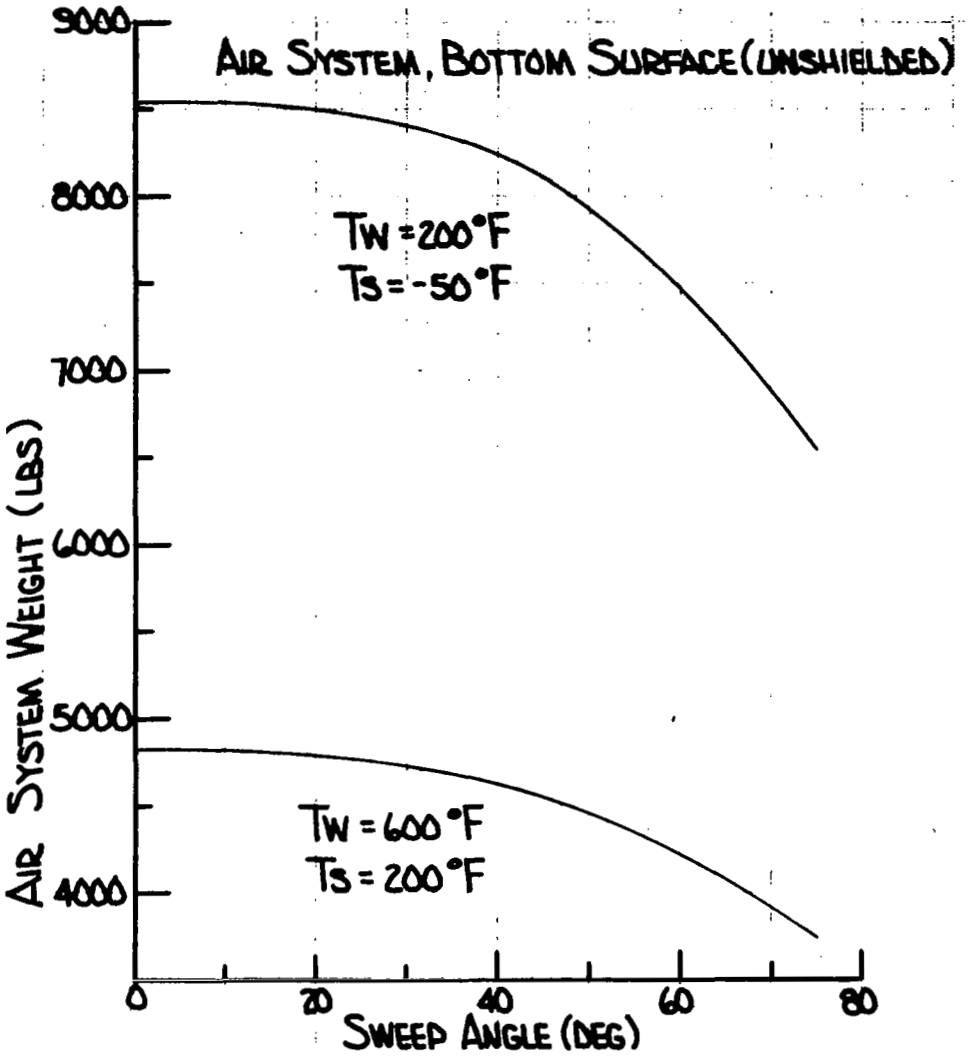

Figure 115. Cooling System Component Weights for a Ram Air System Convective Cooling System for One-Half of the Bottom Surface of the Wing for a 0.05 inch Leading Edge Radius for M = 6.0, α = 10.31°, Altitude = 100,000 ft

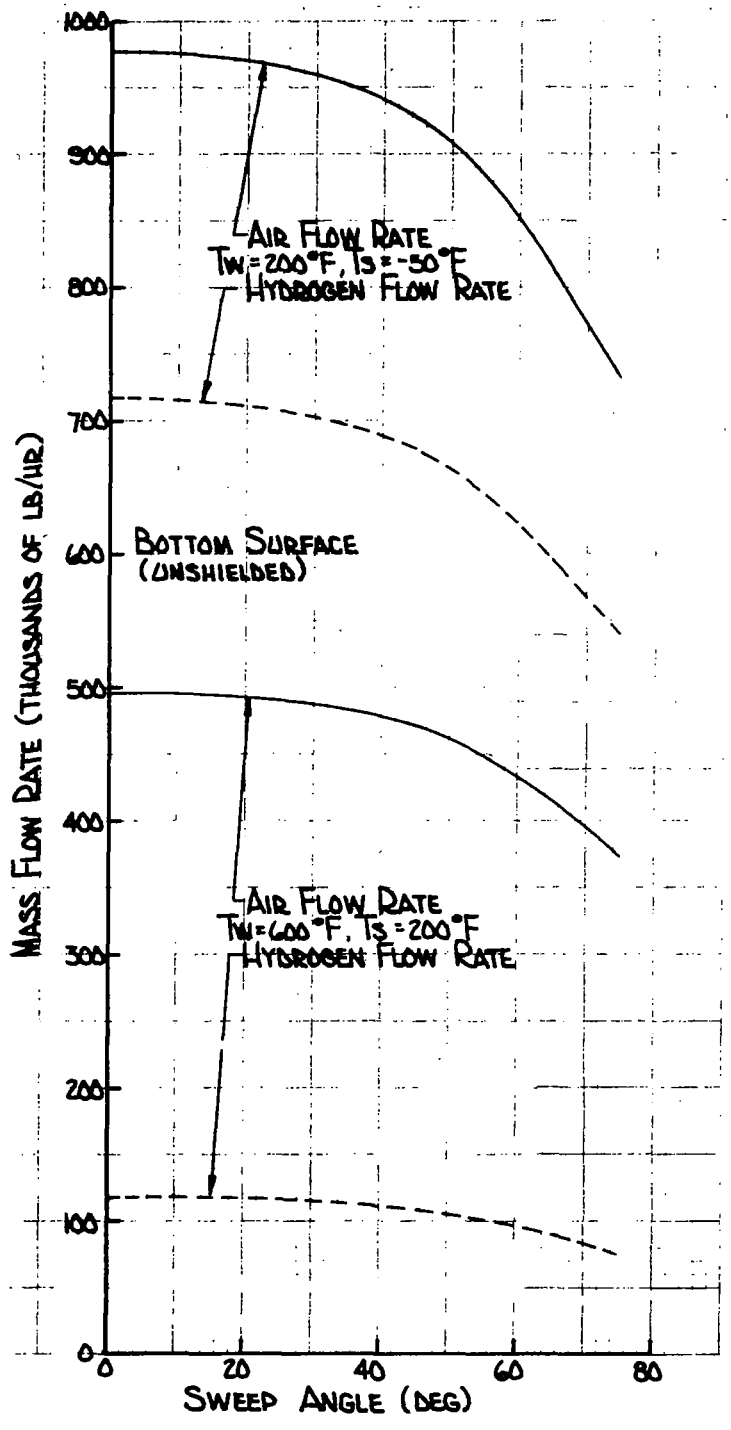

Figure 116. Air and Hydrogen Flow Rates for a Ram Air Convective Cooling System for One-Half of the Bottom Surface of the Wing for a 0.05 inch Leading Edge Radius for M = 6.0, α = 10.31°, Altitude = 100,000 ft

the sink temperatures at which the minimum point occurs are +50°F and +200°F respectively. Convective system weights were determined for operating conditions which minimized the hydrogen flow rate requirements.

Air system weights for the top surface are presented as a function of sweep angle in Figure 112. For a 0° sweep wing and a 200°F wall temperature, system weights would be approximately 14,800 lb while for a 400°F wall temperature and a 75° sweep wing system weights will be approximately 6,500 lb. Air flow rates for the top surface as plotted in Figure 113 range from approximately 183,000 lb/hr for a 200°F wall, 0° sweep angle configuration to 52,000 lb/hr for a 400°F wall, 75° sweep configuration. Hydrogen flow rates vary from approximately 134,000 lb/hr for a 200°F wall, 0° sweep configuration to approximately 24,000 lb/hr for a 400°F wall, 75° sweep configuration. System weights for the bottom surface of a ram air convective-transpiration system in which the bottom surface is convectively cooled vary from approximately 17,100 lb for a 0° sweep, 200°F wall temperature to 7,500 lb for a 200°F 75° sweep configuration. Air flow rates for these configurations are 1,955,000 lb/hr and 750,000 lb/hr respectively. Hydrogen flow rates for these configurations are approximately 1,435,000 lb/hr and 150,000 lb/hr respectively.

Table XXV summarizes the data presented in Figures 111 through 116. This data is meant to show representative system parameters and should not be interpreted as inflexible. Air flow rates would be determined in the final anaylsis by a matching of transpiration flow rate requirements and convective flow rate requirements through changes in the surface temperature of either the top or bottom surface or portions thereof. Hydrogen flow rate requirements are excessive for many of the cases presented in Table XXV. Particularly the 200°F surface temperature case for the bottom surface. It would appear at this point in the study that large sections of the wing could not be convectively cooled with air and that the wing would have to be broken into small segments to allow design of a hybrid ram air convective-transpiration cooling system. Radiation shield techniques such as those described in Section 5 could also be employed to reduce air and hydrogen flow rate requirements for the upper and lower wing surfaces.

2. Ram Air Intake Investigation

For the ram air convection system to be feasible the penalties associated with bringing air onboard the aircraft must be minimal. The penalty most easily estimated is the drag associated with a ram air scoop. This penalty will be the most significant of any penalty associated with a ram air system. The configuration of a scoop, which is both practical and efficient, requires a detailed design effort beyond the scope of this study. However, some significant information about the drag penalty due to a ram air scoop has been obtained.

The drag increment due to the addition of an air induction system to a given configuration consists primarily of two parts: (a) ram drag, D_r, due to decelerating a quantity of air from local velocity to approximately zero internal velocity; and (b) external pressure drag, D_e, on the wedge, cowl and other components which must be added to the aircraft to form the scoop. It can be assumed that the scoop is well designed. (Obviously, if it cannot be, some other cooling concept would be considered.) It follows, therefore, that the ram drag, D_r, will be significantly larger than the external drag, D_e. To a first approximation, therefore, the drag penalty due to an air induction system is due to the ram drag.

TABLE XXV

RAM AIR CONVECTIVE SYSTEM SUMMARY

	Top Surface					Bottom Surface				
	Sweep Angle					Sweep Angle				
	0°	30°	45°	65°	75°	0°	30°	45°	65°	75°
Nominal Surface Temp.	200°F									200°F
Sink Temperature	-50°F									-50°F
Air System Wt. (lb)	14,800	13,800	12,600	9800	7400	17,100	16,800	16,200	14,150	13,100
Air Flow Rate (lb/hr)	183,000	165,000	149,000	115,000	80,000	1,955,000	1,920,000	1,850,000	1,620,000	1,460,000
Hydrogen Flow Rate (lb/hr)	134,000	124,000	112,000	85,000	57,000	1,435,000	1,405,000	1,355,000	1,190,000	1,080,000
Nominal Surface Temp.	400°F				400°F	600°F				600°F
Sink Temperature	50°F				50°F	200°F				200°F
Air System Wt. (lb)	12,400	11,500	10,500	8300	6500	9650	9450	9100	8150	7500
Air Flow Rate (lb/hr)	117,500	107,000	96,000	72,100	52,000	990,000	975,000	940,000	830,000	750,000
Hydrogen Flow Rate (lb/hr)	60,000	54,000	49,000	37,000	24,000	235,000	230,000	215,000	180,000	150,000

The magnitude of the ram drag is given by

$$D_R = \frac{W_A}{g} V_L + (P_L - P_\infty) A_C$$

Where the capture area, $A_C = \frac{W_A}{\rho_L V_L g}$.

The ram drag per unit airflow is therefore

$$\frac{D_R}{W_A} = \frac{V_L}{g} + \frac{P_L - P_\infty}{\rho_L V_L g}$$

The ram drag coefficient is also of interest since it can be compared directly with the aircraft drag coefficient. The ram drag coefficient is defined by

$$C_{D_R} = \frac{D_R}{\frac{1}{2}\rho_\infty V_\infty^2 S} = \frac{2 W_A}{\rho_\infty V_\infty^2 S} \left(\frac{V_L}{g} + \frac{P_L - P}{\rho_L V_L g} \right)$$

The local velocity, V_L, and the local pressure, P_L, are functions of the aircraft configuration and scoop geometry. Their magnitudes will be somewhere between free stream values and the values behind a normal shock. Preliminary trends can be examined by assuming free stream conditions and the local conditions under the wing at an angle of attack of 10.0°. Values of D_R / W_A and C_{D_R} / W_A under these conditions as a function of Mach number are shown in figures 117 and 118. The different local conditions are seen to have little effect on these parameters. Values of C_{D_R} and A_C for a range of air flow rates consistent with those in Table XXV are shown in figure 119. Although the capture areas are not prohibitive and at low air flow rates the drag is not significant, at the higher values, the ram drag approaches the aircraft drag. In these air flow rates, the provision for an efficient air collection system may present a formidable design problem.

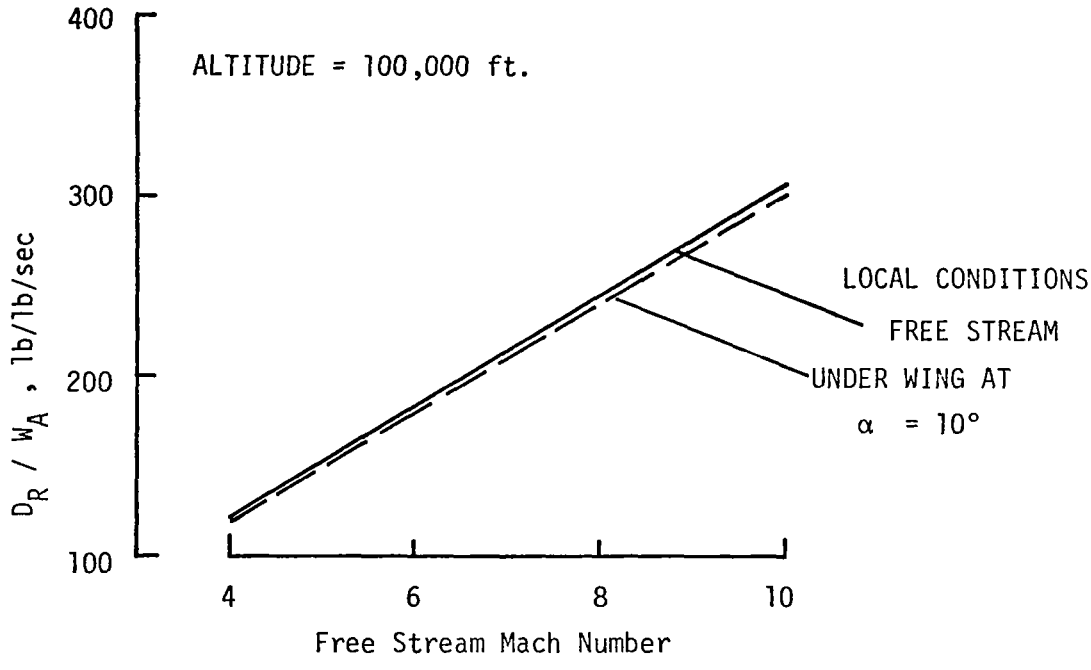

Figure 117. - RAM DRAG PER AIR FLOW RATE.

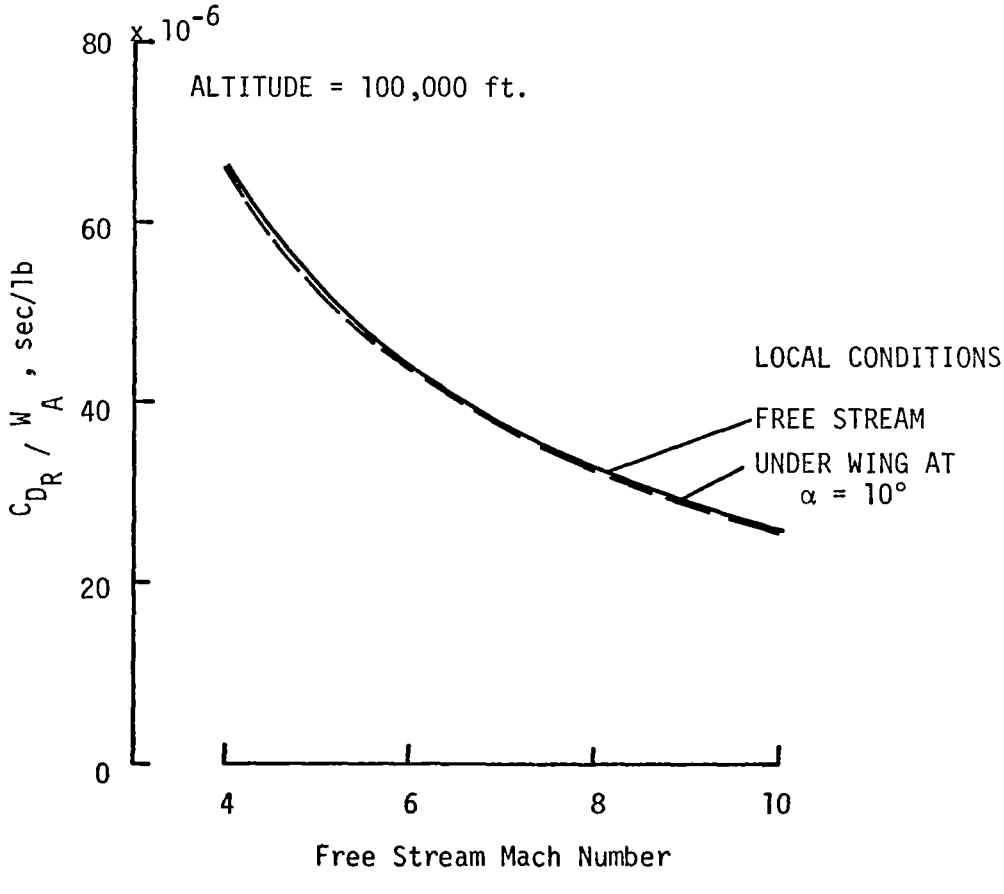

Figure 118. - RAM DRAG COEFFICIENT.

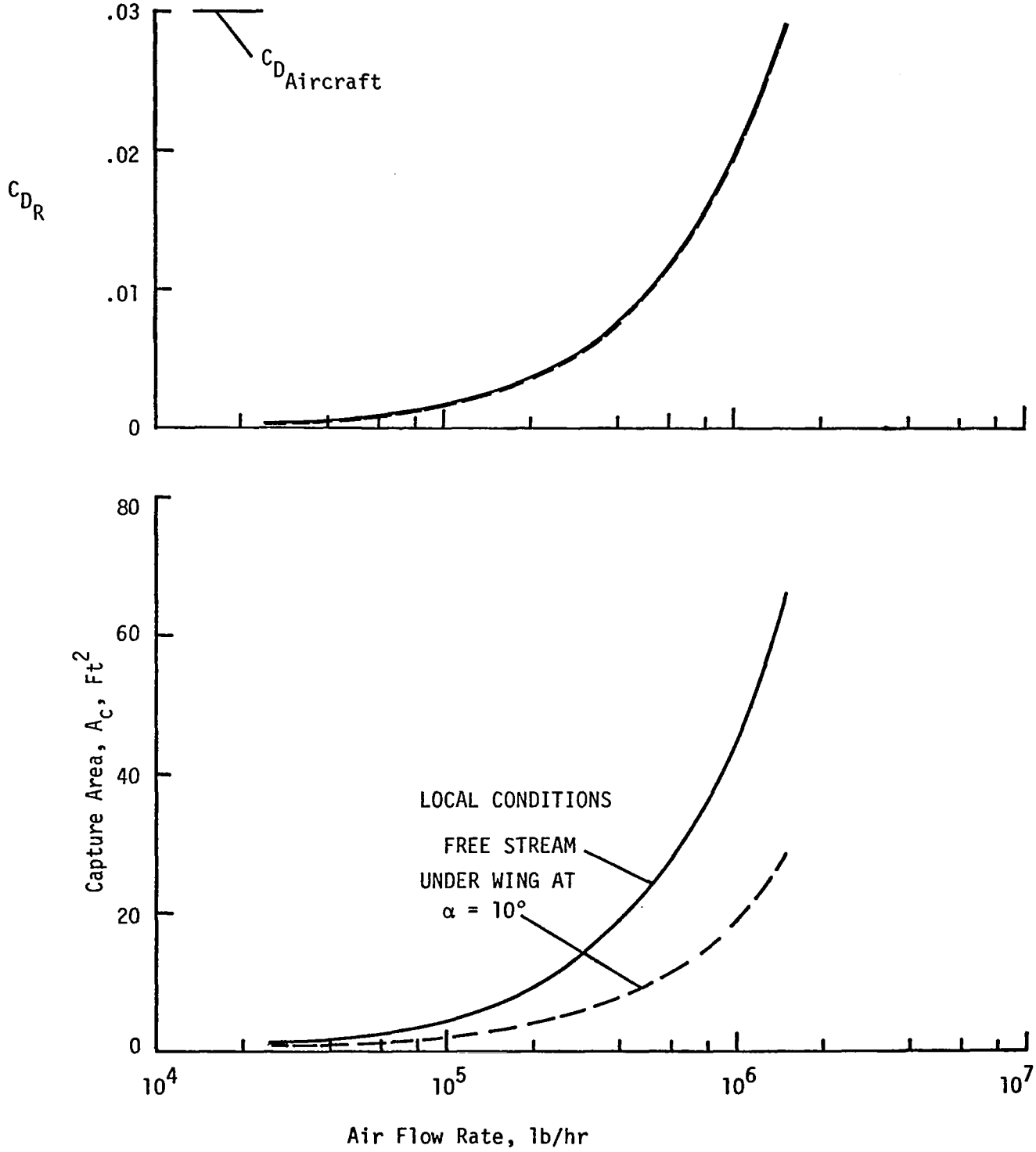

Figure 119. - RAM DRAG COEFFICIENT AND CAPTURE AREA, M = 6, ALTITUDE = 100,000 FEET.

D. SPRAY COOLING SYSTEMS

As mentioned in an earlier section consideration has been given to spray cooling systems using water and lithium as the coolants. For both coolants the property of greatest interest is the latent heat of vaporization when boiling at a pressure corresponding to atmospheric pressure at cruise altitude. At 100,000 ft atmospheric pressure is 0.16 psi. At this pressure water boils at about 50°F with a heat of vaporization of 1065 Btu/lb, while lithium boils at 1600°F with a heat vaporization of 9,060 Btu/lb.

Lithium spray systems have been successfully tested (Reference 13) and based on these test results it is felt that a lithium spray system could be developed for the present application. This system, if carefully designed, should operate at 80% efficiency or with a heat absorbing capability of about 7250 Btu/lb of lithium evaporated. Lithium has a melting point of 357°F and in the liquid form is easily handled and sprayed with its spraying characteristics being very similar to water. The only limitation placed on the use of a lithium spray system in the present application is the minimum operating temperature of 1600°F (corresponding to lithium boiling at P_{atm} = 0.16 psi, h = 100,000 ft). Table XXVI shows the portion of the leading edge hemicylinder that is above 1600°F for the maximum and minimum radii under consideration for all sweep angles being studied. It can be seen that for the sharp leading edge the lithium spray cooling concept could be used effectively over most of the hemicylinder and for a small portion of the lower surface, but that less than half of the 2.0 inch radius hemicylinder could be effectively cooled with lithium spray.

To demonstrate the attractiveness of a lithium spray system, typical system weights have been generated for the severest heating case listed in Table XXVI. For the 0° sweep angle, R = 0.05 inch leading edge a typical lithium spray system would incorporate the components listed in Table XXVII. The system weights are very reasonable and indicate that a lithium spray system could be incorporated into a cooled wing design if the 1600°F operating temperature is allowed. It should be noted that the system will become more attractive as cruise velocity increases and would be more attractive for a Mach 12 excursion than for the Mach 6 case shown here.

Another solution to leading edge cooling would be the use of a water spray system. A water spray cooling system has been tested at Bell and an efficiency approaching 80% was obtained and with development could exceed 90%. Using an 80% efficiency the heat absorbing capability of water would be approximately 800 Btu lb. The recovery temperature in the vicinity of the leading edge is approximately 2650°F. The heat input to the leading edge is given by,

$$Q = (h_{avg})\ (A)\ (T_R - T_W),\ \text{Btu/hr}$$

In a gross manner the water required can be estimated by the relation,

$$\text{water required in lb} = \frac{(Q)\ (1.5\ \text{hr})}{800\ \text{Btu/lb}}$$

TABLE XXVI

PORTION OF LEADING EDGE HEMICYLINDER ABOVE 1600°F

Sweep Angle (deg)	Radius (in.)	S*, Top (in.)	S*, Bottom (in.)
0	0.05	0.062	0.183
0	2.0	1.2	2.0
30	0.05	0.057	0.182
30	2.0	1.05	1.93
45	0.05	0.051	0.180
45	2.0	1.40	3.14
65	0.05	0.043	0.140
65	2.0	0.350	1.75
75	0.05	0.030	0.140
75	2.0	(Max. Temp. = 1450°F)	

* S is measured from centerline of the hemicylinder perpendicular to the leading edge. For reference purposes the value of S to the shoulder of the leading edge hemicylinder is 0.08 inch and 3.14 inches for the 0.05 inch and 2.0 inch radii respectively.

TABLE XXVII

LITHIUM SPRAY COOLING SYSTEM WEIGHTS

Component	Estimated Weight, lb
Lithium	150*
Lithium Tanks Insulation, Heating, Controls, etc.	200*
Nozzles	5
Installation Brackets for Nozzles	20
Supply lines, heaters, etc.	25
Condensing Equipment, lines, controls, etc.	170
Estimated Total Weight (Without condenser)	400 lb

* Lithium could be condensed on rear wedge and recirculated, thus reducing the lithium required but adding system weight.

For a 0° swept wing and a 0.10 inch diameter hemicylinder, examining an area including just the leading edge hemicylinder water requirements were estimated as tabulated below.

Outer Surface Temperature °F	Water Requirement, lb
200	1125
400	1035

These requirements assume the water is expended. In an actual system the water could probably be condensed so that water requirements would be reduced. A water spray system offers greater flexibility in operating temperature than a lithium spray system and might be lighter than a lithium system because of the ease of condensing the water. Estimated component weights for a water spray system, including condensing equipment, to cool the 0.05 inch radius hemicylindrical leading edge for the 0° sweep wing are given in Table XVIII.

TABLE XXVIII

RECIRCULATING WATER SPRAY COOLING SYSTEM WEIGHTS

Component	Estimated Weight, lb
Water	150
Tank, fittings supports, etc.	50
Nozzles, nozzle installation, lines, etc.	30
Condensing Equipment	20
Estimated Total Weight	250

Note: Use of either the lithium spray system or a water spray system depends upon other wing cooling requirements and the choice of the overall aircraft cooling system. Based on the above discussion these spray cooling concepts were considered potential cooling systems for high heating regions of the wing and should be considered in the final cooling system choice for the entire vehicle.

SECTION 8

STRUCTURAL STUDIES

In order to assess the potential of cooled hypersonic wing concepts, it is necessary to examine not only the cooling systems to be used, but also the influence of the cooling systems on the weight of the wing structure. A total wing weight consisting of the cooling system components and structure can then be compared with weights for uncooled approaches. Cooling systems permit greater freedom of choice both with respect to wing configurations and structural materials. Therefore, the influence of sweep angle and structural operating temperature on structural weight of cooled wings was examined. No attempt was made to obtain optimized designs although previous optimization results were utilized to obtain practical configurations which were conservatively sized. Two structural arrangements, a four (4) beam multi-rib concept and a multi-beam, multi-rib concept were compared for a 65° sweep wing. Wing sweep angle variations were made using the four (4) beam multi-rib concept.

The structural studies of both cooled and uncooled wing concepts for the aircraft of interest are summarized in this section. Design requirements are presented and material selection is discussed before the specific structural arrangements are described. Weight predictions are compared with statistical data on previous wing designs. Cooled wing weight trends are shown as a function of sweep angle. A comparison between a cooled and uncooled wing of the 65° sweep configuration is included.

A. LOADS AND BASIC DESIGN PARAMETERS

The wing configurations used for the structural studies are shown in Section 2 and are those with leading edge sweep angles of 0°, 45°, and 65°. For these wing configurations the thickness to chord ratio (t/c) was held constant at 5%. The planform area of all wing configurations was a constant at 6954 ft^2. The fuselage diameter of 20.6 ft is shown in Figures 4 through 8 in Section 2 and strongly influences the wing designs herein. An allowance of 10% of the chord was made for each of the leading edge flaps. The wings considered did not contain fuel tanks because insulated hydrogen tankage within relatively thin wings are quite inefficient from both weight and volume points of view.

For purposes of the structural design studies a wing loading for 1.0 g level flight of 75 psf was used. This 75 psf wing loading can support a 522,000 lb aircraft. Limit load factors for the type of cruise aircraft of interest are given in References 46 and 47 as ±0.2 g longitudinally and laterally and +2.0 g to -1.5 g vertically. The designs herein are based on the +2.0 g vertical load factor along with an ultimate factor of safety of 1.5.

The bending moment at the wing-body intersection resulting from the 2.0 g limit load factor is presented in Figure 120 as a function of leading edge sweep angle. The bending moments were computed by the double integration of the uniformly distributed surface pressure of 2 x 75 = 150 psf. The relieving effect of wing inertia was neglected since it was expected to be less than 10% of the airload. For a wing of constant area,

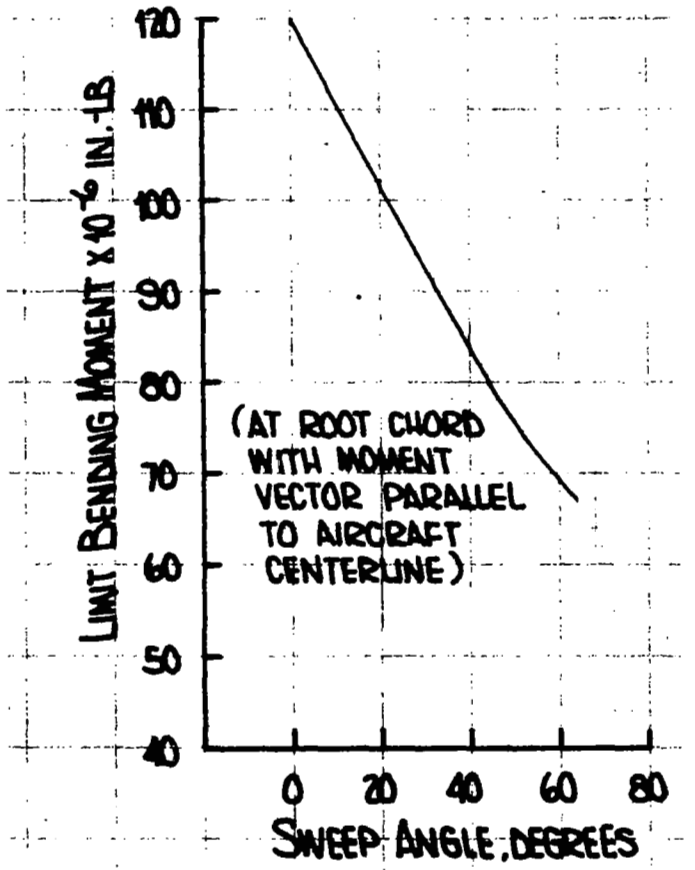

Figure 120. Bending Moment at Root Chord versus Sweep Angle

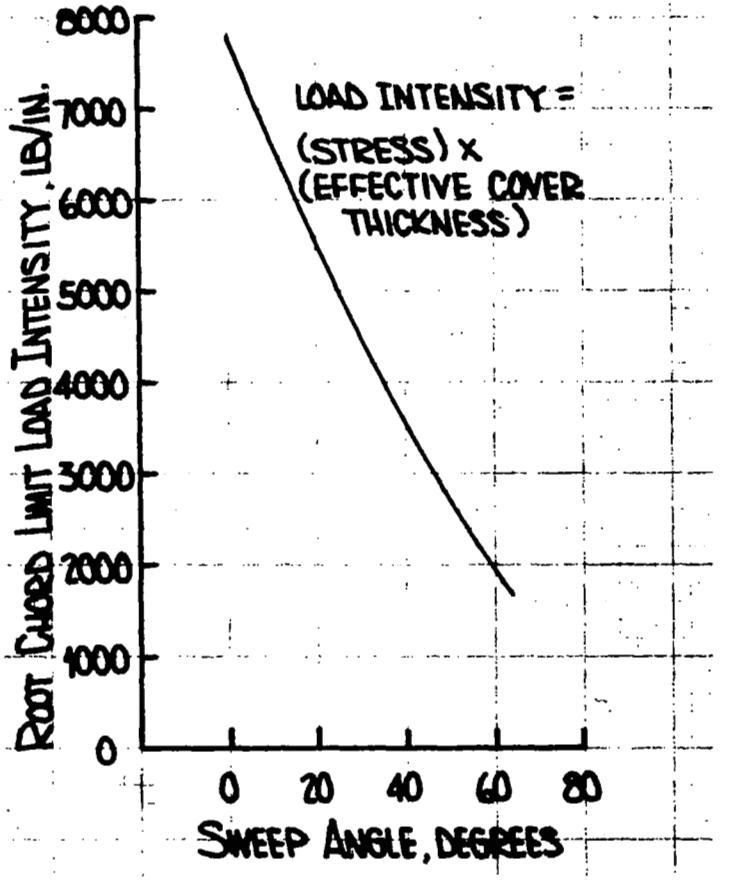

Figure 121. Root Chord Limit Load Intensity versus Sweep Angle

the center of pressure moves inboard as the leading edge is swept, thereby reducing the bending moment at the root. Note that sweeping the leading edge of the wing from 0° to 65° reduces the bending moment at the root by a factor of approximately 2.

Using the bending moment data of Figure 120 and the root section dimensions tabulated below, skin loading intensities due to the bending moment were calculated. These loading intensities are presented in Figure 121 and 122.

Sweep Angle	Root Chord	Maximum Airfoil Thickness at Root
0°	732 in.	36.6 in.
45°	950 in.	47.5 in.
65°	1200 in.	60.0 in.

The load intensities at the root chord are applicable along the entire lower wing surface at the root and at the maximum thickness point on the upper surface at the root for the four (4) beam multi-rib wing concepts which were analyzed using simple beam theory. The multi-beam multi-rib concepts were analyzed using "strip theory" so the loadings in Figures 121 and 122 are averages for the upper and lower surfaces of the multi-beam multi-rib wing arrangements.

Temperature effects were included by selecting allowable strengths which allow for extended exposure to the maximum design temperatures. Thermal stresses were not calculated and are felt to be minimized by the choice of thermal stress relieving structure for the uncooled wing. Fatigue loadings were neglected.

B. MATERIAL SELECTION

The use of cooling systems in the wing structure permits maximum operating temperatures to be controlled to almost any level less than radiation equilibrium values and as a result the designer has a great deal of flexibility in selecting materials of construction. In order to establish representative trends of structural weight as a function of operating temperature the following materials were selected for examination at the temperatures indicated:

200F	7075-T6	Aluminum Alloy
300F	2024-T81	Aluminum Alloy
300F	6A1-4V	Titanium Alloy
600F	6A1-4V	Titanium Alloy
Above 800F	Inconel 718	Nickel Based Alloy

These materials are typical of presently available alloys. The aluminum alloys were selected on the basis of high strength at the operating temperature indicated. The aluminum alloy 2024-T81 at 300°F offers superior strength when compared to 7075-T6 aluminum alloy which is quickly degraded by temperatures much in excess of 200°F.

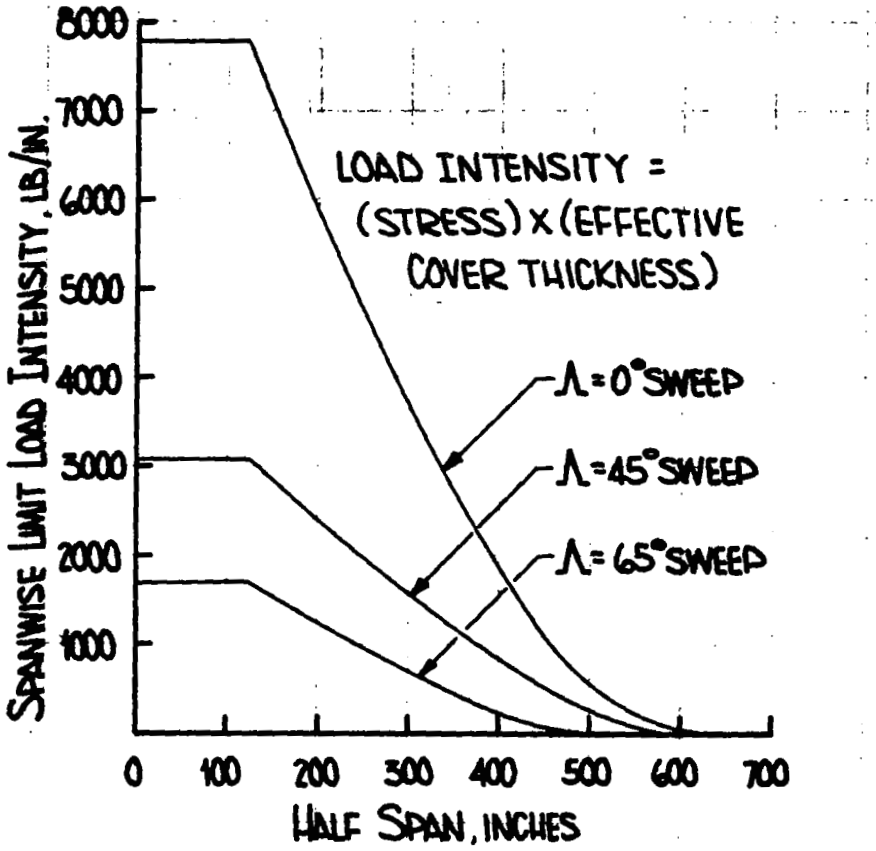

Figure 122. Spanwise Variation of Load Intensity versus Sweep Angle

The 6A1-4V titanium alloy is widely used because of its availability, fabricability, and high strength in the operating temperature range of interest. The Inconel 718 nickel based alloy, cold rolled and aged, was selected for the uncooled wing based on favorable fabrication characteristics as well as good strength to weight ratio in the temperature range of interest.

Design allowable strength data for the aluminum and titanium alloys were obtained from Reference 48. Room temperature strength values were reduced to account for the effects of operating temperature and exposure time at maximum operating temperature. During the 10,000 hour operational life of the aircraft it was assumed that 5,000 hours would be spent the maximum temperature of the cooled structures.

Design allowable strength data for the Inconel 718 material was obtained primarily from Reference 49. Assuming 3000-hour exposure at a temperature of 1000°F the following data is obtained.

Ultimate tensile stress	=	165 kips
Yield tensile and compressive stress	=	113 kips
3000 hour rupture strength	=	140 kips
10,000 hour rupture strength	=	116 kips
0.2% creep deformation, 3000 hours, sustained tensile stress	=	120 kips
0.2% creep deformation, 10,000 hours, sustained tensile stress	=	100 kips

Based on the above data for Inconel 718 a compressive yield stress of 100,000 psi was selected. It is felt that this choice is somewhat conservative and the conservatism will both allow for the degradation due to time at temperature and thermal stress effects which are not included in the analyses. Using Figure 123 (reproduced from Reference 49) the selected 100,000 psi compressive yield stress is 20% below the sustained tensile stress yielding a 0.2%, creep deformation in 3000 hours of flight. Thus, the selected design allowable for Inconel 718 appears adequate to limit creep deformation to reasonable levels.

Minimum thicknesses for each material were specified as indicated below:

Aluminum Alloy	0.063 inch
Titanium Alloy 300F	0.032 inch
600F	0.040 inch
Inconel 718	0.010 inch

For the aluminum and titanium alloys the specified minimum thicknesses are greater than the minimum values currently used in airframe construction to allow cooling system integration. In fact, the large insulated and cooled structure described in Reference 50 utilized a load carrying structure of 0.040 inch aluminum alloy with integral coolant passages as shown in Figure 124. For the doublewall concept the cooled inner wall is

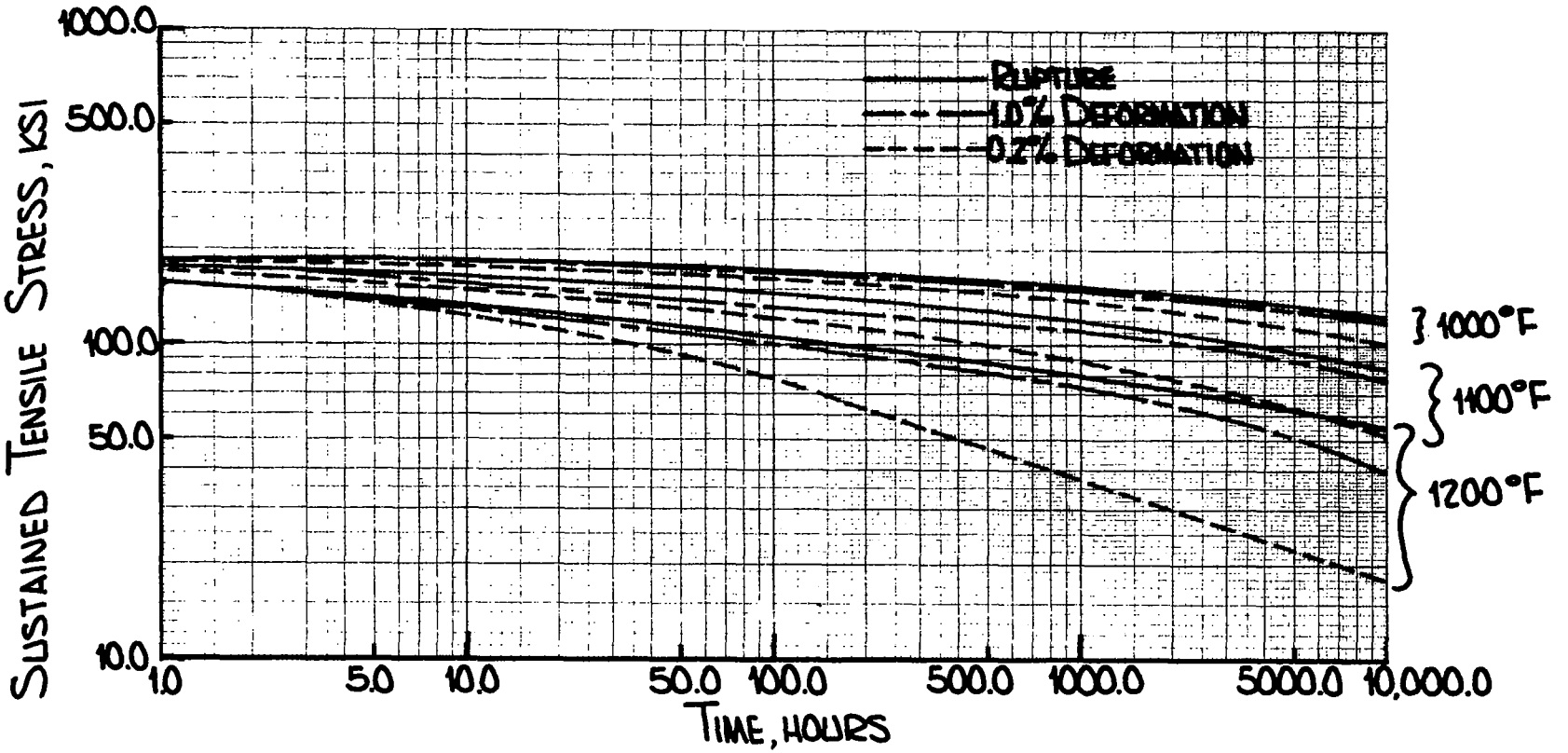

Figure 123. Allowable Creep Stress Properties for Inconel 718 Sheet

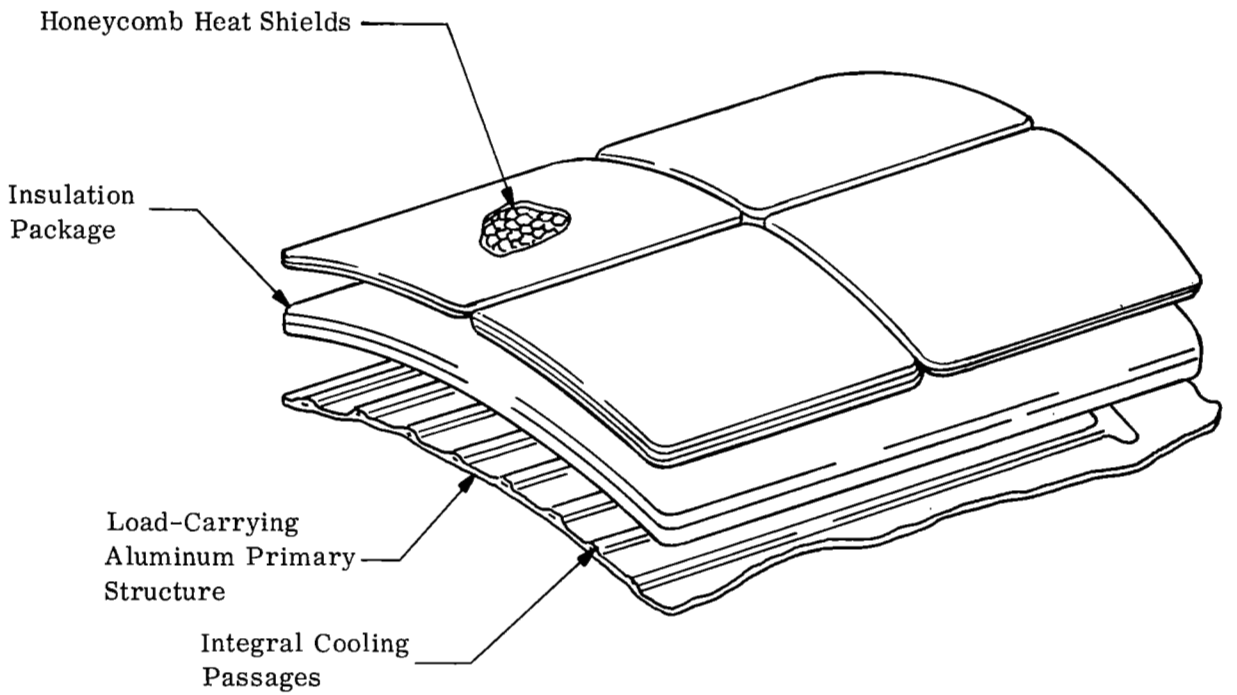

Figure 124. Double-Wall Schematic

the load carrying structure and contains integral cooling passages for an active cooling system. The heat input to the cooling system is lowered by the use of insulation plus a heat shield outer wall which is non-load-carrying. A concept utilizing an 0.040-inch thick non-load-carrying aluminum alloy panel having integral coolant passages is shown in Figure 125. In this case, the corregated, stiffened outer skin is the load carrying structure, and no insulation is used. The minimum thickness for the titanium alloy structures is essentially an estimate since integration of airplane cooling systems with titanium structures has not been studied in detail. The specified minimum thickness for the uncooled superalloy structure is somewhat arbitrary, but should be adequate with respect to handling and oxidation considerations.

C. COOLED WING STRUCTURE

A limited number of cooled wing designs were analyzed in order to establish the relative effects of wing geometry and operating temperature on structural weight. The combinations investigated are listed in the following table.

Mean Outer Surface Temperature		200°F		300°F	600°F
Material		7075-T6		2024-T81 6A1-4V	6A1-4V
Structural Concept (1)		A	B	A	A
Sweep Angle	0°	x	-	x	x
	45°	x	-	-	-
	65°	x	x	-	x

(1) A. Four (4) beam multi-rib arrangement

B. Multi-beam multi-rib arrangement

In sizing the wing structure the forward 10% and the rearward 10% of the chord were assumed to be required for flaps and control surfaces. The 65° sweep wing was an exception; the trailing edge flap was assumed to be of a constant chord equal to 10% of the root chord.

The structural loading index, M/h^2c ranges from about 500 to 50, for sweep angles from 0° to 65°. Consequently, a wide column or plate concept is the most efficient structural arrangement as shown in Reference 19.

For wide column or plate concepts, it is necessary to utilize at least four beams to obtain reasonable shear flow intensities. Wing optimization studies have shown that moderate variations in beam spacing away from the optimum have a minor effect on wing weight as long as shear flow intensities are kept of reasonable magnitude. For the multi-rib arrangement, Figure 126 presents the variation of root station shear flow intensity as a function of sweep angle. Wing cover sizes were determined on the basis of combined interaction

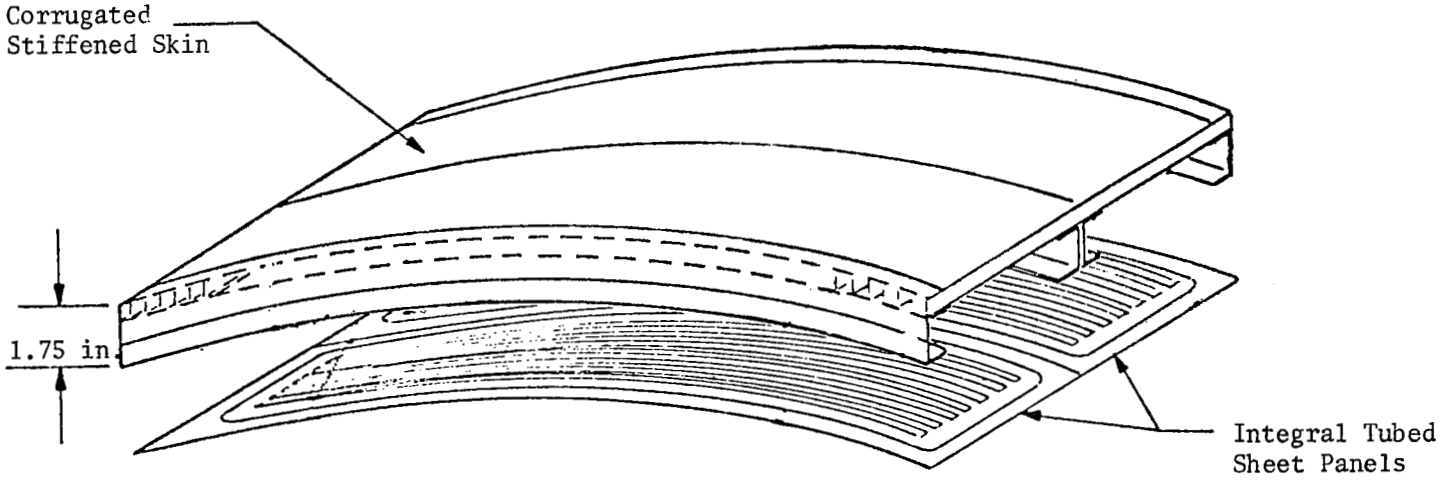

Figure 125. Cooled non-load-carrying panel concept.

effects of shear flow intensity of Figure 126 and axial loading intensity of Figure 121. For all wing concepts the main beam was located at 2/3 chord where wing thickness is a maximum. The other beams were located to intersect the fuselage at locations corresponding to 10%, 39%, and 90% of the root chord as shown in Figures 127, 130, and 131 for the 0° , 45° and 65° sweep angle arrangements. Both cooled and uncooled 65° wing structures of this type were analyzed. In addition, a multi-beam and rib arrangement was analyzed for both a cooled and uncooled 65° sweep configuration. These four concepts, two cooled, and two uncooled gave an adequate basis for comparison of cooled versus uncooled approaches.

Since the use of cooling systems can minimize thermal stresses in the cooled wing structures, conventional structural approaches and methods were used for establishing member sizes. No attempt was made to obtain refined designs although various stiffener types and geometries were considered in conjunction with rib spacing to obtain efficient configurations. The structural configurations chosen were considered to be representative and conservative for the design condition used. Conservatism was considered desirable in order to minimize possible weight increases which might result from consideration of additional design conditions, fatigue effects, aeroelastic requirements, or equipment in the wing (i.e., landing gear). Member sizes were determined for the structural wing box so that its weight could be determined. The average unit weight of the structural box was multiplied by the total wing area to obtain the total wing weight.

For the preliminary design of the four beam and multi-rib arrangement the root section was sized first. It was assumed that element sizes and stiffener spacings would be the same on the tension and compression surfaces and would not vary in a chordwise direction. Sufficient area was added to the compression side of the deepest beam cap to locate the neutral axis at half the maximum wing thickness. On this basis an equivalent thickness of the wing cover was computed. The resultant skin thickness, stringer size, and rib spacing was then determined. The cover thickness was checked for the combined axial and shear flow loadings. Cover proportions were modified, if required, by reproportioning the material between the skin and the stringers. Beam webs were sized by the shear flow. For the type of construction employed, beam caps are light and were assumed to be taken into account by the equivalent cover thickness.

For the preliminary design of the multi-beam and multi-rib wing arrangement, two beams, the mid-chord beam and the rear beam were sized first. Again, it was assumed that the element sizes stay the same on the tension and compression surfaces, but would vary in a chord-wise direction. Beam bending moments were reacted by beam caps and skin cover areas. Beam shear loads were reacted by truss type structural members. Rib sizes were determined on the basis of reacting local airload pressures and transmitting chordwise shear.

After the construction details were determined from the analysis of the root section, several outboard sections were analyzed. The analyses of the outboard sections were based on concepts such as spanwise tapering of the skin, tapering of the stringers by height, width and thickness, and elimination of some of the stringers as the loading intensity decreased. The weight variation with span or chord, as appropriate, between the analyzed sections was plotted and integrated to obtain the weight of the main structural

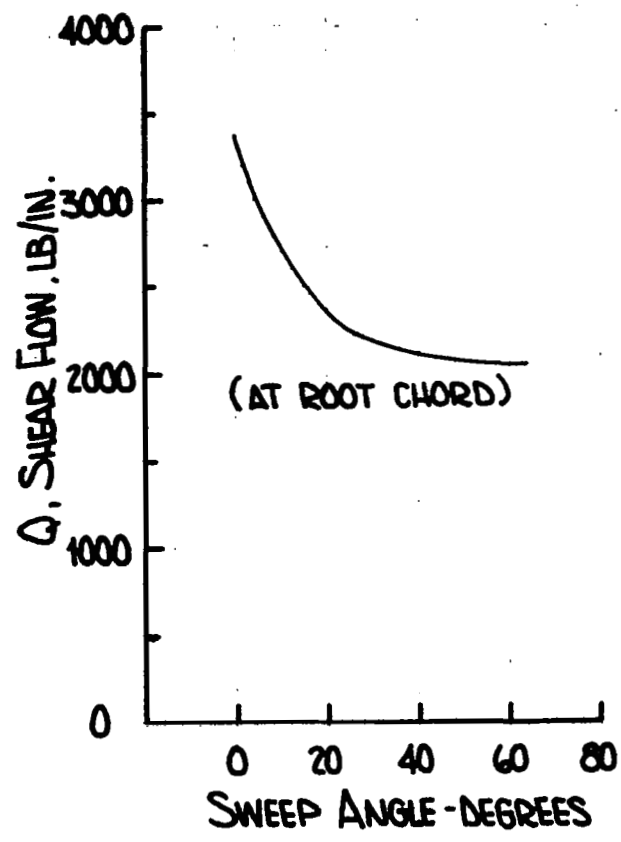

Figure 126. Shear Flow versus Leading Edge Sweep Angle

wing box. The unit weight of the wing box was multiplied by the total wing area to obtain a conservative estimate of the total wing weight. Details of the analyses are discussed for each of the wing sweep angles in later subsections.

1. 0° Sweep

The general arrangement for the 0° sweep wing is shown in Figure 127. Beams run spanwise and are shown as heavy lines. The 31 ribs are spaced on approximately 18 inch centers. Stringer size and spacing were varied for each of the four different combinations of temperature level and construction material investigated.

Because of their high structural efficiency a flanged Y-Tee stringer configuration and the more conventional Zee configuration were examined for one aluminum and one titanium alloy. Using 2024-T81 aluminum alloy at 300°F and comparing combined skin and Zee stringer weights to the weights for the Y-Tee stringer design the Zee stringer design is heavier by about 5%, while using 6A1-4V titanium alloy at 300°F yields a weight difference of 7%. Therefore, a flanged Y-Tee stringer design is recommended for a four beam multi-rib cooled wing design. The web thickness of the titanium Y-Tee stringer were very small, 0.030 to 0.042 inch, which would make the production of such extrusions difficult and expensive. Because of these anticipated fabrication difficulties with a Y-Tee design, weights were reported for the Zee stringer construction only. However, advances over the next decade may offset current processing limitations and then the use of Y-Tee construction is recommended.

In establishing the detailed geometry for the wing outboard stations modifications were made to the stringer proportions, number of stringers and skin thickness so that the load carrying capability of the cross section was determined along with the corresponding local structural weight. Each modified cross section was then assumed to be located at a spanwise position where the maximum cover load corresponded to the load carrying capacity. The covers were then checked for combined shear flow and axial loadings, assuming that the shear flow decreased linearly from root to a value of zero at the tip. Integration of the curve of weight per inch versus span, such as Figures 128 and 129, provided a total weight for the structural box portion of the wing which when divided by the area of the wing box provided the unit weights tabulated below. This unit weight was multiplied by the total wing area to obtain an estimate of the total dry wing weight. For the weights

Material	Temperature °F	Weights Structural Box, lb	Unit Weight lb/ft^2	Total lb
7075-T6	200	32,600	5.87	41,090
2024-T81	300	36,140	6.54	45,700
6A1-4V	300	32,760	5.90	41,300
6A1-4V	600	42,700	7.68	53,800

tabulated above the skin and stringer weight accounted for 87.8% of the total wing weight while the ribs (8.8%) and the beams (3.4%) accounted for the remaining 12.2% of the total wing weight.

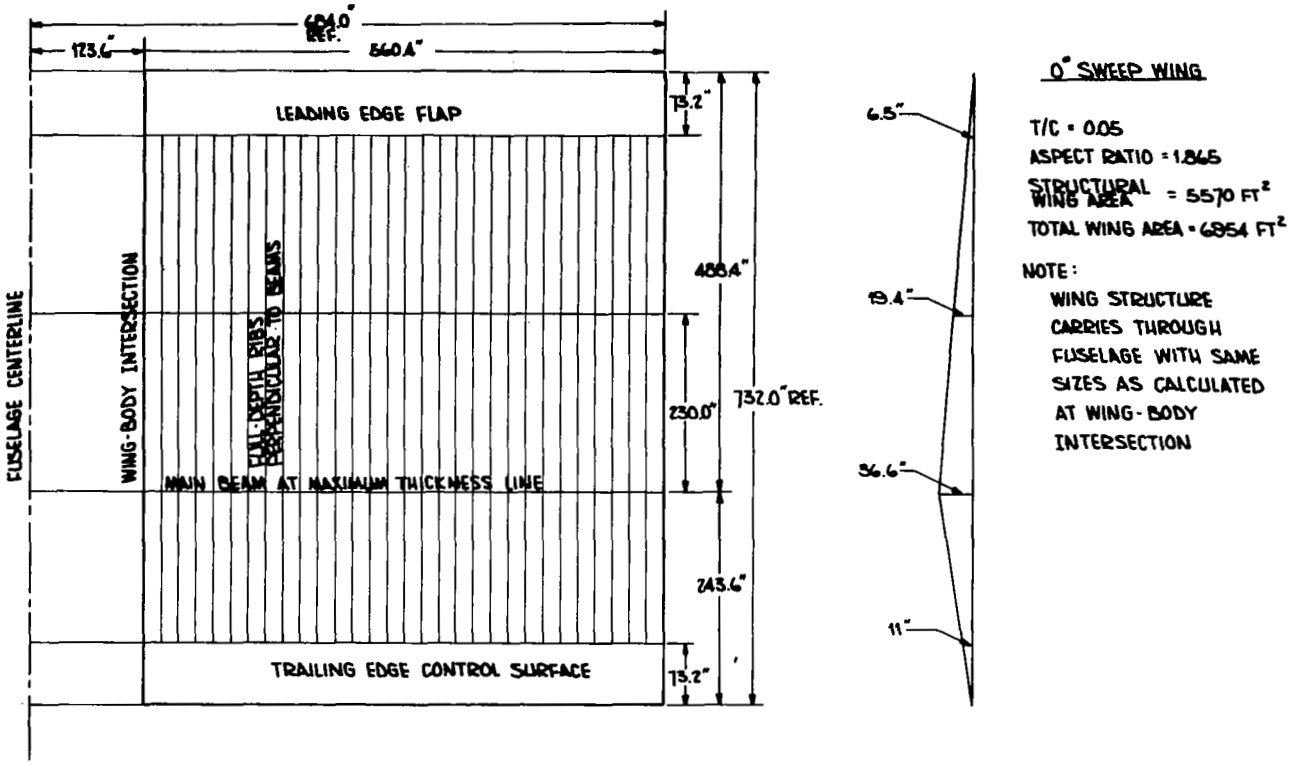

Figure 127. 0°Sweep, Cooled Wing Arrangement

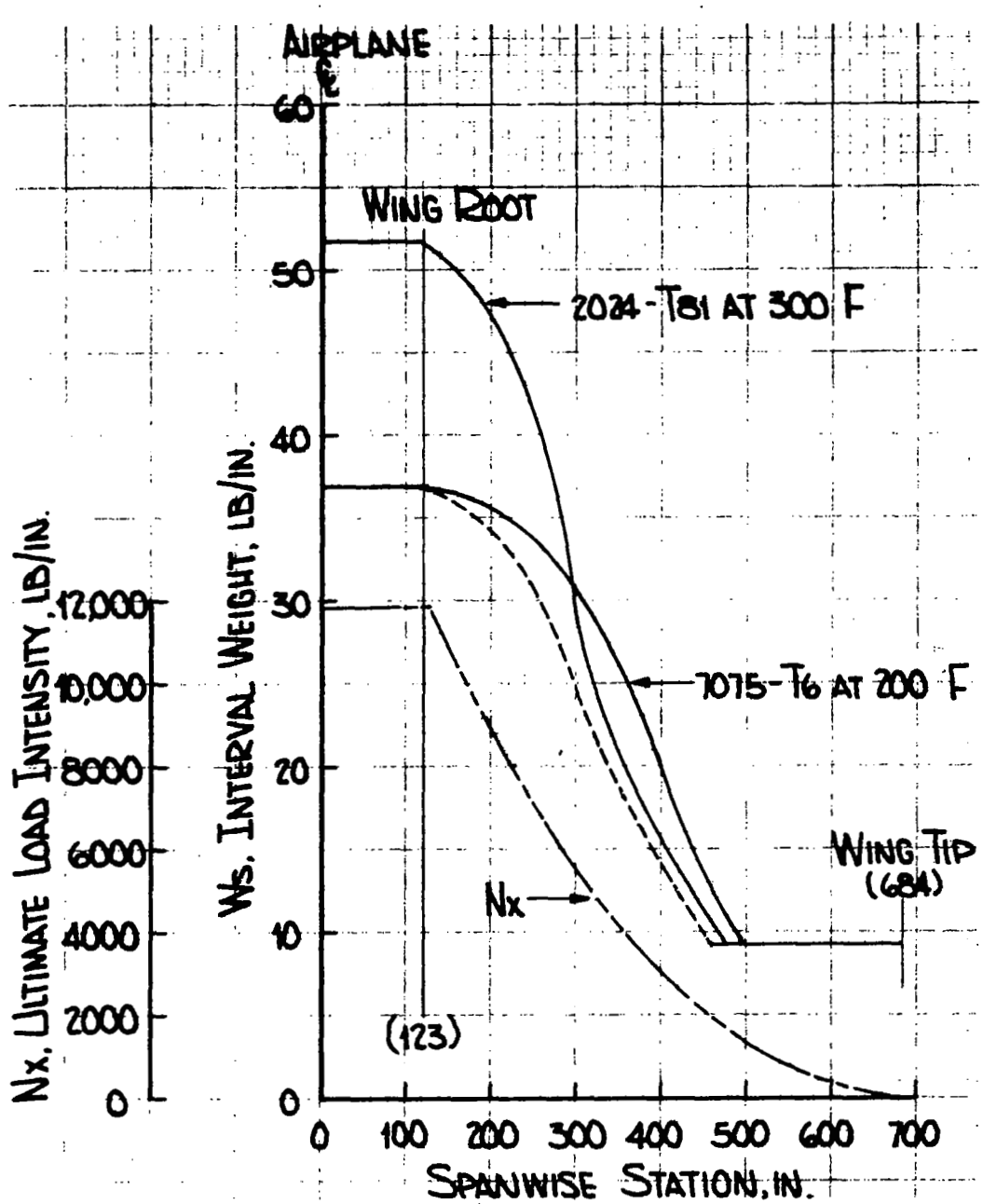

Figure 128. Spanwise Weight Distribution of Aluminum Alloy Wings, 0° Sweep

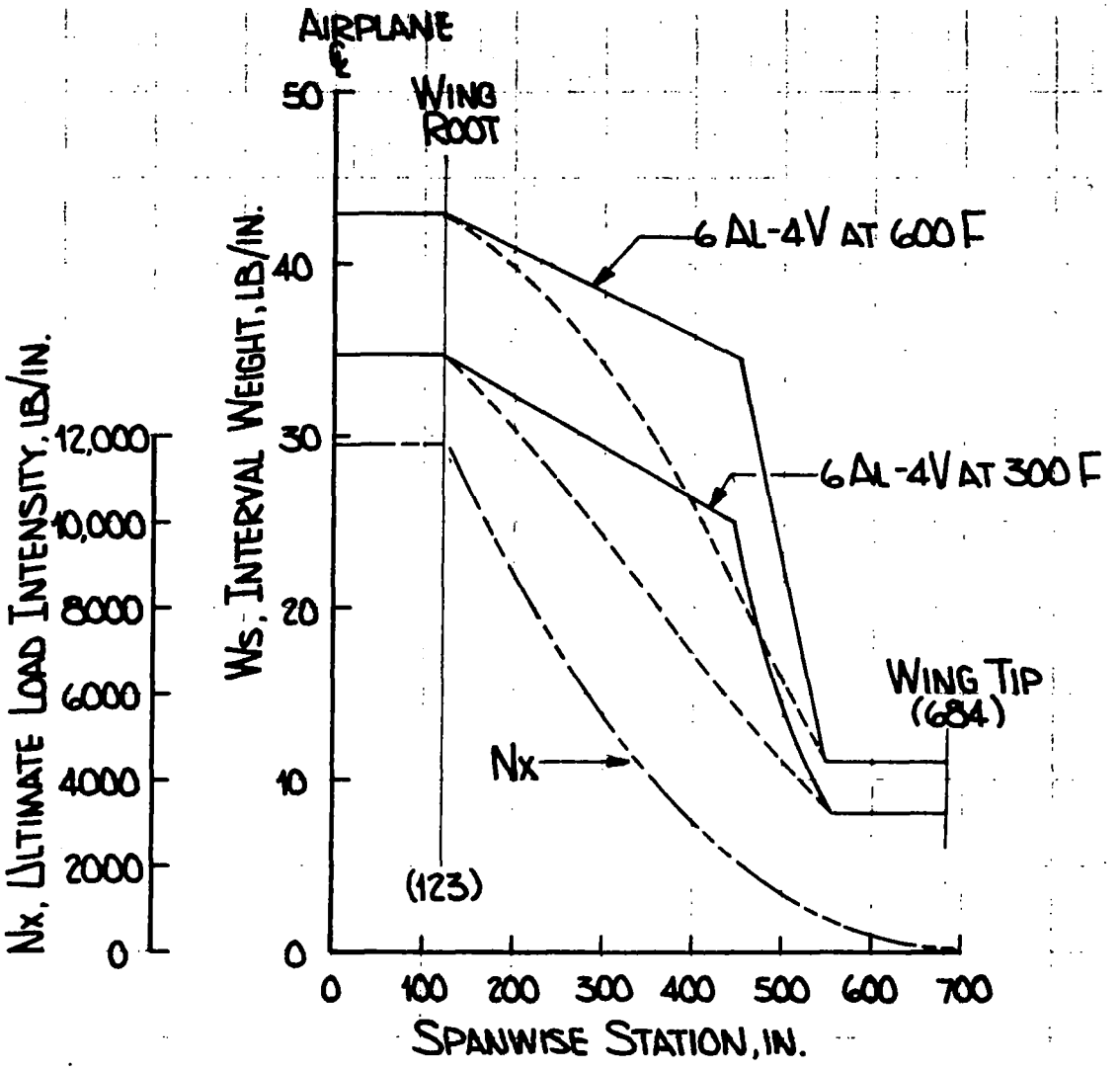

Figure 129. Spanwise Weight Distribution of Titanium Alloy Wings, 0° Sweep

A review of the shapes of the running weight curves of Figures 128 and 129, in comparison with the ultimate load intensity in the covers and the fact that the shear flow decreases linearly with span, suggests that the cross-sectional modifications made were not the most efficient. While the running weight curve for the 2024-T81 wing is almost directly proportional to the loading curve, the running weight curves for the 7075-T6 and the two 6A1-4V wings appear to be heavier than necessary over much of the span. The dashed lines on the figures indicate more likely weight trends with corresponding weight reductions of between 2000 and 3000 pounds estimated for each of these three wings. Wing weights could also be reduced by relaxing the minimum thickness limits, if cooling system design permits with weight decreases of between 200 and 400 pounds. However, since time did not permit detailed checks the wing weights discussed later in the report are those based on the more conservative solid lines.

2. 45° Sweep

The general arrangement for the 45° sweep wing is shown in Figure 130 and is generally similar to that established for the 0° sweep wing. Four beams are located at the 10%, 39%, 66.7% and 90% root chord intersection points. Ribs are spaced on centers of approximately 25 inches. This wing configuration was analyzed for one material, 7075-T6 aluminum alloy operating at 200°F, utilizing Zee stiffened skins. At the root the skin and stringer thicknesses were 0.094 inch. The stringers were spaced on 4.27 inch centers, had 0.80 inch flanges and 1.00 inch webs. The skin and stringers were tapered from root to tip and the stringer spacing was increased by stoping some of the stringers at ribs between the root and the tip. The weight of the structural wing box was 26,600 pounds, an average unit weight of 5.17 lb/ft^2 which gave a total wing weight of 36,190 pounds. For the 45° sweep wing, skin and stringer weights accounted for 85.0% of the total wing weight while the ribs (10.8%) and the beams (4.2%) accounted for the remaining 15.0% of the total cooled wing structural weight.

3. 65° Sweep

The general arrangements for the 65° sweep wing are shown in Figures 131 and 132. In Figure 131 the four beam multi-rib arrangement is shown in which the main structural box was assumed to consist of three beams oriented normal to the aircraft centerline and one along the maximum thickness line. Along the root chord these beams are located at 42%, 67% and 90% chord. Ribs, on approximately 24 inch centers, are perpendicular to the beams. Stringers of a Zee cross section are spaced on 3.5 inch centers. In Figure 132 the multi-beam and rib arrangement is shown and for this arrangement the beams are on 60 inch centers and full depth ribs are spaced on 90 inch centers with former ribs between full depth ribs on 22.5 inch centers. In addition, a full depth beam is placed at the maximum thickness line of the wing.

The geometry of Figure 131, a four beam multi-rib arrangement, was maintained for both the 7075-T6 aluminum alloy wing which was assumed to operate at 200°F and for the 6A1-4V titanium alloy wing which was assumed to operate at 600°F. Minimum skin thicknesses were 0.063 inch and 0.040 inch for the aluminum and titanium wings, respectively. The weights of the structural box for the aluminum and the titanium wings were 18,900 pounds and 23,430 pounds, respectively, corresponding to unit weights of 4.18 lb/ft^2 and 4.92 lb/ft^2. When these unit weights are applied to the entire wing area total weights of 29,160 pounds and 34,200 pounds were estimated for the aluminum and

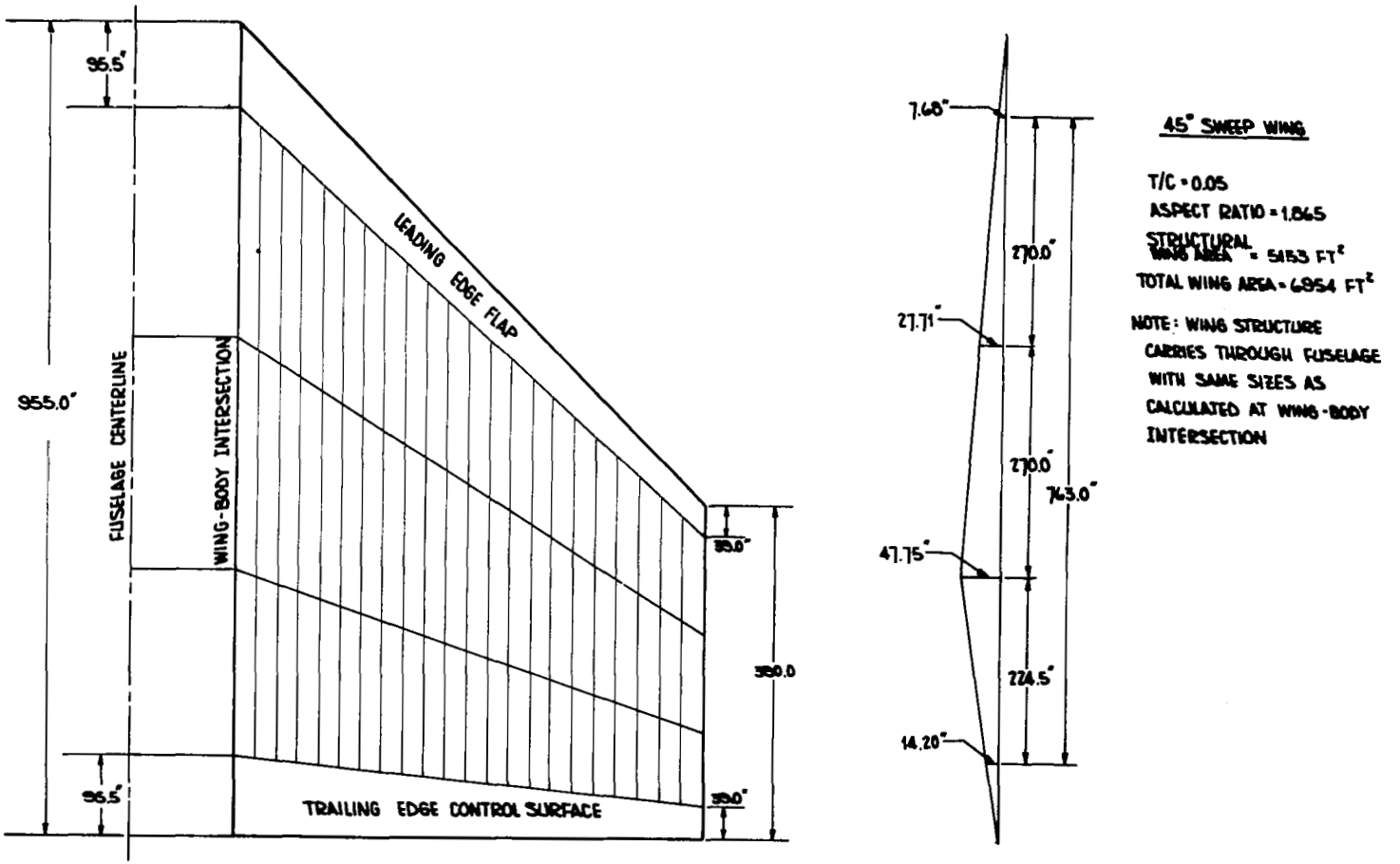

Figure 130. 45° Sweep, Cooled Wing Arrangement

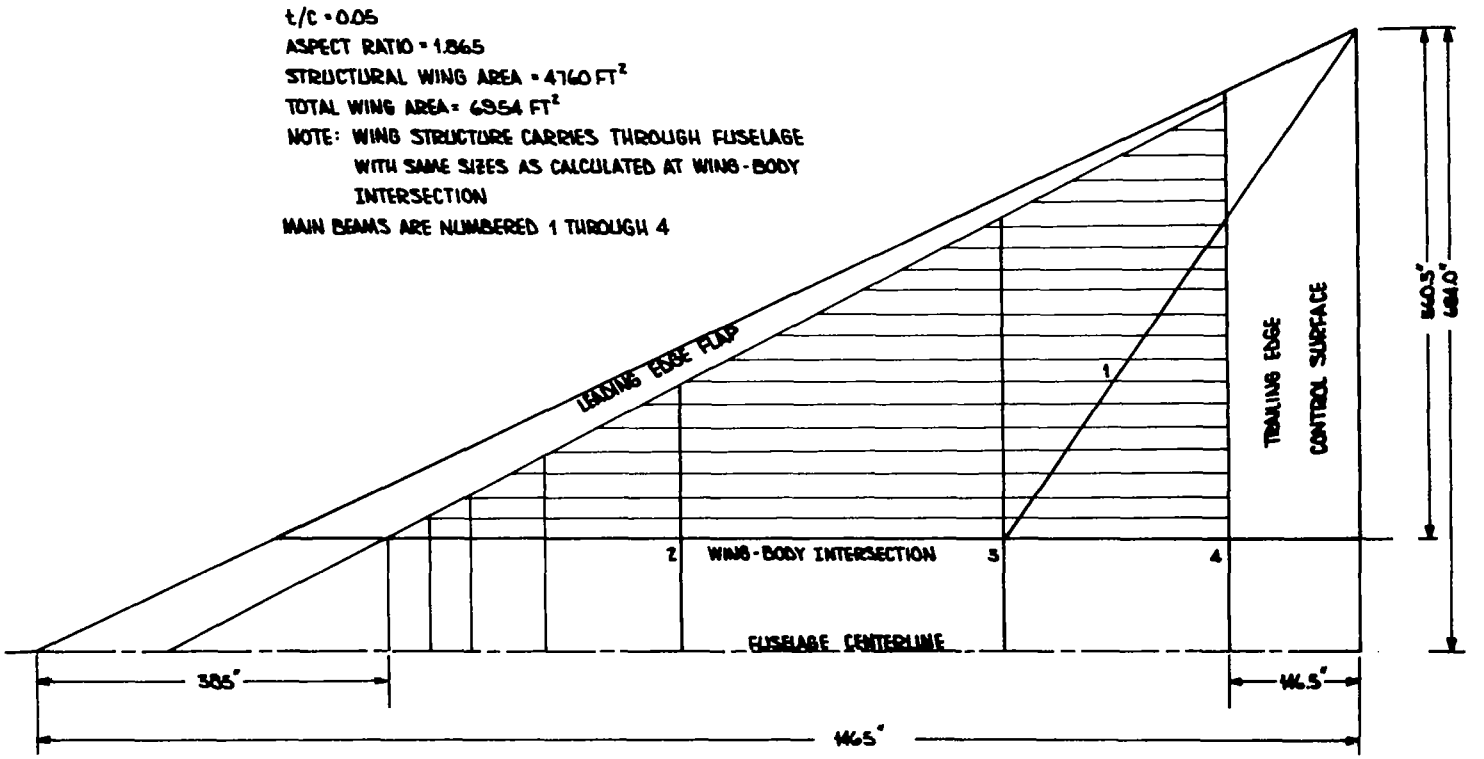

Figure 131. 65° Sweep, Four Beam Multi-Rib Arrangement

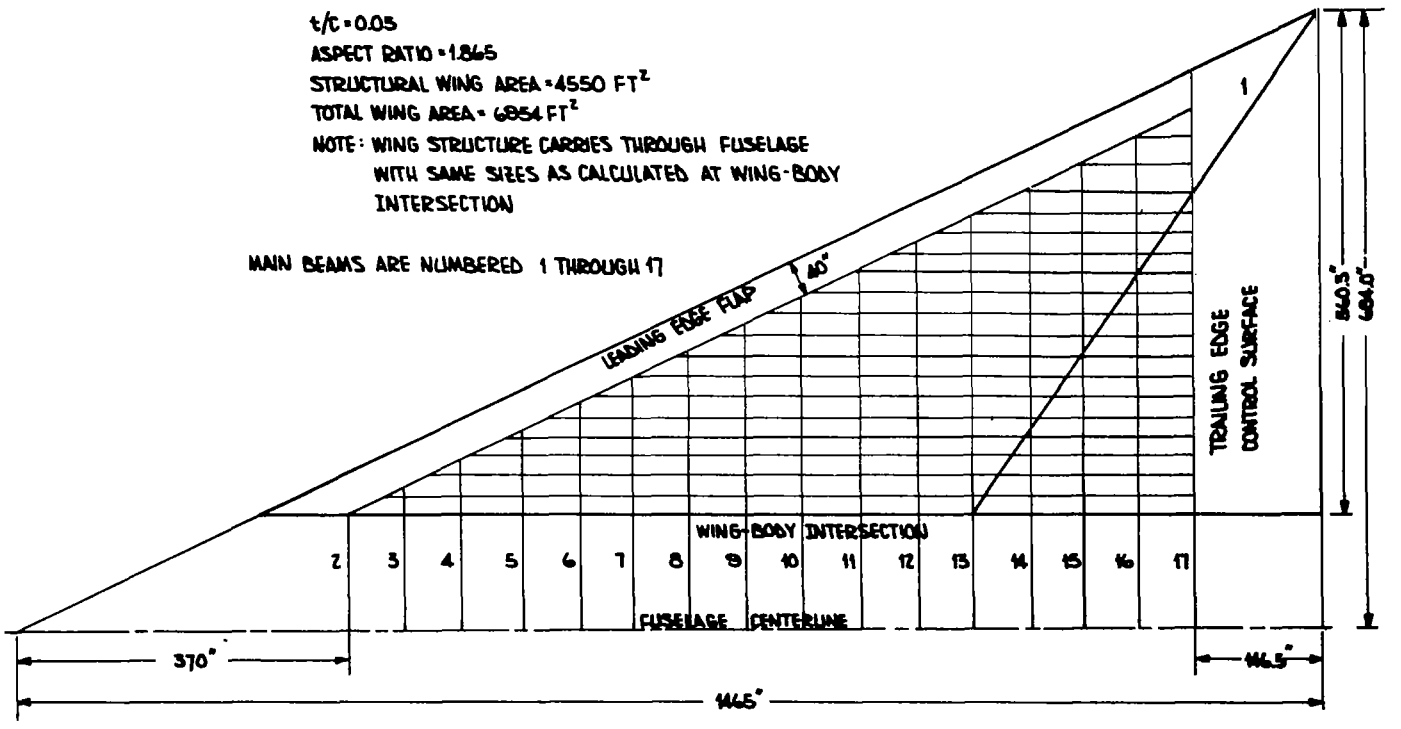

Figure 132. 65° Sweep, Multi-Rib, Multi-Beam Arrangement

titanium wings. These weights are quite conservative because of the assumptions of minimum thicknesses, rib spacing, stringer spacing, and the use of Zee stiffened cover skins. For this cooled 65° sweep wing, four beam multi-rib arrangement, the integrally tubed sheet, Zee stringer stiffened skin covers weighed 73.5% of the total wing weight while the ribs (15.0%) and the beams (11.5%) accounted for the remaining 26.5% of the total cooled wing weight.

The geometry of Figure 132, a multi-beam and multi-rib arrangement, was analyzed for just the 7075-T6 aluminum alloy operating at 200°F. A Zee stringer skin stiffening concept as shown in Figure 133 was used conservatively assuming a maximum compressive allowable stress of 55,000 psi. This value should be easily attainable for practical designs and would provide a margin to accommodate interactions of shear, bending and compressive stresses. The allowable stress sized the skin which was used to determine the wing cover weights. The cover size shown in Figure 133 is for the trailing edge portion of the wing just forward of beam 17 at the root station. Forward of beam 17 and outboard of the root station cover sizes decreased from those shown in Figure 133. This cover concept yields a unit chordwise weight distribution as shown in Figure 134 which decreases from a maximum value of 13.2 lb/ft^2 at the trailing edge to 2.8 lb/ft^2 forward of beam 10. The weight of the structural box for this concept using a multi-beam and rib arrangement is 22,700 lb. The corresponding weight for this structural box is 5.02 lb/ft^2. Applying this unit weight to the total wing area gives a total weight of 35,000 lb. For this cooled 65° sweep wing multi-beam and multi-rib arrangement, the integrally tubed sheet, Zee stringer stiffened skin covers weighed 61.2% of the total wing weight while the ribs (21.1%) and the beams (16.7%) accounted for the remaining 38.8% of the total cooled wing weight.

A summary of the total cooled wing weights for the 65° sweep wing is given below. All of the concepts listed incorporated Zee stringer stiffened skins with integral cooling passages as shown in Figure 135.

Four (4) Beam Multi-Rib Arrangement		Multi-Beam Multi-Rib Arrangement
7075-T6 Al 200°F	6AL-4V Ti 600°F	7075-T6 AL 200°F
29,160 lb	34,200 lb	35,000 lb
4.18 lb/ft^2	4.92 lb/ft^2	5.02 lb/ft^2

D. HOT WING STRUCTURE

In order to provide a comparison with wings utilizing cooled structural concepts, two typical uncooled wings were designed for the 65° sweep configuration. The basic

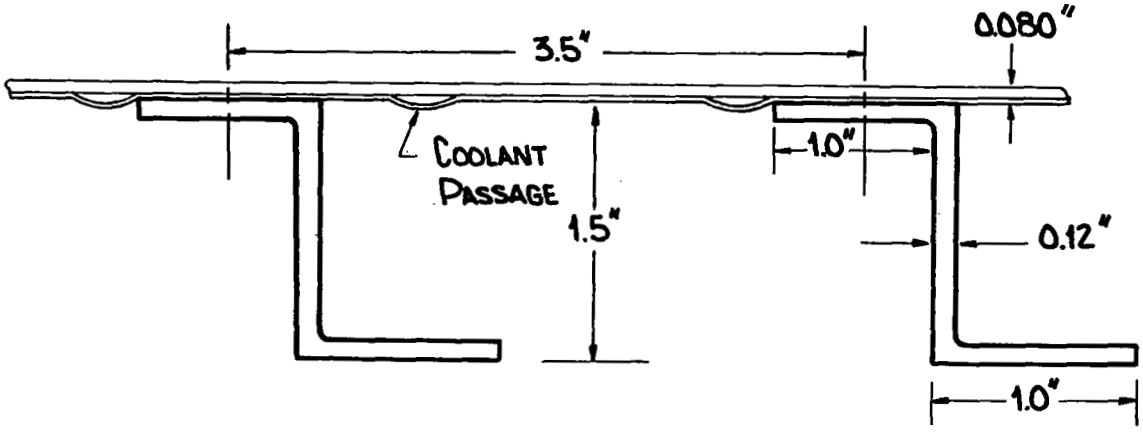

SCALE - FULL

AVERAGE THICKNESS = $\bar{t}$ = 0.20"

RIB SPACING = 22.5"

SECTION RADIUS OF GYRATION = ρ = 0.535"

SLENDERNESS RATIO = L/ρ = 42.0"

Figure 133. Cooled Wing Skin Concept

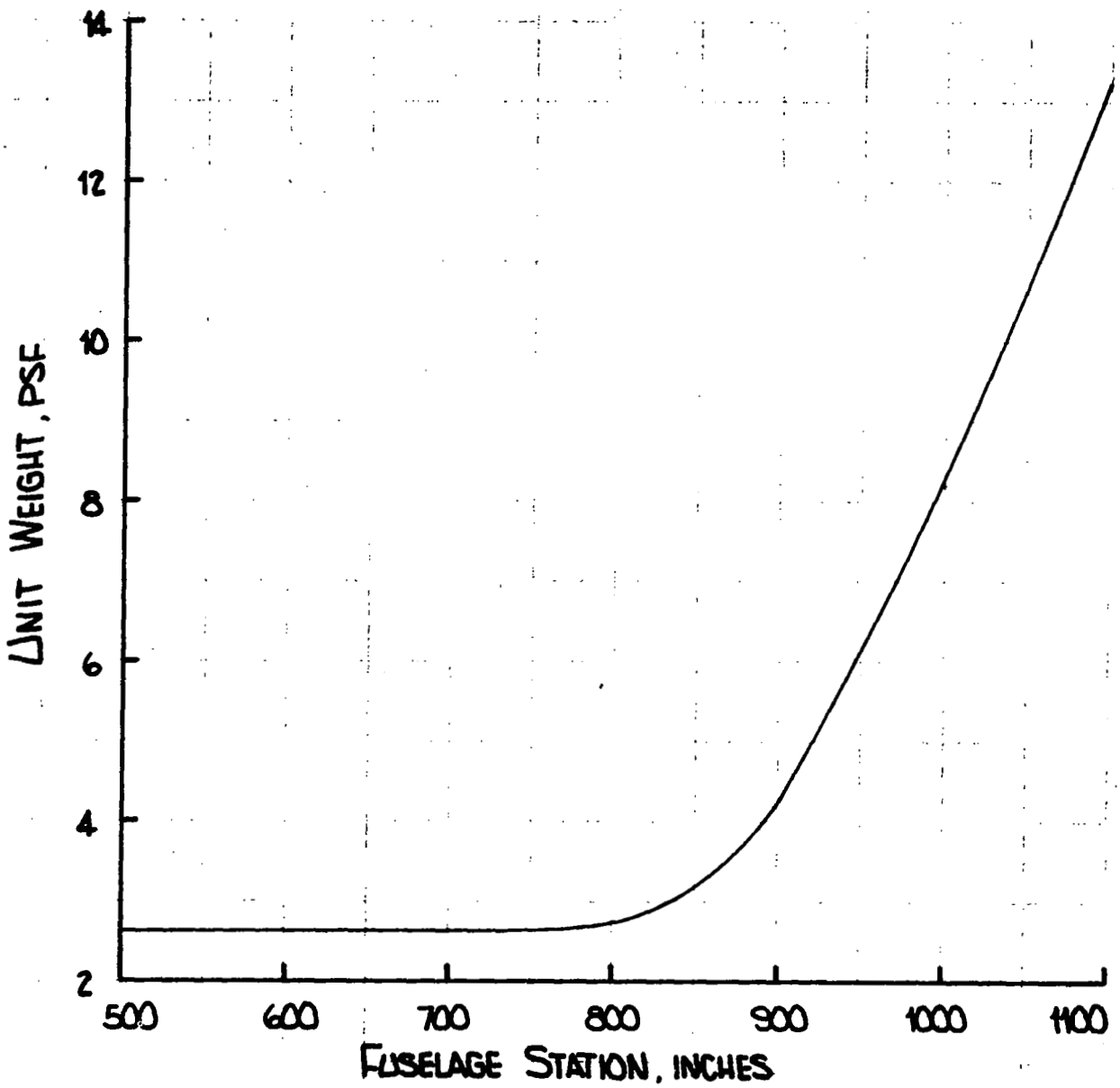

Figure 134. Chordwise Variation in Wing Unit Weight

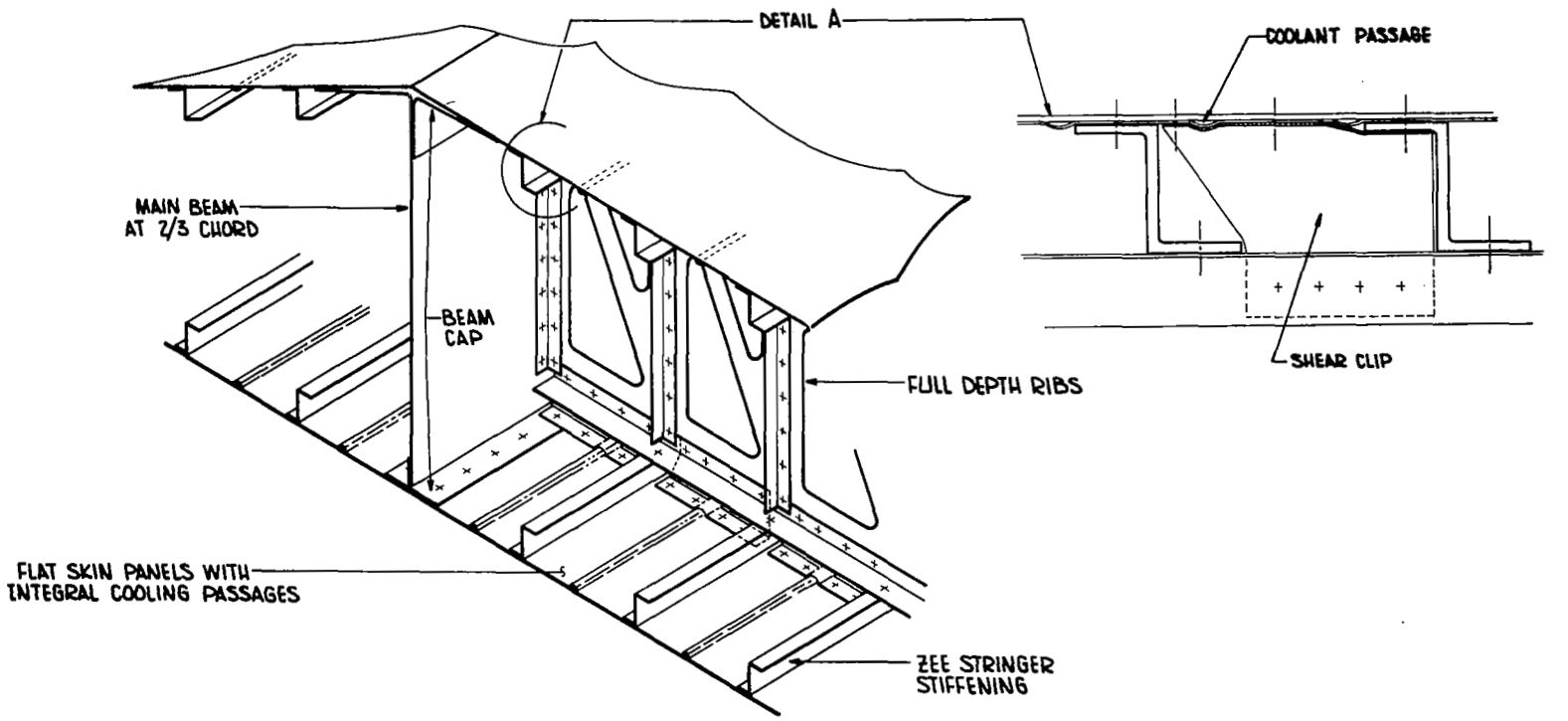

Figure 135. Cooled Wing - Four Beam, Multi-Rib Zee Stringer Stiffened Cooled Skin Arrangement

planforms for these designs were shown previously in Figures 131 and 132 and are the four (4) beam, multi-rib and multi-beam, multi-rib arrangements, respectively. The material of construction was Inconel 718 in the cold rolled and aged condition. Axial and shear load intensities were the same as those for the cooled wing structures. The air-loading of 75 psf with a 2.0g limit load factor and an ultimate factor of safety of 1.5 which gives a root bending moment of 98,700,000 in.-lb was retained. The torsional moment applied by the trailing edge flap was included. Since thermal stresses were not calculated a conservative allowable strength of 100,000 psi was used for design purposes. This is about 20% less than the allowable for 0.2% creep deformation in 3000 hours as shown in Figure 123. Thus, thermal stresses up to 20% of the mechanical stresses can be tolerated in the designs.

For the uncooled wing the rib spacing was determined using the following technique. With a tubular skin stiffening concept optimum weight efficiency parameters were determined from Reference 51. Using the optimum weight efficiency curves shown in Figure 136, a root loading of 3000 lb/in., and a full depth rib of minimum gage with 60% web weight and 40% stiffener weight, an interval weight versus number of ribs in a 115-inch interval can be determined as shown in Figure 137. The minimum interval weight is shown to be relatively insensitive within a rib spacing of 20 to 40 inches.

Figure 138 shows a multi-beam or four beam, multi-rib tubular stiffened skin arrangement. Uncooled wing concepts would utilize sine wave corrugated beam and rib webs. For the wing skins a spanwise oriented tubular stiffened configuration was used. A skin thickness of 0.010 inch was assumed to be a practical minimum. Data for tubular stiffened square panels, as presented in Reference 46, was used as a guide. This design provides high resistance to buckling when loaded parallel to the stiffening and considerable flexibility with respect to in-plane loadings normal to the stiffening. Hence, high structural efficiency is achieved in the spanwise direction and thermal stresses in the chordwise direction are minimized.

Two methods of attaching the tubular skin to the sine wave corrugated ribs can be used. As shown in Figure 138, a continuous tube requires the rib to be attached to the inner half of the tubular skin, thus only 50% of the skin cover is effective in carrying shear load. Thermal stress relief is still achieved through the use of the sine wave type corrugation rib web. Another method of fabrication is forming the tubular skin from two beaded skins welded together. For this concept the tubular cross section is not continuous across a rib, but tapers to form a thick skin at the rib attachment. At this rib attachment a 0.020-inch thick doubler was assumed to reinforce the panel edges and provide stiffening. In this concept, both skins are assumed 100% effective in carrying shear load. In this section, weights for both attachment concepts are presented for comparison.

For the basic multi-beam, multi-rib wing structure shown in Figure 132 about 10% of the chord was assumed to be a leading edge flap while the trailing edge flap was assumed to have a constant chord of 120 inches. The remainder of the wing planform constituted the primary load carrying structure. Sixteen beams were oriented perpendicular to the aircraft centerline while one beam ran along the maximum wing thickness line (2/3 chord) and another was located behind the leading edge flap. Five major full depth ribs were

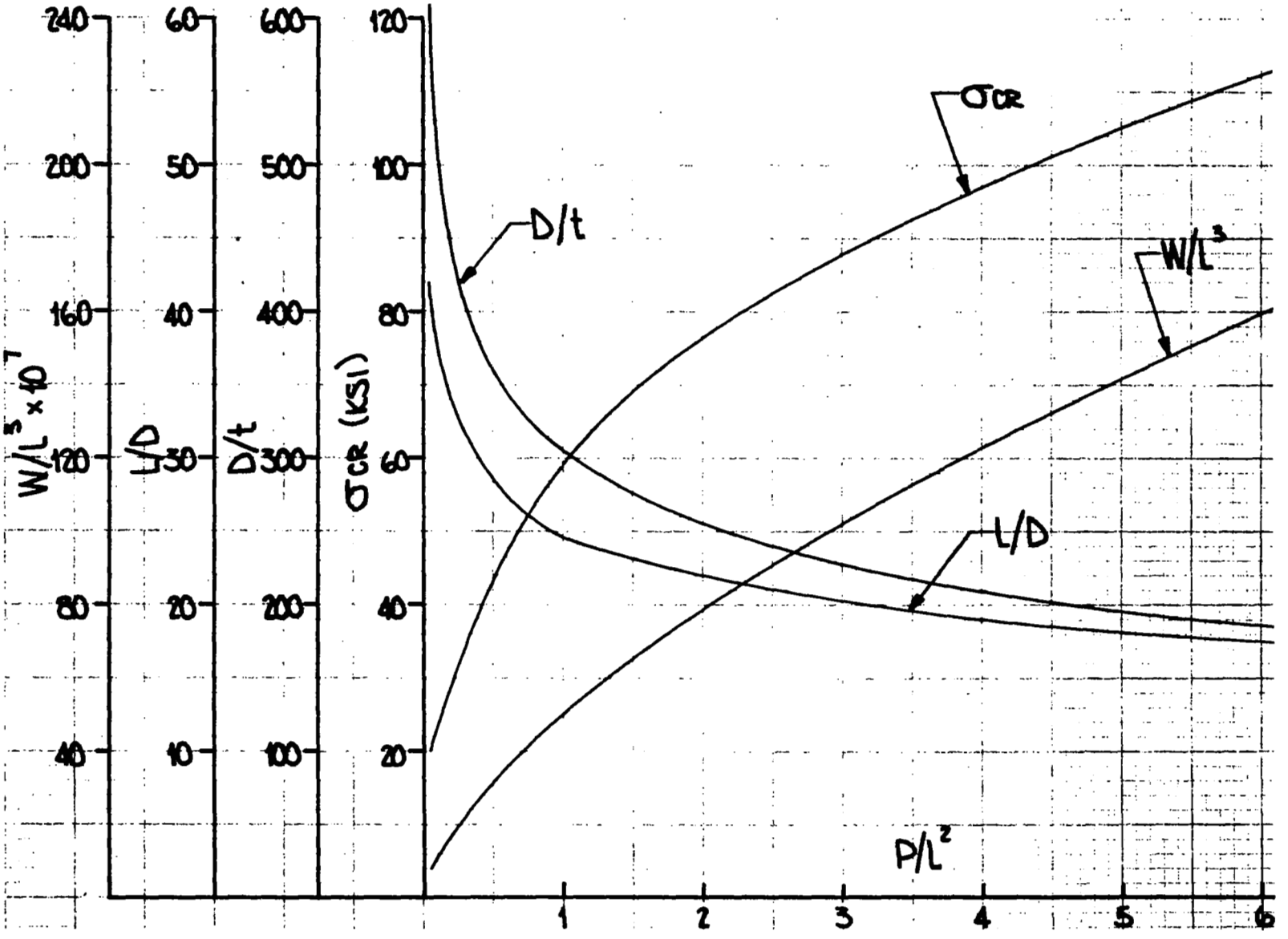

Figure 136. Optimum Weight Efficiency Parameters - Tubular Skin

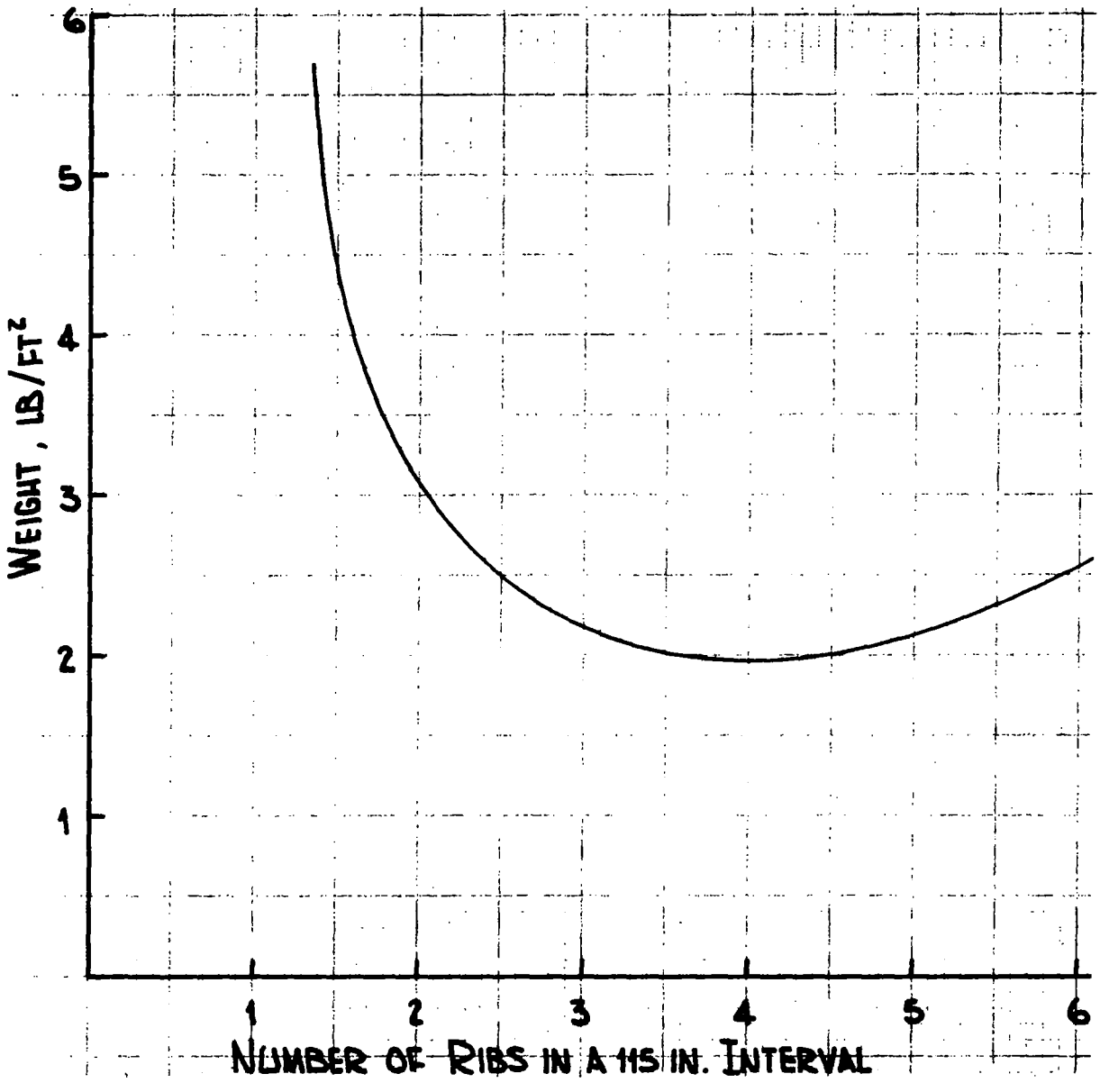

Figure 137. Internal Weight versus Number of Ribs for an Uncooled Wing

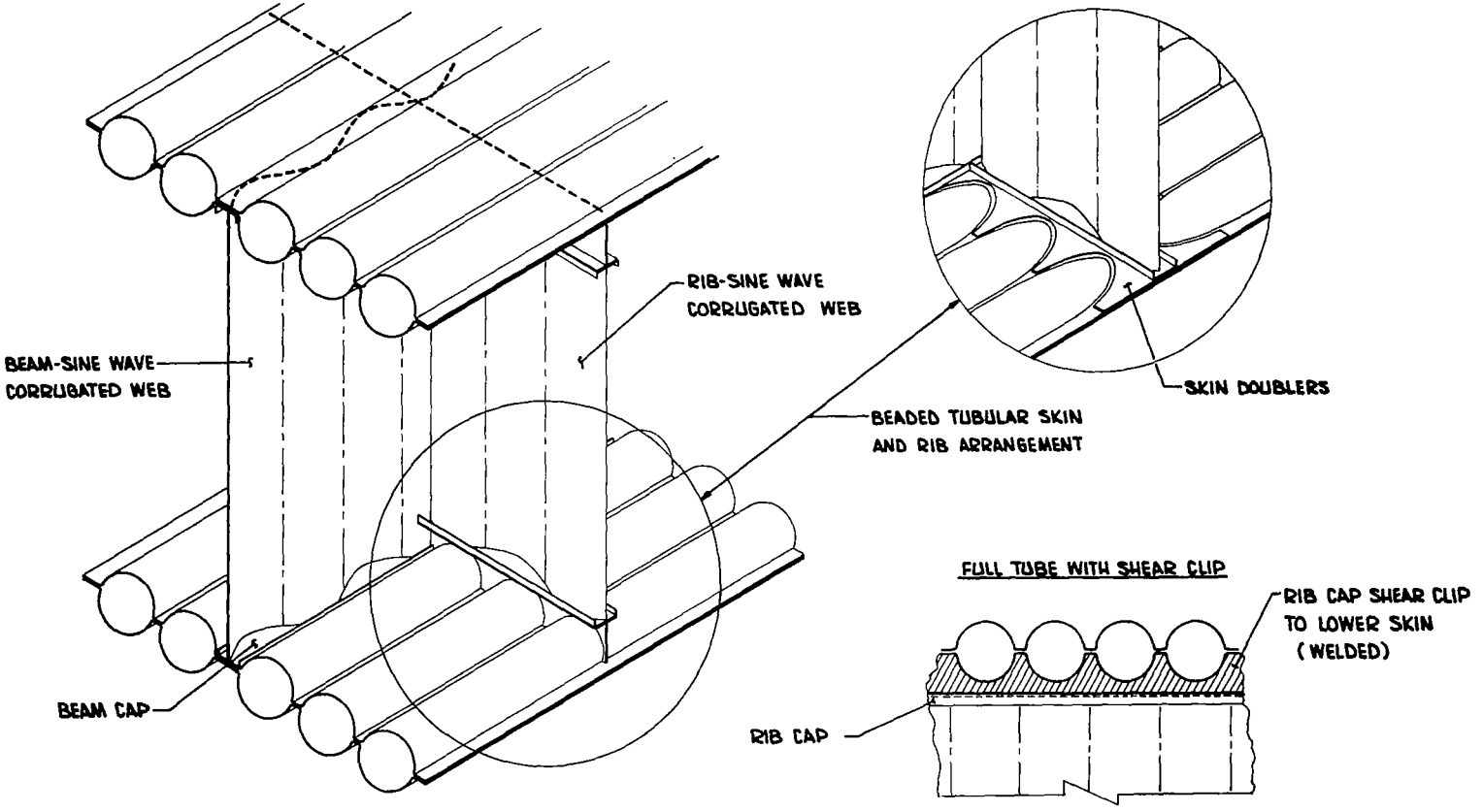

Figure 138. Uncooled Wing - Multi or Four Beam, Multi-Rib Tubular Stiffened Skin Arrangement

provided, along with three former-type ribs between each of the major ribs. Truss type construction was used for all full depth beams and ribs except the leading edge beam. This beam and the former-type ribs employed sine wave type corrugated web construction. The ribs supported the skins which were designed as wide columns. Spacings of the beams and major ribs were based on an optimization study and considerations of control surface support which established a 22.5 inch spacing for the intermediate ribs. After calculating the internal load distributions within the structural box, beam, rib, and stiffened skin cover sizes were calculated based upon shear and axial loading intensities as previously discussed in the cooled wing section.

For the four beam, multi-rib arrangement shown in Figures 131 and 138, the tubular skin sizes for two wing stations are given in Figure 139 along with the corresponding unit weights. A rib spacing of 36.8 inches was used based on the data in Figure 137. The tubular cover weights are 77.2% of the uncooled wing weight while the ribs (14.1%) and beams (8.7%) accounted for the remaining 22.8% of the total uncooled wing weight. Using a linear unit weight distribution between the root station and station 460 and a minimum thickness design the same as station 460 designs for outboard stations, a structural box weight of 14,700 lb was calculated. This corresponds to a unit weight of 6.25 lb/ft^2 and a total wing weight estimate of 43,500 lb. If a beaded tubular skin is utilized and the weight of doublers taken into account, the unit weight is reduced to 5.90 lb/ft^2 with a corresponding total wing weight of 41,000 lb.

Using the multi-beam and rib arrangement of Figure 132, the chordwise distribution of unit structural weight ranged from 4.25 lb/ft^2 to 23 lb/ft^2, as shown in Figure 140. For the more lightly loaded portion of the wing the skin constituted about 70% of the unit weight, beams about 10% and ribs about 20%. For the more heavily loaded rear beam area, the weight distribution was about 40% for the skin, 40% for beams and 12% for ribs. The average weight of the structural box was 7.62 lb/ft^2 which, when multiplied by the total wing area, resulted in a weight of 53,000 pounds for the uncooled 65° sweep wing.

Uncooled 65° Sweep Wing Summary

Material: Inconel 718, Tubular Skin

Four (4) Beam Multi-Rib Arrangement Full Depth Corrugated Beams and Ribs		Multi-Beam Multi-Rib Arrangement Truss Type Beams and Ribs
Full Tube 50% Shear Effectiveness	Beaded Tube 100% Shear Effectiveness	Tubular Skin
6.25 lb/ft^2	5.90 lb/ft^2	7.62 lb/ft^2

NOTE: All of the above concepts require heat shields which weigh about 1.1 lb/ft of wetted surface. This weight is not included in the above.

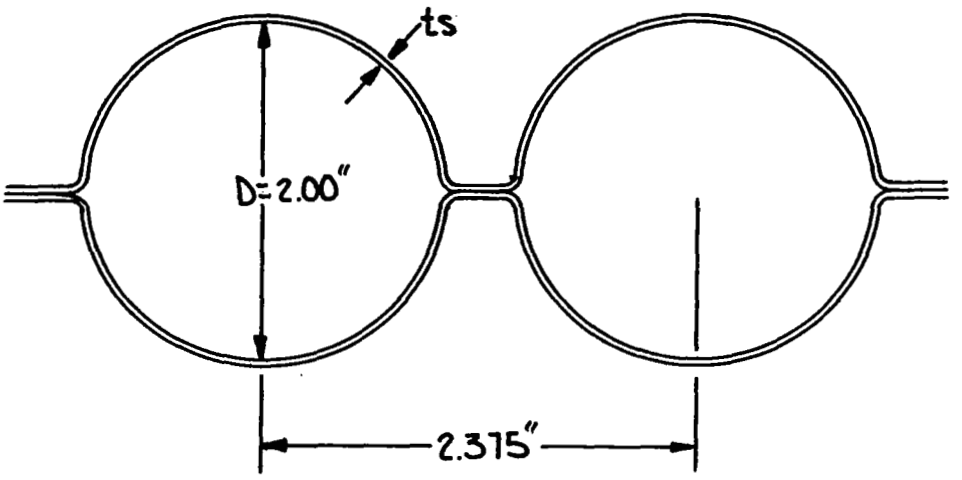

SKIN COVER SIZES:

ROOT STATION:

$t_s = 0.020"$

$\bar{t} = 0.0593"$

UNIT WEIGHT = $2.57\ LB/FT^2 \times 2 = 5.14\ LB/FT.^2$

WING STATION 460" FROM CENTERLINE OF FUSELAGE:

$t_s = 0.010"$

$\bar{t} = 0.0296"$

UNIT WEIGHT = $1.26\ LB/FT^2 \times 2 = 2.52\ LB/FT.^2$

Figure 139. Uncooled Wing Tubular Skin Concept

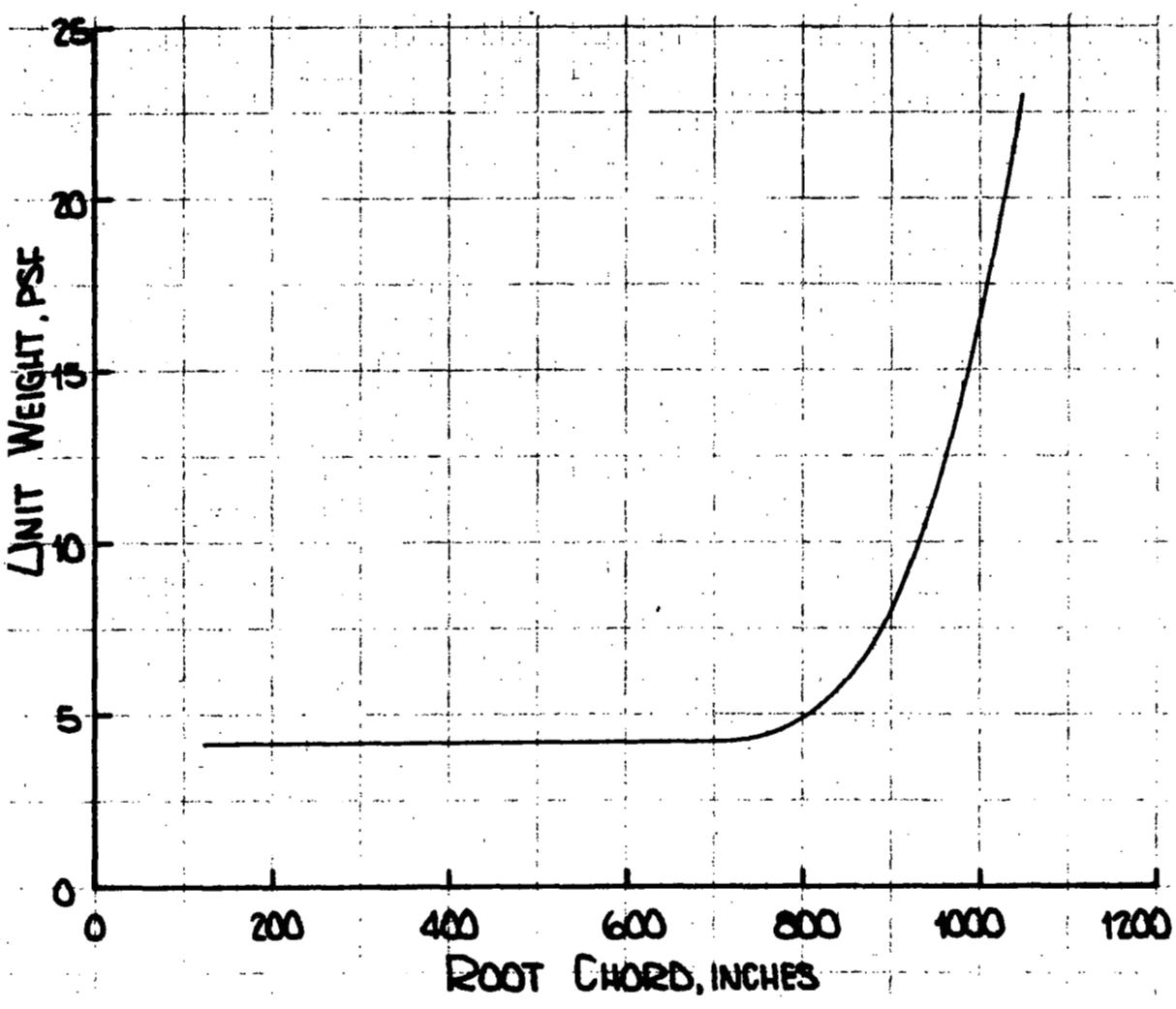

Figure 140. Chordwise Weight Distribution for the Structural Box of the Uncooled Multi-Beam and Rib Uncooled Wing Arrangement

E. WEIGHT SUMMARY

Table XXIX summarizes the structural weights for the cooled and uncooled wings studied in this section. Analyses for 0°, 45° and 65° sweep angles were done for a 200°F aluminum (7075-T6) alloy wing only. These cooled wing designs utilized a four beam, multi-rib arrangement with Zee stringer stiffened cover skins. To obtain a variation in wing weight with wing operating temperature three additional analyses were conducted for the 0° sweep wing. These variations were done for 300°F and 600°F operating temperatures utilizing an aluminum (2024-T81) alloy at 300°F and a titanium (6AL-4V) alloy at both 300°F and 600°F. These wing weight variations are plotted versus sweep angle in Figure 141 in which it is assumed that the curve shape established for the 200°F aluminum alloy is appropriate for the other cooled wing concepts. Shaded areas in Table XXIX indicate weight estimates read from Figure 141 and not based upon actual analyses.

In Figure 141, the structural weights of the 7075-T6 aluminum alloy and the 6A1-4V titanium alloy wings are plotted as a function of leading edge sweep angle as determined from the four beam multi-rib wing designs. The weight of the uncooled 65° sweep wing is plotted also for comparison purposes. As noted in the preceeding discussions, the 2024-T81 (300F) wings are expected to be about 10% heavier than the 7075-T6 wings, while the 6A1-4V (300F) wings would be comparable in weight to the 7075-T6 wings. Although the spanwise loading intensity decreased by a factor of 4.6 as the leading edge sweep is increased from 0° to 65°, the wing weights decreased by factors of only 1.4 to 1.6. This is probably due to the minimum skin gage restrictions assumed for the studies. At the higher sweep angles a greater percentage of the wing is designed by the minimum gage consideration.

Weights of the cooled wings are considered to be conservative by at least 10% as indicated by comparisons of the span-wise weight distributions and spanwide loading distributions. The assumption that the unit weights of the flaps and control surfaces are equal to the unit weight of the structural wing box is a conservatism which is applicable to both cooled and uncooled designs.

In Table XXIX and Figure 141 only structural weights are shown and a true comparison between cooled and uncooled wings must consider cooling system and heat shield weights. This overall comparison is made in Section 12. At this point, structural weights can be compared. Ratioing the uncooled and cooled wing structure weights as given below reveals a weight increase of about 40 to 50% as the change is made from a cooled to an uncooled structure.

$$\frac{\text{Uncooled, Full Tube, MB}}{\text{Cooled, Zee stringer MB}} = \frac{53{,}000}{35{,}000} = 1.52$$

$$\frac{\text{Uncooled, beaded tube, FB}}{\text{Cooled, Zee stringer, FB}} = \frac{41{,}300}{29{,}200} = 1.41$$

TABLE XXIX

STRUCTURAL WEIGHT SUMMARY, NO COOLING SYSTEMS
OR HEAT SHIELDS

		Cooled Wings					Uncooled Wings		
Operating Temperatures		200°F		300°F		600°F	Inconel 718[4] (No Heat Shield Weight)		
Materials		Aluminum 7075-T6		Aluminum 2024-T81	Titanium 6Al-4V	Titanium 6Al-4V			
Structural Concepts[1]		FB	MB	FB	FB	FB	FB	FB	MB
		Zee	Zee	Zee	Zee	Zee	Full Tube	Beaded Tube	Tubular
Sweep Angle	0°	5.87[2]	-	6.54	5.90	7.68	-	-	-
		41,100[3]	-	45,700	41,300	53,800	-	-	-
	45°	5.17	-	5.69	5.26	6.64	-	-	-
		36,200	-	39,500	36,500	46,000	-	-	-
	65°	4.18	5.02	4.39	4.21	4.92	6.25	5.90	7.62
		29,200	35,000	30,500	29,400	34,200	43,500	41,300	53,000

Note: (1) FB, Four Beam-Multirib Arrangement; MB, Multibeam - Multirib Arrangement
(2) Unit Wing Weight, lb/ft^2
(3) Total Wing Weight, lb
(4) Heat Shields Add 1.1 lb/ft^2 of shielded surface area to the uncooled wing weights. Heat shields are an absolute necessity over at least 7000 ft^2 and probably will be needed over 10,000 ft^2 of surface.

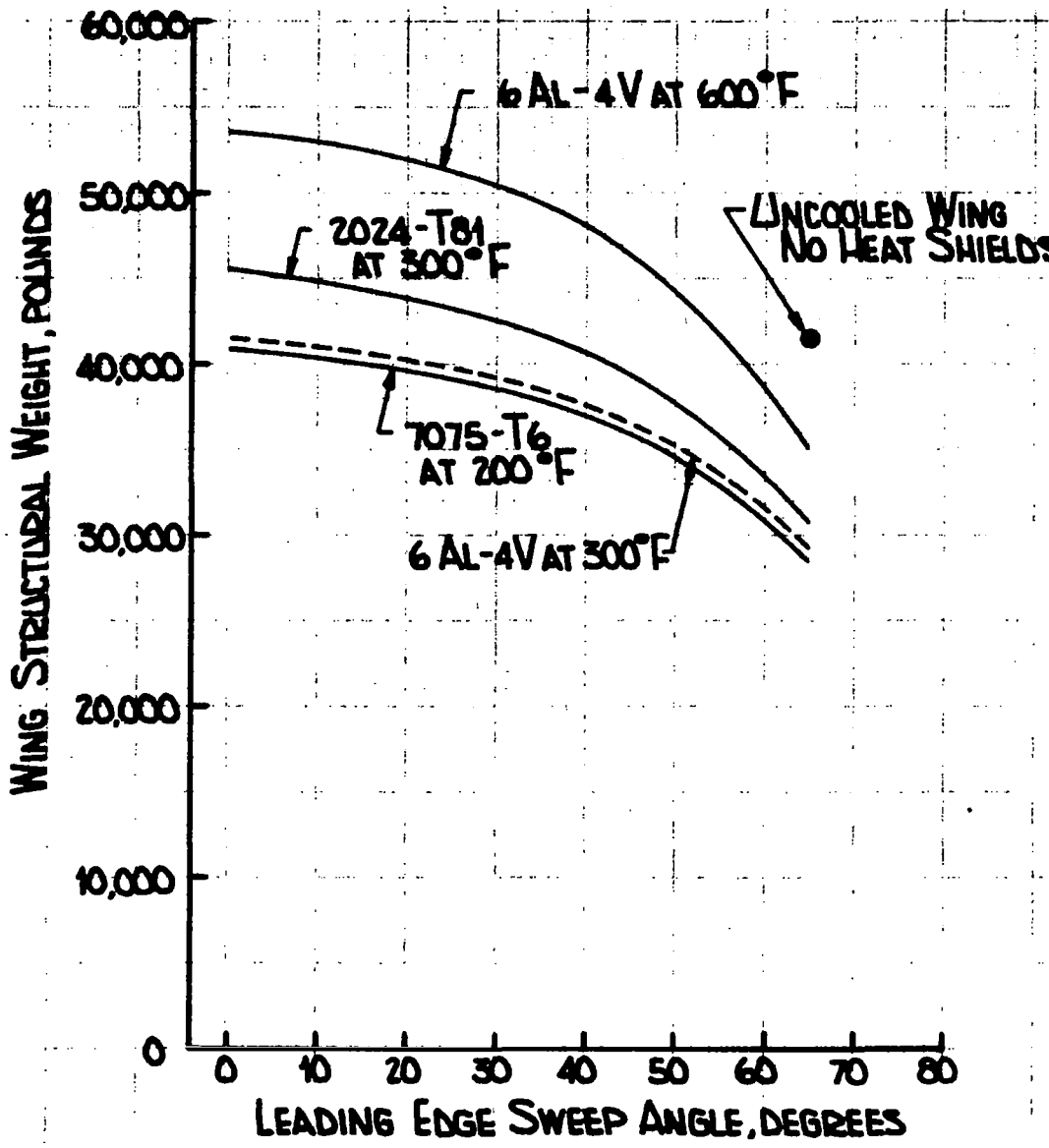

Figure 141. Wing Structural Weight Comparison

F. STATISTICAL WEIGHT ESTIMATES

In order to provide added confidence in the calculated weights for the cooled and uncooled wings, weight prediction techniques based on statistical information were used to generate additional weight estimates. Data comparing cooled and uncooled wings for other aircraft was also obtained from available literature.

1. General Dynamics Weight Estimation Equation

To allow comparison of the data generated during this study and that presented in the reports used as a baseline reference the statistical weight estimating technique presented in Reference 1 is reproduced in this section. Figure 142 presents the wing weight estimation equation and a graph of the material - Mach number coefficient. For the wings studied herein, a 3.0 g ultimate load factor, a 115 ft structural span, a 6954 ft^2 wing area and a root chord thickness of 5 ft were utilized. The takeoff weight is estimated in Figure 9 as 521,000 lb. For the above parameters the following wing weights can be calculated.

Material	Mach Number	Total Weight (lb)	Unit Weight (lb/ft^2)
Inconel 718	6	37,600	5.41
Titanium	3	35,400	5.09

Comparing these weights with those presented in Table XXIX a good correlation is observed for the titanium, 600°F wing, but the above weight for an Inconel 718 wing seems low. It is believed that the use of a thermal stress relieving structure to obtain the weights in Table XXIX is the source of the difference in the uncooled wing weights and that the General Dynamics uncooled wing weights are low.

2. Lockheed Statistical Weight Determination[1]

A statistical wing weight estimation technique applicable to conventional structure has been developed by the Lockheed-California Company. The use of this equation allows an estimate of a cooled hypersonic wing weight to be made based upon projections of present aircraft technology.

Table XXX presents the Lockheed correlation equation along with the aircraft configuration data needed to obtain a wing weight correlation. Figure 143 shows the calculated points for large gross weight aircraft along with at least squares fit to these points. For comparison purposes the correlation for fighter aircraft and light-weight transports is also shown. The wing weights given in Table XXX and Figure 143 are actual weights. Because these wings have been degraded from the theoretical wing weight through the addition of landing gear, access doors, fuel and hydraulic lines, actuating mechanisms and other flight hardware, it would be expected that these actual weights would be about 15 percent above the theoretical weights estimated for these aircraft.

[1] Private communication to C. E. TILYOU, Bell Aerospace Co., from A. BAKER, Lockheed-California Co., Sept. 1965.

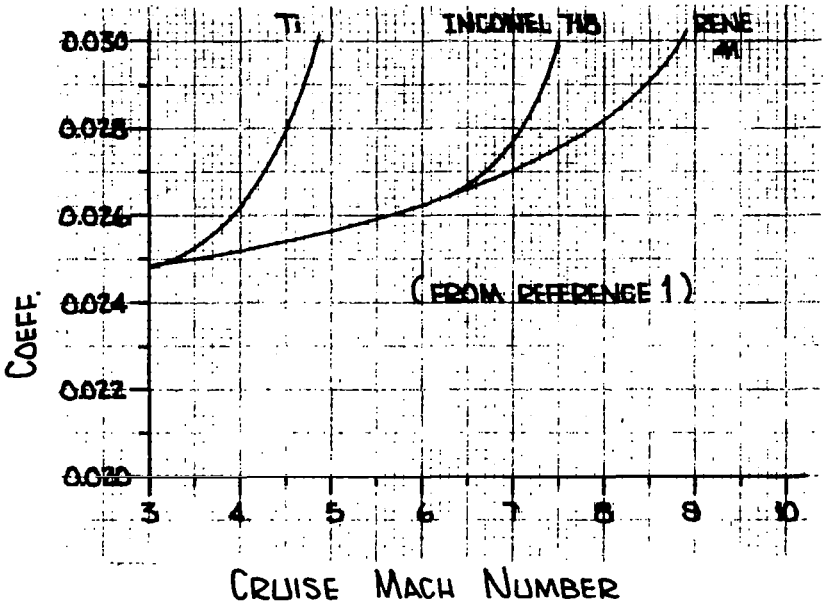

$$\text{Wing Wt.} = \text{Coeff} \left(\frac{W_{TO} \ LF \ b_s \ S}{t_R} \right)^{0.54}$$

where W_{TO} = takeoff weight
LF = ultimate load factor
b_s = structural span
S = wing area
t_R = thickness at root chord

Figure 142. General Dynamics Weight Estimation Equation

TABLE XXX

AIRCRAFT STATISTICAL DATA

Item	Aircraft								
	R6V	C-141A	B-36B	B-52D	DC-8	KC-135	YB-49	C-5A	Bell $\Lambda_o = 65^o$
W_{DG}	184,000	318,000	276,000	450,000	189,000	275,000	213,550	728,000	525,000
N	4.06	3.75	4.0	3.0	3.75	3.0	4.0	3.75	3.0
S	3,610	3,228	4,772	4,000	2,758	2,433	4,000	6,200	6,954
AR	9.9	7.9	11.1	8.6	7.07	7.04	7.4	7.75	1.87
Λ	0	25	9	32	28	28	19	25	32.5
λ	0.33	0.21	0.25	0.40	0.244	0.33	0.25	0.335	0
W_R	24,900	50,200	42,400	45,700	22,000	19,500	27,473	44,254	0
T/C	18.4	12.4	21.0	14.4	10.75	15.2	18.8	11.8	5.0
Q_U	1.0	1.0	1.0	1.0	0.95	1.0	1.0	1.0	1.0
Q_F	1.0	1.0	1.0	1.0	1.0	1.0	1.0	1.0	1.0
Q_I	0.9	1.0	0.9	0.9	0.9	0.9	0.9	0.9	0.9
f	39.1	52.5	70.0	76.5	36.7	34.2	40.7	193.5	67.0
W_W	32,000	34,700	36,000	39,920	27,000	24,800	31,650	83,166	29,160 35,000

$$f = \frac{W_{DG}^{0.6} \times N^{0.6} \times S^{0.8} \times AR^{0.8} \times (1+\lambda)^{0.4} \times \sec^{1.6}\Lambda \times Q_U \times Q_F \times Q_I \times \left[1 - \frac{W_R}{W_{DG}}\right]^{0.4} \times 10^{-5}}{(T/C)^{0.4}}$$

W_W = Wing Weight

W_{DG} = Design Gross Weight (lb)

N = Ultimate Load Factor at D.G.W.

S = Gross Wing Area (ft^2)

AR = Aspect Ratio

Λ = Sweep Angle of 50% Chord

λ = Tip Chord/Root Chord

W_R = Weight of Engines in Wing (lb)

T/C = (4 Root T/C (%) + Tip T/C (%))/5

Q_U = 0.95 for Aircraft with Fuselage Located Undercarriage, 1.0 for Others

Q_F = 1.15 for Wing Folding Provision 1.0 for Others

Q_I = 0.9 for Wings of Integral Skin-Stringer Construction

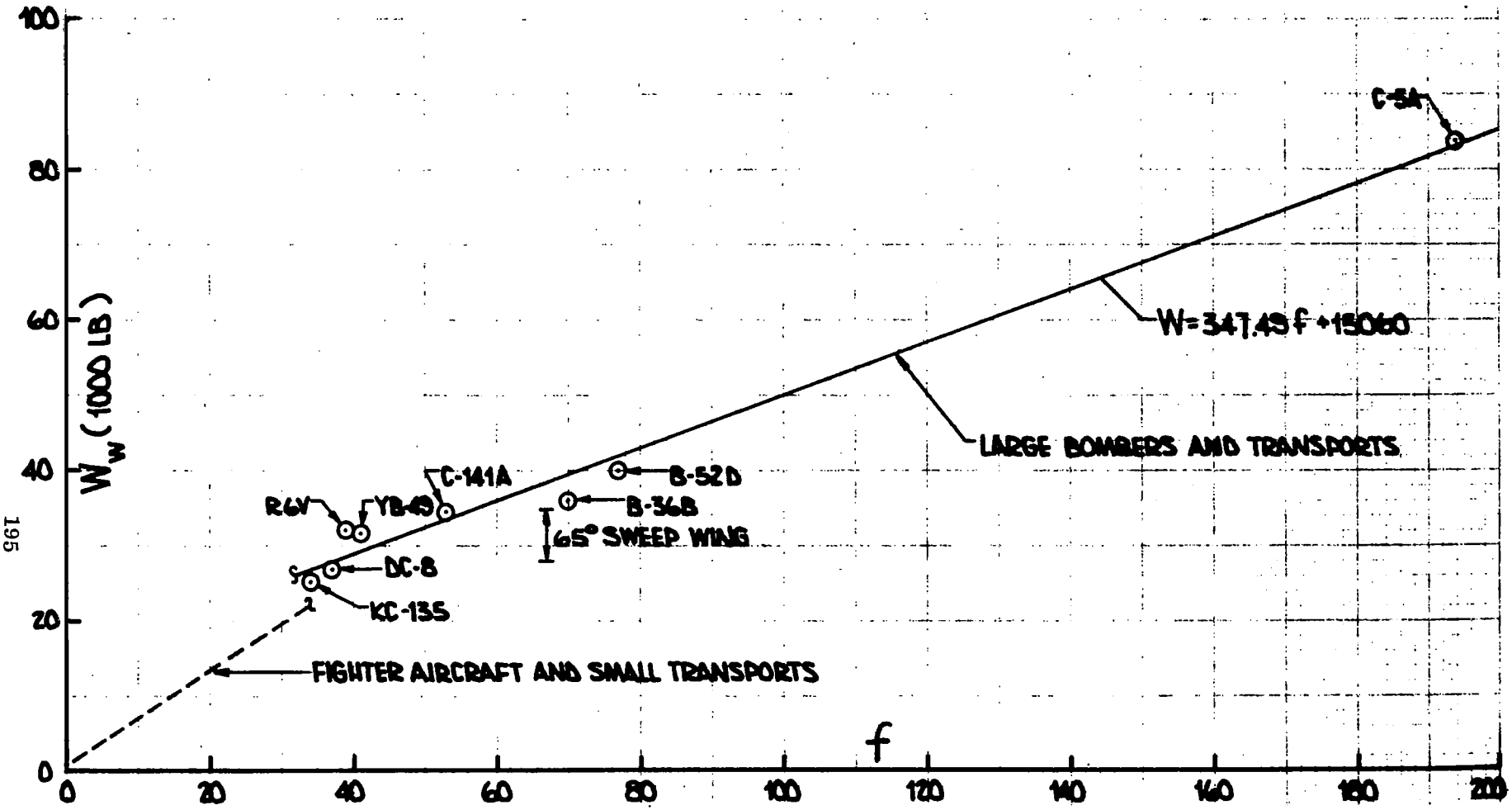

Figure 143. Lockheed Statistical Weight Estimates

The weight of the cooled 65° swept wing as predicted by the equation in Table XXX, 38,200 lb, is significantly higher than the weights calculated for this wing, 29,200 lb to 35,000 lb. This difference, shown graphically in Figure 143 is not surprising. The aircraft on which the correlation is based all have high aspect ratio wings and in most cases the wings are used for fuel storage. Although the correlation equation is a function of both aspect ratio and sweep angle the exponents and coefficient may be related to the aircraft data used for establishing the correlation. As such, significant planform deviations may result in a loss in the accuracy of the prediction. In particular, wings of low aspect ratio and high sweep are expected to be lighter than estimates based on Figure 143. Wet wings are heavier than dry wings regardless of the planform. The internal pressure requirements necessitate increased skin stiffening, somewhat heavier beam webs, and an increase in the weight of skin-to-substructure fasteners. These considerations plus the fact that the scatter band about the correlation line is about ±10% explain the conservative weight prediction made for the wing of the hypersonic cruise aircraft.

3. Bell Aerosystems Statistical Weight Determination

Given in Reference 52 are a series of equations and graphs developed during a Bell study. These equations and graphs can be used to estimate aircraft wing weights. Since the statistical correlation from Reference 52 was developed using a mathematical model different from that used in the Lockheed wing weight estimation technique, it is interesting to compare the projected wing weights. Furthermore, it is believed that the correlation in Reference 52 is particularly good for delta wing aircraft similar in planform to the 65° sweep baseline configuration of this study. Using Reference 52, the correlation curve given in Figure 144 was determined based on data for the F-102, F-106, F-108, and YB-58A aircraft. Comparison of the weight estimate previously determined from the preliminary design of the 65° sweep baseline wing with the prediction based on the statistically founded equations, shows good agreement 29,200 lb as compared to 31,000 lb. This is a result of the similarity of the various delta wing planforms and the fact that no fuel is stored in any of the wings considered. The wing weight data used in the Bell statistical weight equation for the aircraft shown on Figure 144 are summarized as follows.

	Aircraft			
	F-102	F-106	F-108A	YB-58A
Wing Area - (ft^2)	695	698	1160	1543
Aspect Ratio	2.08	2.08	2.72	2.09
Design Gross Weight (lb)	25,500	29,776	-	158,000
Ultimate Design Load Factor	10.5	10.5	8.0	3.0
Root Chord Thickness (%C)	3.9	3.9	2.0	3.4
Wing Weights (lb)	3020	3272	5912	11,400

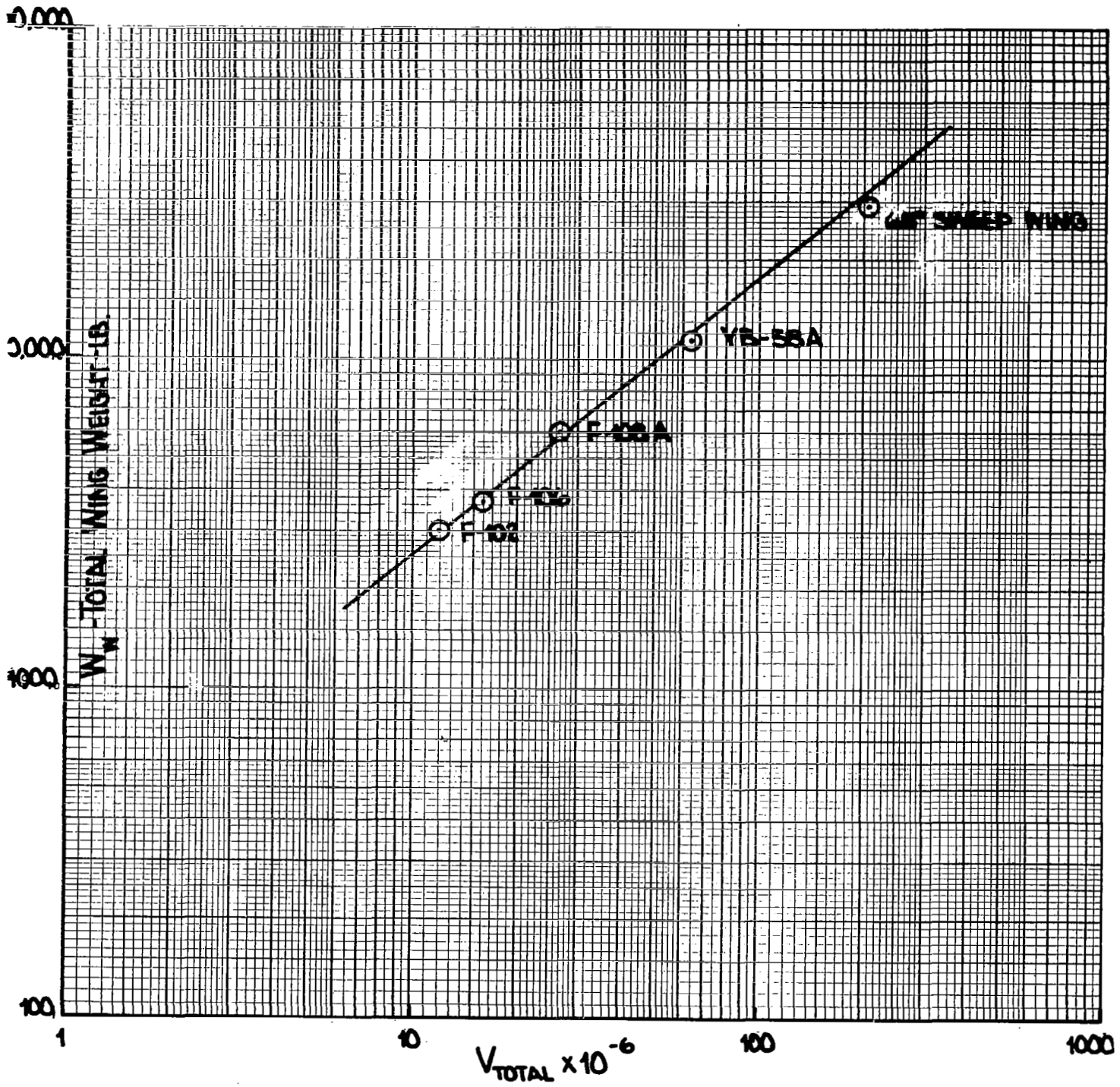

Figure 144. Bell Aerosystems Company Statistical Weight Estimate

4. Comparisons of Cooled and Uncooled Wing Structures

To further establish a level of confidence in the structural weight estimates for the cooled and uncooled wings, data from analytical studies conducted by other organizations were compiled. In Reference 53, a very early study of a hypersonic transport aircraft of interest was obtained by extrapolating data for subsonic transport aircraft. The form of the extrapolation was very simple but was undoubtedly adequate for the authors' purpose; component weight was plotted as a function of takeoff weight. Takeoff weights ranged from 35,000 pounds to 160,000 pounds while wing weights ranged from 3500 pounds to 17,000 pounds. Using the plotted data the authors' projected a unit weight of 7.0 lb/ft^2 for a steel wing with honeycomb sandwich skins for the 500,000 pound Mach 7 transport. This is near the middle of the range of unit weights 5.90 to 7.62 lb/ft^2, predicted on the basis of the preliminary design studies described previously.

In another more recent comparative study of uncooled and cooled structures, the ratio of structural weight was about 1.45, which is in good agreement with the ratios of 1.41 and 1.52 for the two structural concepts examined during this project. Comparison of ratios is considered to be more appropriate than comparison of actual weights because of differences in vehicle configurations, flight trajectories and design life objectives.

SECTION 9

COOLING SYSTEM REFINEMENTS

The weight estimates presented in the previous sections of this report are based upon the use of weight factors for the major cooling system components. As might be expected there is some room for discussion concerning the exact value of these weight factors and their effect on total cooling system weights. In this section the more promising cooling systems are examined with respect to possible weight estimate reductions which might be made as a result of revisions of the weight factors incorporated in the cooling system weight estimates.

A. TRANSPIRATION COOLING

Table XXXI presents a breakdown of the cooling system component weight estimates for two of the most promising transpiration cooling systems, the hydrogen transpiration cooling system with a -400°F inlet temperature and the liquid water transpiration system with the water boiling at 80°F. As noted in Table XVI and Table XVII the outer surface temperatures are near radiation equilibrium values for these systems and as a result the coolant flow rates are low. The data in Table XXXI shows the typical trends of a gaseous versus liquid cooling system. In Section 4 it was shown that to obtain comparable heat transfer characteristics the pumping power requirements for gases are about 1000 times greater than for liquids. This characteristic of gases is manifested in the 6 to 7 times greater plumbing weights for gases than for liquids when used in transpiration cooling systems. Thus, despite the fact that about three times as much water must be transpired as compared to hydrogen the total water system weight is slightly less than the hydrogen system weight. Furthermore, the water coolant occupies only one-fifth the volume required for hydrogen.

Examination of the system components in the hydrogen transpiration cooling system suggests that greatest possible weight savings might be achieved in the plumbing system which constitutes about 70% of the system weight. If liquid or supercritical hydrogen is delivered to the porous surfaces, rather than gaseous hydrogen, weights associated with distribution lines and pumps would obviously be reduced. The degree of reduction can only be assessed through detailed studies which were beyond the scope of the present effort. It is considered very unlikely, however, that plumbing system weights could be halved.

For the water transpiration system, tankage and plumbing weights constitute only about 15% of the total system weight so that refinements in these items are not likely to have a significant influence on system weight. The greatest potential for improvement in the liquid water transpiration system is in refinements of the coolant weight estimate. The method of calculation for water transpiration was given some substantiation in Section 6 by a separate "wet" surface flow rate estimate. Experimental verification of transpiration with water undergoing a phase change and subsequently being heated before injection into the boundary layer was not available in the literature. It is strongly suggested that

TABLE XXXI

COOLANT WEIGHT, TANKAGE WEIGHT AND PLUMBING WEIGHT FOR HYDROGEN AND LIQUID WATER TRANSPIRATION COOLING SYSTEMS

		Hydrogen Transpiration * -400°F Inlet Temperature			Liquid Water Transpiration * 80°F Boiling Water Temperature		
		Sweep Angle			Sweep Angle		
Wing Area	Weight Item (lb)	0°	45°	75°	0°	45°	75°
Leading Edge	Coolant	189	362	620	506	885	1,710
	Tank	26	51	87	10	18	34
	Plumbing	520	734	1,465	155	220	440
Top Surface	Coolant	726	600	296	3,020	2,380	1,090
	Tank	102	84	41	60	48	22
	Plumbing	3,330	2,810	1,850	500	422	278
Bottom Surface	Coolant	2,250	2,140	1,650	7,440	6,800	5,170
	Tank	316	300	231	149	136	103
	Plumbing	6,380	6,150	5,385	958	922	808
Subtotals	Coolant	3,165	3,100	2,570	11,000	10,100	7,970
	Tank	444	435	359	219	202	159
	Plumbing	10,230	9,690	8,700	1,610	1,560	1,530
Total		13,800	13,200	11,600	12,800	11,800	9,655

*Minimum flow rates from Tables XVI and XVII.

such experimental investigations be conducted. Refinements in the weight estimates for a water transpiration system rest upon the results of such experiments and thus cannot be made at this time.

B. FILM COOLING

Refinements in the film cooling system weight estimates are not possible without a greatly improved flow rate prediction method. At present the Hatch-Papell equation is very deficient in its ability to predict film cooling flow rates for either laminar or turbulent flow. A correlation is needed which will relate slot sizes to cooling effectiveness in terms of flow rate requirements and resulting temperature distributions. At this time it is recommended that extensive experimental investigations be conducted to supply data for correlation with theoretical predictions. Both liquid and gaseous coolants should be studied.

C. CONVECTIVE COOLING

The most promising convective cooling concepts are those which employ a water-glycol or silicone transport fluid transporting heat from the vehicle structure to the hydrogen heat sink. Systems of this type can be optimized and refined by changes in operating temperatures and through the use of thermal protection systems. However, when the heat sink is the vehicle fuel and its weight is not included as part of the cooling system weight the cooling system weight optimization is quite different than an optimization in which the expendable coolant weight is charged to the cooling system weight. In the latter case there is a tradeoff between the weight of expended coolant and the weight of thermal protection so that a minimum system weight is found. In the former case, which is being studied here, cooling system weight is not directly related to the heat sink coolant usage.

Since it is assumed that the coolant passages are an integral part of the load carrying structure they do not contribute to the cooling system weight. The coolant distribution system weight of 0.15 lb/ft^2 of cooled surface area is insensitive to coolant flowrate changes due to changes in heat load and is not a significant variable in a weight optimization study. Changes in heat input caused by changes in the thermal protection system affect only the cooling system heat exchanger weight and the transport fluid pump and motor weights. However, changes in the thermal protection system do drastically affect the transport fluid flow rate and the percentage of heat sink heat capacity used for cooling. Since the heat sink is the fuel the optimization process becomes one of flow matching, using thermal protection to reduce the percentage of the fuel heat capacity which is required for structural cooling. Simultaneous reductions in the cooling system heat exchanger and coolant pump and motor weights somewhat offset the thermal protection system weight and a partial weight optimization is obtainable. These facts are demonstrated quantitatively in this subsection.

1. Thermal Protection Systems

Based on the presentation in Section 5 an air gap system (0 radiation shields) and a radiation shield system with some small number of shields were chosen as the most applicable thermal protection systems for a cooled wing. Weight and flow rate data were generated for a water-glycol system and a silicone system with thermal protection on the

TABLE XXXII

AIR GAP OR RADIATION SHIELD THERMAL PROTECTION SYSTEMS
FOR A WATER-GLYCOL COOLING SYSTEM FOR THE BOTTOM SURFACE OF THE WING

	Sink Temperature (^{o}F)	200^{o} F Mean Outer Surface Temperature		Air Gap Thermal[1] Protection System		Radiation Shield[2] Thermal Protection System with Four Radiation Shields	
		0^{o} Sweep	65^{o} Sweep	0^{o} Sweep	65^{o} Sweep	0^{o} Sweep	65^{o} Sweep
Thermal Protection System Weight (lb)		0	0	7,020	6,240	9,580	8,510
Cooling System[3] Weight (lb)	-50 +50	8,560 8,640	7,200 7,300	9,700 9,710	8,580 8,590	11,600 11,600	10,300 10,300
Water-Glycol Flowrate (lb/hr)	-50 +50	584,000 970,000	484,000 810,000	66,000 109,000	54,800 92,000	9,600 16,000	8,070 13,400
Hydrogen Flowrate (lb/hr)	-50 +50	128,400 91,800	106,000 76,000	14,400 10,280	12,100 8,600	2,100 1,500	1,770 1,265

Notes: (1) Outer Surface Temperatures Vary About 1100 ^{o}F ± 25^{o} F

(2) Outer Surface Temperatures Vary About 1150 ^{o}F ±25^{o} F

(3) Cooling System Weight Includes Thermal Protection System Weight

TABLE XXXIII

AIR GAP OR RADIATION SHIELD THERMAL PROTECTION SYSTEMS
FOR A SILICONE COOLING SYSTEM FOR THE BOTTOM SURFACE OF THE WING

	Sink Temperature (^{o}F)	400^{o} F Mean Outer Surface Temperature		Air Gap Thermal[1] Protection System		Radiation Shield[2] Thermal Protection System with Four Radiation Shields	
		0^{o} Sweep	65^{o} Sweep	0^{o} Sweep	65^{o} Sweep	0^{o} Sweep	65^{o} Sweep
Thermal Protection System Weight (lb)	–	0	0	7,020	6,240	9,580	8,510
Cooling System[3] Weight (lb)	0 200	8,000 8,200	6,270 6,860	9,660 9,680	8,550 8,570	11,600 13,200	10,300 10,300
Silicone Flowrate (lb/hr)	0 200	590,000 1,200,000	496,000 980,000	69,500 139,000	58,300 116,500	10,200 20,400	8,550 17,100
Hydrogen Flowrate (lb/hr)	0 200	97,200 58,600	81,000 48,400	11,400 6,840	9,540 5,730	1,670 1,000	1,400 840

Notes: (1) Outer Surface Temperatures Vary About 1100^{o}F ±25^{o}F

(2) Outer Surface Temperatures Vary About 1100^{o}F ±25^{o}F

(3) Cooling System Weight Includes Thermal Protection System Weight

TABLE XXXIV

AIR GAP THERMAL PROTECTION SYSTEM FOR A WATER-GLYCOL COOLING SYSTEM FOR THE TOP SURFACE OF THE WING

	Sink Temperature (^{O}F)	200^{O}F Mean Outer Surface Temperature		Air Gap Thermal Protection System (1)	
		0^{O} Sweep	65^{O} Sweep	0^{O} Sweep	65^{O} Sweep
Thermal Protection System Weight (lb)	–	0	0	3,670	2,680
Cooling System Weight (2) (lb)	+50	1,650	1,146	4,770	3,480
Water-Glycol Flowrate (lb/hr)	+50	91,200	57,200	23,400	14,800
Hydrogen Flowrate (lb/hr)	+50	8,600	5,400	1,230	544

Note: (1) Outer Surface Temperatures Vary about 625^{O}F ±25^{O}F
(2) Cooling System Weight Includes Thermal Protection System Weight

bottom surface as summarized in Table XXXII and XXXIII respectively. The bottom surface was assumed to be protected by a high temperature radiation shield system such as that described in Section 5 and for which weights are presented in the first column of Table VII. For such a system a simple air gap shield of an outer surface made from 0.020 inch thick superalloy weighs 1.10 lb/ft^2. With four Rhodium radiation shields this system weighs 1.50 lb/ft^2.

The data in Tables XXXII and XXXIII demonstrate the effectiveness of a radiation barrier in reducing the heat input to the cooling system. The simple air gap shield reduces the transport fluid and hydrogen flow rates by a factor of almost nine while increasing the weight of the thermal protection plus cooling system by about 3,000 lb. Since heat exchanger weights and pump and motor weights are reduced as flow rates are reduced the weight increase due to adding heat shields is almost nullified and the effective increase in system weight is only 0.17 lb/ft^2. A radiation shield system employing four radiation shields reduces the transport fluid and hydrogen flow rates by a factor of more than 60 times. For this arrangement, the weight of the bottom surface cooling system increases by about 3,000 lb, or about 0.47 lb/ft^2. As shown in Table XXXIV adding a thermal protection system to the top surface is not as advantageous weightwise as adding thermal protection to the highly heated bottom surface.

Using Figures 42 and 43 from Section 5 these reductions in flow rate can be verified for the 200°F active cooling system temperature (water-glycol system). The 0° sweep wing with an average heat transfer coefficient on the bottom surface of 7.7 BTU/hr-ft^2-°F, may be taken as an example. From Figure 42 the corresponding heat input to the 200°F active cooling system for zero and four radiation shields is 1850 BTU/hr-ft^2- F and 275 BTU/hr-ft^2-°F respectively. The heat input for no protection and a 200°F outer surface temperature is 16,900 BTU/hr-ft^2-°F (2200 x h). This means that the heat input has been reduced by 9.1 times and 61.0 respectively for the air gap (zero shields) and four radiation shield systems. From Figure 43 the corresponding outer surface temperature are 1100°F and 1150°F respectively as noted in Table XXXII. Using Figures 42 and 43 estimates of the water-glycol and hydrogen flow rate changes can be made for any combination of radiation shields and heat transfer coefficient.

To correctly assess the effect of this thermal protection system weightwise, a series of computations must be performed to determine how the reduced flow rates affect the system component weights. In Section 10 the data in Tables XXXII and XXXIII is used to obtain total wing weights for both water-glycol and silicone systems with a thermal protection system on the bottom surface.

2. System Operating Temperature Variations

In Section 7, Figure 91, a schematic of the indirect liquid convective cooling systems was presented showing the assumed operating temperatures which were chosen to obtain representative cooling system weight estimates and typical performance characteristics. Past experience has shown that system weights are not particularly sensitive to exact values of the operating temperatures. In this section these operating temperatures were varied to suggest refinements in the indirect liquid cooling system design. Since hydrogen flow rate reductions are of greatest interest, emphasis was placed on reducing the hydrogen flow rates without increasing system weights. The systems of interest are

the indirect cooling systems using water-glycol and silicone transport fluids previously described in Section 7 and therefore have no thermal protection.

Referring to Figure 91, variations in T_S the sink temperature, vary the hydrogen flow rate. As T_S increases the hydrogen flow rate decreases. The assumption of the hydrogen outlet temperature being 100°F below T_S is conservative and can be changed by careful examination of the transport fluid-hydrogen heat exchanger.

The thermodynamically limited, maximum possible heat transfer rate is realized only in a counterflow heat exchanger of infinite heat transfer area, Reference 26. Assuming that a counterflow heat exchanger of reasonable size is the correct choice for this application then Figure 145 shows a corresponding temperature versus area plot. To insure that a compact heat exchanger could be designed a conservative assumption of δ = -100°F was used in Section 7 and the resulting flow rates for the water-glycol and silicone systems were presented in Table XXIII. If the resulting hydrogen flow rates are excessive then heat exchanger designs are possible with the hydrogen outlet temperature as much as 50°F above T_S (δ = +50°F). Figure 146 presents hydrogen flow rate reduction factors for various sink temperatures and hydrogen outlet temperatures. Using the data in Table XXIII and the curves in Figure 146 hydrogen flow rates can be determined for sink temperatures from -100°F to +200°F and hydrogen outlet temperature from -200°F to +250°F. Using the curves in Figure 146 hydrogen flow rate reductions can be estimated for the water-glycol and silicone systems.

Another technique for reducing hydrogen flow rates is through reduction of the heat input to the cooling system by raising the average value of the outer surface temperature. Figure 147 presents a set of curves for both the water-glycol system and the silicone systems. For the water-glycol system a titanium structural skin would allow a 300°F mean outer surface temperature and a reduction in hydrogen flow rates of 5 to 6% below the 200°F case. For the silicone system the mean outer surface temperature could go as high as 600°F and still allow a titanium structural skin. Raising the mean outer surface temperature to 600°F from the 400°F used in Table XXIII would reduce hydrogen flow rates by 15 to 20%. To achieve higher outer surface temperatures and thus greater hydrogen flow rate reductions the thermal protection systems previously discussed would be required.

D. SPRAY COOLING

For a Mach 6 cruise vehicle spray cooling techniques could be used to alleviate problems in the severest heating regions such as, the leading edges of the wing, control surfaces, the fuselage nose, or engine structure. At this time it does not appear advisable to pursue spray cooling for Mach 6 wing application because convective and transpiration cooling techniques can be used. However, for higher Mach number vehicles convective and transpiration techniques may be severely taxed and then spray cooling will appear more attractive.

E. RADIATION COOLING ON REAR WEDGE SURFACE

The possibility of a radiation-convection system incorporating a radiator on the wing rear wedge surface was described in earlier sections. To determine the feasibility

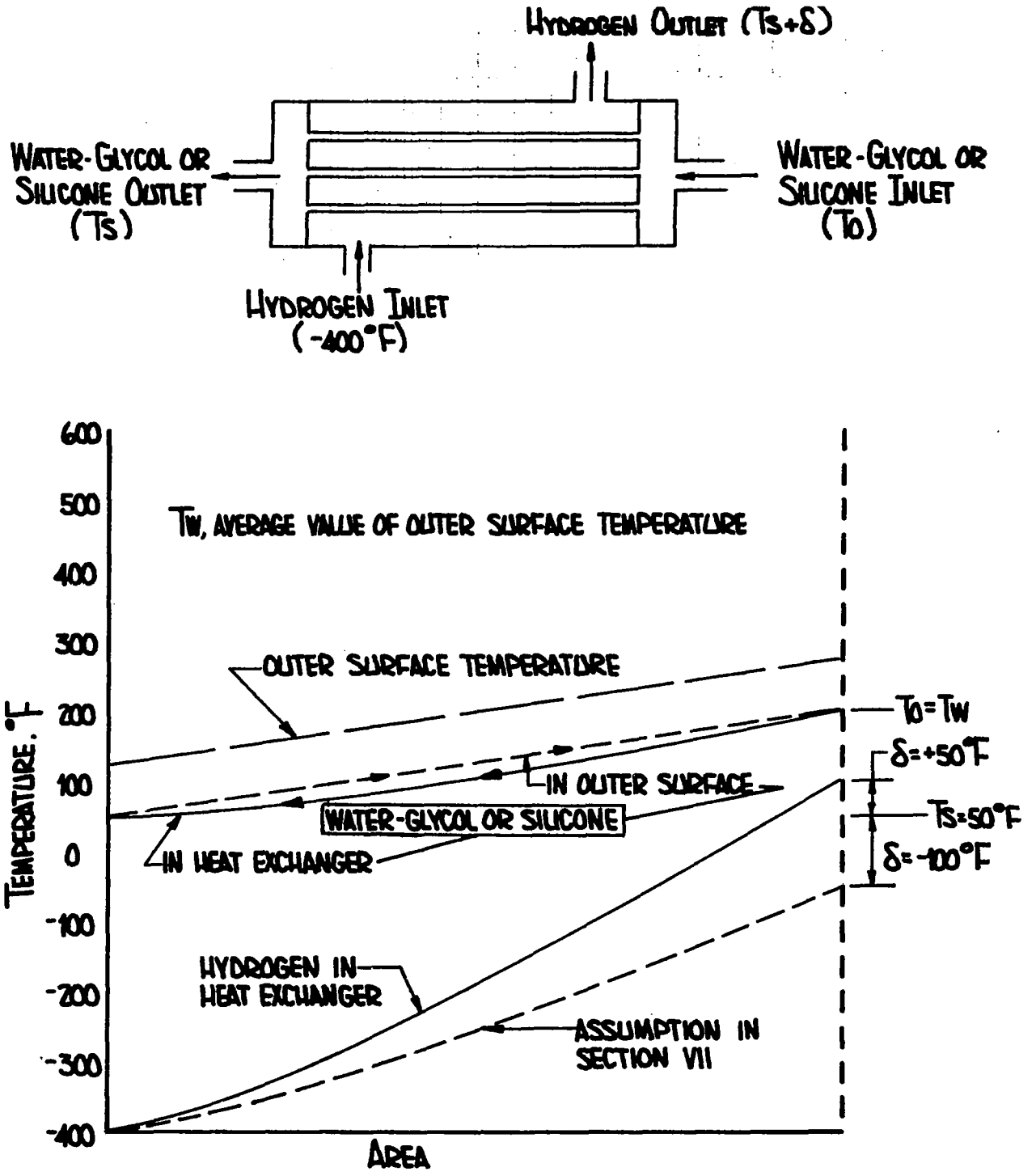

Figure 145. Temperature Variations in a Water-Glycol or Silicone Indirect Cooling System for a Minimum Transport Fluid Temperature, T_s of +50°F

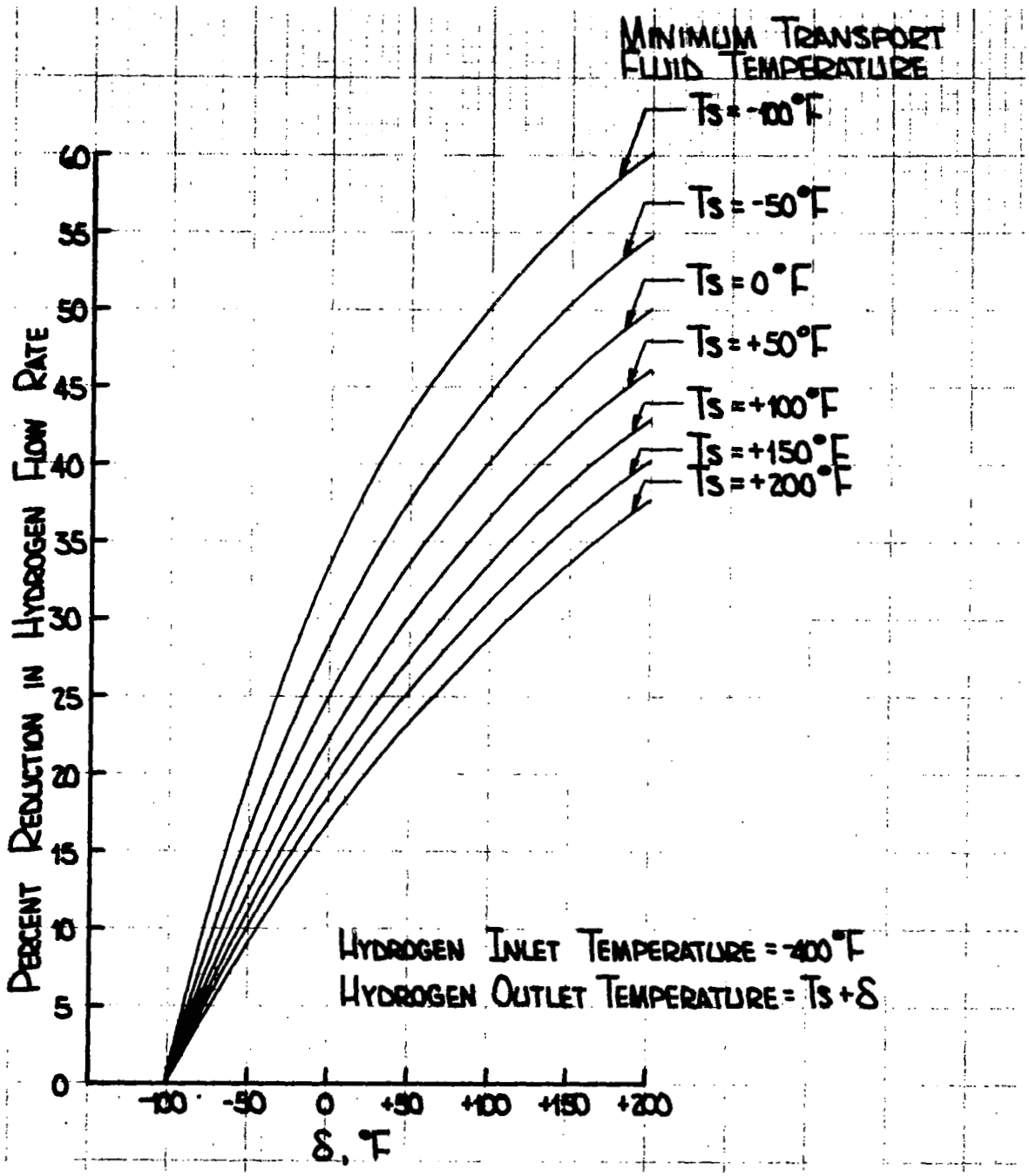

Figure 146. Percent Reduction in Hydrogen Flow Rate versus Variation in Hydrogen Outlet Temperature

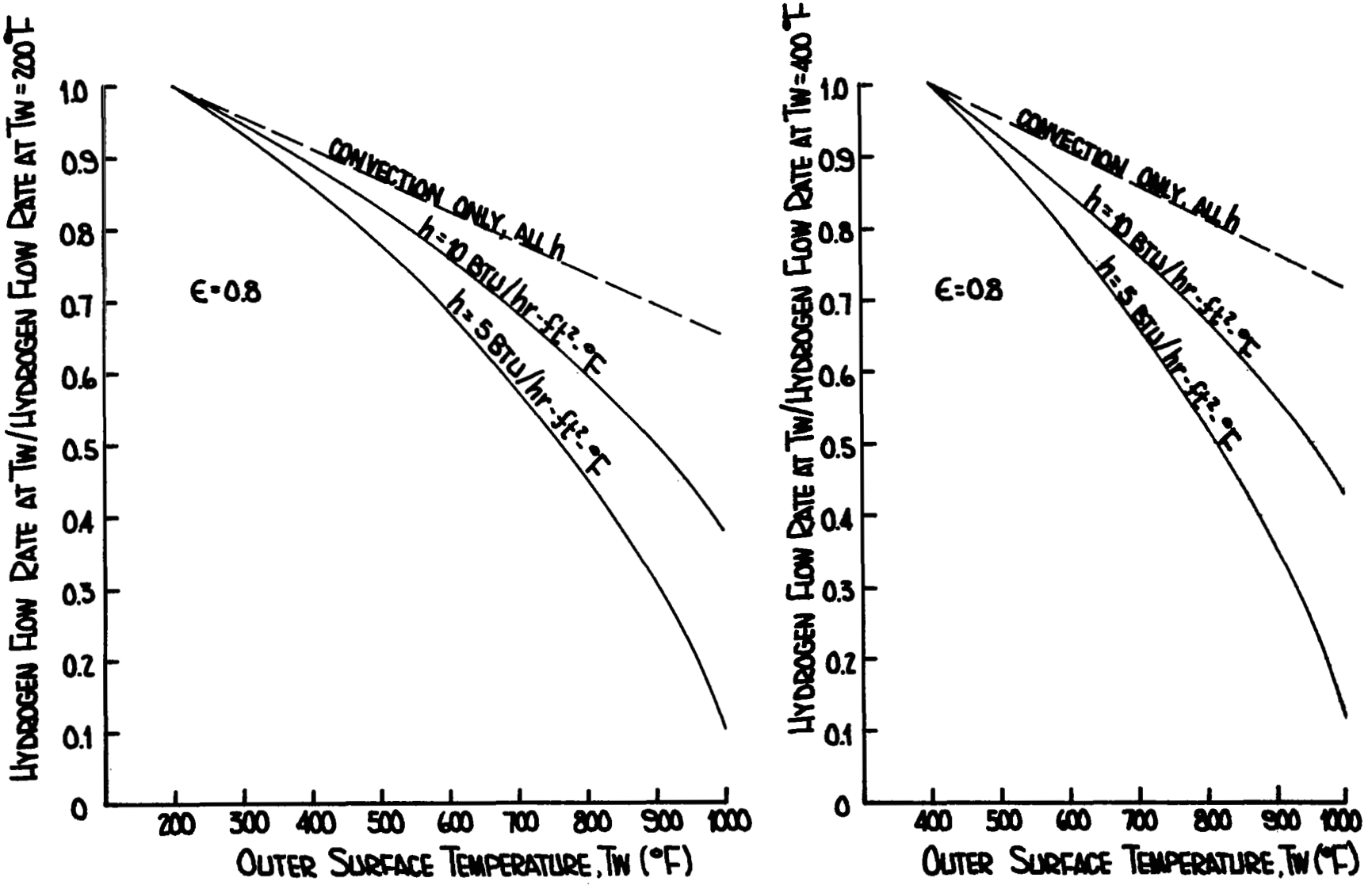

Figure 147. Hydrogen Flow Rate Variations with Outer Surface Temperature

of such a system an estimate of heat rejection rate from such a radiator is needed. Figure 148 presents data for such a rear wedge radiator assuming that the convective heat transfer coefficient on the rear wedge surface is 0.075 BTU/hr-ft^2-°F. It is felt that this is a reasonable estimate for a highly expanded flow regime, but admittedly little data exists to confirm or deny this estimate.

In this figure the vertical distance between the curves represents the quantity of heat transferred to or from the surface. For surface temperatures to the left of the radiation equilibrium temperature line heat is convected into the surface. For surface temperatures to the right of the radiation equilibrium line heat is radiated away from the surface. For a surface temperature of 400°F the heat rejection rate is the heat radiated out minus the heat convected in and is approximately 600 BTU/hr-ft^2. On the wing front wedge surface heating rates range from about 2850 BTU/hr-ft^2 for 0° sweep to about 2250 BTU/hr-ft^2 for 75° sweep with a 400°F surface temperature. Using estimates such as those above it was concluded that although a rear wedge radiator can reject a large quantity of heat, when compared to the total heat input to the wing such a radiator would not be a significant heat sink. However, it must be noted that the use of this radiator concept might be very practical for cooling local hot spots such as wing control surfaces which might be deflected for short periods of time and be subjected to heating intensities compatible with the radiator concepts.

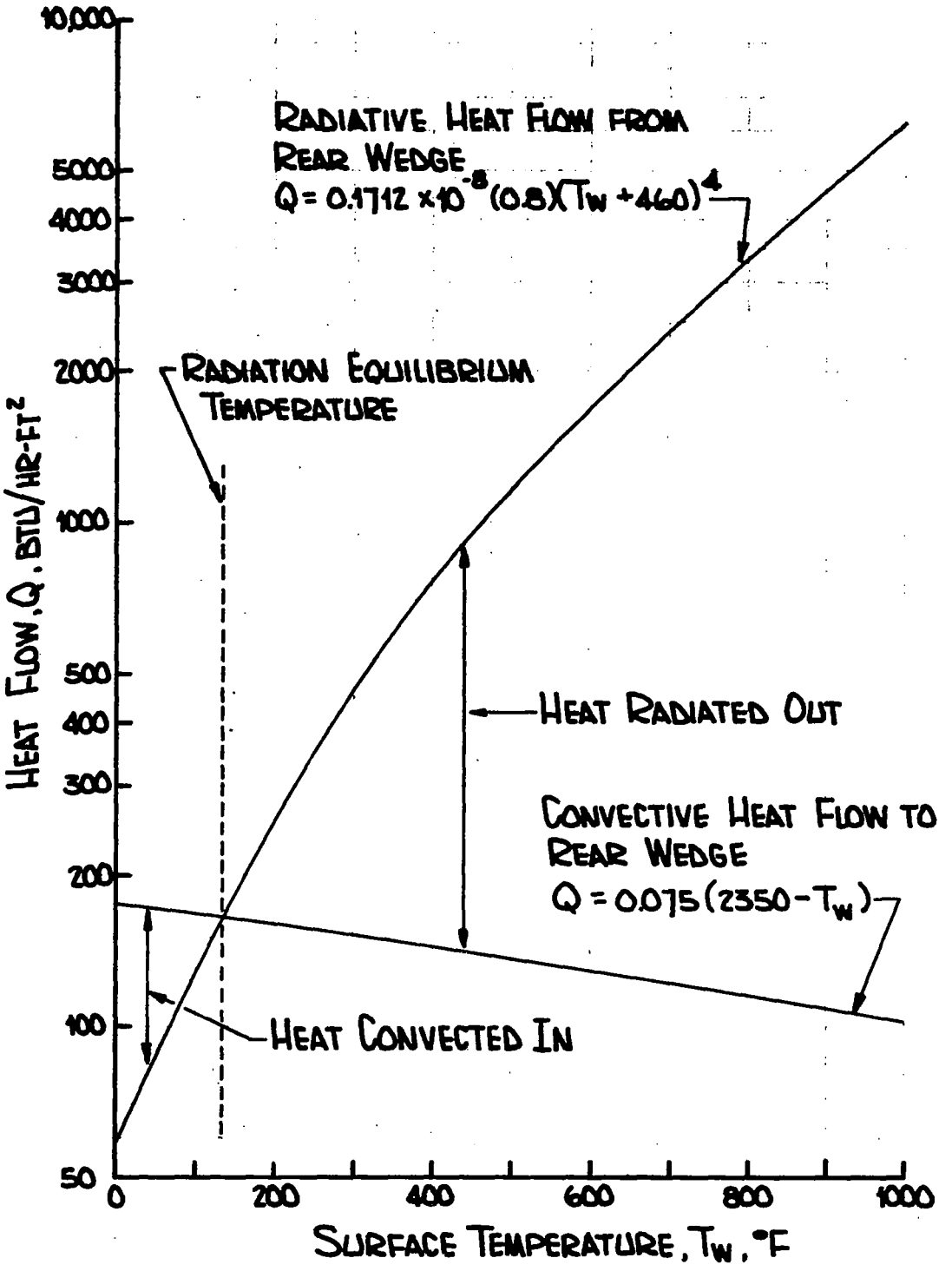

Figure 148. Heat Rejected by Radiation on Back Wedge versus Surface Temperature

SECTION 10

SUMMARY OF ACTIVE COOLING SYSTEMS

In order to assess the relative merits of various cooling system concepts it is necessary to combine the cooling system weight estimates from Sections 6 and 7 with the weight estimates for the cooled load carrying structure as developed in Section 8. In this section total wing weights are given for sweep angles of 0° and 65°. System weights, system operating temperatures, and fluid flow rates are summarized for three transpiration cooling systems and two convective systems. The selected transpiration systems were those employing hydrogen, helium, and water as tranpirants and operating with outer surface temperatures near radiation equilibrium values to minimize coolant flow rate requirements. For these systems total cooled wing weights for the 65° sweep configuration were approximately 50,000, 55,000, and 51,000 lb respectively. For the transpiration cooled wings, the expendable coolant weight is included in the total cooled wing weight estimate.

Both of the selected convective cooling systems used transport fluids, either water-glycol or silicone, to move heat from the wing surface to a heat exchanger where heat was rejected to the hydrogen fuel. The convective systems were compared with and without thermal protection (heatshields) on lower surface of the wing. For the 65° sweep configuration without thermal protection, weights of 40,600 and 42,300 lb were estimated for the water-glycol and silicone fluid cooled wings respectively. When thermal protection was added on just the bottom surface of the wing, wing weights increased slightly to about 41,900 and 44,000 lb for the water-glycol and silicone systems respectively. Although the addition of thermal protection to the lower surface of the wing increased weights slightly, the hydrogen flowrate requirement was reduced by more than 50%.

For the various configurations of convective cooling systems examined the percentage of available hydrogen heat capacity utilized for wing cooling ranged between 5 and 20%.

Using the weights for the various cooled wing concepts as described in detail in this section it is possible to make comparisons with the estimated weight of the hot wing concept described in Section 8. From the analyses described in Section 8 typical hot wing concepts weighed more than 50,000 lb for the 65° sweep configuration with heat shields. Thus, weight savings of up to 10,000 lb might be expected for cooled concepts as compared to hot concepts.

A. TRANSPIRATION COOLING SYSTEMS

For the present application either gaseous transpiration systems using hydrogen or helium, or a liquid system using water appeared feasible. In order to minimize coolant requirements transpiration cooling system operating temperatures must maximize the change of coolant temperature as it passes through the porous wall. Thus, the leading edge, top and bottom surface temperatures should be near the radiation equilibrium values. For Mach 6 with a 10.31° angle of attack at an altitude of 100,000 ft these values are about 1400°F for the leading edge, 600°F for the top surface, and 1100°F for the bottom surface. Assuming all the coolants to be stored as liquids the minimum coolant temperature is approximately -400°F for the hydrogen, -450°F for helium, and +80°F for water. For the hydrogen and helium systems the heat of vaporization was not included in the coolant heat capacity since they are likely to be used in a supercritical condition. For the water system, however, the heat of vaporization was accounted for by using a fictitious minimum coolant temperature.

The total weights for a transpiration cooled wing is the sum of a cooling system component weight, the coolant weight, and a cooled structure weight. Cooling system component weight is the sum the individual weights of the coolant, tankage, tank insulation, tank support, plumbing which includes insulation where necessary, and a porous material with its associated supports. In Table XXXV coolant weights for each system are tabulated in addition to the cooling system component weight. For the systems listed the cooled structure operates at about 100°F and is made from 7075-T6 aluminum tubed sheet plus appropriate beams, ribs, and stringers. For all transpiration systems considered the cooled structure weighs about 41,100 lbs for a 0° sweep wing and about 29,200 lb for a 65° sweep wing.

For the hydrogen system total wing weights vary from about 63,000 lb for a 0° sweep wing to about 49,300 lb for a 65° sweep wing. Cooling system weights are about 18,000 lb. The coolant weighs about 3000 lb. The helium system weights are higher than the hydrogen system weights primarily due to the increased coolant requirement of about 5,000 lb. This increased coolant requirement also increases the tankage weight estimates for the helium system as compared to the hydrogen system.

The water transpiration system weights are between those for hydrogen and helium systems, but for this system the coolant weight requirement is a larger fraction of the cooling system weight estimate. Approximately 10,000 lb of water is required to cool the wing to which is added about 13,000 lb of associated hardware. The resulting cooled wing weights range from 65,500 lb for a 0° sweep wing to 51,000 for a 65° sweep wing.

B. CONVECTIVE COOLING SYSTEMS

The indirect convective cooling system concepts selected use liquid transport fluids to exchange heat from the structure to the hydrogen fuel. Water-glycol and silicone were selected as possible liquid transport fluids; the choice depends on the desired system operating temperature range. Choice of a system operating temperature range is primarily based on two factors. First, the choice of structural

TABLE XXXV
TRANSPIRATION COOLING SYSTEM COMPARISON
FOR HYPERSONIC WING

			Hydrogen		Helium		Water	
			0^{o} Sweep	65^{o} Sweep	0^{o} Sweep	65^{o} Sweep	0^{o} Sweep	65^{o} Sweep
Weights (lb)	Structure		41,100	29,200	41,100	29,200	41,100	29,200
	Cooling System Components		18,700	17,200	20,400	18,300	13,400	12,400
	Coolant		3,160	2,910	8,510	7,260	11,000	9,380
	Total Wing		63,000	49,300	70,000	54,800	65,500	51,000
Temperature (^{o}F)	Structure		100	100	100	100	100	100
	Maximum Coolant	L.E.	1,400	1,400	1,400	1,400	1,400	1,400
		Top	600	600	600	600	600	600
		Bottom	1,100	1,100	1,100	1,100	1,100	1,100
	Minimum Coolant		-400	-400	-450	-450	80	80

materials and second, the permissible hydrogen usage. For the present application the hydrogen fuel can be used as the heat sink as long as the hydrogen heat capacity used is a reasonable fraction of the total hydrogen heat capacity available. The question of what is a reasonable fraction is not easily answered, but as will be shown later, this fraction of hydrogen heat capacity utilization never exceeded 20%.

Rather than restrict the studies to a particular temperature or material a range of temperatures from 200°F to 600°F was investigated. Preliminary investigations revealed the possibility of cooling the entire wing to 200°F without any thermal protection systems such as heat shields or insulation. These investigations also concluded that if a thermal protection system were to be used heat shield/radiation barrier concepts would probably be superior to heat shield/insulation concepts. In this section cooled wing concepts with and without thermal protection are presented for comparison purposes. The systems tabulated herein are identified by three parameters, namely the transport fluid, the structural operating temperature and corresponding structural material, and whether or not a thermal protection system is used on the bottom surface of the wing. Tables XXXVI through XXXIX summarize the weights of wings which employ water-glycol and silicone transport fluids, operate at structural temperature levels between 200°F and 600°F, are fabricated from aluminum and titanium alloys, and utilize structures exposed to the boundary layer or protected by heat shields.

For these systems a total cooled wing weight is presented which is the sum of a cooling system weight estimate,a cooled wing structural weight estimate, and a thermal protection system weight where applicable. The cooling system weight estimate includes such items as plumbing, transport fluid pump and motor, APU fuel, heat exchanger, and thermal protection system if utilized. The wing structural weight was calculated assuming material properties based on the mean structural temperature. Minimum gage restrictions were placed on the structural skin surface to account for the cooling system. In addition to this skin weight, appropriate weights were included in the wing structural weight estimate for beams, ribs, and stringers.

The lightest cooled wing concept is the water-glycol system with an aluminum structure and no thermal protection system. For systems without thermal protection on the bottom wing surface the cooling system weights are almost independent of sweep angle and are approximately 11,400 lb. As the mean outer surface temperature is increased from 200°F to 300°F the heat input to the cooling system is decreased by about 6% thus reducing both the water-glycol and hydrogen flow rates and slightly reducing cooling system weight estimates. Wing structural weights are a function of mean outer surface temperature because material property degradation with increasing structural operating temperature (from 200°F to 300°F) changed the structural material from aluminum to titanium and increased the structural weight estimate by approximately 200 lb. Structural weights for the water-glycol cooled aluminum alloy wing structure varied from about 41,100 lb for a 0° sweep wing to about 29,200 lb for a 65° sweep wing. Addition of the cooled wing structure and the cooling system weights resulted in a water-glycol cooled wing weight which ranged from about 52,500 lb for 0° sweep to about 40,600 lb for 65° sweep. From a total cooled wing weight standpoint either the 7075-T6 aluminum wing or the 6Al-4V titanium wing appeared attractive. Ease of fabrication will probably favor the choice of a cooled aluminum alloy wing.

To examine the possibility of significantly reducing the percentage of the available hydrogen heat capacity required to cool the wing, a radiation shield thermal protection system was added to the bottom surface of the wing. An air gap system (superalloy heat shield outer surface) increases the bottom surface weight by approximately 1.10 lb/ft^2, but the large reductions in both the water-glycol flow rate and hydrogen flow rate yield large reductions in cooling system component weights which partially offset the added heat shield weight. Comparing Tables XXXVI and XXXVII, an increase in the total cool wing weight of about 1000 lb is noticed when an air-gap thermal protection system is added to the lower wing surface. Adding four 1 mil rhodium radiation shields increases the thermal protection system weight to 1.50 lb/ft^2, but reduces water-glycol and hydrogen flow rates more than the air gap thermal protection system reductions, and results in a total system weight increase of approximately 3,000 lb. The addition of the thermal protection system reduces the percentage of the hydrogen heat capacity required for wing cooling by about approximately 6% for an increase in system weight of 1000-3000 lb.

Table XXXVIII summarizes an actively cooled wing concept using a mean outer surface temperature of from 400°F to 600°F. Although raising the mean outer surface temperature degrades the titanium structural properties and raises wing structural weights some reduction in cooling system component weight results from the reduced heat load. Changes in mean outer surface temperature from 300°F to 400°F and then to 600°F increase wing structural weights for the titanium structure 0° sweep wing from 41,300 lb to 45,700 lb and then to 53,800 lb. For a 65° sweep wing the mean outer surface temperature changes from 300°F to 400°F to 600°F increase the structural weight estimates from 29,400 lb to 31,500 lb to 34,200 lb. This effect of sweep angle results primarily from the decreased loading intensities at high angles of sweep. Cooling sytem component weights for the silicone system with no thermal protection are approximately 10,800 lb. Total wing weights for the unprotected silicone system range from about 42,300 lb for a 400°F mean outer surface temperature, 65° sweep wing, to 63,800 lb for a 600°F mean outer surface temperature, 0° sweep wing.

Adding a thermal protection system to the bottom surface of the wing increases cooling system weights by approximately 2000 and 4500 lb for the air gap and four radiation shield thermal protection systems respectively for the 400°F titanium wing structure. The thermal protection system yields approximately a 5% reduction in the amount of hydrogen heat capacity required for this case, but increases total wing weights to about 60,000 lbs for a 0° sweep wing and to about 45,000 lb for a 65° sweep wing.

Transport fluid flow rates listed in Tables XXXVI through XXXIX were computed assuming constant fluid properties. Thus the fluid flow rate is the quotient of the heat absorbed by the cooling system and the product of the specific heat multiplied by the coolant temperature change. Maximum and minimum coolant temperatures are listed in the tables. For water-glycol and silicone the suggested maximum coolant temperatures are 200°F and 400°F respectively. The minimum coolant temperatures are a function of the transport fluid to hydrogen heat exchanger design and were chosen as 50°F and 200°F for the water-glycol and silicone respectively. Transport fluid flow rates range

TABLE XXXVI

WATER-GLYCOL CONVECTIVE COOLING SYSTEM COMPARISON
FOR HYPERSONIC WING WITH NO THERMAL PROTECTION SYSTEM

		200°F Mean Outer Surface Temperature (7075-T6 Struct.)		300°F Mean Outer Surface Temperature (6Al-4V Struct.)	
		0° Sweep	65° Sweep	0° Sweep	65° Sweep
Weights (lb)	Total Cooled Wing Weight	52,500	40,600	52,300	40,400
	Cooling System Components	11,400	11,400	11,000	11,000
	Wing Structure	41,100	29,200	41,300	29,400
Water-Glycol	Maximum Temperature (°F)	200	200	200	200
	Minimum Temperature (°F)	50	50	50	50
	Flow Rate (lb/hr)	1,170,000	1,180,000	1,116,000	1,121,000
Hydrogen	Maximum Temperature (°F)	-50	-50	-50	-50
	Minimum Temperature (°F)	-400	-400	-400	-400
	Flow Rate (lb/hr)	110,000	112,000	105,000	106,000
Hydrogen	Maximum Temperature (°F)	50	50	50	50
	Minimum Temperature (°F)	-400	-400	-400	-400
	Flow Rate (lb/hr)	85,600	87,100	81,700	82,500
Hydrogen	Maximum Temperature (°F)	150	150	150	150
	Minimum Temperature (°F)	-400	-400	-400	-400
	Flow Rate (lb/hr)	69,850	71,100	66,700	67,300

TABLE XXXVII

WATER-GLYCOL CONVECTIVE COOLING SYSTEM COMPARISON FOR HYPERSONIC WING WITH RADIATION SHIELD THERMAL PROTECTION SYSTEM ON THE BOTTOM SURFACE ONLY

		Air Gap		Four Radiation Shields	
		0^{o} Sweep	65^{o} Sweep	0^{o} Sweep	65^{o} Sweep
Weights (lb)	Total Cooled Wing Weight	53,500	41,900	55,400	43,600
	Cooling System Components	5,390	6,480	4,720	5,920
	Thermal Protection System	7,020	6,240	9,580	8,510
	Wing Structure	41,100	29,200	41,100	29,200
Water Glycol	Maximum Temperature (^{o}F)	200	200	200	200
	Minimum Temperature (^{o}F)	50	50	50	50
	Flow Rate (lb/hr)	304,000	452,000	211,000	373,000
Hydrogen	Maximum Temperature (^{o}F)	-50	-50	-50	-50
	Minimum Temperature (^{o}F)	-400	-400	-400	-400
	Flow Rate (lb/hr)	28,600	44,200	19,800	36,900
Hydrogen	Maximum Temperature (^{o}F)	50	50	50	50
	Minimum Temperature (^{o}F)	-400	-400	-400	-400
	Flow Rate (lb/hr)	22,300	34,300	15,400	28,700
Hydrogen	Maximum Temperature (^{o}F)	150	150	150	150
	Minimum Temperature (^{o}F)	-400	-400	-400	-400
	Flow Rate (lb/hr)	18,200	28,200	12,600	23,500

TABLE XXXVIII

SILICONE CONVECTIVE COOLING SYSTEM COMPARISON FOR HYPERSONIC WING WITH NO THERMAL PROTECTION SYSTEM

		400°F Mean Outer Surface Temperature (6A l-4V Struct.)		600°F Mean Outer Surface Temperature (6A l-4V Struct.)	
		0° Sweep	65° Sweep	0° Sweep	65° Sweep
Weights (lb)	Total Cooled Wing Weight	56,000	42,300	63,800	44,200
	Cooling System Components	10,800	10,800	10,000	10,000
	Wing Structure	45,700	31,500	53,800	34,200
Silicone	Maximum Temperature (°F)	400	400	400	400
	Minimum Temperature (°F)	200	200	200	200
	Flow Rate (lb/hr)	1,440,000	1,430,000	1,290,000	1,292,000
Hydrogen	Maximum Temperature (°F)	100	100	100	100
	Minimum Temperature (°F)	-400	-400	-400	-400
	Flow Rate (lb/hr)	70,200	70,800	63,200	63,500
Hydrogen	Maximum Temperature (°F)	200	200	200	200
	Minimum Temperature (°F)	-400	-400	-400	-400
	Flow Rate (lb/hr)	58,300	58,800	52,500	52,700
Hydrogen	Maximum Temperature (°F)	300	300	300	300
	Minimum Temperature (°F)	-400	-400	-400	-400
	Flow Rate (lb/hr)	50,000	50,400	45,000	45,300

TABLE XXXIX

SILICONE CONVECTIVE COOLING SYSTEM COMPARISON FOR HYPERSONIC WING WITH RADIATION SHIELD THERMAL PROTECTION SYSTEM ON THE BOTTOM SURFACE ONLY

		Air Gap		Four Radiation Shields	
		0^{o} Sweep	65^{o} Sweep	0^{o} Sweep	65^{o} Sweep
Weights (lb)	Total Cooled Wing Weight	57,900	44,000	61,500	45,700
	Cooling System Components	5,220	6,230	6,180	5,690
	Thermal Protection System	7,020	6,240	9,580	8,510
	Wing Structure	45,700	31,500	45,700	31,500
Silicone	Maximum Temperature (^{o}F)	400	400	400	400
	Minimum Temperature (^{o}F)	200	200	200	200
	Flow Rate (lb/hr)	371,000	573,000	252,000	473,000
Hydrogen	Maximum Temperature (^{o}F)	100	100	100	100
	Minimum Temperature (^{o}F)	-400	-400	-400	-400
	Flow Rate (lb/hr)	18,300	28,200	12,400	23,300
Hydrogen	Maximum Temperature (^{o}F)	200	200	200	200
	Minimum Temperature (^{o}F)	-400	-400	-400	-400
	Flow Rate (lb/hr)	15,250	23,500	10,300	19,430
Hydrogen	Maximum Temperature (^{o}F)	300	300	300	300
	Minimum Temperature (^{o}F)	-400	-400	-400	-400
	Flow Rate (lb/hr)	13,100	20,200	8,860	16,650

from about 200,000 lb/hr to about 1,500,000 lb/hr for the entire cooled wing. Although these values may appear high at first, for 10,000 ft^2 of cooled wing surface area maximum transport fluid flow rates do not exceed 500 $lb/hr/ft^2$ for any local area and result in Reynolds numbers in the moderately turbulent range (3,000 to 10,000). For this range of flow rates and Reynolds numbers cooling system design is not difficult.

Hydrogen flow rate estimates were made assuming a counterflow heat exchanger design. A range of hydrogen temperatures is given for each system resulting in a corresponding range of hydrogen flow rates. For the various systems presented, hydrogen flow rates from 7,800 lb/hr to 110,000 lb/hr can be obtained depending upon the particular choice of system and operating temperatures. Rather than discussing hydrogen flow rate it is more applicable to consider the percent of the total hydrogen heat capacity utilized by the various system combination.

Listed in Table XL is an estimate of the percent of the total available hydrogen heat capacity that is used by the various wing cooling systems. These estimates were made assuming a hydrogen flow rate of 147,000 lb/hr. with a maximum temperature change of 1800°F. As shown in Table XL in no case is more than 20% of the available hydrogen heat capacity utilized and if a silicone system is used with four radiation shields plus a heat shield on the bottom surface less than 5% of the available hydrogen heat capacity is used for cooling the wing.

These results, of course, are for the design conditions, assumed herein, of Mach number 6, altitude 100,000 feet, and angle of attack of 8.3°, where the aircraft is climbing to cruise altitude. It is of interest to examine also the cooling requirements under the steady state conditions of cruise. At the start of cruise, the altitude is 102,120 feet and the fuel flow rate, 81,300 lb/hr. At the end of cruise the altitude is 106,360 feet, and the fuel flow rate, 71,800 lb/hr. The angle of attack at both conditions is 5.14°. Estimates of the cooling system heat loads and hydrogen flow rates were made for each of these conditions, and the start of cruise was found to be the more critical. The percentages of available heat capacity and total heat capacity used by the various wing cooling systems for this condition is shown in Table XLI. These results indicate that although the heat capacities required during cruise are increased over the design point requirements, less than 25 percent of the hydrogen heat capacity is used to cool the wing.

TABLE XL

PERCENTAGE OF HYDROGEN HEAT CAPACITY UTILIZATION FOR CONVECTIVE COOLING OF A 65° SWEEP WING. DESIGN POINT, H = 100,000 ft., α = 8.3°, fuel flow = 147,000 lb/hr.

		HEAT ABSORBED (BTU/HR) x 10^{-6}	HYDROGEN TEMPERATURE CHANGE, °F	HYDROGEN FLOW RATE (LB/HR)	PERCENT OF AVAILABLE HEAT CAPACITY	PERCENT OF TOTAL HEAT CAPACITY
Water-Glycol	200°F MEAN OUTER SURFACE TEMPERATURE, UNSHIELDED	137	550	71,100	48.4	14.8
	AIR GAP THERMAL PROTECTION SYSTEM ON BOTTOM SURFACE	54.2	550	28,200	19.2	5.9
	FOUR RADIATION SHIELDS ON BOTTOM SURFACE	45.2	550	23,500	16.0	4.9
Silicone	400°F MEAN OUTER SURFACE TEMPERATURE, UNSHIELDED	124	700	50,400	34.3	13.3
	AIR GAP THERMAL PROTECTION SYSTEM ON BOTTOM SURFACE	49.4	700	20,200	13.7	5.3
	FOUR RADIATION SHIELDS ON BOTTOM SURFACE	40.8	700	16,650	11.3	4.4

FOR T_w = 200° AVAILABLE HEAT CAPACITY IS 30.6% OF TOTAL HEAT CAPACITY.

FOR T_w = 400° AVAILABLE HEAT CAPACITY IS 30.9% OF TOTAL HEAT CAPACITY.

TABLE XLI

PERCENTAGE OF HYDROGEN HEAT CAPACITY UTILIZATION FOR CONVECTIVE COOLING OF A 65° SWEEP WING. Start of Cruise, H = 102,120 ft. α = 5.14°. Fuel Flow = 81,300 lb/hr.

		HEAT ABSORBED (BTU/HR) x 10^{-6}	HYDROGEN TEMPERATURE CHANGE, °F	HYDROGEN FLOW RATE (LB/HR)	PERCENT OF AVAILABLE HEAT CAPACITY	PERCENT OF TOTAL HEAT CAPACITY
Water-Glycol	200°F MEAN OUTER SURFACE TEMPERATURE, UNSHIELDED	115	550	59,800	73.5	22.5
	AIR GAP THERMAL PROTECTION SYSTEM ON BOTTOM SURFACE	36.2	550	18,800	23.2	7.1
	FOUR RADIATION SHIELDS ON BOTTOM SURFACE	25.5	550	13,300	16.3	5.0
Silicone	400°F MEAN OUTER SURFACE TEMPERATURE, UNSHIELDED	94.3	700	38,500	47.0	18.3
	AIR GAP THERMAL PROTECTION SYSTEM ON BOTTOM SURFACE	28.1	700	11,500	14.1	5.5
	FOUR RADIATION SHIELDS ON BOTTOM SURFACE	18.2	700	7,400	9.1	3.5

FOR T_w = 200° AVAILABLE HEAT CAPACITY IS 30.6% OF TOTAL HEAT CAPACITY.

FOR T_w = 400° AVAILABLE HEAT CAPACITY IS 38.9% OF TOTAL HEAT CAPACITY.

SECTION 12

CONCLUSIONS AND RECOMMENDATIONS

As discussed in previous sections of the report, transpiration, film, and convective cooling concepts were examined. Coolants included hydrogen, helium, air, and water. Various structural temperatures were considered which permitted comparison of aluminum alloy, titanium alloy, and superalloy construction materials for the primary load carrying function. Heat shields, radiation barriers, and thermal insulation were considered to reduce heat flow to the cooled structures. Wing sweep angles were varied from 0° to 75°. The cooled wing concepts were compared, among themselves and with the uncooled concept, on the basis of structural weight, cooling system weight, and coolant weight. The results of the analyses and comparisons led to the conclusions presented in this section. In reviewing these conclusions, it must be remembered that for the convective cooling system the hydrogen fuel was assumed to provide an adequate heat sink. Therefore, no weights for an expendable coolant were included in the total weights of convectively cooled concepts. This basic assumption had two significant influences on the results. First, the normally expected order of cooling effectiveness is changed from transpiration, film, and convection to convection, transpiration, and film. Second, the normally expected optimization of convective cooling system weight as a tradeoff between the weights of insulation and expendable coolant is of no significance.

The primary conclusion reached as a result of this study is that the weights of wings cooled by any of several techniques are equal to or less than the weight of an uncooled wing. For the 65° swept wing of the Mach 6 vehicle, the total weights for the cooled wings without heat shields or insulation were 40,600 lb for water-glycol convection cooling, 42,300 lb for silicone convection cooling, 50,000 lb for hydrogen transpiration cooling, 51,000 lb for water transpiration cooling, and 55,000 lb for helium transpiration cooling. The weight of the uncooled wing was estimated to be 52,300 lb assuming heat shields are required over 10,000 sq. ft., the entire lower surface and approximately half of the upper surface. When the external surface of the wing was cooled by convective systems, about 15 percent of the heat capacity of the fuel was required to absorb the aerodynamic heat load. The use of heat shields and radiation barriers reduced the required percentage of fuel heat capacity to about 5 percent, but increased wing weight by between 1000 and 3000 lb.

The study resulted in a number of other conclusions of importance. For convenience these can be divided into the following seven categories: (1) identification of applicable cooling concepts, (2) evaluation of cooling systems, (3) comparison of cooling systems, (4) influence of auxiliary thermal protection techniques on cooling system performance, (5) aerodynamic-thermodynamic-structural interactions, and (6) available transpiration and film cooling theories. Subsequent paragraphs present the conclusions in each category.

The concepts studied included transpiration, film, and convective cooling. Convective concepts included direct, indirect, and spray cooling systems. The following conclusions were reached with respect to the use of convective, transpiration, or film cooling concepts for the hypersonic wing of interest:

1. Indirect convective cooling concepts and transpiration cooling concepts are attractive for cooling the wing structure of hypersonic cruise vehicles.

2. The high coolant flow rates predicted for film cooling makes it unattractive despite a lower coolant distribution system weight than for transpiration cooling. Since this result is based on film cooling theories verified only at low supersonic speeds, a reevaluation of film cooling is recommended when a hypersonic theoretical/experimental basis becomes available.

3. For the transpiration cooling concepts studied, the selected hydrogen, helium, and water systems have very low local flow rates due to the use of high outer surface temperatures. These low flow rates cause a very slight reduction in wing drag, and these reductions were so small that they were not believed to be significant in evaluation of transpiration cooling systems.

4. Direct convective concepts are unattractive for reasons which differ depending on whether the coolant is a liquid or a gas. For liquids, the available heat capacity is limited because of the narrow operating temperature range or if advantage is taken of the heat of vaporization two phase flow problems are encountered. For gases, high heat transfer coefficients can be achieved only through high mass flows which result in large piping sizes in the coolant distribution system, large pressure drops through the heat exchange components, and high distribution system weights.

5. Spray cooling is unattractive because the heat fluxes and temperature levels experienced by the wing are too low to take advantage of coolants with sufficiently high heat capacities.

Conclusions reached with respect to the evaluation of the two promising concepts, transpiration and indirect convection, are as follows:

1. When system weights were combined with coolant weights, the ranking of the transpiration systems was hydrogen, water, and helium in order of decreasing transpirant effectiveness with percentage increases in total system weights of approximately 10% and 30% as compared to the hydrogen system. Transpiration cooling with air was not selected as a cooling system for the entire wing because of the problems associated with removing the heat from ram air and the attractiveness of the alternate systems both from system wieght and simplicity viewpoints.

2. The use of stored air as a transpirant was not selected because of the lower weights estimated for the hydrogen and helium systems.

3. The close comparison of hydrogen and water transpiration results from the fact that the cooling system component weights of the water system are much less than for the hydrogen system and almost balance the difference in coolant weights.

4. Transpiration coolant flow rates are very sensitive to the allowable operating temperature of the outermost surface of the structure to be cooled. For the wing studied, an increase of outermost temperature from 200°F to 1000°F decreased flow rates by a factor of 10.

5. Transpiration cooling flow rates required for surface temperatures of 200°F result in drag reductions of less than 5%. Surface temperatures near radiation equilibrium values result in low rates and the corresponding drag reductions are less than 1%. These drag reductions were not included in the cooling system evaluations.

6. Indirect convective cooling systems using the hydrogen fuel as a heat sink are not sensitive weightwise to changes in outer surface temperature, for example, changing the outer surface temperature from 200°F to 600°F reduced the cooling system component weights by about 5%.

7. For the indirect convective cooling systems outer surface temperature changes from 200°F to 600°F change the percent of the hydrogen heat capacity utilized for cooling from 16.3% to 13.2%.

Despite the superior heat transfer and blocking characteristics of transpiration cooling as compared to convective cooling, the weight penalties associated with the expended coolant, porous material, and plenum chambers overshadow the thermal performance benefits when it is assumed that the aircraft fuel supply provides a sufficient heat sink for the aerodynamic heat input such that no expendable coolant weight is charged against the convective concepts. If this assumption is not valid the relative merits of the two concepts must be reassessed. During such a revaluation it will be necessary to consider techniques for reducing the amount of aerodynamic heat input which must be absorbed by the convective cooling system.

When convective systems are used to cool the external surface of the 65° swept wing of the Mach 6 vehicle approximately 15% of the heat capacity of the fuel is required to absorb the aerodynamic heat input. It may be desirable, however, to minimize the percentage of fuel heat capacity used by structural cooling. Therefore, studies of auxiliary thermal protection techniques were conducted and significant conclusions are listed below:

1. The percentage of aerodynamic heat load absorbed by the cooling system can be reduced by the use of thermal protection techniques such as insulation or heat shields external to the cooled load carrying structure.

2. For the heat loads associated with this particular application the use of an external thermal protection system which includes an outer protective metallic surface and a thin layer of insulation or no insulation at all increases total wing weight when the expendable coolant weight is not charged to the cooling system.

3. The use of heat shields, radiation barriers, and/or thermal insulation between the external surface and cooled load carrying structure can reduce the heat loads which must be absorbed by convective cooling system by 1 or 2 orders of magnitude as compared with direct cooling of the external surface.

4. Over most of the wing surface, an air-gap/radiation barrier concept appears to be more desirable than fibrous insulation with respect to both thermal efficiency and all-weather operation.

5. If sharp leading edges are used, it may not be practical to employ thermal protection concepts in the forward portion of the wing because of limited available structural depth.

6. The aerodynamic heat load which must be absorbed by the fuel can be reduced by using that portion of the upper wing surface which is in an expanded flow field as a space radiator surface.

During the course of the investigation certain interactions among aerodynamic, thermal, and structural design considerations became apparent. Conclusions in this regard are listed below:

1. Cooling system weight is essentially independent of wing sweep angle for constant wing area thus permitting greater design flexibility than is possible with uncooled wing concepts. This is the result of the increased length of leading edge at higher sweep angles.

2. As sweep angle is decreased the weight of the load carrying wing structures increases.

3. Heating at the leading edge of the wing is greater for the sweep angles which just caused transition from laminar to turbulent flow than for wings with 0° sweep. For large leading edge diameters a change in flow from laminar to turbulent at the leading edge is noted as sweep angles go from 0° to 45°.

4. The heat load to a wing with a sharp leading edge is less than that to one with a blunt leading edge because of both the difference in leading edge heat load and the downstream effect of higher surface pressures due to the blunt nose effect.

5. Since the weight of the structure is much greater than the weight of the cooling system components, wing temperature levels should be established to achieve minimum weight by optimizing structural configurations accounting for material property temperature dependence.

6. The incorporation of cooling systems into the wing structure does not reduce the structural depth to any significant degree.

During the course of the study some limitations in presently available theories were found as noted below:

1. Present transpiration and film cooling theories cannot adequately deal with the introduction of a liquid film on the external surface of the porous media.
2. Film cooling theory for turbulent flow including downstream effects is almost completely lacking thus making realistic evaluation of this concept difficult
3. Aerodynamic heating theory can not adequately define the heat loads on the upper rear portion of the wing that is in a highly expanded flow field.

Based on the results of the study as summarized above it is possible to identify areas in which future efforts would be most profitable. It is recommended that the studies of cooled structural concepts be extended to encompass the entire aircraft. Such analyses would permit an assessment of the cooled concept on a total aircraft system basis. The results would provide a basis for assigning percentages of the fuel heat capacity to those aircraft systems which can use it to greatest advantage rather than arbitrarily assigning most of the fuel heat sink capacity to the engine cooling problem. The present studies suggest that overall vehicle system efficiency might be improved if cooling concepts other than regenerative cooling with fuel are used for selected portions of the propulsion system. It is also recommended that more than one aircraft configuration be investigated with respect to cooled structural concepts in order to assess the sensitivity of cooling concepts with respect to vehicle configuration parameters.

In addition to the overall aircraft studies, a number of recommendations of more specialized scope are presented below:

1. Analytical studies of a typical cooled wing section should be conducted using a transient analysis computer program with a feedback control capability to determine the exact temperature distributions in highly heated wing areas.
2. Mission profile variations should be conducted to determine the sensitivity of the cooled wing concepts to off-design conditions.
3. Experimental evaluations of transpiration and film cooling with water should be conducted to permit a more reliable basis for comparison with other cooling concepts.
4. Reliability studies and analyses should be conducted on the various types of cooling systems and should include examination of the consequences of cooling system failures of various types.
5. Febrication studies should be conducted to establish manufacturing procedures required to produce usable structural configurations which incorporate porous, perforated, and/or convectively cooled external surfaces.

6. A relatively large convectively cooled structure should be fabricated and experimentally evaluated under simulated heating and loading conditions, including vibration and acoustic excitation, in order to demonstrate system reliability.

7. Work should be conducted to improve the theoretical capabilities for predicting transition from laminar to turbulent flow and for predicting aerodynamic heating under expanded flow conditions typical of the rear upper surface of the wing.

SYMBOLS FOR APPENDICES

A_{Ref}	area of underwing
b	wing span dimension
Bu	mass transfer driving function
C	wing chord dimension
C_D	drag coefficient
C_F	skin friction coefficient
C_L	lift coefficient
C_p	specific heat
D	diameter of hemicylindrical nose
dA	nodal surface area
F	equation of arbitrary surface
$\overline{F_c C_F}$	postulated function defined by Spalding
F_R	postulated function defined by Spalding
H	enthalpy
h	heat transfer coefficient
K	thermal conductivity
L	unit vector parallel to leading edge
M	Mach number
N	normal vector to surface
Nu	Nusselt number
P	pressure
P_R	Prandtl number
q	heat flux
R	gas constant
R_E	Reynolds number
R_N	radius of hemicylindrical leading edge
$\frac{S}{R_N}$	normalized distance perpendicular to leading edge
T	temperature

SYMBOLS (CONT)

T	tangent vector
t	wing thickness
V	velocity
w	mass flow rate.
$\frac{X}{R_N}$	normalized distance from leading edge in streamwise direction

GREEK

α	direction cosine with respect to X axis
α_θ	time varying body angle of attack
β	direction cosine with respect to Y axis
β	velocity gradient at stagnation line
β_i	deflected stream angle
δ	direction cosine with respect to Z axis
δ	angular location of stagnation line
δ	boundary layer displacement thickness
δ_i	compliment of flow deflection angle
Λ	sweep angle
μ	viscosity
ρ	density
ϕ	wedge angle

SUBSCRIPTS

AU	aft upper surface
QW	adiabatic wall conditions
B	blast pressure component
e	effective angle
FU	forward upper surface
H	hemicylindrical surface
i	element number
L	vector normal to leading edge

SYMBOLS (CONT)

N	normal to surface
SN	surface normal
u	unit vector
V	vector tangent to velocity vector
VL	velocity vector normal to leading edge
w	wall conditions
δ	local free stream conditions
0	stagnation conditions
1	conditions upstream of shock
2	conditions downstream of shock
02	conditions on surface at stagnation line
∞	free stream conditions

APPENDIX A

GEOMETRICAL CONSIDERATIONS

In order to include the effects of the nonsymmetrical shape and varying angles of attack on the heat flux and temperature distribution, an analytical method was derived for calculating the local surface angle of attack and the effective sweep angle for the vehicle at any angle of attack. This was done by defining two parameters which are independent of flight attitude and are therefore known for the vehicle, and by relating the other necessary parameters to these two parameters and the flight attitude.

Two configuration angles, the wing wedge angle ϕ and the sweep angle, Λ, and the wing angle of attack α_θ were chosen to be the independent variables. (The wedge angle is the angle between the wing surface and the plane of the leading edges.)

The leading edges of the hypersonic wing are assumed to be hemicylindrical. The plane containing the center lines of the cylindrical leading edges is considered to be the reference plane of the wing.

The sweep angle Λ is contained in the plane of the leading edges and is the complement of one-half the angle between the two leading edges. The wing angle of attack α_θ is the angle between a streamline in the free stream flow and the plane of the leading edges. The angle of attack can, of course, be either positive or negative.

The effective sweep angle, Λ_e, is the sweep angle the air stream "sees" and is less than the actual sweep angle when the wing angle of attack is not zero. It is the complement of the acute angle between the leading edge and the free stream flow. The equation relating effective sweep angle to geometric sweep angle and wing angle of attack is:

$$\sin \Lambda_e = \sin \Lambda \cos \alpha_\theta \tag{A-1}$$

The stagnation line of the cylindrical leading edge is defined as the intersection of the cylinder with a plane through the center line of the cylinder parallel to the free stream flow. For a wing angle of attack of zero, this plane is the plane of the leading edge. The angular location of the virtual stagnation line, i.e., the angle δ, in the plane perpendicular to the leading edge is given by

$$\text{TAN } \delta = \frac{\text{TAN } \alpha_\theta}{\text{COS } \Lambda} \tag{A-2}$$

The location of lines of flow along the flat surface can be determined by defining the angle β as the angle on the wing surface between the leading edge and the deflected streamline. The angle β is related to the effective sweep and the normal wedge angle by the equation:

$$\text{TAN } (90 - \beta) = \frac{\text{TAN } \Lambda_e}{\text{COS } \phi_n} \tag{A-3}$$

The streamline length is computed by

$$\frac{X}{R_N} = 1 + \left\{ \frac{\left|\frac{S_{ie}}{R_N}\right| - (90 - \phi_n)\ \frac{\pi}{180}}{\text{Sin } \beta_e} \right\} \tag{A-4}$$

The normal wedge angle ϕ_n is determined from the complement of the flow deflection angle, computed by the dot product of the unit velocity vector and the unit vector normal to the surface as discussed below.

A. SURFACE NORMALS

Classical methods of vector analysis were used to determine the direction cosines of the surface normals. An illustration of this method follows, as it applies to the subject vehicle.

For any surface, F (x, y, z) = 0, the gradient vector

$$\text{grad } F = \frac{\partial F}{\partial x}\vec{i} + \frac{\partial F}{\partial y}\vec{j} + \frac{\partial F}{\partial z}\vec{k} \tag{A-5}$$

is normal to the tangent plane at (x_1, y_1, z_1). The unit vector normal to the surface is then,

$$\frac{\text{grad } F}{|N|} = \frac{\text{grad } F}{\sqrt{\left(\frac{\partial F}{\partial x}\right)^2 + \left(\frac{\partial F}{\partial y}\right)^2 + \left(\frac{\partial F}{\partial z}\right)^2}} \tag{A-6}$$

thus yielding the direction cosines:

$$\text{COS } \alpha_{SN} = \frac{\partial F/\partial x}{|N|}$$

$$\text{COS } \beta_{SN} = \frac{\partial F/\partial y}{|N|}$$

$$\text{COS } \gamma_{SN} = \frac{\partial F/\partial z}{|N|}$$

The wing geometry is defined based on the following constraints:

1. The maximum thickness ratio (t/c) is constant and occurs at a specified percent chord
2. The wing area is constant
3. The trailing edge sweep angle is zero
4. The wing has a flat bottom, i.e., the bottom wedge angle is zero
5. The span b is a function of the sweep angle

The wedge angle for the forward upper surface is measured in a plane normal to the leading edge and the aft upper surface wedge angle is measured normal to the trailing edge of the wing. Since the thickness ratio and percent chord for maximum thickness are constant, this angle is also constant.

Since the upper and lower surfaces of the wing are planar, the wedge angles and sweep angles provide sufficient information to define the surface normals. Thus, for the forward upper surface, the direction cosines are:

$$\left.\begin{aligned} \cos \alpha_{FU} &= \sin \phi_{FU} \cos \Lambda \\ \cos \beta_{FU} &= \sin \phi_{FU} \sin \Lambda \\ \cos \gamma_{FU} &= \cos \phi_{FU} \end{aligned}\right\} \qquad \text{(A-7)}$$

and for the aft upper surface the direction cosines are:

$$\left.\begin{aligned} \cos \alpha_{AU} &= -\sin \phi_{AU} \\ \cos \beta_{AU} &= 0 \\ \cos \gamma_{AU} &= \cos \phi_{AU} \end{aligned}\right\} \qquad \text{(A-8)}$$

In a similar manner the surface normal and direction cosines may be determined for the lower surface. Remembering that it is flat and has a zero wedge angle, the direction cosines are:

$$\left.\begin{aligned} \cos \alpha_{L} &= 0 \\ \cos \beta_{L} &= 0 \\ \cos \gamma_{L} &= -1 \end{aligned}\right\} \qquad \text{(A-9)}$$

For the hemicylindrical leading edge any location may be defined by the angular surface distance S/R_N from the reference point, i.e., the stagnation point at zero angle of attack. In terms of S/R_N, the outward pointing normal as defined by its direction cosines is:

$$\left.\begin{aligned} \cos \alpha_H &= \cos (S/R_N) \cos \Lambda \\ \cos \beta_H &= \cos (S/R_N) \sin \Lambda \\ \cos \gamma_H &= -\sin (S/R_N) \end{aligned}\right\} \qquad \text{(A-10)}$$

wherein S/R_N is considered positive in the direction of the lower surface trailing edge.

B. VEHICLE VELOCITY VECTOR

Assuming the view point of stationary vehicle and a moving environment, the free stream unit velocity vector, assuming zero yaw, is given by:

$$\vec{V}_u = \frac{\vec{V}}{|V|} = -\cos \alpha_\theta \, \vec{i} + \sin \alpha_\theta \, \vec{k} \qquad \text{(A-11)}$$

and the direction cosines of the free stream velocity vector are:

$$\left.\begin{aligned} \cos \alpha_V &= -\cos \alpha_\theta \\ \cos \beta_V &= 0 \\ \cos \gamma_V &= \sin \alpha_\theta \end{aligned}\right\} \qquad \text{(A-12)}$$

By considering a unit vector along the centerline of the cylindrical lower leading edge ($\vec{L}$) and writing the vector triple product,

$$\vec{V}_L = (\vec{L} \times \vec{V}_u) \times \vec{L} \qquad \text{(A-13)}$$

the component of $\vec{V}$ normal to the leading edge ($\vec{V}_L$) will be defined.

Evaluation of (13) yields:

$$\vec{V}_L = (-\cos \alpha_\theta \cos^2 \Lambda) \, \vec{i} - (\sin \Lambda \cos \Lambda \cos \alpha_\theta) \, \vec{j} + \sin \alpha_\theta \, \vec{k}, \qquad \text{(A-14)}$$

and the direction cosines of the velocity vector normal to the leading edge, which are:

$$\cos \alpha_{VL} = \frac{-\cos \alpha_\theta \quad \cos^2 \Lambda}{\sqrt{\sin^2 \alpha_\theta \quad + \cos^2 \alpha_\theta \quad \cos^2 \Lambda}}$$

$$\cos \beta_{VL} = \frac{-\sin \Lambda \cos \Lambda \cos \alpha_\theta}{\sqrt{\sin^2 \alpha_\theta \quad + \cos^2 \alpha_\theta \quad \cos^2 \Lambda}} \qquad \text{(A-15)}$$

$$\cos \gamma_{VL} = \frac{\text{Sin } \alpha_\theta}{\sqrt{\sin \alpha_\theta \quad + \cos^2 \alpha_\theta \quad \cos^2 \Lambda}}$$

C. SURFACE TANGENTS

Knowing the surface normals, and the free stream velocity vector, the surface tangent can be determined by the triple product

$$T_i = \vec{N} \times \vec{V} \times \vec{N} \qquad \text{(A-16)}$$

The tangent vector may be described as

$$T_i = \cos \alpha_i \, i + \cos \beta_i \, j + \cos \gamma_i \, k \qquad \text{(A-17)}$$

where $\cos \alpha$, $\cos \beta$, and $\cos \gamma$ are the direction cosines.

The direction cosines for upper surface tangent are

$$\left.\begin{aligned} \cos \alpha_u &= -\cos \phi_u \cos \Lambda \\ \cos \beta_u &= -\cos \phi_u \sin \Lambda \\ \cos \gamma_u &= \sin \phi_u \end{aligned}\right\} \qquad \text{(A-18)}$$

and for the lower surface are

$$\left.\begin{aligned} \cos \alpha_L &= -1 \\ \cos \beta_L &= 0 \\ \cos \gamma_L &= 0 \end{aligned}\right\} \qquad \text{(A-19)}$$

On the hemicylinder, the tangent vector reverses direction at the stagnation line. On the lower side of the stagnation line, the direction cosines are

$$\left.\begin{aligned} \cos \alpha_H &= -\sin\left(\frac{S}{R_N}\right) \cos \Lambda \\ \cos \beta_H &= -\sin\left(\frac{S}{R_N}\right) \sin \Lambda \\ \cos \gamma_H &= -\cos\left(\frac{S}{R_N}\right) \end{aligned}\right\} \qquad \text{(A-20)}$$

On the upper side of the stagnation line, the direction cosines are

$$\left.\begin{aligned} \cos \alpha_H &= \sin\left(\frac{S}{R_N}\right) \cos \Lambda \\ \cos \beta_H &= \sin\left(\frac{S}{R_N}\right) \sin \Lambda \\ \cos \gamma_H &= \cos\left(\frac{S}{R_N}\right) \end{aligned}\right\} \qquad \text{(A-21)}$$

D. FLOW DEFLECTION ANGLE

The angle of interest in calculating the pressure distribution is the flow deflection angle, δ_i. The complement of the flow deflection angle may be obtained from the dot product of the velocity vector and the surface normal. Therefore, the complement of the flow deflection angle between the velocity vector normal to the leading edge and the surface normal to the hemicylinder is:

$$\cos \delta_H = \cos \alpha_{VL} \cos \alpha_H + \cos \beta_{VL} \cos \beta_H + \cos \gamma_{VL} \cos \gamma_H \qquad \text{(A-22)}$$

Similarly the complement of the flow deflection angle between the free stream velocity vector and the forward upper surface is

$$\cos \delta_{FU} = -\cos \alpha_\theta \cos \alpha_{FU} + \sin \alpha_\theta \cos \gamma_{FU} \qquad \text{(A-23)}$$

The complement of the flow deflection angle between the free stream velocity vector and the aft upper surface is:

$$\cos \delta_{AU} = -\cos \alpha_\theta \cos \alpha_{AU} + \sin \alpha_\theta \cos \gamma_{AU} \qquad \text{(A-24)}$$

The complement of the flow deflection angle between the free stream velocity vector and the lower surface is:

$$\cos (90 - \alpha_L) = -\sin \alpha_\theta \qquad \text{(A-25)}$$

The local angle of attack on the lower surface of the wing, α_L, may be related to the effective sweep angle and the effective wedge angle by:

$$\sin \alpha_L = \sin \phi_e \cos \Lambda_e \tag{A-26}$$

The flow deflection angles for the upper surfaces are:

$$\alpha_{FU} = 90 - \delta_{FU} \tag{A-27}$$

$$\alpha_{AU} = 90 - \delta_{AU} \tag{A-28}$$

APPENDIX B
DETERMINATION OF LOCAL FLOW FIELDS

Determination of the local flow field parameters, i.e., pressure temperature and velocity is requisite to evaluation of the local heat transfer coefficient, However, the flow field surrounding a vehicle in hypersonic flight is dependent on the geometry of the vehicle, i.e., the presence of blunt leading edges tends to increase static temperature and pressure and decrease velocity at the boundary layer edge. This effect which may extend many diameters downstream can cause a substantial decrease (30 to 40%) in aerodynamic heating rates.

Nose bluntness effects are dependent on the vehicle configuration, Mach number, Reynolds number, wall cooling, and total enthalpy (real gas effects). Two limiting cases are immediately recognized. A good estimate of the upper bound on heating can be obtained by assuming sharp body values for local velocity and enthalpy. Conversely, the lower limit is obtained by assuming all of the fluid in the boundary layer has passed through a normal shock in computing local flow properties. The flow conditions at the boundary layer edge are then obtained assuming an isentropic expansion from the stagnation to the local pressure. This approach is restricted to equilibrium or frozen flows.

A. LOCAL PRESSURE

The local pressure on the hemi-cylindrical leading edge is determined on the basis of modified Newtonian Impact theory (Reference 37),

$$\frac{P_\delta}{P_{02}} = \frac{P_\infty}{P_{02}} \sin^2 \delta_H + \cos^2 \delta_H \qquad \text{(A-29)}$$

where, for ideal air ($\gamma = 1.4$) and $M_\infty \operatorname{Cos} \Lambda_e \geq 1$, the stagnation line pressure ratio is:

$$\frac{P_\infty}{P_{02}} = \frac{6.0228 \times 10^{-3}}{M_\infty^2 \cos^2 \Lambda_e} \left[\frac{7 M_\infty^2 \cos^2 \Lambda_e - 1}{M_\infty^2 \cos^2 \Lambda_e} \right]^{5/2} \qquad \text{(A-30)}$$

Pressures aft of the leading edge are predicted using the method of Creager (Reference 11) which presumes that superposition of the wedge pressures and blast wave pressures is valid. The wedge pressures are computed on the basis of real gas attached oblique shock relations. For a compression surface, i.e., positive flow detection angle, the wedge pressure is given by:

$$\frac{P_\delta}{P_\infty} = 1 + (2.97596\text{x}10^{-2}\,\alpha_i - 1.3848\text{x}10^{-5}\,\alpha_i^2 + 1.0846\ \text{x}10^{-5}\,\alpha_i^3)\,M_\infty + (-6.9146\text{x}10^{-4}\,\alpha_i + 2.53666\text{x}10^{-4}\,\alpha_i^2 + 3.4355\text{x}10^{-6}\,\alpha_i^3)\,M_\infty^2 + (4.2138\text{x}10^{-6}\,\alpha_i + 8.9207\text{x}10^{-6}\,\alpha_i^2 - 1.6784\text{x}10^{-7}\,\alpha_i^3)\,M_\infty^3 \quad \text{(A-31)}$$

and α_i is limited to the maximum angle for shock attachment defined by:

$$\alpha_{max} = 45.6 - \frac{45.6 + 2.43\,(M_\infty - 1)}{1 + 0.498\,(M_\infty - 1) + 0.599\,(M_\infty - 1)^2} \quad \text{(A-32)}$$

The blunt nose overpressures for a compression surface are predicted by the blast wave type equation.

$$\frac{P_B}{P_\infty} = 0.112\left[\frac{1.2}{(S/R_N)}\right]^{2/3} M_\infty^2 \cos^2 \Lambda_e \quad \text{(A-33)}$$

In regions of expansion, Prandtl-Meyer relations are applied to compute the wedge pressures and a technique suggested by Wallace and McLaughlin (Reference 38) is applied to compute the blunt nose overpressures. For ideal air ($\gamma = 1.4$), the overpressure equation becomes:

$$\frac{P_B}{P_\infty} = \frac{0.1134\,M_\infty^2 \cos^2 \Lambda_e}{1.0627\,(\frac{X}{R_N})^{2/3} + 2.151\,(\frac{X}{R_N} - 1)\tan|\delta|} \quad \text{(A-34)}$$

B. LOCAL TEMPERATURE

The local stream temperature is then computed assuming the flow passes through a normal shock and subsequently expands isentropically to the local pressure.

$$T_\delta = T_\infty \left[\left(\frac{P_\delta}{P_\infty}\right)\left(\frac{P_{T1}}{P_{T2}}\right)\right]^{2/7} \quad \text{(A-35)}$$

C. LOCAL VELOCITY

Similarly, the local stream velocity is given by

$$V_\delta = V_\infty \left[\frac{M_\infty^2 + 5}{M_\infty^2} \left[1 - \left(\frac{P_\delta}{P_{T2}} \right)^{2/7} \right] \right]^{1/2} \qquad \text{(A-36)}$$

APPENDIX C

AERODYNAMIC HEATING

Aerodynamic heat input is a function of trajectory and external geometry of the wing; i.e., sweep angle of the wing, altitude, velocity, angle of attack and radius of curvature at the stagnation point. The problem of predicting heat flux to the stagnation line of unswept leading edges and the heat flux distribution over an unswept wing has been the subject of numerous investigations. In general the theories developed for predicting heat flux distribution are based on knowledge of flow conditions; however, an exact definition of flow conditions around a three-dimensional blunt body is quite complex. The existence of shock boundary layer interaction and the blunt nose induced vorticity effects at hypersonic speeds complicate the problem considerably. However, recent attempts have been made to account for these effects (Reference 39). Thus, use of a swept leading edge at angle of attack introduces two additional problems: (1) predicting the flow field which the air stream actually sees, and (2) predicting the effect of sweep on the heat flux. The first is a geometry problem and relationships between the important leading edge geometry parameters and the angle of attack were developed in a previous section. The effect of sweep on the heat flux is much more complicated and approximate methods based in part on theory and in part on experimental results have been developed for determining heat flux distribution over a swept leading edge. These methods have been compared with some experimental results for swept leading edges at angle of attack and generally the comparison is good.

The prediction of heating rates in the leading edge region has been divided into two main parts (1) the heat flux q_o at the stagnation line, and (2) the ratio q/q_o aft of the stagnation line. This allows the use of different methods for each part and provides greater overall accuracy.

A. LAMINAR FLOW

In the region of the stagnation line, heat fluxes are predicted for a laminar leading edge using the method of Reshotko and Cohen (Reference 4). Although this method is based on simpler assumptions than the theoretically more exact method of Faye and Riddell (Reference 40) comparisons have shown that the two agree within ten percent for all practical conditions. The method of Reshotko and Cohen has been further simplified at Bell Aerosystems (Reference 41) until the final expression for the heat transfer coefficient is

$$h_o = \left(\frac{N_U}{\sqrt{R_E}}\right)\left(\frac{K_w}{\mu_w}\right)\left(\frac{T_o}{T_w}\right)^{1/2}\left(\frac{T_o}{T_\delta}\right)^{5/4}\left(\frac{\beta D}{V_\delta}\right)^{1/2}\left(\frac{P_\infty V_\infty}{D_N}\right)^{1/2} \qquad \text{(A-37)}$$

The parameter $(Nu/\sqrt{Re_{e_w}})$ is obtained from Reference 4 and is shown in Figure A-1 for air. The parameter $k_w/\sqrt{\mu_w}$ is illustrated graphically in Figure A-2. The velocity gradient parameter, $\frac{\beta D}{V}$, was obtained from Reference 42 and is presented in Figure A-3.

The variation of the laminar heating rate aft of the stagnation point is known less accurately. A method derived by Lees, Reference 6, allows the prediction of heating rates to an unswept wing for laminar flow and invloves a continuous integral from the stagnation point to the point in question. For a two-dimensional body, the applicable equation is

$$q = 0.51\, P_R^{-2/3} (H_o - H_w) \frac{P_\delta\, V_\delta}{\sqrt{2\int_o^S P_\alpha\, V_\delta\, d_S}} \qquad \text{(A-38)}$$

In this equation H is the enthalpy and S the arc length from the stagnation point. The solution of Lees is employed herein as a ratio of local heat flux to stagnation heat flux, q/q_o, which allows the use of the more accurate method of Reshotko and Cohen at the stagnation line.

Knowledge of the heating rates is far more advanced than knowledge of the flow conditions on which the heating rates are based. Methods which apply at low supersonic speeds have been found to be highly inaccurate at hypersonic speeds, when shock-boundary layer interaction and blunt leading edge effects produce substantially higher pressures than would normally be expected. The method used herein has attempted to account only for the latter of these effects.

Since the method of Reshotko and Cohen does not account for sweep, a technique was employed at Bell which is based on an empirical correlation of test data. It was found that a simple cosine curve correlates the data up to an angle of yaw of 60°, i.e.,

$$h_{\Lambda_e}/h_{(\Lambda_e = 0)} = \cos \Lambda_e \quad \text{for } \Lambda_e \leq 60^\circ$$

A polynomial expression with (A-39)

$$h_{\Lambda_e}/h_{(\Lambda_e = 0)} = 0.35 \quad \text{for } \Lambda_e = 75^\circ$$

is employed for $60^\circ < \Lambda_e \leq 90^\circ$.

This method was substantiated by an analysis based on real gas relations.

The distribution of heat flux around the swept wing is based on the distribution around an unswept cylinder using the method of Lees. In particular, the value of h at the shoulder of a swept hemi-cylinder is assumed equal to $\sqrt{h\,\Lambda_e/h_o}$ times the unswept value and a fairing is made between the stagnation point and the shoulder. The method of Lees is used aft of the shoulder, based on a modified blunt nose pressure distribution.

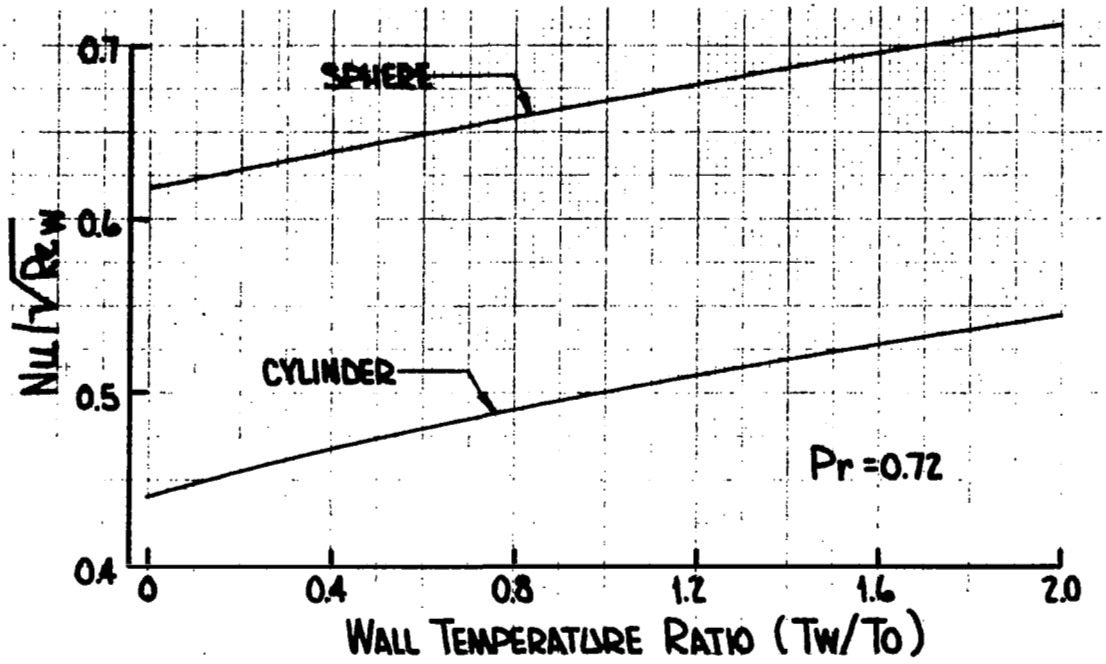

Figure A-1. $Nu/\sqrt{Re_w}$ versus Wall Temperature Ratio for Stagnation Point Heating on a Sphere and a Cylinder

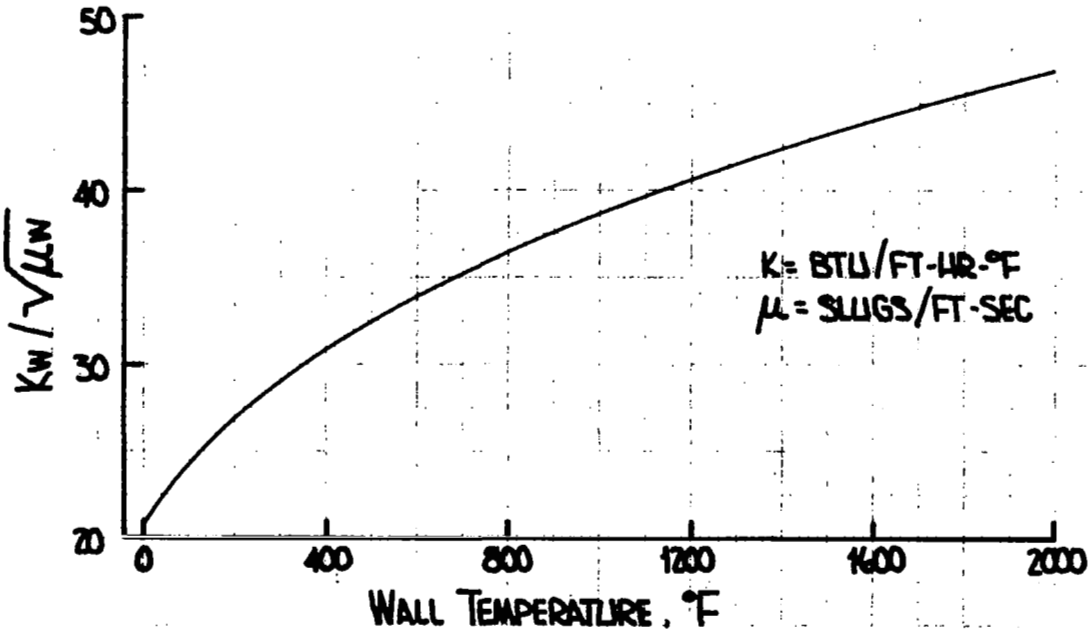

Figure A-2. $K_w/\sqrt{\mu_\omega}$ versus Wall Temperature for Stagnation Point Heating on a Sphere and a Cylinder

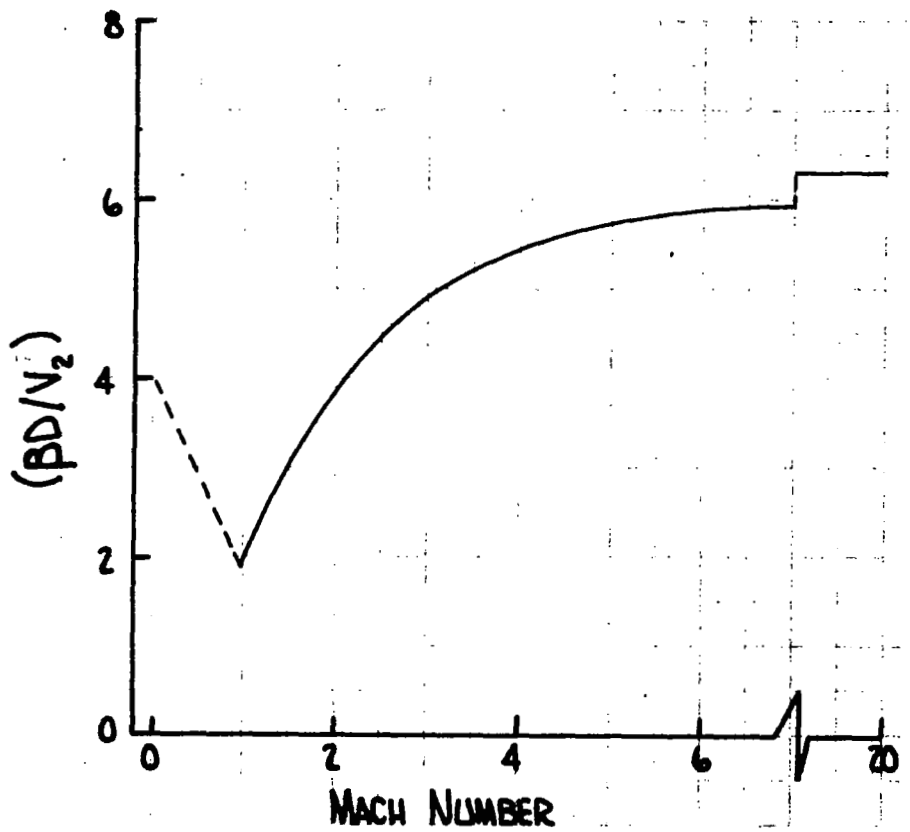

Figure A-3. Stagnation Point Flow Velocity Gradient versus Mach Number

B. TURBULENT HEAT FLUX DISTRIBUTION

In the region of the stagnation line, the turbulent heat flux is predicted by employing the method of Beckwith and Gallagher (Reference 8). The theory gives fairly good agreement with test data for sweep angles greater than 20° sweep. After simplification, the equation for the turbulent heat transfer coefficient at the stagnation line becomes

$$h_o = \frac{1.4206 \times 10^{-4}}{R_N^{1/5}\, \mu_\infty^{3/8}\, T_o^{0.608}\, T_w^{0.192}} \left(\frac{K_\infty}{\sqrt{\mu_\infty}}\right) \left(\frac{\beta D}{V_2}\right)^{1/5} \left(\frac{P_{02}}{P_\infty}\right)^{4/5} \left(P_\infty\, V_\infty\right)^{4/5} \left(\frac{V_2}{V_\infty}\right)^{1/5} \left(\frac{T_o}{T_\infty}\right)^{0.152} \left(\sin^{3/5} \Lambda_e\right)\left(\cos^{1/5} \Lambda_e\right) \tag{A-40}$$

The parameters $\frac{K_\infty}{\sqrt{\mu_\infty}}$ and $\frac{\beta D}{V_2}$ are obtained from Figures A-2 and A-3, respectively.

The chordwise distribution of heat flux for turbulent flow is computed using the method of Beckwith and Gallagher. Similar to laminar flow, the equation involves an integral from the stagnation point to the point of interest. The applicable equation is

$$\frac{h}{h_o} = \left(\frac{P_\delta}{P_{02}}\right)^{8/7} \left[\frac{\left(\frac{P_{02}}{P_\delta}\right)^{2/7} - \left(\frac{T_2}{T_o}\right)}{1-\left(\frac{T_2}{T_o}\right)}\right]^{3/8} \left(\frac{\delta_s}{\delta}\right)^{1/4} \tag{A-41}$$

where $\frac{\delta_s}{\delta}$ is given by the integral equation

$$\left(\frac{\delta_s}{\delta}\right)^{1/4} = \left\{\frac{5}{8}\left(\frac{\beta D}{V}\right)\sqrt{T_o/T_2}\left(\frac{1}{U_1}\right)^{1/4} \int_o^{S/R_N} U_1^{1/4} \left[\frac{\left(\frac{P_{02}}{P_\delta}\right)^{2/7} - \left(\frac{T_2}{T_o}\right)}{1 - T_2/T_o}\right]^{3/8} \left(\frac{P_\delta}{P_{02}}\right)^{8/7} d\left(\frac{S}{R_N}\right)\right\}^{-1/5} \tag{A-42}$$

In this equation S/R_N is the normal distance along the surface perpendicular to the leading edge. The solution accounts for sweep through its dependence on the stagnation point value.

Aft of the shoulder the heat flux distribution is computed by a relationship outlined by Bertram and Neal (Reference 9) using the Von Karman form of the Reynolds analogy employing the Spalding and Chi skin friction function (Reference 10).

The turbulent flat plate convective film coefficient is

$$h = \frac{C_f C_p V_\infty P_\infty}{2 R T_\infty}\left[1 + 5\sqrt{\frac{F_C C_F}{2}}\left\{P_R - 1 + \ln\left(\frac{5 P_R + 1}{6}\right)\right\}\right] \qquad \text{(A-43)}$$

the parameter F_C is obtained from the equation

$$F_C = \left(\frac{T_{AW}}{T_\delta} - 1\right)\left\{\sin^{-1} \frac{2\sqrt{T_{AW}/T_\delta} - 1\left[T_{AW} - T_W - T_{AW}\left(2 - \frac{T_{AW}}{T_\delta} - \frac{T_W}{T_\delta}\right)\right]}{\frac{\left(T_{AW} + T_W\right)^2}{T_\delta} - 4 T_{AW}}\right\}^{-2} \qquad \text{(A-44)}$$

The parameter C_F, i.e., the skin friction coefficient, is

$$C_F = \frac{0.1 \left(F_R R_e\right)^{-0.268} + 0.001}{F_C} \qquad \text{(A-45)}$$

which is obtained from a curve fit of experimental data presented in Spalding and Chi's report.

The parameter F_R is a postulated function based on the Reynold's Number which was fit to experimental data by Spalding and Chi. The resultant expression yields a least mean square error of 9.9% over a Mach number range of 0 to 12. The equation for F_R is:

$$F_R = \left(\frac{1}{F_C}\right)\left(\frac{T_\infty}{T_W}\right)^{0.702}\left(\frac{T_R}{T_w}\right)^{0.772} \qquad \text{(A-46)}$$

To evaluate the heat transfer coefficient on the flat plate regions, it is necessary to iterate on both the wall temperature and the heat transfer coefficient since the function, F_C, depends on the wall temperature. For proper convergence of the heat transfer coefficient, the inverse sine in the equation for F_C must be evaluated in the proper quadrant. The proper quadrant in which to evaluate the inverse sine is shown in Figure A-4

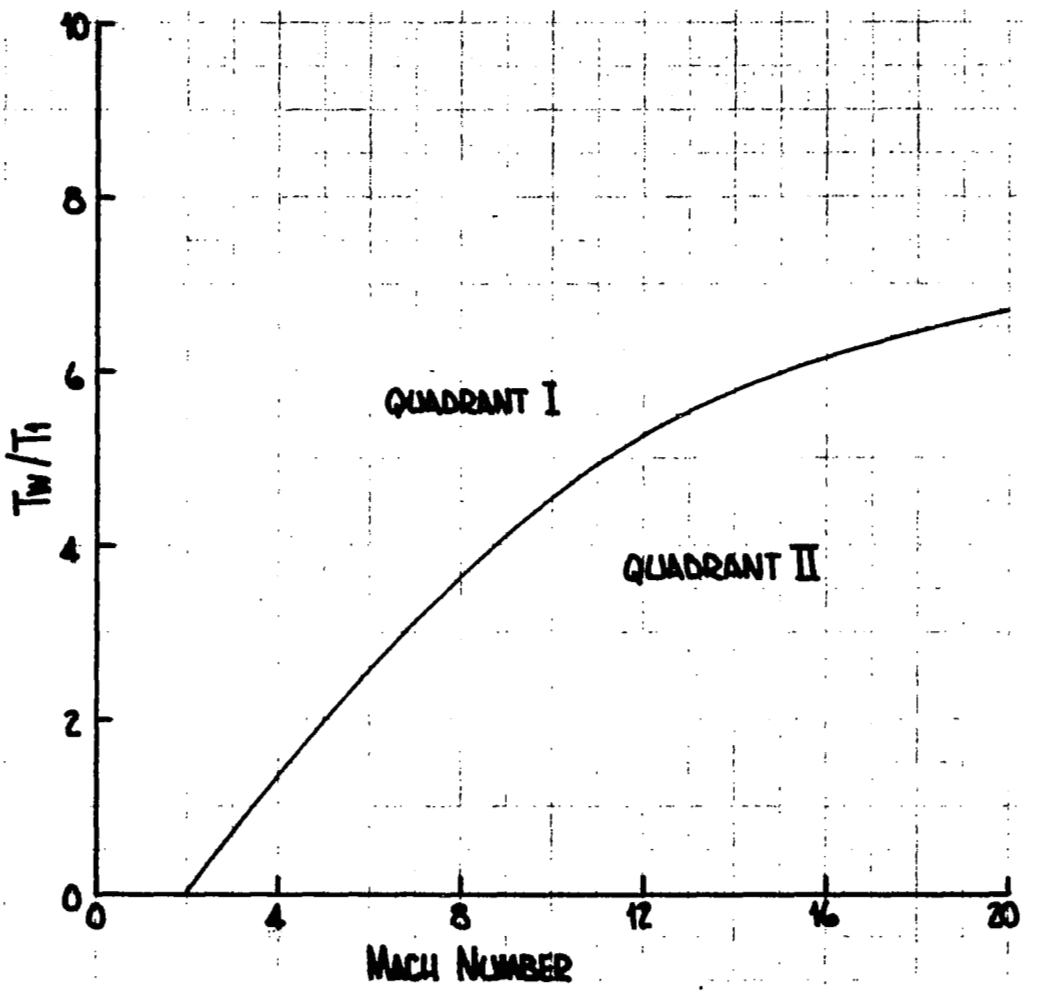

Figure A-4. Quadrent Evaluation for Inverse Sine Function versus Temperature Ratio and Mach Number

reproduced here from Reference 9. The present computer program evaluates the heat transfer coefficients using a wall temperature equal to the radiation equilibrium wall temperature.

To obtain heat transfer coefficients for wall temperatures other than the radiation equilibrium values a correction factor technique can be employed. For purposes of this study correction factors were generated for a range of wall temperatures using a reference temperature of 500°F. Figure A-5 presents the correction factors for laminar flow as determined in Reference 5. Within the bounds of expected wall temperatures in the laminar flow regime, 200°F to 2500°F, correction factors are within 5%. Using the relationships in Reference 10, turbulent flow correction factors were generated for a Reynolds number of 10,000,000 which is a typical Reynolds number on the lower wing surface. In turbulent flow on the lower surface of the wing the expected range of wall temperatures is 200°F to 1200°F and correction factors are within 10%.

C. TRANSITION

It is of utmost importance to predict the onset of turbulent flow because of the increased heating rates which occur due to the turbulent action. The onset of transition from laminar to turbulent flow may be computed on the basis of the steramwise Reynold's number defined by the equation

$$Re = R_N \int_0^{X/R_N} \frac{\rho_\delta V_\delta}{\mu_\delta} d\left(\frac{X}{R_N}\right) \tag{A-47}$$

On the wedge surface the distance $d\left(\frac{X}{R_N}\right)$ is given by

$$d\left(\frac{X}{R_N}\right) = d\left(\frac{S}{R_N}\right) / \sin \beta \tag{A-48}$$

where β is the angle between the direction perpendicular to the leading edge and the streamwise direction.

For the flat lower surface, it is defined as

$$\beta_L = 90 - \Lambda \tag{A-49}$$

and for the wedge upper surfaces as

$$\beta_T = 90 - \tan^{-1} \frac{\tan \Lambda}{\cos \phi_T}$$

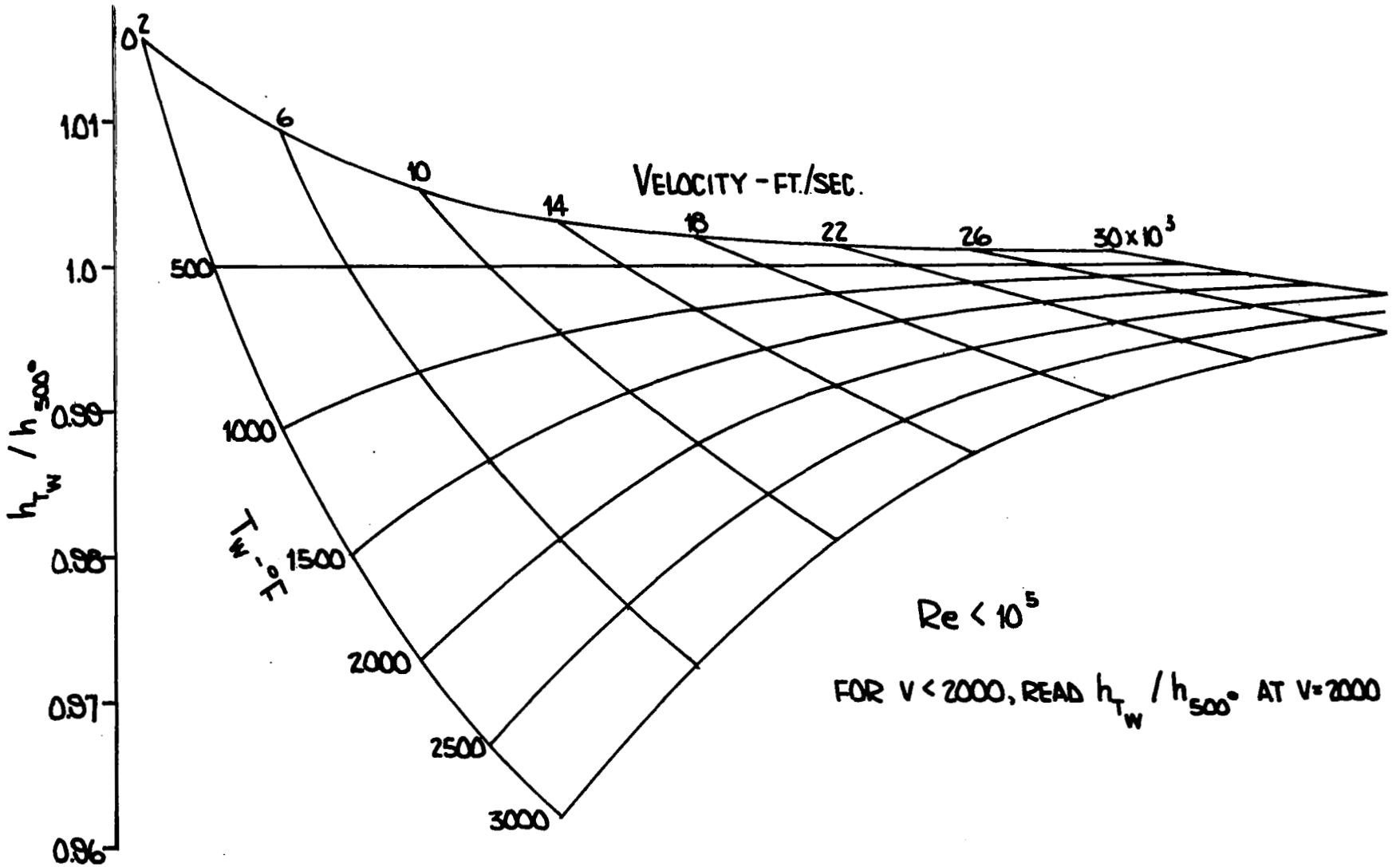

Figure A-5. Correction to Heat Transfer Coefficient for Different Wall Temperatures for Laminar Flow

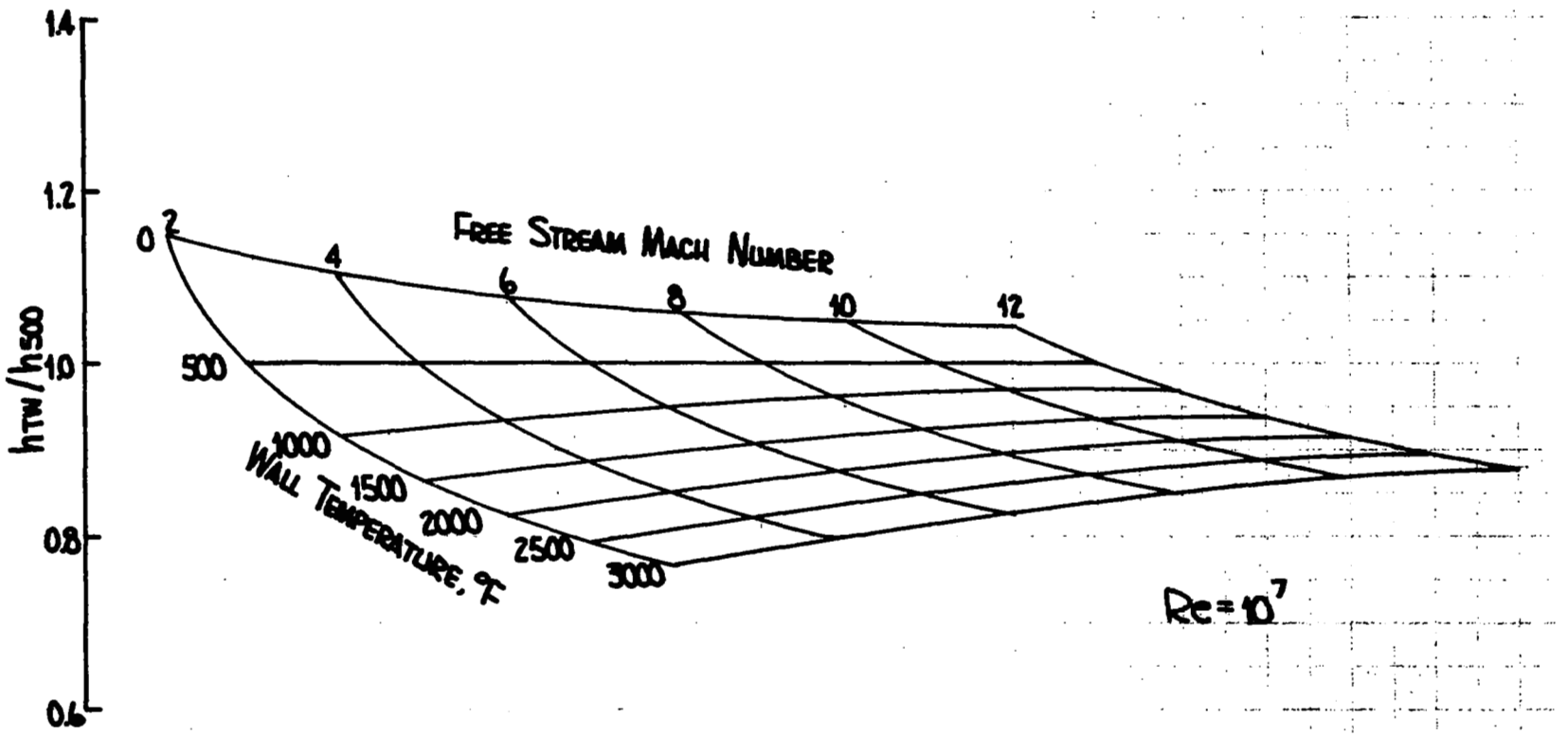

Figure A- 6. Correction to Heat Transfer Coefficient for Different Wall Temperatures for Turbulent Flow

On the hemicylinder the streamwise direction is approximated by

$$d\left(\frac{X}{R_N}\right) = d\left(\frac{S}{R_N}\right) \frac{1 + \cos^2 \Lambda_e}{2 \cos^2 \Lambda_e} \tag{A-50}$$

It should be noted that the computer program assumes that as soon as the streamwise Reynolds number exceeds the critical Reynolds number, fully developed turbulent flow commences. In other words, a step change in the heat transfer coefficient and coolant flowrate will result, rather than a continuous variation which must exist in reality.

The inputted value of the critical Reynolds number of 500,000 is corrected for a premature onset of turbulence due to a swept leading edge as suggested by Czarnecki et al (Reference 43). Figure A-7 shows the effect of sweep on transition.

Bushnell (Reference 7) has shown that the presence of a forebody has a distablizing effect on the leading edge cross flow thus causing an earlier onset of transition. then predicted by the streamwise Reynolds number corrected for sweep angle. Experimental data indicates that for sweep angles greater than 10°, transition to turbulent flow results when the Reynolds number exceeds the value given by

$$Re_c = 7.87 \times 10^8 \Lambda_e^{-2.43} + 0.2 \times 10^5 \tag{A-51}$$

where the leading edge diameter is to be used as the characteristic dimension when calculating the Reynold's number, i.e.,

$$Re = \frac{\rho_\infty V_\infty d}{\mu_\infty} \tag{A-52}$$

D. RECOVERY TEMPERATURE

The forcing function used to compute the cold wall heating rates is the local recovery temperature, i.e., the adiabatic wall temperature. This value is somewhat less than the total or stagnation temperature. In fact, the recovery temperature can be written in terms of the stagnation temperature

$$T_R = T_\delta + r\,(T_o - T_\delta) \tag{A-53}$$

where r is the recovery factor and the total temperature T_o is obtained from the following equation

$$\int_{T_\delta}^{T_o} C_p\,dt = \frac{V_\delta^2}{2gJ} \tag{A-54}$$

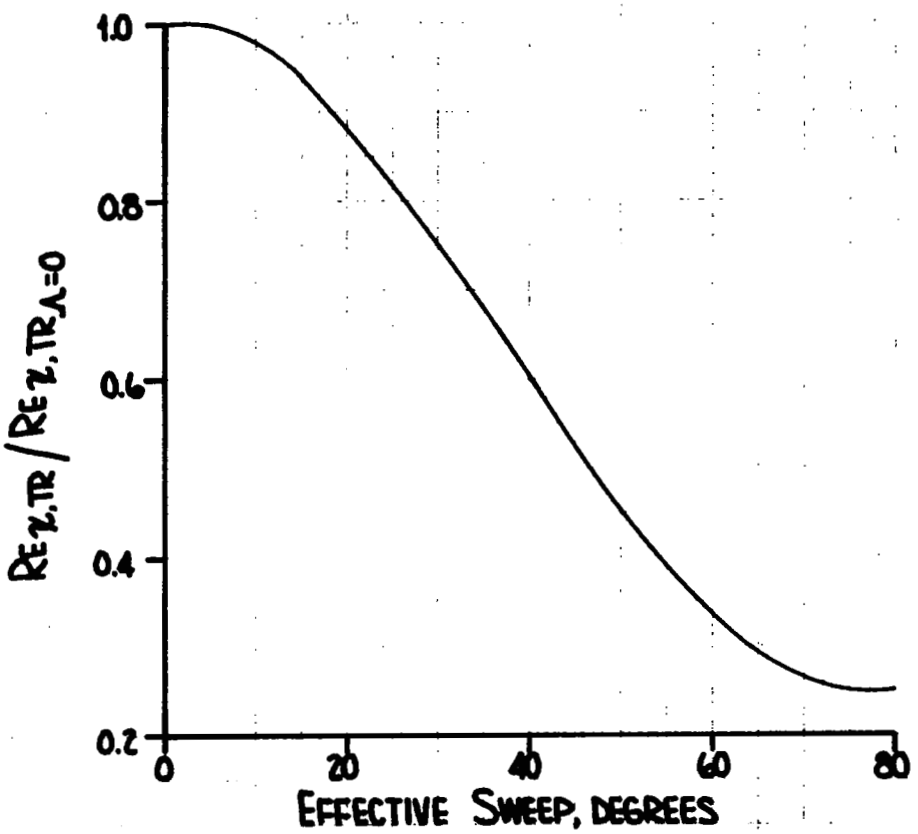

Figure A-7. Effect of Sweep on Transition Reynolds Number

Figure A-8 is a plot of $T_o - T$ versus V_δ based on the following equation for the specific heat which assumes no dissociation.

$$C_p = 0.24 \left[1 + \left(\frac{\gamma-1}{\gamma}\right)\left(\frac{5500}{T}\right)^2 \frac{\exp(5500/T)}{(1-\exp(5500/T))^2}\right] \quad \text{(A-55)}$$

The local recovery factor on the hemicylindrical leading edge varies with the sweep angle and chordwise location. This variation of the recovery factory may be approximated by

$$r_i = (\cos^2 \Lambda_e + r \sin^2 \Lambda_e) \cos^2 \eta + r \sin^2 \eta \quad \text{(A-56)}$$

where η is an angle which varies from 0 at the stagnation line to $\pi/2$ at the shoulder of the hemicylinder. The recovery factor variation around a laminar swept leading edge is given in Figure A-9.

For flow over the upper and lower surfaces the recovery factor is defined as

$$r_i = \sqrt{P_R} \quad \text{(A-57)}$$

for laminar flow and

$$r_i = \sqrt[3]{P_R} \quad \text{(A-58)}$$

for turbulent flow.

E. COLD WALL HEATING RATES AND RADIATION EQUILIBRIUM TEMP.

Subsequently, the cold wall heating rate is calculated from

$$\dot{q} = h\, T_r \quad \text{(A-59)}$$

and the radiation equilibrium wall temperature is determined from solution of the local heat balance:

$$\sigma \epsilon_o T_w^4 - h (\dot{T}_r - T_w) = 0 \quad \text{(A-60)}$$

It should be noted that the methods described above presume that strip theory is applicable, i.e., the spanwise component of the flow may be neglected. It has been shown in Reference 44 that the heat transfer is best predicted by assuming a strip type flow in the angle of attack range from 0 to 25° which encompasses the nominal angle of attack, i.e., 12°.

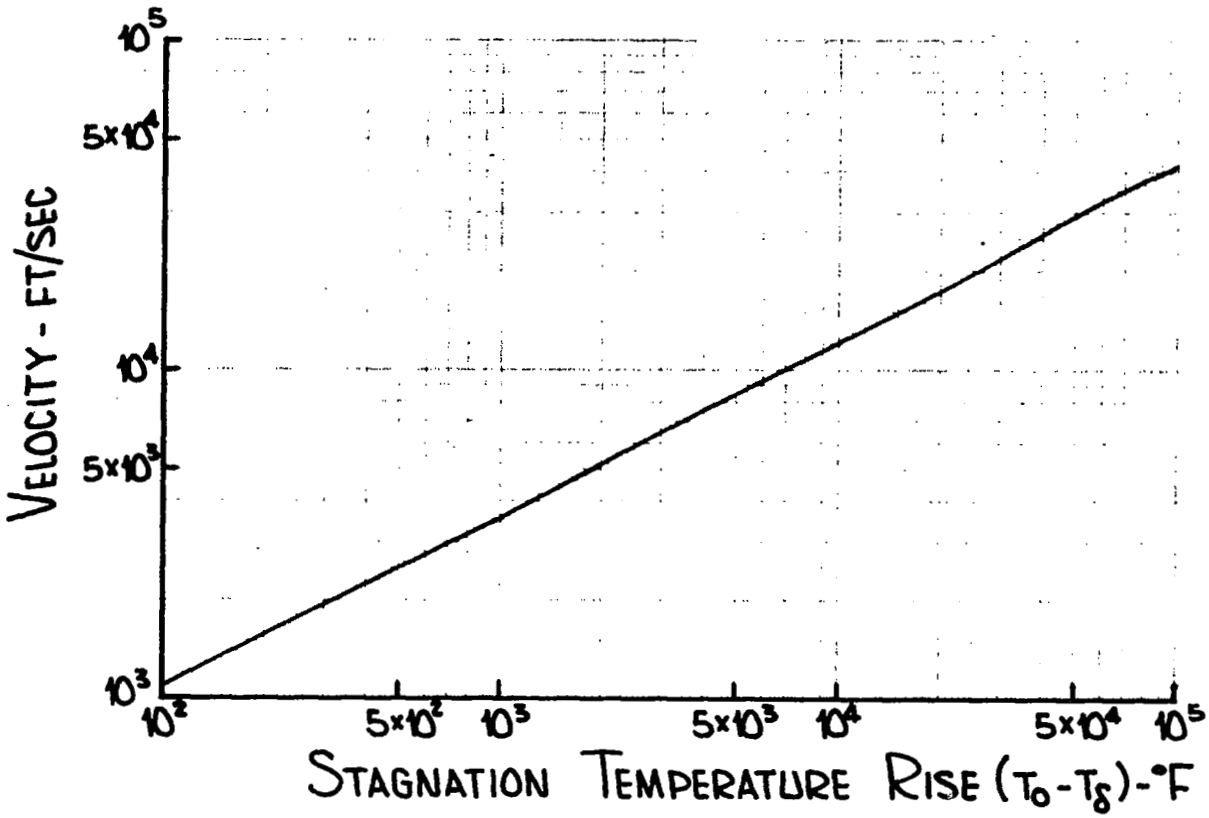

Figure A-8. Stagnation Temperature Rise versus Velocity

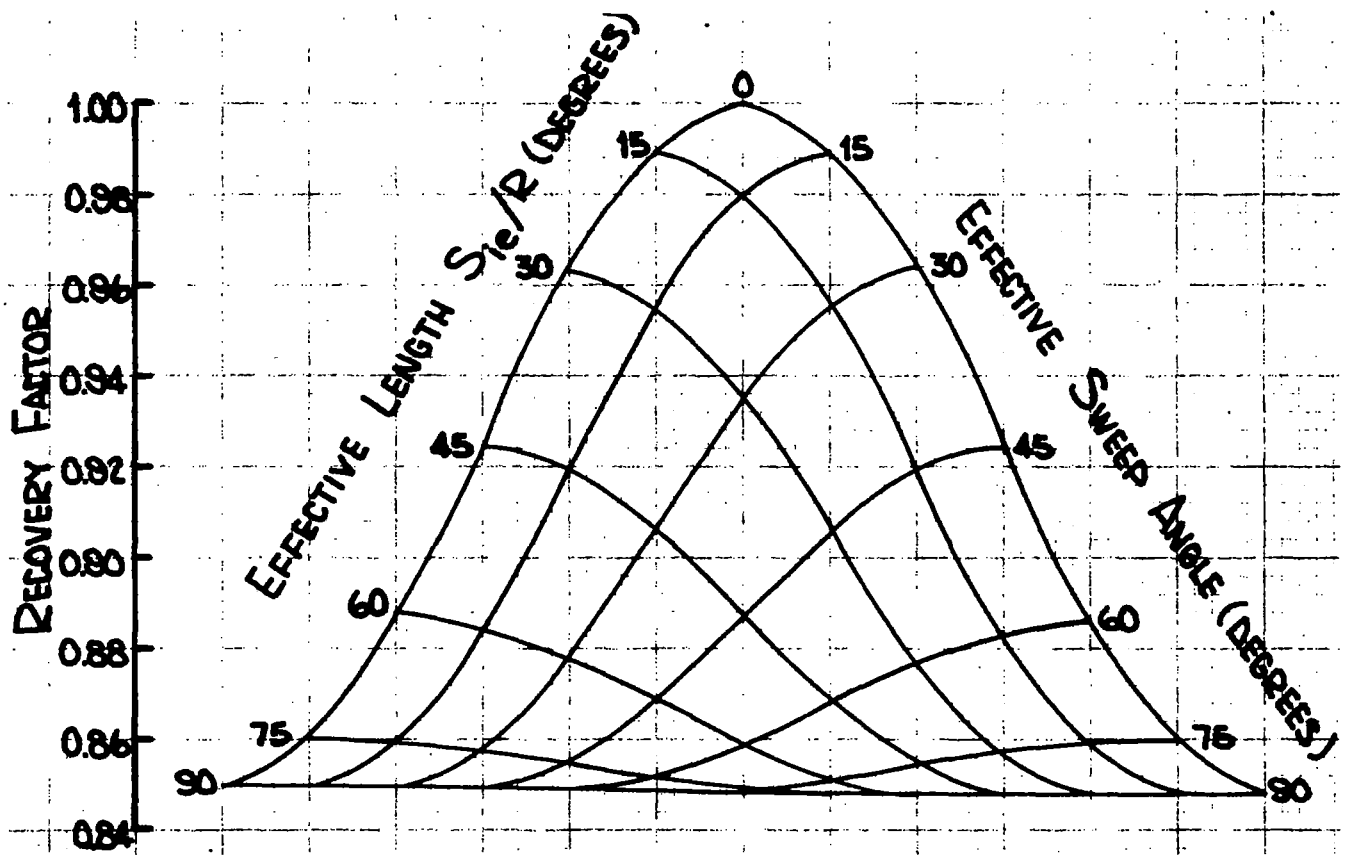

Figure A- 9 . Variation of Recovery Factor around Swept Leading Edge

It is also noted that previous studies have indicated that at zero angle of attack the theory presented herein somewhat over-predicts the heat fluxes on the slab portion of the wing. However, at an angle of attack of 15° experimental data is correlated quite well.

APPENDIX D
TRANSPIRATION COOLING

Transpiration cooling is a function of many of the same parameters as aerodynamic heating. It is a means of cooling an aerodynamic surface by injecting a cool fluid with a high specific heat into the boundary layer. The injection performs two functions: (1) it removes heat by an increase in internal energy of the fluid and (2) it thickens the boundary layer thus reducing the aerodynamic heat input.

The coolant flowrate on a turbulent flatplate is predicted using the method outlined by Spalding, Auslander and Sundaram (Reference 27) which will be referred to as Spalding's method in this paper. The analysis is an extension of the work by Spalding and Chi (Reference 10) for a turbulent boundary layer on a hot plate without mass transfer. The postulated functions F_C, F_R and F_{RX} are extended to include the effects of mass transfer in the form of B_u, the driving force for mass transfer.

The driving force for a chemically inert coolant in terms of enthalpy may be expressed as

$$B_u = \frac{1}{P_R^{2/3}} \frac{C_{p_\infty} (T_\infty - T_w) + \frac{r_i V_\infty^2}{2 g J}}{C_{p_c} (T_w - T_c) + q_{RAD}/\dot{W}_c} \qquad \text{(A-61)}$$

where r_i is the recovery factor corrected for coolant injection q_{RAD} is the radiation heat transfer rate and $\dot{W}_c$ is the coolant flowrate.

Spalding, through the definition of the driving force, Reynolds analogy, and shear stress has shown the flowrate can be obtained from the following equation

$$W_c = \frac{1}{2} \rho_\infty V_\infty C_F Bu \qquad \text{(A-62)}$$

where the skin friction coefficient, C_F, is obtained from

$$C_F = \frac{\overline{F_c C_F}}{F_c} \qquad \text{(A-63)}$$

F_c is obtained from numerical integration of

$$F_c = \left[\int_0^1 \left(\frac{\delta / \delta_\infty}{1 + Bu\, z} \right)^{1/2} dz \right]^{-2} \qquad \text{(A-64)}$$

and $\overline{F_c C_F}$ is an empirical correlation.

$$\overline{F_c C_F} = 0.01 \, (F_{RX} \, R_E)^{-0.268} + 0.001 \qquad \text{(A-65)}$$

where F_{RX} is given by

$$F_{RX} = \left(\frac{\mu_\infty}{\mu_w} \right) \frac{1}{F_c \, (1 + Bu)^{1/2}} \qquad \text{(A-66)}$$

Unfortunately, the above equations must be solved simultaneously rather than sequentially as indicated in Reference 27.

The flowrate on a laminar flat plate is obtained by employing the same method as the turbulent flat plate with the skin friction coefficient modified for laminar flow. Since the wall temperature would be cooled to a constant temperature and the blowing function is nearly a constant, C_F is the only parameter in equation (63) that depends on the type of flow. Spalding showed that transpiration reduces the skin friction coefficient in turbulent flow, and this analysis assumes that a similar reduction results in laminar flow. The skin friction coefficient is obtained by ratioing the Blasius laminar value to the Blasius turbulent value by the relationship

$$\frac{C_{FL}}{C_{FT}} = \frac{11.25}{Re^{0.3}} \qquad \text{(A-67)}$$

Thus, the laminar skin friction coefficient with transpiration is

$$C_F = \frac{11.25}{Re^{0.3}} \, \frac{0.01 \, (F_{RX} \, Re)^{-0.268} + 0.001}{F_c} \qquad \text{(A-68)}$$

On the hemicylinder the pressure and velocity, which Spalding assumed to be constant, vary with circumferential location. However, Spalding suggests that his procedure can be extended to regions of moderate variations of stream velocity by using an integrated Reynolds number as suggested by Ambrok (Reference 45). Initial solutions indicated that this technique results in an unrealistic trend near the stagnation point, i.e., within 30° of the stagnation point. Therefore, for this region, the curves of flowrate and heat flux are assumed to be proportional. Thus, the flowrates are obtained from

$$\dot{W}_c = \dot{W}_{30°} \, \frac{h}{h_{30}} \qquad 0 < \frac{S_i}{R_n} < \pi/6 \qquad \text{(A-69)}$$

APPENDIX E

AERODYNAMIC STRUCTURAL LOADS

The aerodynamic forces on the wing are a summation of the pressure and viscous shear forces. These forces are presented in the dimensionless form of lift and drag coefficients. The lift is based upon a lateral projected area and the drag is based upon a frontal projected area. The relative direction of lift is normal to the free stream velocity vector and the relative direction of drag is parallel to the free stream velocity vector.

A. DRAG

The component of pressure forces that contribute to the drag coefficient are obtained by the vector dot product of the inward surface normal and the free stream velocity vector. The differential drag coefficient is then obtained by:

$$C_{DP} = \frac{P_i \, dA_i}{q_\infty \, A_{Ref}} \; \vec{V} \cdot \vec{N} \tag{A-70}$$

where N is the unit vector normal to the surface; V is the unit velocity vector, dA is the unit width area of the i^{th} element; A_{Ref} is a unit width area of the undersurface; and q_∞ is given by

$$q_\infty = \frac{1}{2} \rho_\infty \, V_\infty^2 \tag{A-71}$$

The total pressure drag coefficient is obtained by a chordwise integration of the differential drag coefficients, i.e.,

$$C_{DP} = \sum C_{Di} = \frac{1}{q_\infty A_{Ref}} \sum_{i=1}^{N} P_i dA_i \; (\vec{V} \cdot \vec{N}) \tag{A-72}$$

The viscous shear forces are expressed in the dimensionless form of the skin friction coefficient, C_F. As described in a previous section, the skin friction coefficient is determined using the method of Spalding et al.

The viscous forces that contribute to the drag coefficient are obtained by the vector dot product of T, the unit vector tangent to the surface and V_N, the normal to the free stream velocity vector. The i^{th} element drag coefficient due to shear force i is then

$$C_{DS} = \sum_{i=1}^{N} C_{Fi} (V_N \cdot T) \frac{dA_i}{A_{Ref}} \qquad \text{(A-73)}$$

The total drag coefficient is given as

$$C_D = C_{DP} + C_{DS} \qquad \text{(A-74)}$$

B. LIFT

Similarly the lift coefficient is obtained from the following equation

$$C_L = \sum_{i=1}^{N} \frac{C_{Di} d_{Ai}}{q_\infty A_{Ref}} (V_N \cdot N) + C_{Fi} \frac{d_{Ai}}{A_{ref}} (V_N \cdot T) \qquad \text{(A-75)}$$

where V_N is the unit vector which is normal to the free stream velocity vector as previously defined.

REFERENCES

1. Jarlett, F.E., "Performance Potential of Hydrogen Fueled, Airbreathing Cruise Aircraft," Report Numbers GDC DCB 66-004/1/2/2A/3/4.

2. Anthony, F.M. and Huff, R.D., "Analytical Evaluation of Actively Cooled Modified Monocoque Structural Sandwich Concepts," AFFDL - TR-65-124, Bell Aerosystems Co., July 1965.

3. Anthony, F.M., et al , "Fluid Cooled Cabin Wall Design for Hypersonic Aircraft," Interim Technical Report No. 2331-900201, Contract No. AF33(615)-5351, Bell Aerosystems Company, March 1967.

4. Reshotko, E. and Cohen, C.B., "Heat Transfer at the Forward Stagnation Point of Blunt Bodies," NACA Rep. 3513, 1955.

5. "A Manual for Determining Aerodynamic Heating of High-Speed Aircraft," Bell Aircraft Corporation Report No. 7006-3352-001, Volume I, June 1959.

6. Lees, L., "Laminar Heat Transfer over Blunt-Nosed Bodies at Hypersonic Flight Speeds," Jet Propulsion, Vol. 26, No. 4, April 1956, pp. 259-269.

7. Bushnell, Dennis M., "Interference Heating on a Swept Cylinder in Region of Intersection with a Wedge at Mach Number 8," NASA TN D-3094, 1965.

8. Beckwith, Ivan E. and Gallagher , James J., "Local Heat Transfer and Recovery Temperatures on a Yawed Cylinder at a Mach Number of 4.15 and High Reynolds Numbers," NASA TR R-104, 1961.

9. Neal, Luther, Jr., and Bertram, Michael H., "Turbulent-Skin-Friction and Heat-Transfer Charts Adapted from the Spalding and Chi Method," NASA TN-D-3969, 1967.

10. Spalding, D.B. and Chi, S.W., "The Drag of a Compressible Turbulent Boundary Layer on a Smooth Flat Plate with and Without Heat Transfer," Journal of Fluid Mechanics, Vol. 18, Part 1, January 1964, pp. 117-143.

11. Creager, M.O., "The Effect of Leading Edge Sweep and Surface Inclination on the Hypersonic Flow Field over a Blunt Flat Plate," NASA M 12-26-58A, January 1959.

12. Kelley, J.B. and L' Ecuyer, M.R., "Transpiration Cooling - Its Theory and Application," Report No. TM-66-5, Purdue University and Purdue Research Foundation, Lafayette, Indiana, June 1966.

13. Mistretta, A.L., "Lithium Spray Structural Cooling," AFFDL-TR-64-169, November 1964.

14. "Brass Bell Test Results and Test Program Plans - Liquid Metal Coolant System ," Report D143-941-015, October 1956.

15. Nixon, A.C., et al, "Vaporizing and Endothermal Fuels for Advanced Engine Application," Quarterly Progress Report No. 1, Contract AF-33(615)-3789, August 1966.

16. "Manned Orbiting Space Station, Environmental Control and Life Support System Study, " Hamilton Standard Report SLS 410-3, Vol. 3, Contract NAS 9-1498, May 1964.

17. SEA Aerospace Applied Thermodynamics Manual, Society of Automotive Engineers, Inc., 1969.

18. Anthony, F.M. et al, "Design and Analysis of Lightweight Thermal Protection Systems," Technical Report No. AFML-TR-67-377, Bell Aerosystems Co., December 1967.

19. Dukes, W.H. and Schmitt, A. "Structural Design for Aerodynamic Heating," WADC Technical Report 55-305, Parts I and II, Bell Aerosystems Co., October 1955.

20. Ryan, J.M. "Lightweight Thermal Protection System Development," Volume II, Insulation Material Data and Test Apparatus, AFML-TR-65-26, January 1965.

21. Hinckley, R.B., "Liquid Propellant Losses During Space Flight," Final Report, NASA Contract NAS 5-664, A.D. Little, Inc., October 1962.

22. Anthony, F.M. et al, "Design, Fabrication and Test of Hydrogen Cooled Structural Panels," Interim Technical Report, Report No. 2328-900201, Bell Aerosystems Company, January 1967.

23. "Integration and Optimization of Space Vehicle Environmental Control Systems," Technical Report ASD-TR-61-176, Part II, April 1963.

24. "Final Report on Lightweight Metal Foil Heat Exchangers," AFML-TR-65-52, Volume 1, Analysis, Design and Fabrication Methods, February 1965.

25. AFML-TR-65-52, Volume II, Hydrogen Precooler Development.

26. Kays W. and London, A.L., Compact Heat Exchangers, 2nd Edition, New York: McGraw-Hill, 1964.

27. Spalding, D.B., Auslander, D.M. and Sundaram, T.R., "The Calculation of Heat and Mass Transfer through the Turbulent Boundary Layer on a Flat Plate at High Mach Numbers, With and Without Chemical Reaction," Supersonic Flow Chemical Processes and Radiative Transfer, New York: McMillian Company, 1964.

28. Kays, W.M., "Convective Heat and Mass Transfer," New York: McGraw-Hill Book Company, 1966.

29. Hatch, J.E., and Papell, S.S., "Use of a Theoretical Flow Model to Correlate Data for Film Cooling or Heating an Adiabatic Wall by Tangential Injection of Gases of Different Fluid Properties," NASA TN-D-130, Lewis Research Center, November 1959.

30. Eckert, E.R.G., and Livingood, J.V.B., "Comparison of Effectiveness of Convection, Transpiration and Film Cooling Methods with Air as Coolant," NACA Report 1163, 1954.

31. Wieghardt, K., "Hot Air Discharge for De-Icing," AAF Translation, F-TS 919 RE, 1946.

32. Harnett, J.P., Birkebak, R.C. and Eckert, E.R.G., "Velocity Distributions, Temperature Distribution, Effectiveness and Heat Transfer for Air Injected Through a Tangential Slot into a Turbulent Boundary Layer," Trans. ASME, Ser. C 83, 1961, p. 293.

33. Papell, S.S., and Grout, A.M., "Experimental Investigation of Air Film Cooling Applied to an Adiabatic Wall by Means of an Axial Discharging Slot," NASA TN D-9, 1959.

34. Rosenbaum, H., "Turbulent Compressible Boundary Layer on a Flat Plate with Heat Transfer and Mass Diffusion," Thesis submitted to the Polytechnic Institute of Brooklyn, 1965.

35. McRee, D.I., Peterson, J.B., Braslow, A.L., "Effect of Air Injection Through a Porous Surface and Through Slots on Turbulent Skin Friction at Mach 3, "NASA TN D-2427, 1964.

36. Dally, J.W., "Design Data for Materials Employed in Thermal Protective Systems on Advanced Aerospace Vehicles," ML-TDR-64-204, Volume III, August 1965.

37. Jones, R.A. and Trimpi, R.L., Heat Transfer and Pressure Distribution at a Mach. No. 6.0 for 70° Swept Slab Wing with Sharp and Spherical Noses and Cylindrical Leading Edges," NASA, TMX-682, May 1962.

38. Wallace, J.E. and McLaughlin, E.J., "Experimental Investigations of Hypersonic, Turbulent Flow and Laminar Leeward-Side Flow on Flat Plates," USAF FDL TR-66-63 Volume I, 1966.

39. Moretti, G. et al, "Supersonic Flow About General Three Dimensional Blunt Bodies, Flow Field Analysis of Reentry Configurations by a General Three-Dimensional Method of Characteristics," ASD TR 61-727, Volume III, October 1962.

40. Faye, J.A. and Riddell, F.R., "Theory of Stagnation Point Heat Transfer in Dissociated Air," AVCO Research Laboratory, RR-1, June 1956.

41. "MX-2276 Reconnaissance Aircraft Weapon System, Aerodynamics," Bell Aircraft Corporation, Report No. D143-945-024, December 1955 (SECRET).

42. Beckwith, I.E., "Theoretical Investigation of Laminar Heat Transfer on Yawed Infinite Cylinders in Supersonic Flow and Comparison with Experimental Data," NACA RM L55F09, 1955.

43. Czarnecki, K.R., Allen J.M. and Jackson, M.W., "Boundary Layer Transition on Hypersonic-Cruise Aircraft," Conference on Hypersonic Aircraft Technology, NASA SP-148, 1967.

44. Dunavant, J.C., "Investigation of Heat Transfer and Pressures on Highly Swept Flat and Dihedraled Delta Wings at Mach Numbers of 6.8 and 9.6 and Angles of Attack to 90°, NASA TM X-688, June 1962.

45. Ambrok, G.S., "Approximate Solution of the Equation for the Thermal Boundary Layer with Variations of the Boundary Layer Structure," Soviet Physica Technical Physics, Volume 2, 1957.

46. Anderson, M. L., et al, "Analysis of Wing Structures for Hypersonic Aircraft", Report No. 31, Conference on Hypersonic Aircraft Technology, NASA-SP-148, May 1967.

47. Plank, P. O., et al, "Hypersonic Cruise Vehicle Wing Structure Evaluation," Prepared by Lockheed Missiles and Space Co. NASA CR 1568, Dec. 1969.

48. MIL-HDBK-5, Strength of Metal Aircraft Elements, March 1959, Armed Forces Supply Support Center, Washington, D. C.

49. Air Weapons Materials Application Handbook, Metals and Alloys, ARDC-TR-59-66.

50. Dukes, W. H., et al, Manufacturing Methods for Insulated and Cooled Double-Wall Structures, ASD Technical Report 61-7-799, Section I, Volumes I and II, May 1961.

51. Krivetsky, A., "Minimum Weight Design of Isotropic Plates and Shells Under Various Loading Conditions," Bell Aerosystems Company Report No. 2500-941024, November 1, 1968.

52. Liebermann, C. L., et al, "A Method for Estimating Airplane Wing and Tail Weights," Bell Aircraft Corporation, Report No. 2-59-942001, October 1959.

53. Pietrangeli, G. J. et al, "The Feasibility of a Mach 7 Transport Employing Airbreathing Propulsion Systems," AD-654-428, JHU/APL CG-2900, 15 November 1960.

UNITED STATES GOVERNMENT PRINTING OFFICE—1972/720-369/315-3-1